EXERGY ANALYSIS OF A STIRLING CYCLE

by

James Alexander Wills

A Dissertation Submitted to the Department of Mechanical Engineering at the University of Cape Town in fulfilment of the Degree of Master of Science in Engineering in Mechanical Engineering

Supervised by:
Professor Tunde Bello-Ochende

October 17, 2017

"Clearly, there are many places where diesel is king or gas-turbine is king, or IC engines will win, but there are many places in the world where as we've seen they just won't do the job. The modern version of the Stirling engine has some very, very attractive characteristics, and we're trying to optimize it for some of those applications."

Dean Kamen

American Inventor

Excerpt from a 2009 interview with Popular Mechanics magazine

Plagiarism Declaration

I know the meaning of plagiarism and declare that all the work in the document, save for that which is properly acknowledged, is my own. This thesis/dissertation has been submitted to the Turnitin module (or equivalent similarity and originality checking software) and I confirm that my supervisor has seen my report and any concerns revealed by such have been resolved with my supervisor.

Signed: Signed by candidate

Date: October 17, 2017

Abstract

In this dissertation the analysis of the Stirling engine is presented, this research topic falls within the category of thermal energy conversion. The research that was conducted is presented in three chapters of which the topics are: the effects of allocation of volume on engine performance, the GPU-3 (Ground Power Unit - developed by GM) Stirling engine analysis, and the optimisation of a 1000 cm^3 Stirling engine with finite heat capacity rates at the source and the sink.

The Stirling engine has many advantages over other heat engines, as it is extremely quiet, has multi-fuel capabilities and is highly efficient. There is also significant interest in using Stirling engines in low to medium temperature solar thermal applications, and for waste heat recovery. To develop high-performance engines that are also economically viable, advanced mathematical models that accurately predict performance and give insight into the different loss mechanisms are required.

This work aims to use and adapt such a model to analyse the effects of different engine parameters and to show how such a model can be used for engine optimisation using the Implicit Filtering algorithm. In the various analyses that are presented, the dynamic second order adiabatic numerical model is used and is coupled to equations that describe the heat and mass transfer in the engine.

The analysis shows that the allocation of volume has a significant effect on engine performance. It is shown that in high-temperature difference (HTD) engines, increasing dead-volume ratio increases efficiency and decreases specific work output. In the case of low-temperature difference (LTD) and medium-temperature difference (MTD) engines, there is an optimal dead-volume ratio that gives maximum specific work output. It was also found that there are optimal swept volume ratios and that the allocation of heat exchanger volume has a negligible effect on engine performance - so long as the dead-volume ratio is optimal.

The second order model with irreversibilities included was used to perform an exergy analysis of the GPU-3 Stirling engine. This model compared well with experimental results and the results from other models found in the literature. The results of the study show the two different approaches in modelling the engine losses and the effect that the various engine parameters have on the GPU-3 power output and efficiency.

The optimisation of the 1000 cm^3 Stirling engine was performed using a model with finite heat capacity rates at the source and the sink, fixed number of heater and cooler tubes, and four different regenerator mesh types. The engine geometry was optimised for maximum work output using the implicit filtering algorithm, and the results show the dominant effect that the regenerator has on engine performance and the geometry that gives maximum work output.

The critical insights obtained from this research are the importance of the dead-volume ratio in engine analysis, the merits of the novel Second law Stirling engine model, and the importance of regenerator mesh choice and geometry. The Implicit filtering algorithm is also shown to be a suitable choice of optimisation algorithm to use with Stirling engine mathematical models.

Acknowledgements

The financial assistance of the National Research Foundation (NRF) and the University of Cape Town (UCT) towards this research is hereby acknowledged. Opinions expressed and conclusions arrived at, are those of the author and are not necessarily attributed to the NRF and UCT.

I would like to acknowledge the help, support, and encouragement of my supervisor Professor Tunde Bello-Ochende. Without your advice and direction, I would not have made it this far.

To my mother, father and grandfather, thank-you for the 24 years of support and encouragement.

To my sister Nicola, thank you for always being there when I needed to go for coffee or needed to chat.

To Jay, thank you for the forest runs and the Greek adventures.

To my good friends Dean and Emma, thank you for the campus meetings, coffee breaks and encouragement.

I also place on record my sincere thanks to all who, directly or indirectly helped me on my journey.

Research Output

The following papers were produced in the course of this study and were published at the time of submission:

1. Wills J.A., Bello-Ochende T., Theoretical Thermodynamic Analysis and Optimisation of a Stirling Engine in Terms of Dead Volume, *In Conference Proceedings of the 4th Southern African Solar Energy Conference*, SASEC 2016, 31st October - 2nd November,Faculty of Theology at Stellenbosch University, Stellenbosch, South Africa. Paper ID. 72.

2. Wills J.A., Bello-Ochende T., Second Law Analysis and Optimisation of an MTD Stirling Engine Regenerator, *In Conference Proceedings of the 10th Constructal Law and Second Law Conference*, CLC 2017, 15th - 16th May,Romanian Academy, Bucharest, Romania.

Contents

List of Figures

List of Tables

Nomenclature

Alphabetical Symbols

A	area (m^2)
b	variable used in rhombic drive analysis
C	heat capacity rate ($kW.K^{-1}$)
C_p	isobaric heat capacity ($kJ.kg^{-1}.K^{-1}$)
C_v	isochoric heat capacity ($kJ.kg^{-1}.K^{-1}$)
d	direction
D	diameter (m)
e	eccentricity (m)
E	energy (kJ)
e	unit vector
f	frequency (Hz)
FR	flush ratio
f	function
g	gradient (∇f)
g	gravitational constant ($9.81 m.s^{-2}$)
H	Hessian ($\nabla^2 f$)
h	enthalpy ($kJ.kg^{-1}.K^{-1}$)
h	heat transfer coefficient ($kW.m^{-2}.K^{-1}$)
h	stencil step size
$\bar{h}$	Runge-Kutta and Adam's-Bashforth step size
$\dot{I}$	irreversibility rate (kW)
k	thermal conductivity ($kW.m^{-1}.K^{-1}$)
$\bar{k}$	Runge-Kutta k value
L	length (m)

L	lower bound
m	mass (kg)
$\dot{m}$	mass flow rate $(kg.s^{-1}$ or $kg.\theta^{-1})$
N	engine Speed (rpm)
N	number of tubes
NTU	number of transfer units
P	pressure (kPa)
Po	power (kW)
q	specific energy (kJ/kg)
$\dot{q}$	specific energy rate (kW/kg)
Q	energy (kJ)
$\dot{Q}$	energy rate (kW)
r	radius (m)
R	ideal gas constant $(kJ.kg^{-1}.K^{-1})$
$\mathbb{R}$	reals
s	specific entropy $(kJ.kg^{-1}.K^{-1})$
S	entropy $(kJ.K^{-1})$
S	stencil
S	secant
$\dot{S}$	entropy rate $(kW.K^{-1})$
$\bar{S}$	Sutherland temperature (K)
t	time (s)
T	temperature (K)
U	overall heat transfer coefficient $(kW.m^{-2}.K^{-1})$
U	upper bound
U	steepest Decent Vector
v	velocity $(m.s^{-1})$
V	volume (m^3)
w	specific work (kJ)
$\dot{w}$	specific power (kW/kg)
W	work (kJ)
$\dot{W}$	power (kW)
x	vector
X	temperature ratio

$\dot{X}$	exergy (kW)
y	scalar or vector at time t
y	gradient difference
z	height difference (m)
z	normalised vector

Greek Symbols

α	Armijo rule coefficient
α	phase difference ($^\circ$ or rad)
γ	ratio of specific heats
δ	differential
ε	effectiveness
ϵ	shape factor
ζ	regenerator volume to dead-volume ratio
η	efficiency
θ	angle ($rads$)
λ	step size in line search
μ	viscosity ($kg.m^{-1}.s^{-1}$)
ρ	density ($kg.m^{-3}$)
τ	shear stress (Pa)
ϕ	porosity
ω	angular velocity ($rad.s^{-1}$)
Ω	hyper-rectangle

Subscripts

$+$	future
0	environment
1	state 1
2	state 2
c	current
c	compression space
cb	compression space to cooler boundary

ccl	compression space clearance
$charge$	properties related to engine with all compartments at T_0
$cond$	conduction
$disp$, d	displacer
$dead$	dead/unswept
e	expansion space
eb	expansion space to heater boundary
ecl	expansion space clearance
$flow$	parallel with flow direction
gen	generated
h	heater
hb	regenerator to heater boundary
hyd	hydraulic
H	source
$H1$	source entering
$H2$	source exiting
i	index
in	in/entering
$internal$	internal
k	cooler
kb	cooler to heater boundary
K	sink
$K1$	sink entering
$K2$	sink exiting
$lost$	lost/destroyed
max	maximum
$mean$	average
$mesh$	mesh
min	minimum
n	upper limit of summation
net	net
out	out/leaving
$pist$, p	piston
r	regenerator

rev	reversible
$reference$	reference
$surf$	surface
$swept$	swept
th	thermal
$total$	total
ΔP	pressure effects
ΔT	temperature effects

Superscripts

0	methalpy shorthand
$*$	optimal scalar or vector
N	number

Dimensionless Numbers

B_N	Beale Number	$\frac{Po}{P_{mean}V_{swept}N}$
f_D	Darcy friction factor	$\frac{2\Delta PD}{L\rho v^2}$
f_F	Fanning friction factor	$\frac{2\tau}{\rho v^2}$
f_r	Reynolds friction factor	Ref_D
Nu	Nusselt number	$\frac{hD}{k}$
Pr	Prandtl Number	$\frac{C_p\mu}{k}$
Re	Reynolds number	$\frac{\rho vD}{\mu}$

St	Stanton Number	$\frac{h}{\rho u C_p}$
W_N	West Number	$\frac{Po}{P_{mean} V_{swept} N(\frac{T_h - T_k}{T_h + T_k})}$

Chapter 1

Introduction

1.1 Background

The Stirling engine was invented by Rev. Robert Stirling in 1816 approximately 80 years before the Diesel engine. It was developed as an alternative to the steam engines of the day and was commercially a success up until the early 1900's. At this point, there was rapid development in internal combustion engine technology which resulted in a steep decline in Stirling engine development and use. Then in the 1950's, there was renewed interest in the Stirling engine with the development of the Philips Stirling electric generators. Then again in the 1970's during the various oil and energy crises, there was concern surrounding energy availability and security which resulted in significant investment into Stirling engine research and development programmes. This renewed interest mainly revolved around developing Stirling engines for use in the automotive industry and military. Although there were many programmes, a widely adopted Stirling engine that could compete with internal combustion engines was never successfully commercially developed.

That being said, Stirling engines are currently considered the most efficient and economically viable low power solar thermal conversion devices available. They are also able to operate through a low-temperature difference and can, therefore, be used cheaply and efficiently with waste heat or cheap low-temperature sources of energy. The ability of the Stirling engine to operate through extremely low-temperature differences was aptly demonstrated by James Senft who designed a Ringbom type engine which operated with a temperature difference of 0.5 °C [92].

The Stirling cycle is a closed thermodynamic cycle that is regenerative and involves the cyclic compression and expansion of the working fluid at varying temperatures. Figure 1.1 is a diagram of the ideal isothermal Stirling cycle.

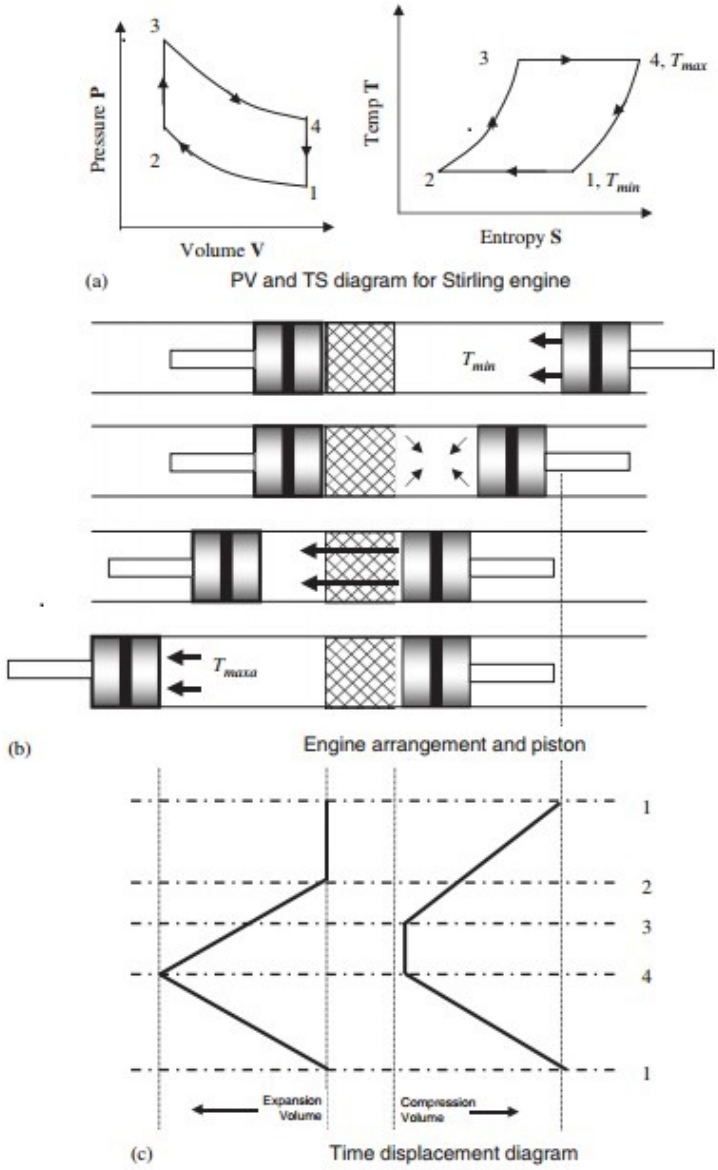

Figure 1.1: Idealised Stirling cycle diagram [109]

Stirling engines are generally classified based on the temperature difference through which they operate. Low-temperature difference (LTD) engines have a heater temperature of between 80 °C and 150 °C, medium-temperature difference (MTD) engines 150 °C to 400 °C and high-temperature difference (HTD) engines 400 °C to 800 °C [61].

With the current uncertainty over future oil supply, peak oil and the ever-present need for more efficient energy solutions, there is renewed interest in Stirling engines. DEKA Research and Development Corporation is currently developing the Beacon 10, a gas-powered Stirling engine and water heater. These units produce 10 kWe and are being designed for domestic and small-scale commercial combined heat and power(CHP) applications. Figure 1.2 is an image of a Beacon 10 prototype that DEKA is currently developing.

Figure 1.2: DEKA Beacon 10 gas powered CHP Stirling generator [65]

1.2 Problem Statement

Africa as a continent is facing a potential energy shortage which needs to be swiftly addressed to allow for sustainable development. The continent is rich in renewable energy resources that have electricity generation potential, and a significant share of these resources require heat engines to convert the thermal energy to electricity. Often the optimal geographic location for renewable power generation is far removed from the conventional power distribution network. Due to the high cost of connecting these areas to existing electricity distribution systems, it is often more suitable for the power generated to be used by local consumers.

Due to many different factors, the Stirling engine has been identified as a prime candidate for small-scale power generation. However, current Stirling engine technology has not seen widespread application. Recently there has been renewed interest due to its multi-fuel capabilities, low noise output, and high efficiency. Stirling engines have a low power density when compared to internal combustion engines. Therefore, it is of interest to optimise these engines for maximum power output as this results in a smaller engine which is more economical regarding space and material requirement. The cycle is optimised thermodynamically in terms of allocation of volume to give maximum power density. The whole engine is then looked at and optimised using exergy analysis methodology. Stirling engines are complicated devices as the working fluid flow through the heat exchangers is transient and completely reversing. The modelling of the entire system and the irreversibilities present requires an understanding of thermodynamics, heat transfer and fluid dynamics. The areas of Exergy Analysis (EA), Finite Time Thermodynamics (FTT) and, Entropy Generation Minimization (EGM) are where these three fields meet. The component configuration of the system is optimised by maximising the work output of the engine. Similarly, the efficiency of the engine can also be optimised, but this has not been included in the scope of this study.

1.3 Objectives of the Investigation

The main objective of the investigation is to optimise a Stirling engine through the following research objectives:

- Modelling of the Stirling cycle.
- Analysis into the effects of dead-volume ratio on the Stirling cycle.
- Optimisation of the cycle specific work output in terms of volume allocation.
- Application of the second law to the second order ideal adiabatic model of the Stirling engine.
- Exergy analysis and modelling of the GPU-3 (Ground Power Unit - developed by GM) Stirling engine.
- Exergy analysis and optimisation of a 1000 cm^3 Stirling engine for maximum work output with finite heat capacity rates at the source and the sink.

1.4 Originality of Work

It has always been thought that the effect of unswept or dead-volume negatively affects the performance of Stirling engines. This study has found that this is not the case, as when the adiabatic working space assumption is made there exist optimal dead-volume ratios for LTD and MTD Stirling cycles that give maximum specific work output. This result is not available in the literature. The use of a linear multi-step method (Adam's-Bashforth) is also a new approach to finding a numerical solution to the ideal adiabatic model. It decreases the solution time as it does not require intermediate steps like the Runge-Kutta method which has been conventionally used in Stirling cycle models. The approach to optimising the physical design parameters through the exergy analysis of a dynamic numerical Stirling engine model is novel. In the literature, this approach has only been applied to highly idealised Stirling engine mathematical models.

1.5 Dissertation Overview

The dissertation is composed of 9 chapters. Chapter 1 describes the background to the research, the research problem, the objectives of the investigation, the originality of the work and the layout of the dissertation. Chapter 2 is the literature review, which presents a summary of the literature published on the topics of renewable energy, Stirling engines, and second law analysis. This chapter briefly describes the current energy situation in the world and Africa. Stirling cycle literature is then discussed along with different thermodynamic models and previous Stirling engine studies. The literature on the second law of thermodynamics is then discussed along with the application of the second law to Stirling engines and other engineering devices. Chapter 3 is the mathematical modelling chapter which presents and explains the Stirling cycle mathematical model and objective function. Chapter 4 is the optimisation chapter where the optimisation procedure is discussed and explained. Chapter 5 is the dead-volume analysis that presents and explains the results of the dead-volume and allocation of volume analyses. Chapter 6 is the exergy analysis of the GPU-3 Stirling engine, and chapter 7 is the optimisation of the 1000 cm^3 Stirling engine with finite heat capacity rates at the source and the sink. Chapter 8 is the conclusion which presents the discussion of results and concluding remarks. Chapter 9 is the recommendations chapter which proposes recommendations for future work and research.

Chapter 2

Literature Review

2.1 Introduction

The following chapter discusses the literature on renewable energy, the Stirling engine and, the second law of thermodynamics and its use in the analysis of power cycles. The literature review was conducted over the entirety of the time that this research was being carried out and was under continual revision as the topic progressed and evolved.

There is currently a concern over the certainty of future energy supply and the threat of global climate change. These issues are of utmost importance when considering the electrification of developing regions and addition of generating capacity to meet the ever-increasing demand for energy. South Africa faces both of these challenges as the demand for electricity is continuously rising due to increased consumption in developed areas, and the electrification of developing regions. To guarantee future energy supply and mitigate global climate change a realistic and easily implementable cost-effective solution is required. Currently, the most favourable solution to these looming crises is to utilise a variety of the abundant renewable energy resources that are available. This solution is the most feasible, as these sources of energy are non-polluting and inexhaustible [35].

The use of Stirling engines with renewable thermal sources of energy is one of the many potential renewable energy solutions that are available. The Stirling engine is a closed cycle and therefore requires external heating. This characteristic makes them suitable for use with all forms of thermal energy. In recent years there has been a notable interest in using Stirling engines with solar concentrators as a means of generating electricity. In the literature, second law Stirling engine optimisation has not been given much attention, and this study aims to

add knowledge to this crucial area of renewable energy technology research. The effects of volume allocation in the Stirling engine are also analysed, as this is another area in the literature that has not been given significant attention. To properly optimise a system, the exergy or available work should be maximised for the system as a whole, rather than being maximised for individual components. By spreading the entropy generation over the entire system, the result is a truly optimised system. Whereas, optimising individual components does not guarantee an optimised system.

The literature review was conducted throughout the dissertation writing process and is broken up into six main sections. The first part is the renewable energy section. In this section, the renewable energy situation in the world and renewable sources that are compatible with Stirling engines are discussed. The second section is concerned with the Stirling engine; a brief history is given along with the discussion of Stirling cycle modelling and previously conducted theoretical and experimental analyses. The third section discusses Stirling engine heat exchangers as these components have the most significant effect on Stirling engine performance and are the interfaces between the engine, the source and the sink. The fourth section discusses solar thermal power in the context of the Stirling engine. The fifth and final section describes the second law of thermodynamics and, the entropy generation minimisation and exergy analysis methods of optimisation. The application of the second law to the different components is also discussed along with the interpretation and implications of the results.

2.2 Renewable Energy

2.2.1 Background

The extended historical use of fossil fuels has resulted in global warming due to the emission of greenhouse gases; it is, therefore, a priority that non-polluting sources of energy be employed to mitigate these effects[45]. Renewable energy sources are currently considered the most effective solution to this problem and are termed renewable as they are clean and unbounded sources of energy[77]. According to [83], at the end of 2014 renewable generating capacity had reached 1712 GW which represented 27.7 % of the worlds generating capacity, an increase of 8.5 % over the 2013 levels. In 2014 it was estimated that renewables provided 22.8 % of the worlds electricity needs and that renewables made up 58.5 % of additions to the global generating capacity.

Figure 2.1 is a diagram that shows the potential of renewable sources to provide for the worlds energy needs[35].

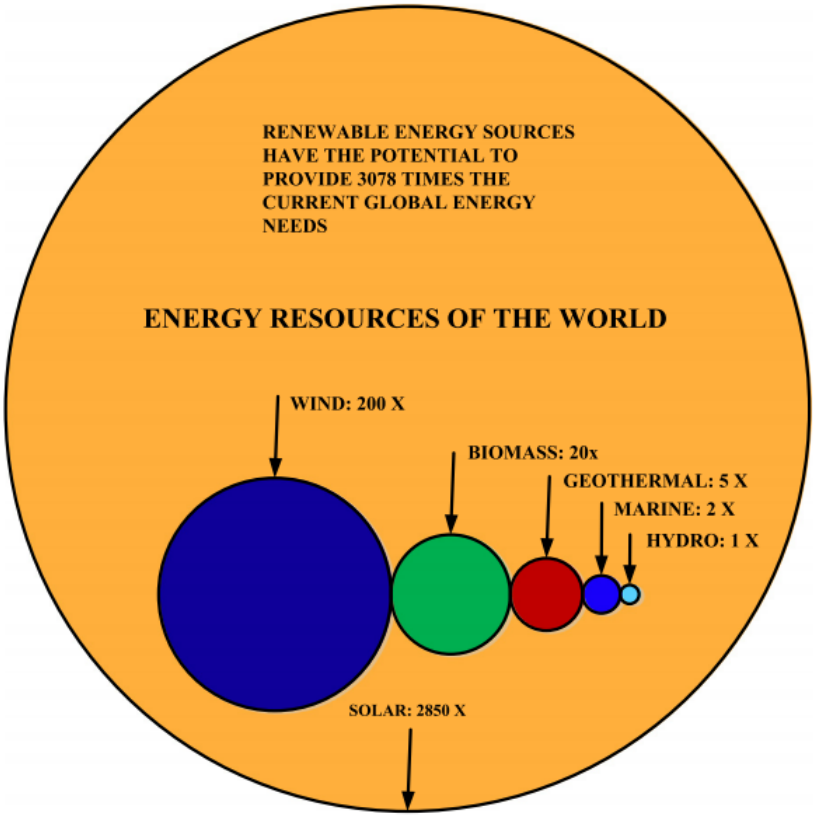

Figure 2.1: Renewable energy source potential chart [35]

From figure 2.1 it can be seen that renewable energy resources can provide 3078 times the current global need if all utilised. Solar makes up the bulk of this, with solar having the potential to provide 2850 times the worlds energy requirement.

As referred to in [83], the sustainable energy for all initiative launched by the United Nations secretary general in 2011 has pledged to double the renewable energy share from a baseline of 18 % in 2010 to 36 % by the year 2030. This increase in renewables is to be done while increasing energy efficiency and access to modern energy services. Renewable energy research is therefore of utmost importance if these objectives are to be achieved. Current sources of renewable energy are categorised as follows: solar, geothermal, wind, bioenergy and marine energy. Three of these sources can be used as heat sources for a Stirling engine; these are bioenergy, solar and geothermal energy.

Figure 2.2 below gives a breakdown diagram of the different renewable energy sources[35].

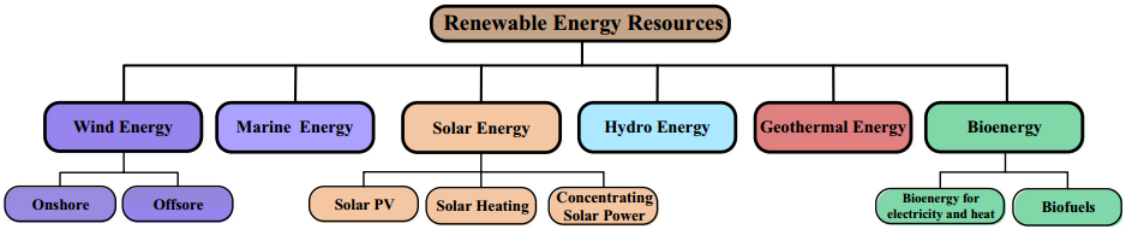

Figure 2.2: Renewable energy source chart [35]

2.2.2 Solar Energy

According to [108], the sun constantly emits 3.8×10^{17} GW. 1.8×10^{8} GW is intercepted by the earth of which approximately 1.08×10^{8} GW reaches the surface of the earth. If 0.1 % of this energy is converted to electricity at an efficiency of 10 %, the generating capacity would be 10800 GW which is 3.6 times the worlds current generating capacity of approximately 3000 GW. This calculation illustrates that if energy storage were not an issue the sun would easily be capable of satisfying the worlds energy need. There are currently two methods of generating electricity using solar irradiance; these are photovoltaics (PV) and solar thermal energy (STE). Of these two methods solar thermal energy can be used as a source of heat energy for a Stirling engine. According to [83], global solar thermal capacity reached 4.4 GW in 2014 with a capacity increase of 27 % over 2013.

Concentrating solar power works by concentrating incoming solar irradiance, which in turn heats a solid, liquid or gas medium [35]. This medium exchanges heat with a cycle working fluid which in turn is used to generate power. The majority of current plants use parabolic trough technology as a means of concentrating solar irradiance. The advantages of solar power are its potential to be an unlimited energy source, as well as the fact that it does not yield any air or water pollution. However, there are shortcomings to solar energy which includes lack of economic competitiveness, reliance on sunlight availability, the pressing need for energy storage technologies and landscape damage due to erosion.

2.2.3 Geothermal Energy

According to [35], geothermal energy is considered to be a reliable, potentially unlimited energy source that does not contribute to air or water pollution. However, there have been issues with cost, as geothermal plants often have high start-up and maintenance costs.

There are three different categories of geothermal reservoir. These are water-dominant fields, wet steam fields and vapour-dominant fields [8]. Water-dominant fields produce water at temperatures up to 100 °C, wet steam fields produce pressurised water at temperatures higher than 100 °C and vapour-dominant fields produce dry steam at pressures higher than atmospheric. There are very established methods for generating electricity with vapour-dominant and wet steam fields, but not for water-dominant fields. Historically, in the case of a water-dominant field, the organic Rankine cycle is used, or the heat is used for direct heating [8]. However, according to [55], the low-temperature difference (LTD) Stirling engine is also a viable option. The Stirling engine is well suited for low-temperature geothermal electricity generation as it is a feasible option for use with water-dominant wells that were previously thought to only be suitable for direct heating or organic Rankine cycle applications.

According to [83], in the last five years, geothermal capacity has maintained steady growth at a rate of 3.6 %, with an addition of 640 MW in 2014.

2.2.4 Bioenergy

In the 2015 renewables status report, it was highlighted that liquid biofuel production had reached its highest levels ever recorded, with a production increase of 9 % in the year 2014 [83].

As discussed in [35], bioenergy is considered a renewable energy source that is relatively inexpensive. Waste products from many agricultural and industrial processes are deemed to be biofuels, and if used correctly, the load on landfills and other conventional waste management programmes can be significantly reduced. Biomass is also very widely distributed and can be locally produced in many regions, providing unparalleled energy access when compared to conventional fossil fuels. Another benefit is the involvement of the agricultural sector in biomass production, which has a positive impact on rural employment. According to [77], the two primary biofuels which are produced from biomass are biogas and biodiesel. Both of these fuels have significant advantages over conventional fuels and have the potential to enormously reduce the emissions that are linked to fossil fuels, as they can directly replace fossil fuels. Biogas is produced from primarily organic waste that has gone through an anaerobic digestion process. This process is one of the most efficient methods of biofuel production currently available. It also allows biogas to be produced when it is required rather than continuously. Biodiesel, on the other hand, is produced from primarily fats and

oils and is biodegradable. Biofuels do have disadvantages, as they contribute to air pollution through carbon dioxide and other greenhouse gas emissions. There is also concern over particulate emissions often associated with the burning of unprocessed biofuels. These particulate emissions are primarily a concern with wood and other solid fuels. Regarding the production of biofuels, agricultural air and soil pollution due to the intensive farming methods, as well as a loss of biodiversity are a concern [35].

There is interest in utilising biomass as a fuel source for Stirling engines because the combustion process is external and therefore less fuel processing is required. A Stirling engine is also very flexible when it comes to fuel type and can, thus, be designed to cater for multiple fuels. This capability is an especially important characteristic, as in the case of biomass the fuel composition can often be inconsistent.

2.2.5 Renewable Energy in the African Context

In 2015, it was estimated that there were approximately 1 billion people in the world that did not have access to electricity [83]. Many of these people live in Africa, and due to the developing nature of many African economies, a lot of the countries lack the grid infrastructure required for countrywide electricity supply. The total generating capacity in Africa is 147 GW, which at the time of writing was less than was present in Germany [83]. Sustainable energy use and development has also been at the forefront of the considerations in policies and plans put forward in many African countries [17].

Africa as a continent has significant availability of renewable energy resources when compared to other continents, and it is imperative that these be harnessed in the future to provide electricity for sustainable development [17]. The primary sources of thermal renewable energy found on the African continent are solar and bioenergy. According to [8], there is also geothermal potential on the African continent as there are geothermal resources present in East Africa, found in locations around the East African rift. These resources are situated in mainly Kenyan and Ethiopian territory, with geothermal sources supplying 8.41 % of Kenyas energy requirement in the year 2000.

2.2.6 Summary

Renewable energy research and technology development is currently growing at a rapid rate. However, it has been pointed out that there needs to be even more rapid growth if the

looming threats of climate change and fossil fuel resource depletion are to be mitigated. Regarding thermal renewable energy, the Stirling engine has been cited as a prime candidate for use in this industry, as a small to medium scale converter.

2.3 The Stirling Cycle

2.3.1 Background

The Stirling engine which has also been called a hot-air or hot-gas engine was invented by Robert Stirling in 1816 [102]. The Stirling cycle is a closed thermodynamic cycle that involves the cyclic compression and expansion of gas at different temperatures and incorporates regeneration. The Stirling engine is categorised as part of the Reitlinger class of cycles, which is a class of cycles that can theoretically attain Carnot efficiency [93].

The Stirling engine had moderate commercial success up until the early 1900's when internal combustion engines and electric motors achieved widespread adoption [109]. However, after the energy crisis of 1979, there was renewed interest in Stirling engine technology. This renewed interest manifested itself as a high research output during the 1980's. The main reason for the attention was the multi-fuel capabilities and low fuel consumption of the Stirling engine which was of importance at the time because of the global uncertainty around energy security.

The Stirling engine is currently considered the most effective device for low power solar thermal conversion in the range of 1-100 kWe [56]. It does not contribute to air and noise pollution to the same levels that are associated with internal combustion engines and is highly efficient when compared to other gas power cycles. The engine is also fit for use with low-temperature heat sources and is therefore suitable for waste heat recovery. The thermodynamic cycle is a closed cycle, with the highly simplified ideal model being made up of four thermodynamic processes, these being: two isothermal processes and two constant volume processes. In reality, these processes are not realised as real Stirling engines are seen to have adiabatic working spaces rather than isothermal ones [116, 115].

Figure 2.3 below is a pressure-volume diagram of the cycle originally analysed by Gustav Schmidt in 1871 [91]. In the analysis, the working spaces are assumed to be isothermal.

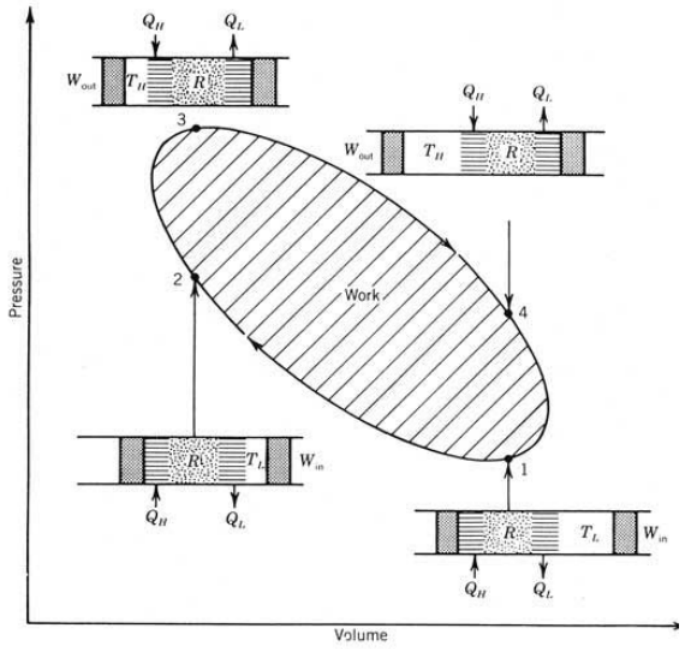

Figure 2.3: P-V diagram of the idealised Stirling cycle for an alpha type engine with sinusoidal volume variation [101]

There are three different mechanical configurations for Stirling engines, and they are the alpha, beta and gamma-type engines [109]. Figure 2.4 is a diagram of these three configurations.

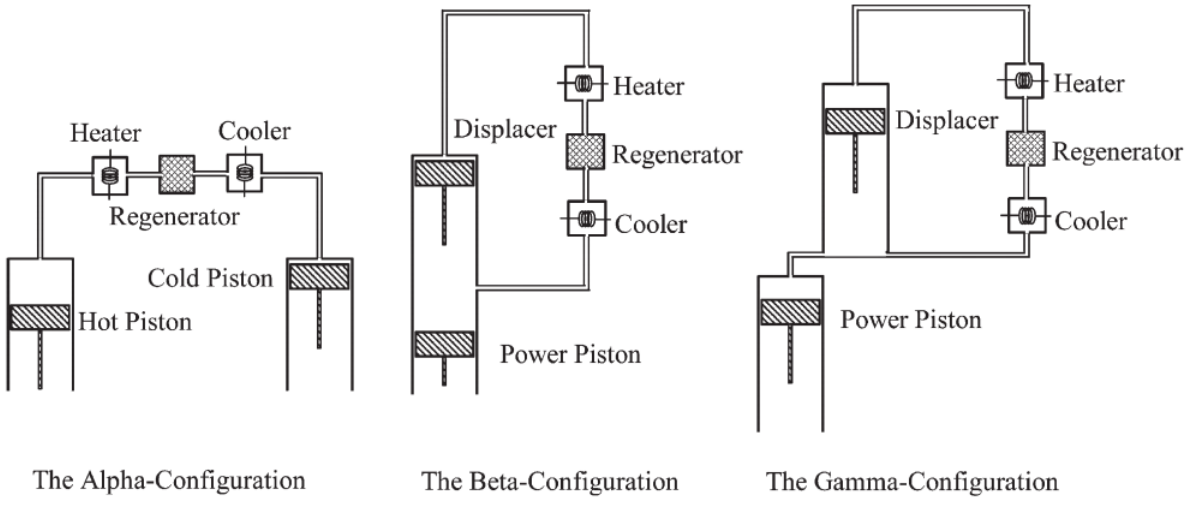

Figure 2.4: Stirling engine mechanical configurations [56]

These three different mechanical configurations each have their advantages and disadvantages. The alpha type engine gives the highest power density, as this coupling allows for a large swept volume. However, the beta and gamma configurations are preferred in practice as they do not require the hot (expansion space) cylinder to be sealed [109]. The sealing of the expansion space cylinder is difficult and expensive in practice as specialised high-temperature seals are required.

2.3.2 Stirling Cycle Modelling

As discussed in [70], [24] and [34], there are a wide variety of Stirling engine models. According to these review articles, the different Stirling engine models are categorised according to their complexity and ability to accurately predict real engine performance. The following sub-headings each describe one of these categories, and they are zeroth order models, first order models, second order models, third order models, the method of characteristics and multi-dimensional models.

Zeroth Order Models

Zeroth order models are models based on Stirling engine experimentation and the empirical findings from these experiments [34]. Professor William Beale, the inventor of the free piston Stirling engine, found that the maximum output power of a Stirling engine is proportional to the mean engine pressure, engine volume and speed [109]. However, Beale based his relation on experiments that involved Stirling engines operating with a relatively high-temperature difference notably a heater temperature of 650 °C and a cooler temperature of 65 °C. The Beale number relation can be seen as equation 2.1 [34].

$$B_N = \frac{Po}{P_{mean} V_{swept} N} \tag{2.1}$$

The Beale number is approximately 0.15 for Stirling engines with a heater temperature of 650 °C or greater [49]. The shortfall of the relation is that it did not account for the temperature difference. However, these effects were considered by West and the West number relates the maximum output power to the mean engine pressure, volume, speed and, the source and sink temperatures.

The West number relation can be seen as equation 2.2 [49].

$$W_N = \frac{Po}{P_{mean} V_{swept} N (\frac{T_h - T_k}{T_h + T_k})} \tag{2.2}$$

It has been found that the West number is approximately 0.25 for devices with outputs of between 5 and 150 kW [49]. Whereas, a West number of 0.35 has been recommended for smaller Stirling engines.

The above relations are usually used by engine designers as a way of quickly estimating the power output for a set of specified engine parameters [24].

First Order Models

First order models are the simplest mathematical models that are available. These models are used for simplified initial Stirling engine analysis and performance predictions [24]. They usually start with an ideal loss free isothermal analysis, then a correction factor that accounts for all the losses is applied to calculate the estimated actual efficiency and power output. The first analysis of this kind was done by Gustav Schmidt in 1871 for the case of sinusoidal volume variations in the expansion and compression spaces [34]. This analysis resulted in the now well-known Schmidt equations [91].

Second Order Models

Second order models are more complex than first order models and are more insightful as they identify and quantify the different losses present in the cycle. In all second-order models, it is assumed that the energy losses are decoupled from one another. As explained in [24], [70] and [34], these models begin with an idealised analysis of the cycle to determine the heat input and power output, the different losses are then identified and included in the analysis to find the adjusted heat input and power output. The losses included in the analysis are pumping power losses and heat transfer losses, the pumping power losses are subtracted from the calculated ideal power output, and the heat transfer losses are added to the calculated ideal heat input. Once the new input heat and output power have been calculated, the new loss inclusive efficiency is evaluated.

Second order models are further categorised by how the expansion and compression spaces are modelled. They are modelled as either being isothermal, adiabatic or semi-adiabatic [24].

Isothermal compression and expansion space modelling is based on the Schmidt analysis and assumes that the rate of heat transfer between the cylinder walls and working fluid is infinite. The solution to the isothermal cycle equations can be found analytically for sinusoidal volume variation in the working spaces. Adiabatic modelling assumes that the working spaces are adiabatic and therefore the rate of heat transfer between the cylinder walls and working fluid is zero. A solution to the adiabatic cycle equations cannot be found analytically, and an iterative numerical scheme is required to obtain a solution. Semi-adiabatic compression and expansion space modelling assumes finite heat transfer rate between the cylinder walls and working fluid, and the working space wall temperatures are assumed to be constant. A solution to the semi-adiabatic cycle equations cannot be found analytically, and an iterative method is required to obtain a solution. The first example of a non-isothermal analysis was conducted by Finkelstein in the 1960's, and this study represented a significant advancement in Stirling engine numerical modelling and analysis [38]. These models along with the inclusion of various losses into the models have laid the foundation for modern Stirling engine analysis [119].

It has been suggested that the standard Stirling cycle model should be the second order adiabatic model, as the working spaces in actual Stirling engines are adiabatic and not isothermal [116, 115]. This model was extensively analysed and experimentally validated over a period of ten years by Dr Berchowitz while working at the University of the Witwatersrand [15, 16].

Third Order Models

Third order modelling of the Stirling engine is broken down into three steps. First, the engine is divided up into control volumes, then the differential equations of energy, mass and momentum conservation, along with the equations of state are defined for each control volume. The differential equations are then solved simultaneously using numerical methods [24]. There are two different categories of numerical method for solving the set of differential equations. These are the implicit and explicit integration methods. Explicit integration involves computing values at a new time using the derivatives evaluated at the previous time. Implicit integration involves computing values at a new time using the derivatives evaluated at the new time. There have been many commercial packages that have been developed for Stirling engine analysis. The code by David Gedeon, named SAGE has been used with success and utilises implicit methods to solve the governing equations in space

and time [41].

The Method of Characteristics

According to [24], these models utilise the method of characteristics to solve the governing thermodynamic equations. This method is realised by transforming these governing equations from partial differential equations of the hyperbolic type to linear differential equations. The method has been applied with a high degree of success to the analysis of compressible gas flow and is suitable for use in the analysis of the unsteady flow through Stirling engine heat exchangers.

Multi-Dimensional Models

Multi-dimensional models are the most complex of all the models and involve computational fluid dynamics (CFD) methodology [120]. According to [34], two-dimensional CFD models can greatly improve the accuracy of analysis as the complex heat transfer, and gas dynamics can be more accurately modelled. In this area of Stirling engine modelling, there is a clear lack of work that has been done, as in the past third order models have been adequate. Also, it is only recently that computers have been able to simulate the Stirling engine in a reasonable amount of time using multi-dimensional models. However, if Stirling cycle engines are to be improved further this research area needs to be expanded as far higher accuracy can be achieved. This decrease in simulation time is especially significant in the case of modelling turbulence and transient effects.

2.3.3 Stirling Cycle Analysis in Literature

There have been some studies in the literature that have analysed and optimised Stirling engines using several different techniques and methodologies. This section presents these studies and briefly summarises what was analysed and the outcome of each study.

In [28], a theoretical model was presented that investigated the optimisation of the Stirling cycle using a linear variation of the overall heat transfer coefficients and temperature difference. It examined the effects of the cases where the source and sink had finite thermal capacity or were at constant temperature. The results of the study indicated an optimal range of parameters and provided insight into the optimal design of Stirling engines.

In [121], a model utilising finite time thermodynamics was presented. The model accounted

for the effects of irreversible heat transfer, as well as imperfect regeneration. The relationships between power output and efficiency, optimised power output and conductance characteristics, and optimised power output and regenerator effectiveness were established. The model provides a baseline from which the performance of real machines can be judged and improved.

In [110], a new thermodynamic model of the Stirling engine was presented. The analysis of the GPU-3 Stirling engine was presented, and the effects that different design parameters have on performance was analysed. The losses in the regenerator were also analysed, and engine performance using different regenerator matrix materials was explored.

In [68], a first order analysis of the Stirling cycle along with exergetic, energetic and entropic analyses was presented. The Stirling cycle was then optimised according to the performance requirements of the exergetic, energetic and entropic analysis methodologies. Similarly, [43] employed finite time and finite size thermodynamics to optimise the Stirling engine from an engineering design perspective. The exo-irreversible Stirling cycle with imperfect regeneration was used to obtain analytical relations for all engine operating parameters as functions of given engine specifications and engine speed. Another similar study [69] analysed the low-temperature difference (LTD) Stirling engine at steady state operation. The engine was divided into components, and for each component, energy, entropy and exergy balances were written in terms of the different engine parameters. The result of the analysis was the optimal conditions for operation that resulted in the minimum amount of exergy destruction or production of entropy, and thus minimisation of operating cost.

In [93], an analysis was presented that aimed to gain some insight into the nature of Stirling engine losses and the effect that these losses have on engine performance. The model took into account limited heat transfer at the source and sink, mechanical friction and internal thermal losses. The combination of heat losses was represented as a heat flow, proportional to the difference between the source and sink temperatures. The study found that the maximum efficiency was at a specific temperature ratio.

In [94], the Stirling engine was optimised and analysed to produce maximum shaft work, rather than maximum cyclic work as has been the focus of many optimisations. The gamma type engine configuration was chosen, and it was shown that maximum shaft work occurs at smaller swept-volume ratios than the swept volume ratio that gives maximum cyclic work. It was also shown that smaller swept volume ratios are in favour of shaft work and that

dead-volume negatively affects performance.

In [37] and [36], the maximum power density technique was applied to Stirling engines, as utilising this technique will result in smaller engines with higher efficiencies. The studies present the maximum efficiency and maximum power density points along with the optimal compression ratio for maximum power density. In [36], the optimisation was a multivariate optimisation that gave the maximum power density for different engine parameters.

In [79], a new Stirling engine model named the Direct method was presented. This method has been suggested as a means of accurately simulating the Stirling engine and assumes finite time processes, and that the mechanisms that result in the irreversibilities present in the system can be intuitively analysed and separated. The direct method results were compared to experimental Stirling engine results, and there was a good agreement.

In [114], the ecological function of the irreversible Stirling and Ericsson cycles was presented, the ecological function is defined as the power minus the irreversibility due to various losses. The ecological function was maximised, and the expression for the power output and thermal efficiency derived. Using these expressions the effects that different parameters have on engine performance was explored. It was found that the internal irreversibilities are always greater than the external irreversibilities and that the cooler heat capacity rate and effectiveness have a far more significant effect than the heater heat capacity rate and effectiveness. The effect of the effectiveness for both of these heat exchangers was far outweighed by the regenerator effectiveness which has the most significant effect on engine performance.

In [1], an analysis that used finite time thermodynamics to calculate the thermal efficiency and power output of the Stirling engine was presented. The analysis included finite-rate heat transfer, regenerative losses, bridging losses and finite time regeneration. A sensitivity analysis of the operating and engine parameters was presented, showing the effects that these different parameters have on performance.

In [112], the second order adiabatic model was used, and a multi-objective optimisation of the model with pressure drop and external conduction losses was presented. The analysis used the NSGA-II multi-objective evolutionary algorithm that sought to optimise the output of the engine. The result of the optimisation was a Pareto frontier of equally optimal solutions in terms of engine efficiency and power loss. The same authors presented the optimisation of the GPU-3 Stirling engine using a third order model and multi-objective optimisation

criteria, which can be seen in [113].

In [18], a Stirling engine with a swashplate drive mechanism was analysed, and it was found that there was an engine geometry that maximised the thermal efficiency of the engine. The analysis also presented the optimal variables that give maximum efficiency, and it was found that the performance was highly sensitive to change in some variables but not others. The optimisation was also seen to be robust in the sense that changing some variables had limited effect on engine performance.

In [78], a model based off of the work of Urieli and Berchowitz [116, 115] was presented. The model was used to optimise the geometry of a gamma type Stirling engine using the quasi-steady flow approach. In optimising the engine the power output and corresponding thermal efficiency were maximised.

In [7], a new Stirling cycle polytropic model with various losses (PSVL) was presented. The model was applied to the GPU-3 Stirling engine and showed good agreement with experimental results, with the output power and efficiency being predicted within a 14.34 % and 3.14 % difference respectively.

In [25], a model for predicting the performance of a thermal-lag type Stirling engine was presented. This type of Stirling engine is a beta type engine with no displacer and just a piston. The analysis was used to predict the optimal engine speed for maximum power output and thermal efficiency. The effects of some other parameters were also analysed and presented.

In [4], a model for a gamma type Stirling engine was presented and experimentally validated. The model assumed adiabatic working spaces, finite heat transfer rate and, mechanical and thermal losses were included. The model showed good agreement with experimental data, with the heater and cooler temperatures being predicted with a high degree of accuracy. The effect of the buffer pressure on engine performance was also predicted.

To summarise the different analyses and optimisations seen in this section, it can be concluded that in most cases highly idealised Stirling engine models were used. It can also be seen that limited exergy analysis has been carried out on more complex Stirling cycle models.

2.3.4 Stirling Engine Experimental Results

There have been some experimental efforts concerned with the design and testing of Stirling engines. Some of the most profound design and experimental results were achieved by Senft who designed and tested a Ringbom type Stirling engine that operated with a temperate difference of 0.5°C [92]. There have been many other Stirling engine tests, the different tests and corresponding abbreviated results can be seen in table 2.1.

Table 2.1: Table of Stirling engine experimental results

Name	Po(w)	η(%)	N(rpm)	T_H(K)	T_K(K)	$V_{swept}(cm^3)$	$P_{charge}(bar)$
Kontragool [58]	1.69	0.645	52.1	436	307	893.8	1
Kontragool [59]	11.8	0.494	133	589	307	893.8	1
Kontragool [60]	6.1	0.44	20	439	307	7391	1
Kontragool [59]	32.7	0.809	42.1	771	307	7391	1
Iwamoto [48]	145	5	142	403	313	25100	1
Ishiki [47]	91	-	500	635	305	1767	1
Ishiki [47]	79.43	4.2	351	635	305	1767	1
Basic 400hp [49]	291000	-	452	967	313	17400	110
NS-03M [49]	3810	-	1401	971	313	62	161
4-275 [49]	118000	-	2600	1023	313	4×275	150
4-215 [49]	127000	-	4000	923	313	4×215	150
NS-03T [49]	4140	-	1299	991	313	190	64
GPU-3 [49]	8950	-	3600	1019	313	120	69
MELSE II [49]	3100	-	1000	858	313	302	45
MP1002CA [49]	250	-	1500	973	313	59.4	15
102C [49]	480	-	1600	1073	313	67	12
Batmaz [9]	118	11	784	953	318	190	2
Cinar [26]	128.3	-	891	1273	293	276	4
Cinar [27]	5.98	-	208	1273	303	192	1
Sripakagorn [99]	95.4	9.35	360	773	308	165	7

From table 2.1 it can be seen that there has been a large number of Stirling engine experimental efforts. During the review, it was found that the experimental data from these efforts varied considerably in quality and availability.

2.3.5 Summary

There is a wide range of different approaches to modelling real Stirling engines, some of them are more complex than others. There are many challenges faced in choosing an appropriate Stirling engine model, a very simplified model will be computationally inexpensive, but

it will not accurately represent a real machine. A highly complex model will accurately model a real machine but will be too computationally expensive to conduct a multivariate optimisation. Therefore, it is important to use a model that is complex enough to accurately predict Stirling engine performance and losses while still being simple enough, such that a multivariate optimisation is feasible. There have been a large number of experimental investigations into Stirling engine performance, and some of the gained practical knowledge can be drawn upon to limit variable ranges, thus reducing computation time.

2.4 Heat Exchangers

2.4.1 Background

Depending on the Stirling engine configuration, the heat transfer into and out of the engine either occurs through the cylinder walls or the heater and cooler. In the case of Stirling engines where the heat transfer occurs through the cylinder walls, the engine is divided into three control volumes, whereas if the engine has a heater and cooler the engine is divided into five control volumes. The typical Stirling engine has a heater and cooler and therefore has three main heat exchangers. These heat exchangers each have a different role in the operation of a Stirling engine. These three heat exchangers are the **heater**, **regenerator** and **cooler**. There are almost always auxiliary heat exchangers that are incorporated into the system to allow for the optimal operation of the Stirling engine. However, these have not been included, as this section only deals with the heat exchangers in direct contact with the cycle working fluid.

In Stirling engine design the heat exchangers are critical components as the type and sizing of these components has the most significant effect on engine performance. It is therefore imperative that careful consideration be given to the design of these heat exchangers. The flow experienced in the heat exchangers is oscillating, however oscillating flow relations are not always available, and quasi-steady flow assumptions are often made. In the modelling of the heat exchangers, the parameters of critical importance are the friction factor and heat transfer coefficient. If the relationship between the heat exchanger geometry and these parameters is known, then it is possible to optimise the heat exchanger geometry for a specified engine performance.

Figure 2.5 is a diagram of the different heat exchangers in relation to other engine components for a typical beta type engine.

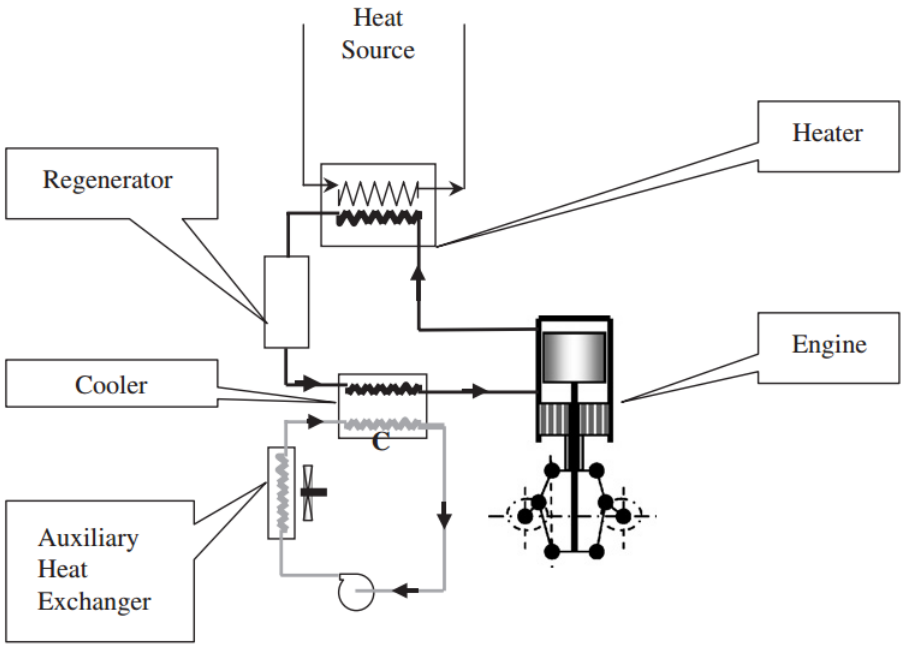

Figure 2.5: Diagram showing Stirling engine heat exchangers [109]

The modelling of flow and heat transfer in Stirling engine heat exchangers has predominantly been done using steady-state correlations [96]. The reason for this is that it has been impossible to accurately measure velocities, temperatures and pressure drop using experimental oscillating flow rigs [46]. To better understand these phenomenon complex multi-dimensional models have been developed, along with simplified oscillating flow rigs. These rigs have been used to validate the models. One of the phenomena that make the study of oscillating flow difficult is the annular effect, which is where the maximum velocity is near the pipe wall rather than the centre of the pipe, as is the case for steady-state flow [64]. The effects of thermal and hydrodynamic entrance lengths are also poorly understood, and it has been estimated that approximately 15% to 50% of the pressure loss in the Stirling engine heat exchangers occurs at the entrance and exit of the heat exchanger [109]. In the case of a tubular heater and cooler the study conducted by [64], found that the frictional coefficient for oscillating flow was lower than predicted by the unidirectional turbulent approximation of the flow.

2.4.2 Heater

The heater is the heat exchanger that enables the heat transfer between the heat source and the working fluid. The design of this heat exchanger is often highly challenging as the heat transfer coefficient on the inside and outside of the heater tubes is often significantly different, resulting in incomparable surface area requirements [109]. This problem is mostly encountered when heat transfer between combustion products and the working fluid is occurring in the heater, as the pressures and flow rates are often very different. The heater is also adversely affected by heat exchanger fouling when biofuels are used. This heat exchanger fouling degrades the engine performance by decreasing the heat transfer coefficient on the combustion products side of the heater tubes [63]. This fouling means that the heater has to be cleaned regularly to combat the degradation of heater performance. It has also been found that increasing the working fluid pressure increases the heat transfer coefficient and thus decreases the heater wall temperature [122].

Figure 2.6 is a photograph of a bundle of heater tubes, seen on the cylinder head of a Stirling engine.

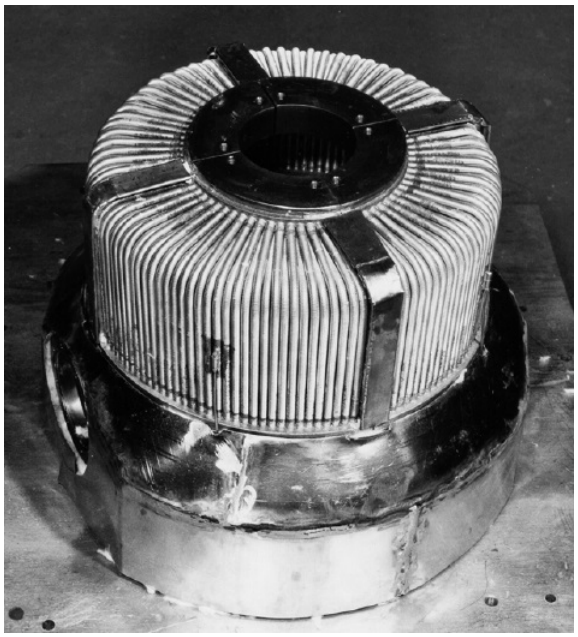

Figure 2.6: Photograph of a Stirling engine heater head showing the heater tubes [97]

2.4.3 Cooler

The cooler allows for the transfer of heat from the engine working fluid to the sink. The cooler is an important component as the working fluid temperature in the cooler has a significant effect on efficiency and therefore should be minimised as far as possible. Stirling engines are usually either air cooled or water cooled, with designers using water cooling in modern Stirling engine designs [109]. Water cooled Stirling engine coolers have coolant and working fluid heat transfer characteristics that are comparable. Therefore, the working fluid side heat transfer is a parameter that heavily influences efficiency [52].

Figure 2.7 is a photograph of cooler tubes that fit around the Stirling engine cylinder to facilitate flow between the working spaces.

Figure 2.7: Photograph of a Stirling engine cooler tube bundle [97]

2.4.4 Regenerator

The regenerator is the most important component of a Stirling engine, as it has the biggest effect on engine performance. This influence on performance is because the regenerator effectiveness significantly affects the engine efficiency, as it directly affects the heating and cooling requirement [109].

The regenerator is very simply put, a thermal sponge which absorbs and releases thermal energy to the working fluid as it moves through the engine. In the ideal cycle, the heat

transfer in the regenerator is isothermal and therefore reversible, with the one end of the regenerator being at the compression space temperature and the other at the expansion space temperature. In reality, the conditions are usually far from ideal, and to optimise the regenerator the heat capacity and heat transfer coefficient need to be maximised while the flow losses are minimised [109]. In heat exchangers, these are competing irreversibilities, and therefore the optimal geometry needs to be found for the case of minimum destruction of exergy or available work [11].

Figure 2.8 is a photograph of three different regenerator mesh types under a microscope.

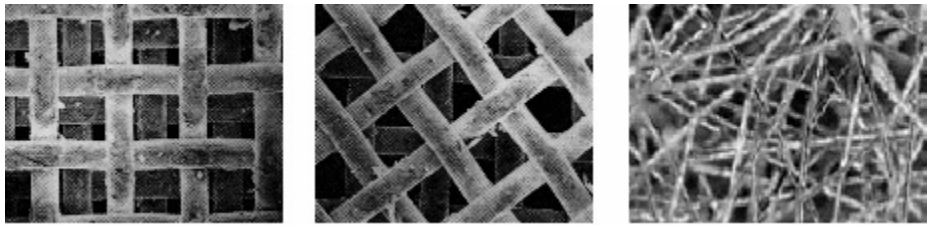

Figure 2.8: Photograph of three different regenerator meshes under a microscope [97]

When computing the regenerator effectiveness, there have been some relations that have been proposed, all requiring that the NTU be computed first.
Martini proposed equation 2.3 [40].

$$\varepsilon_r = \frac{NTU}{NTU + 2} \tag{2.3}$$

Organ proposed equation 2.4 [40].

$$\varepsilon_r = 1 - \frac{1}{NTU} \tag{2.4}$$

De Monte proposed equation 2.5 [40].

$$\varepsilon_r = \frac{NTU}{NTU + 2} + \frac{2FR}{NTU(NTU + 2)} \tag{2.5}$$

It has been found that the measured friction factor for oscillating flow through regenerator material is about 30% higher than that for unidirectional flow [104]. This study also developed flow loss and heat transfer correlations for different regenerator materials [104].

When designing the Stirling engine regenerator, it is essential to look at the pressure drop and heat transfer performance and the tradeoff between these two competing irreversibilities. The analysis presented in [33] is concerned with the losses in the regenerator most notably the thermal and dissipative losses. The losses are analysed using the ratio of Stanton number (St) to Fanning friction factor (f_F), and the outcome can be seen as figure 2.9.

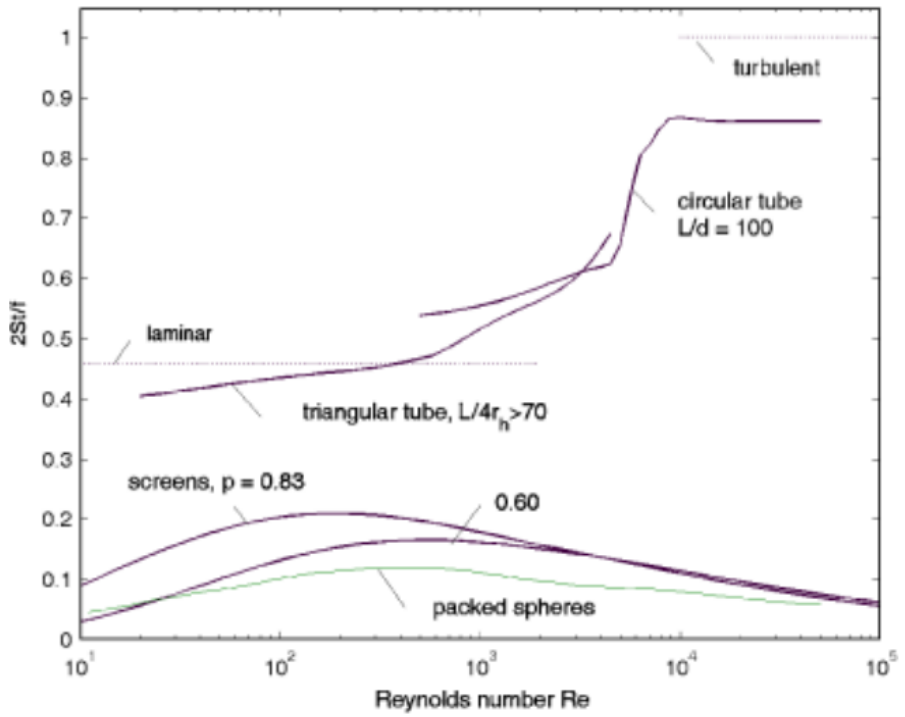

Figure 2.9: Ratio of thermal to dissipative loss ($2St/f_F$) versus Reynolds number (Re) for different regenerator materials and configurations [33]

Figure 2.9 shows that variation in loss ratio varies only slightly with Reynolds number for the wire mesh and packed spheres when compared to the tubes. It is also quite simple to see that the meshes and packed spheres have pressure dominant losses whereas the losses in the pipes are heat transfer dominant losses.

Some studies have been conducted that look at losses in the regenerator and the effect that these losses have on engine performance. The study conducted in [3] found that the temperature within the regenerator oscillates in two different modes. The first mode is the oscillation of the regenerator matrix temperature profile and the second mode is the oscillation of the matrix temperatures at the ends of the regenerator, thus "bending" the approximately linear temperature profile. This first mode of oscillation is caused by the

direction of fluid flow in the regenerator and was seen to slightly increase the efficiency of the engine while reducing the power output. The second mode is caused by the large temperature difference between the fluid entering the regenerator and the matrix temperature and was seen to reduce efficiency and power output of the engine. The analysis presented in [32] is a first order model that accounts for the pressure drop across the regenerator. The study showed that for optimised non-dimensional power output the maximum attainable efficiency is half of the Carnot efficiency and that the efficiency of the engine is independent of regenerator conductance.

The Constructal law has been applied to the design of regenerators to optimise the geometry for maximum heat transfer and minimum pressure drop [12]. This Constructal law approach to regenerator design can be used to reduce the effects of the second mode of temperature oscillation discussed in [3], as there has been research into using wrinkled ducts in the entrance length to maximise heat transfer [13]. This same principle could also be used to reduce the temperature oscillations in the regenerator increasing engine performance.

2.4.5 Heat Exchanger Dead-Volume

The heater, cooler and regenerator have void volumes through which the working fluid flows. These heat exchanger void volumes along with the clearance volumes make up the dead-volume in real Stirling engines, the dead-volume is also sometimes referred to as the unswept volume. It is thought that dead-volume decreases engine performance and therefore should be minimised as far as possible while still allowing enough void volume for adequate heat transfer. In most idealised theoretical analyses this dead-volume is assumed to be zero.

There have been a few studies that have analysed the effects of dead-volume on engine performance. The study conducted by [57], used a first order isothermal model and found that dead-volume negatively affects engine performance by decreasing specific work output and efficiency. Other studies have all come to similar conclusions, with the study conducted by [81] and similarly by [44], concluding that dead-volume in the regenerator while necessary to allow for adequate heat transfer, negatively affects engine performance. The study conducted by [78] stated that the dead-volume decreased the engine performance and should, therefore, be zero. The second order dynamic model that was introduced in [110] was used to calculate the optimal characteristics of an MTD solar Stirling engine. The study also analysed the effect of increasing dead-volume, concluding that it decreased power output.

Senft conducted a study using the classical Schmidt analysis with mechanical losses included and found that there is an optimal swept volume ratio. Additionally, it was found that increasing the dead-volume degrades performance [94]. The analysis conducted by de Boer showed that the efficiency limit of a Stirling engine is half of Carnot efficiency and that the efficiency is also independent of regenerator conductance, in the analysis the ideal case of a regenerator with zero dead-volume and perfect regeneration was assumed [32]. The analysis presented in [37], assumed polytropic processes for the compression and expansion spaces to more accurately model the regenerator. The maximum efficiency and maximum power density points were found along with the optimal compression ratio. The analysis presented in [36], optimised the irreversible Stirling cycle using the maximum power density technique and it was suggested that using this technique yields smaller sized engines with high efficiencies. The optimisation presented was a multivariate optimisation that gave the maximum power density for different engine specifications.

There have been some studies that have investigated the effects of dead-volume on engine performance. However, almost all of these studies have used highly idealised models or have not meticulously explored the effects of dead-volume on engine performance.

2.4.6 Summary

One of the main areas of Constructal research is its application to heat exchangers and the 'morphing' of the configuration to fit the body of the flow, thus giving optimal flow conditions [14]. This application of Constructal theory gives a better heat exchanger architecture for maximum heat transfer and minimum flow loss. The application of Constructal tree shape heat exchangers in Stirling engines is an area of research that has been given little attention and shows promise for the future. The regenerator is such an integral part of the Stirling engine, and therefore this is an area where research is required, as significant increases in Stirling engine regenerator performance could drastically increase engine performance.

When increasing the size of Stirling engine heat exchangers, their efficiency increases, however, the power density of the engine often decreases which is a direct result of the increase in the dead-volume ratio. From the literature, it can be seen that there has been limited detailed analysis into the effects of dead-volume on engine performance. These effects need to be analysed using more complex models so that the nature of dead-volume can be more accurately understood, which will result in the design of more efficient engines.

2.5 Solar Thermal Power

2.5.1 Background

The interest and research into solar thermal energy has seen a significant increase in recent years, as it is an attractive alternative source of energy. The idea of using a solar concentrator, thus using the power of the sun is not a new idea and the first recorded use of this technology was by Archimedes in 212 BC. Two millennia later the solar-powered steam engine was pioneered by August Monchot, who built several examples [51].

In the last 50 years, there have been big advances in utilising collectors that focus the sun's rays to heat a fluid. In solar collectors the temperatures range from 100 °C to 1500 °C. As seen in the literature, this is the only area of solar thermal power where Stirling engines have seen widespread adoption. The reasons for this is that they offer high efficiency and good reliability. There have been many efforts by different organisations to develop the technology [100].

Figure 2.10 is a photograph of a dish Stirling system that was developed by Boeing.

Figure 2.10: Photograph of the solar Stirling converter developed by Boeing [72]

Concentrating collectors concentrate the solar irradiance by a factor termed the concentration ratio. This concentration ratio is the ratio of concentrator aperture area to absorber area

and the factor by which the radiation flux is increased when it reaches the surface of the absorber. Solar concentrators can have varying concentration ratios, as the concentration ratio increases the temperature at which energy is supplied at increases. However, there is an optimal design point as the thermal receiver losses also increase with increasing absorber temperature.

Figure 2.11 is a plot of concentration ratio versus temperature showing the optimal concentration ratio ranges for different power cycles.

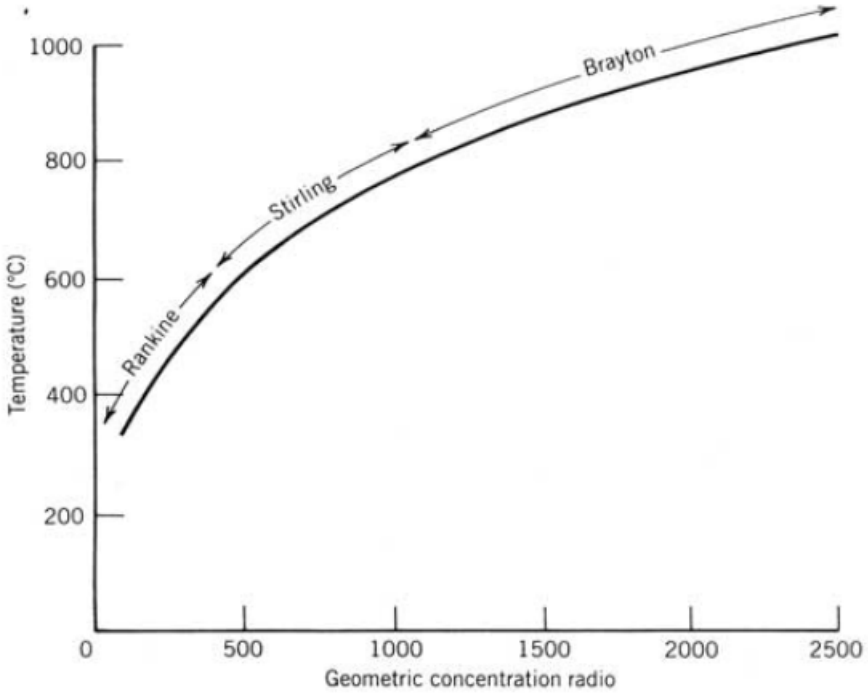

Figure 2.11: Graph showing heat engines used for different concentration ratios [101]

Figure 2.11 shows that the Stirling cycle is the optimal cycle to use when the concentration ratio is in the range of 500 - 1000.

Stirling engines have historically always been used as converters with parabolic dish collectors, for distributed power generation. There have been a number of studies done that optimised a dish Brayton cycle for use in South Africa [88, 67, 86, 87, 85, 89, 66]. South Africa has areas that are extremely suitable for solar thermal systems, and it is estimated that the daily solar irradiance is 7 $kW.h.m^2$ [39]. This solar irradiance makes South Africa a prime location for the application of solar energy technologies, as the direct nominal irra-

diance(DNI) is far higher than in other parts of the world.

2.5.2 Solar Stirling Engine Analysis

There have been many studies that have analysed and optimised solar thermal Stirling engines, using several different techniques and methodologies. This section presents some of these studies and briefly summarises what was analysed and the outcome of each study.

In [111], the optimisation of a mean temperature difference solar Stirling engine was investigated. The critical engine parameters were initially optimised using a dynamic model, with pressure drops and heat losses included. Once this optimisation was complete, the swept volume was optimised for a given operating speed, temperature difference and dead-volume.

In [29], the effects of pressure losses and irreversible heat transfer on the solar Stirling cycle were analysed. The model took into account external and internal irreversibilities, and the results indicated that the maximum attainable efficiency of an engine with optimised parameters is approximately half of Carnot efficiency.

The analysis presented in [2] gave a model that optimised the thermal efficiency and output power of a solar Stirling engine through the use of an evolutionary algorithm. The variables in the optimisation were the source temperature, sink temperature and absorber temperature.

The analysis conducted by [62], utilised a genetic algorithm along with a novel second-order model to find the optimal design parameters for an LTD solar Stirling engine. The paper presented a new dynamic second order LTD model, the optimisation results from the model were validated using a 3D CFD model, and the optimisation results gave noticeable improvements in performance over the experimental results presented in [58].

The analysis conducted by [123], applied the method of finite time thermodynamics to maximise power and thus efficiency of a solar-powered dish Stirling engine. The outcome of the study was that the absorber temperature, concentration ratio of the collector and regenerator effectiveness were all fundamental characteristics that have a significant effect on the maximum power output. The analysis provides a set of technical guidelines for the design of collectors and Stirling engines, the optimal absorber temperature was found to be 1100 K, and the optimal concentration ratio was found to be 1300.

The study presented in [21] gave a model of a solar Stirling engine, the model was a combined

model involving the Stirling engine and the solar collector and was used to determine the maximum efficiency and operating temperature for the system. For the collector, a linearised heat loss model was used, and the Stirling engine was modelled as an irreversible cycle. The irreversibilities incorporated into the model were regenerative losses and heat conduction losses.

2.5.3 Summary

The literature shows that the dish solar Stirling engine has been exhaustively researched, as it is an area where Stirling engines are seen to be promising. However, research is still required in this field, as more recently the Stirling engine has been suggested as a converter for low grade solar thermal energy [59, 56]. This area of research holds promise as these engines are speculated to be significantly cheaper to manufacture and operate than dish Stirling systems. If this technology is implemented at low cost, it could make the Stirling engine competitive with photovoltaic systems.

2.6 Second Law Analysis

2.6.1 Background

The second law of thermodynamics is elegantly explained in [80], "the first law defines changes in state in that only changes where energy is conserved are realisable. However, this includes many potential changes that do not occur in practice. At this point, the second law becomes relevant as it defines which processes can occur in practice." The second law was initially formulated as a statement, and in the engineering context, the most reasonable statement is the Kelvin-Planck statement which, is appropriate to heat engines. The statement reads:

"It is impossible to devise an engine which, working in a cycle, shall produce no effect other than the extraction of heat from a reservoir and the performance of an equivalent amount of work."

Historically the implications of the second law of thermodynamics were first discovered by Sadi Carnot who proved that no thermodynamic cycle could achieve a higher thermal efficiency than the theoretical Carnot engine. This result although not recognised as significant

at the time and virtually ignored, subsequently had a massive impact on physics and engineering [11]. More than a century after this profound discovery, the fields of finite time thermodynamics (FTT) as it is known in physics and entropy generation minimization (EGM) as it is known in engineering began. These methods of thermodynamic optimisation first appeared in the 1970's as stand-alone fields, and there was substantial growth in the 1980's and 1990's due to other global factors [10].

One of the first finite time thermodynamics applications was the application of the technique to the ideal Carnot engine. After applying the principles and finding the point of maximum power a different efficiency limit was found [75, 20, 30]. This maximum achievable efficiency at maximum power conditions, which first appeared in nuclear engineering literature, can be seen as equation 2.6 and is known as the Curzon-Ahlborn efficiency.

$$\eta = 1 - (T_K/T_H)^{1/2} \tag{2.6}$$

Equation 2.6 is a performance limit for finite-sized heat engines where finite duration thermodynamic processes occur, whereas the ideal Carnot efficiency is based on heavily idealised processes.

The effects that result in irreversibility are heat transfer through a finite temperature difference, friction, unrestrained expansion, spontaneous chemical reaction, mixing of fluids at different states, flow of electric current through a resistance, magnetic hysteresis and inelastic deformation [11]. However, in thermodynamic analysis, all these irreversibilities can be regarded as secondary to the irreversibilities due to combustion and heat transfer. The importance of studying thermodynamics processes in finite time is so that the limits of the processes can be fully understood. The most straightforward analyses show how different sources of irreversibility effect and limit real thermodynamic processes [90].

2.6.2 Entropy

Entropy was first defined and named by Rudolph Clausius in 1865. However, it was discovered earlier by Rankine who named it Thermodynamic Function [11]. The equation defined by Clausius can be seen as equation 2.7.

$$dS = \frac{\delta Q_{rev}}{T} \tag{2.7}$$

As defined in [11], the entropy balance for an open system is equation 2.8 [11].

$$\dot{S}_{gen} = \frac{dS}{dt} - \sum_{i} \frac{\dot{Q}_i}{T_i} + \sum_{out} \dot{m}s - \sum_{in} \dot{m}s \geq 0 \tag{2.8}$$

The direction of the inequality is very important in this equation, as the second law of thermodynamics states that the transfer of entropy never exceeds the entropy change of a system. Therefore the rate of entropy generation is always positive.

Simplifying equation 2.8, the equation for the entropy change of a substance can be seen as equation 2.9

$$s_2 - s_1 = \int_1^2 \frac{\delta Q}{T} + s_{gen} \tag{2.9}$$

Assuming constant specific heats and integrating the equation yields equation 2.10, which can be used to calculate the entropy change of an ideal gas.

$$s_2 - s_1 = C_P \ln\left(\frac{T_2}{T_1}\right) - R \ln\left(\frac{P_2}{P_1}\right) \tag{2.10}$$

From equation 2.10, it can be seen that change in entropy is only due to the transfer of heat and not the transfer of work. It is also crucial to note that when using the equation, the entropy generation (S_{gen}) is not the same as ($S_2 - S_1$) which is the change in the property entropy.

2.6.3 Exergy

Exergy is defined as the maximum amount of energy that is available to do work [11], and it is also known as the quality of the energy or the availability. In the realm of thermodynamic optimisation, it is an important variable that should be maximised to maximise power output within specified design constraints.

As discussed in [90], the choice of constraints is critical as they can limit or extend the processes that can be chosen to optimise the thermodynamic system. In choosing the constraints, there are often two extremes the maximum power case, and the maximum efficiency or minimum entropy generation case. These extremes can be thought of in the operation of a heat engine that converts the energy at a certain cost to power at a certain price, in optimising the profit there exists a range of operating conditions that exist between maximum

power generation and minimum rate of entropy generation. With the optimal solution to the problem depending on the respective prices of fuel and power.

Applying the first and second law for an open system, equation 2.11 is derived, which describes the exergy of an open system [11].

$$\dot{W} = -\frac{d}{dt}(E + P_0V - T_0S) + \sum_{i=1}^{n}\left(1 - \frac{T_0}{T_i}\right)\dot{Q}_i + \sum_{out}\dot{m}(h^0 - T_0S) - \sum_{in}\dot{m}(h^0 - T_0S) - T_0\dot{S}_{gen} \tag{2.11}$$

Where the methalpy (h^0) is the shorthand for the generalised enthalpy group, seen below:

$$h^0 = h + v^2/2 + gz$$

Utilising equation 2.11 it can be seen that the rate of destruction of available work for an open system is only dependant on the rate of entropy generation. This statement is expressed mathematically as equation 2.12.

$$\dot{W}_{lost} = T_0\dot{S}_{gen} \tag{2.12}$$

This result is known as the Guoy-Stodola theorem and defines what is known as the "lost available work". This equation when interpreted means that whenever a system is operating irreversibly, the rate at which exergy is destroyed is proportional to the rate at which entropy is generated [11]. It is from this result that the field of entropy generation minimization (EGM) was developed [10].

2.6.4 Entropy Generation Minimization

According to [10], the first area to which EGM methodology was applied was in the field of solar thermal power generation. The first study being conducted in 1957, where an engine driven by solar heating was optimised.

Entropy Generation Minimization (EGM) or Finite Time Thermodynamics (FTT) draw on three previously distinctly separate fields, namely pure thermodynamics, heat and mass transfer, and fluid mechanics, it also bridges the gap between physics and engineering [22]. Utilising aspects of each field the EGM methodology can be used to show that when finite size or finite time constraints are imposed on a system optima exist that result in minimum rate of entropy generation. This minimum rate of entropy generation is of significance as it results in the minimum rate of work destruction due to thermodynamic irreversibility.

When optimising the global performance of a system, it is essential to spread the entropy generation rate across components. In doing so, the entire system is optimised giving the best performance of the system and not of the individual components. This concept is significant as individually optimised components do not necessarily result in an optimal system. EGM may be used in the initial stages of design to identify the existence of optima and to analyse the trends that changing different parameters have on the system [76]. Following this, these optima can be further refined through global cost analysis and optimisation.

There are many different areas to which optimisation through EGM can be applied. Some of these areas are listed below:

- External flow
- Internal flow
- Heat exchangers

2.6.5 The Second Law Applied to Heat Exchangers

Heat exchangers when incorporated into a system are usually responsible for a great deal, if not the majority of the irreversibility present in the system. Therefore, heat exchangers should be optimised for minimum rate of entropy generation so that they destroy the minimum amount of exergy while still fulfilling their engineering design purpose. In a heat exchanger that consists of two streams, the rate of entropy generation is the sum of the rates of entropy generation on each side of the heat transfer surface of the heat exchanger.

In heat exchanger design there are two mechanisms through which irreversibilities occur, namely heat transfer through a finite temperature difference and flow friction. In heat exchangers these irreversibilities compete with one another, therefore to optimise the heat exchanger the most desirable trade-off between these competing irreversibilities needs to be found. In doing so, the maximum entropy generation rate paradox also needs to be considered, as it is known that when $\varepsilon = 1$ or $\varepsilon = 0$ the rate of entropy generation may be zero. However, these are not feasible design points.

There have been many second law optimisations of heat exchangers seen in the literature. The analysis by [76] applied the EGM methodology to a parallel plate counterflow heat exchanger. The geometry of the heat exchanger was optimised to give minimum entropy

generation number. The analysis conducted constrained the mass and volume of the heat exchanger as the heat exchanger was optimised for use in an aircraft. The analysis by [117] optimised a finned cross-flow heat exchanger for application in an aircraft's environmental control system. The optimisation used the EGM methodology to optimise the geometry of the heat exchanger, and it was shown that using smooth surface models in initial analysis is justified from a simplicity standpoint as the models can be refined later to include more complicated geometries.

The analysis conducted by [82], presented the thermodynamic optimisation of a cross-flow plate-fin heat exchanger using a particle swarm optimisation algorithm. A similar optimisation is carried out in [73], however, this optimisation used a genetic algorithm. The analysis also looked into the effects that changing parameters had on entropy generation number.

2.7 Conclusion

From the literature review, five main conclusions can be drawn. These conclusions point to areas where research effort is needed and explain why it is needed. These conclusions can be seen in the list below:

1. The renewable energy industry is rapidly growing, and the Stirling engine stands to play a vital role. The engine is well suited for use with solar thermal, biofuels and even geothermal heat sources. So that high-performance, low-cost Stirling engines can be developed, there needs to be an effort to understand better and model the Stirling cycle. This research effort needs to be undertaken so that engines can efficiently and reliably be analysed, optimised and designed.

2. The use of Multidimensional models to analyse and optimise Stirling engines is a relatively new area of Stirling engine research. There is vast scope to conduct CFD analyses of different Stirling engines and use these models to develop better heat transfer and flow friction relations and gain understanding of the different loss mechanisms. There is also scope to develop ways of reducing computation time while maintaining a high degree of accuracy.

3. The choice of heat exchanger volume on the Stirling cycle has a significant effect on engine performance that has not been studied in detail. It is stated in literature that the effect of dead-volume on Stirling engine performance is detrimental and that it should

be minimised as far as possible. The investigation into the effects and potential for cycle optimisation in terms of dead-volume is lacking. This physical design parameter needs to be studied in-detail as dead-volume is unavoidable in real engines. This goes hand-in-hand with the exergy analysis or entropy generation minimization methodology as a fixed volume or area criteria is required when optimising heat exchangers.

4. It is evident in the literature that there has been limited exergy analysis of Stirling engines. There has also not been any multivariate optimisation of Stirling engines using exergy analysis methodology, especially when using dynamic Stirling engine models that include pressure drop irreversibility. This methodology has been used with success in other areas of thermal design and optimisation and should, therefore, be used in Stirling engine optimisation.

5. Most literature referred to the optimisation of components rather than the optimisation of the entire system. This is notable in the case of the regenerator geometry which many studies have analysed. It has been mentioned by [10], that optimising specific components does not always result in an optimised system. Therefore, studies need to be done that optimise the regenerator while also optimising other engine components to give a truly optimised system.

Chapter 3

Mathematical Modelling

3.1 Introduction

The following chapter introduces the mathematical modelling of the Stirling cycle. In the literature, many different Stirling cycle models have been used, and the choice of model and approach is an important decision. The exergy analysis approach to modelling of power cycles has been applied successfully to many different cycles and idealised Stirling engine mathematical models. However, this approach has not been applied to more complex Stirling engine numerical models and is presented in this chapter. The ideal adiabatic model presented is used in chapter 5, and the model with losses and exergy analysis (EA) methodology applied is used in chapters 6 and 7. After researching the different models available in the literature the ideal adiabatic model was chosen. This decision was based on the following criteria:

- The accuracy of the model to capture the thermodynamic processes occurring in the Stirling cycle.
- The complexity of the model and how computationally expensive it is.

Using these criteria, two models were looked at; they were the ideal isothermal and ideal adiabatic models. The ideal isothermal model is the simpler of the two models, as in this model an analytical solution exists. For the ideal adiabatic model this is not the case and iterative methods need to be used to solve the set of equations, which is defined as convergence between the start and end temperatures in the expansion and compression spaces, making the ideal adiabatic model far more complicated than the ideal isothermal model. However, it has been noted that the ideal adiabatic model is a far more accurate

representation of the Stirling cycle, as in reality, no heat transfer occurs through the cylinder walls, and the expansion and compression spaces are adiabatic rather than isothermal [116] [115]. For these reasons, the ideal adiabatic model has been chosen over the ideal isothermal model.

This chapter starts by presenting and explaining the different Stirling engine configurations and the equations that describe the volume variations and heat exchanger geometry. Following this, the ideal adiabatic model is presented and explained. Next, the heat transfer and flow friction relations used to link the physical system to the thermodynamic equations, and used to describe the flow and heat transfer in the different heat exchangers is presented and explained. Followed by the presentation and explanation of the second law and exergy analysis equations.

3.2 Stirling Engine Configurations

There are a variety of different Stirling engine configurations that are available to a Stirling engine designer. The three couplings, namely the alpha, beta and gamma couplings with slider crank mechanism are considered in this section. In all Stirling engine configurations there is a phase difference between the compression and expansion space volumes, which has been shown to be 90° for optimal thermodynamic performance. This phase difference between the spaces is not always achievable and is dependent on the configuration and linkage type. Figure 3.1 is a diagram that shows the phase difference between the volumes [115].

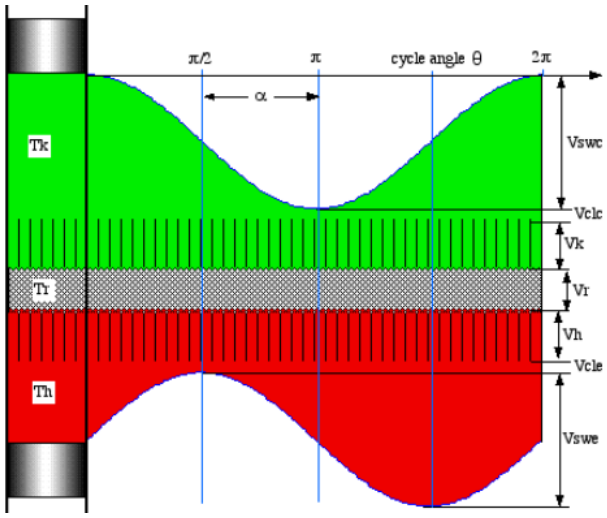

Figure 3.1: Diagram showing phase difference (α) between the working space volumes [115]

3.2.1 Alpha Type

Alpha type engines typically have two pistons that are each in a separated cylinder connected by the cooler, regenerator and heater. This configuration suffers from the disadvantage of requiring sealing of both engine compartments. However, the configuration can be compounded which allows for a high specific power output [109].

Figure 3.2 shows a diagram of the compression and expansion spaces in the alpha type configuration and is used to show the formulation of the equations for volume variation in these spaces.

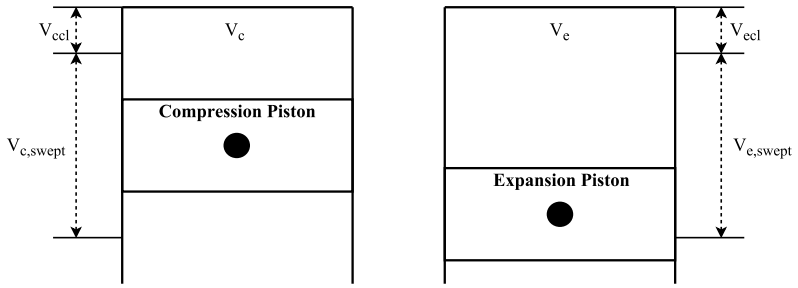

Figure 3.2: Alpha type Stirling engine expansion and compression space diagram

Equation 3.1 is an expression for the volume in the compression space in terms of crank angle. Equation 3.2 is an expression for the volume in the expansion space in terms of crank angle and the phase difference between volumes.

$$V_c = V_{ccl} + \frac{V_{c,swept}}{2}\Big(1 + cos(\theta)\Big) \tag{3.1}$$

$$V_e = V_{ecl} + \frac{V_{e,swept}}{2}\Big(1 + cos(\theta + \alpha)\Big) \tag{3.2}$$

Equation 3.3 and 3.4 are the derivatives with respect to crank angle of equations 3.1 and 3.2 respectively.

$$\frac{dV_c}{d\theta} = -\frac{V_{c,swept}}{2} sin(\theta) \tag{3.3}$$

$$\frac{dV_e}{d\theta} = -\frac{V_{e,swept}}{2} sin(\theta + \alpha) \tag{3.4}$$

3.2.2 Beta Type

The beta configuration has a piston, and a displacer in the same cylinder which is an advantage as only one cylinder seal is required. The sealing is also on the cold side of the engine which means expensive high-temperature seals are not required. The compression space is located between the displacer and piston. The expansion space is located above the displacer, and these spaces are connected serially by the cooler, regenerator and heater.

Figure 3.3 shows a diagram of the compression and expansion spaces in the beta type configuration and is used to show the formulation of the equations for volume variation in these spaces.

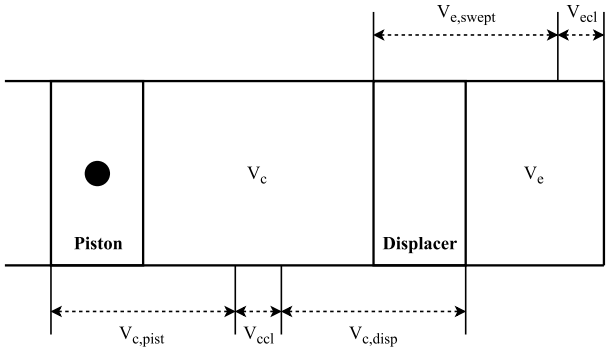

Figure 3.3: Beta type Stirling engine expansion and compression space diagram

Equation 3.5 is an expression for the volume in the compression space in terms of crank angle. Equation 3.6 is an expression for the volume in the expansion space in terms of crank angle.

$$V_c = V_{ccl} + \frac{V_{c,disp}}{2}\Big(1 - \cos(\theta + \alpha)\Big) + \frac{V_{c,pist}}{2}\Big(1 + \cos(\theta)\Big) \tag{3.5}$$

$$V_e = V_{ecl} + \frac{V_{e,swept}}{2}\Big(1 + \cos(\theta + \alpha)\Big) \tag{3.6}$$

Equation 3.7 and 3.8 are the derivatives with respect to crank angle of equations 3.5 and 3.6 respectively.

$$\frac{dV_c}{d\theta} = \frac{V_{c,disp}}{2}\sin(\theta + \alpha) - \frac{V_{c,pist}}{2}\sin(\theta) \tag{3.7}$$

$$\frac{dV_e}{d\theta} = -\frac{V_{e,swept}}{2}\sin(\theta + \alpha) \tag{3.8}$$

3.2.3 Gamma Type

The gamma configuration is similar to the beta configuration in the fact that the configuration consists of a displacer and piston. However, each is in a separate cylinder. The compression space is located in the piston cylinder and the bottom half of the displacer cylinder, and the expansion space is located at the top of the displacer cylinder. In the same way as the beta configuration the compression and expansion spaces are connected serially by the cooler, regenerator and heater.

Figure 3.4 below shows a diagram of the compression and expansion spaces in the gamma type configuration and is used to show the formulation of the equations for volume variation in the working spaces.

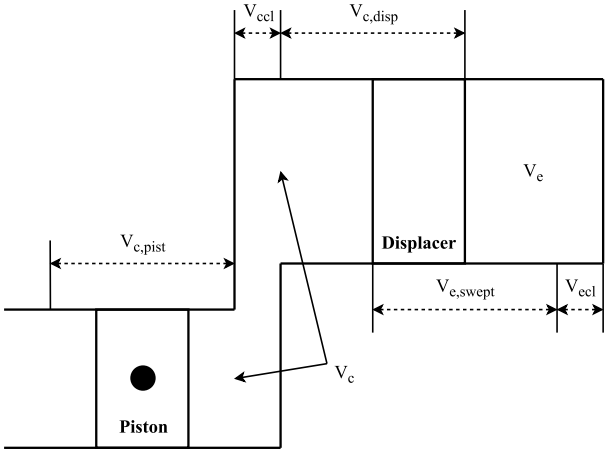

Figure 3.4: Gamma type Stirling engine expansion and compression space diagram

Equation 3.9 is an expression for the volume in the compression space in terms of crank angle. Equation 3.10 is an expression for the volume in the expansion space in terms of crank angle.

$$V_c = V_{ccl} + \frac{V_{c,disp}}{2}\Big(1 - \cos(\theta + \alpha)\Big) + \frac{V_{c,pist}}{2}\Big(1 + \cos(\theta)\Big) \tag{3.9}$$

$$V_e = V_{ecl} + \frac{V_{e,swept}}{2}\Big(1 + \cos(\theta + \alpha)\Big) \tag{3.10}$$

Equation 3.11 and 3.12 are the derivatives with respect to crank angle of equations 3.9 and 3.10 respectively.

$$\frac{dV_c}{d\theta} = \frac{V_{c,disp}}{2}\sin(\theta + \alpha) - \frac{V_{c,pist}}{2}\sin(\theta) \tag{3.11}$$

$$\frac{dV_e}{d\theta} = -\frac{V_{e,swept}}{2}\sin(\theta + \alpha) \tag{3.12}$$

3.2.4 Heat Exchanger Geometry

In the Stirling engine model the geometry of the heat exchangers is specified, and from these variables, the volumes and areas need to be calculated. The equations outlined below are used to calculate the volume and surface area in the heater, cooler and regenerator.
Defining the volume and surface area of the heater in terms of the number of tubes, tube length and tube diameter, yields equations 3.13 and 3.14.

$$V_h = \frac{N_h L_h \pi D_h^2}{4} \tag{3.13}$$

$$A_h = N_h L_h \pi D_h \tag{3.14}$$

Defining the volume and surface area of the cooler in terms of the number of tubes, tube length and tube diameter, yields equations 3.15 and 3.16.

$$V_k = \frac{N_k L_k \pi D_k^2}{4} \tag{3.15}$$

$$A_k = N_k L_k \pi D_k \tag{3.16}$$

The regenerator is more complex that the heater and the cooler, and the hydraulic diameter needs to be defined before the volume and surface area are defined. The hydraulic diameter is defined as equation 3.17.

$$d_{hyd} = \frac{4\phi d_{mesh}}{\epsilon(1-\phi)} \tag{3.17}$$

Therefore, defining the regenerator void volume and surface area, yields equation 3.18 and 3.19.

$$V_r = \phi \frac{\pi L_r D_r^2}{4} \tag{3.18}$$

$$A_r = \frac{4\phi V_r}{d_{hyd}} \tag{3.19}$$

These equations for heat exchanger area and volume along with the equations for volume variation in the expansion and compression spaces are required as inputs to the ideal adiabatic model.

3.3 The Ideal Adiabatic Model

The ideal adiabatic model was developed by Urieli and Berchowitz in the 1980's as a means of modelling real Stirling engines [116, 115]. The model was developed, as the ideal isothermal model was deemed inadequate for predicting the performance of real machines. In the ideal isothermal model all the heat transfer occurs through the cylinder walls, this makes the heat exchangers unnecessary which in reality is not the case. Hence, the ideal adiabatic model assumes the working spaces are adiabatic, and all the heat transfer occurs in the heat exchangers. This model is seen to more accurately model heat transfer and mass flow in real Stirling engines.

The ideal adiabatic model is based on the following assumptions.

1. The pressure throughout the engine is constant.
2. The compression and expansion processes are adiabatic.
3. The regeneration process is perfect ($\varepsilon_r = 1$).
4. There is negligible gas leakage from the engine.
5. The working fluid in the engine is an ideal gas.
6. The heat exchangers and regenerator are perfectly insulated.
7. The engine operates under steady state conditions.
8. The working fluid in the heater and cooler is isothermal.

The five serially connected component approach is used to model the ideal adiabatic Stirling engine. These five components are the compression space, cooler, regenerator, heater, and expansion space.

The layout of the compartments along with the symbols denoting the different thermodynamic properties in the compartments and the temperature plot showing the temperature of working fluid in each compartment can be seen as figure 3.5.

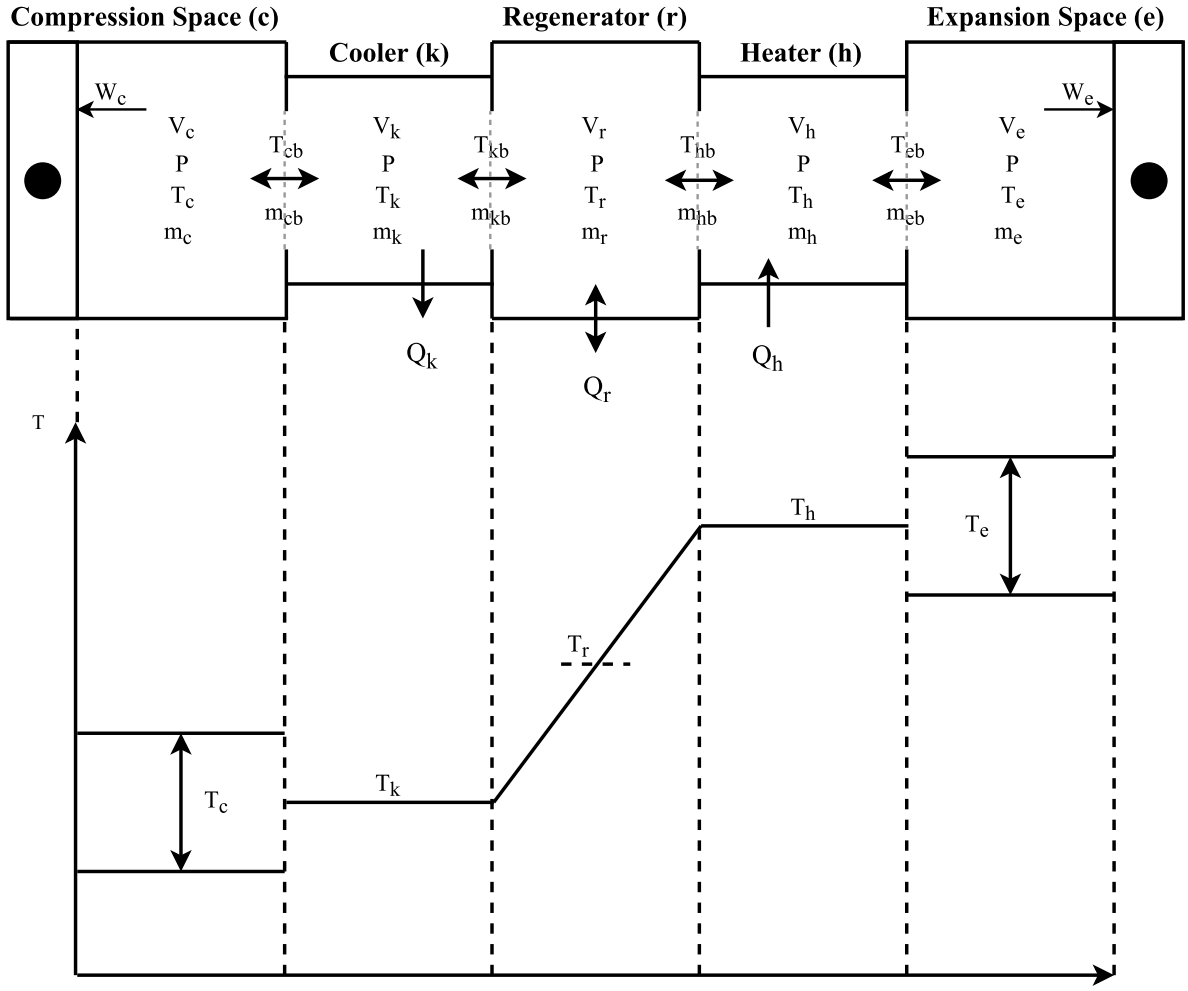

Figure 3.5: Component and temperature diagram for the ideal adiabatic model [116]

3.3.1 Regenerator Temperature

The mean effective temperature of the gas in the regenerator is assumed to be the log mean temperature of the entrance and exit temperatures of the regenerator [91, 116], seen as equation 3.20.

$$T_r = \frac{T_h - T_k}{ln(T_h/T_k)} \tag{3.20}$$

3.3.2 Mass of Working Fluid

To calculate the total mass of working fluid the isothermal model is used, as is suggested in [116, 115]. To do this the mean engine pressure and volume of the different components are specified, and from this, the mass of working fluid in the engine is calculated. The equations and derivation of the equations for computing the mass of working fluid in the alpha and beta/gamma configurations can be seen in Appendices A1 and A2 respectively.

To calculate the mass of working fluid in each engine component the ideal gas law is used. Equation 3.21 is the mass in the compression space, equation 3.22 is the mass in the cooler, equation 3.23 is the mass in the regenerator, equation 3.24 is the mass in the heater and equation 3.25 is the mass in the expansion space.

$$m_c = \frac{PV_c}{RT_c} \tag{3.21}$$

$$m_k = \frac{PV_k}{RT_k} \tag{3.22}$$

$$m_r = \frac{PV_r}{RT_r} \tag{3.23}$$

$$m_h = \frac{PV_h}{RT_h} \tag{3.24}$$

$$m_e = \frac{PV_e}{RT_e} \tag{3.25}$$

Similarly, using the derivative of the ideal gas law, the mass differential in each component is calculated. In the case of the heater, cooler and regenerator the volume differential and temperature differential are zero. Equation 3.26 is the mass differential in the compression space, equation 3.27 is the mass differential in the cooler and equation 3.28 is the mass differential in the regenerator.

$$dm_k = m_k \frac{dP}{P} \tag{3.26}$$

$$dm_r = m_r \frac{dP}{P} \tag{3.27}$$

$$dm_h = m_h \frac{dP}{P} \tag{3.28}$$

In the case of the compression and expansion spaces this assumption can't be made and the derivation begins by looking at a generalised cell of working space, seen as figure 3.6.

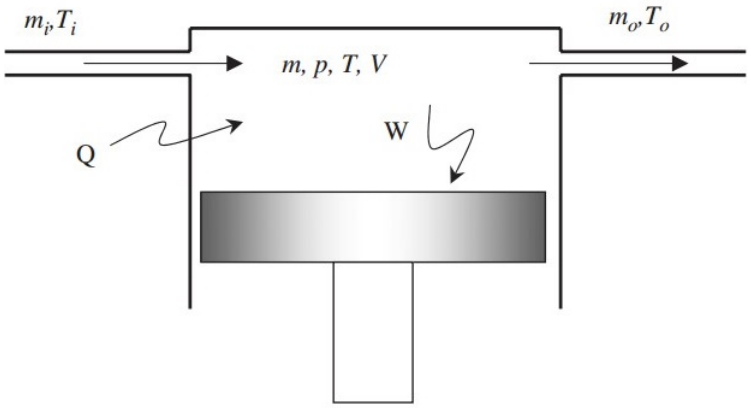

Figure 3.6: Generalised cell of working space [109]

The mathematical form of the first law is applied to the cell, yielding equation 3.29.

$$C_v d(mT) = dQ - dW + C_p(\dot{m}_{in}T_{in} - \dot{m}_{out}T_{out}) \tag{3.29}$$

Looking at the expansion space, equation 3.29 simplifies to equation 3.30 because there is only one flow boundary, and no heat transfer through the cylinder walls as per the adiabatic assumption.

$$C_v d(m_e T_e) = -dW_e + C_p \dot{m}_{eb} T_{eb} \tag{3.30}$$

Therefore, as the mass flux is directly related to the mass differential equation 3.31 is obtained.

$$\frac{C_v}{R}(PdV_e + V_e dP) + dWe = C_p T_{eb} dm_e \tag{3.31}$$

After rearranging the expression, equation 3.32 which describes the mass differential in the expansion space is obtained.

$$dm_e = \frac{1}{RT_{eb}}\left(PdV_e + \frac{1}{\gamma}V_e dP\right) \tag{3.32}$$

Similarly equation 3.33, defines the mass differential in the compression space.

$$dm_c = \frac{1}{RT_{cb}}\left(PdV_c + \frac{1}{\gamma}V_c dP\right) \tag{3.33}$$

3.3.3 Pressure

The ideal adiabatic model assumes a constant pressure throughout the device. Therefore, the pressure and temperature can be defined using the instantaneous volume and temperature in each compartment, seen as equation 3.34.

$$P = mR/\Big(\frac{V_c}{T_c} + \frac{V_k}{T_k} + \frac{V_r}{T_r} + \frac{V_h}{T_h} + \frac{V_e}{T_e}\Big) \tag{3.34}$$

Summing the mass in all the components to give the total mass of working fluid, yields equation 3.35.

$$m = m_c + m_k + m_r + m_h + m_e \tag{3.35}$$

Taking the derivative of equation 3.35, we obtain equation 3.36. This expression must be equal to zero due to the no working fluid leakage assumption.

$$dm = 0 = dm_c + dm_k + dm_r + dm_h + dm_e \tag{3.36}$$

Substituting equations 3.26, 3.27, 3.28, 3.32 & 3.33 into equation 3.36 we obtain equation 3.37.

$$\frac{1}{RT_{cb}}\Big(PdV_c + \frac{1}{\gamma}V_c dP\Big) + \frac{1}{RT_{eb}}\Big(PdV_e + \frac{1}{\gamma}V_e dP\Big) + \frac{dP}{R}\Big(\frac{V_k}{T_k} + \frac{V_r}{T_r} + \frac{V_h}{T_h}\Big) = 0 \tag{3.37}$$

Rearranging equation 3.37 to explicitly describe the pressure differential we obtain equation 3.38.

$$dP = \frac{-\gamma P\Big(dV_e/T_{eb} + dV_c/T_{cb}\Big)}{V_c/T_{cb} + \gamma\Big(V_k/T_k + V_r/T_r + V_h/T_h\Big) + V_e/T_{eb}} \tag{3.38}$$

3.3.4 Mass Flows

Using the mass differentials in each component, we can define the mass flows between engine components. Equation 3.39 is the mass flow between the compression space and cooler, equation 3.40 is the mass flow between the cooler and regenerator, equation 3.41 is the mass flow between the expansion space and heater, and equation 3.42 is the mass flow between the heater and regenerator.

$$\dot{m}_{cb} = -dm_c \tag{3.39}$$

$$\dot{m}_{kb} = \dot{m}_{cb} - dm_k \tag{3.40}$$

$$\dot{m}_{eb} = dm_e \tag{3.41}$$

$$\dot{m}_{hb} = \dot{m}_{eb} + dm_h \tag{3.42}$$

3.3.5 Conditional Temperatures

In order to define the temperature of the fluid passing through the expansion and compression space boundaries an "if statement" is required, as this temperature changes depending on the direction of the flow.

$$if \quad \dot{m}_{cb} > 0 \quad T_{cb} = T_c$$

$$else \quad T_{cb} = T_k$$

$$if \quad \dot{m}_{eb} > 0 \quad T_{eb} = T_h$$

$$else \quad T_{eb} = T_e$$

3.3.6 Temperature Derivatives

Rearranging the differential form of the ideal gas law, the temperature differential in the compression space can be defined as equation 3.43.

$$dT_c = T_c\Big(\frac{dP}{P} + \frac{dV_c}{V_c} + \frac{dm_c}{m_c}\Big) \tag{3.43}$$

Similarly the temperature differential in the expansion space is equation 3.44.

$$dT_e = T_e\Big(\frac{dP}{P} + \frac{dV_e}{V_e} + \frac{dm_e}{m_e}\Big) \tag{3.44}$$

3.3.7 Energy Equations

Calculating the energy absorbed and rejected in the heat exchangers, equation 3.29 is applied to the cooler, regenerator and heater. Equation 3.45 is the energy differential in the cooler, equation 3.46 is the energy differential in the regenerator and equation 3.47 is the energy differential in the heater.

$$dQ_k = \Big(\frac{C_v}{R}\Big)V_k dP - C_p(\dot{m}_{cb}T_{cb} - \dot{m}_{kb}T_k) \tag{3.45}$$

$$dQ_r = \Big(\frac{C_v}{R}\Big)V_r dP - C_p(\dot{m}_{kb}T_k - \dot{m}_{hb}T_h) \tag{3.46}$$

$$dQ_h = \Big(\frac{C_v}{R}\Big)V_h dP - C_p(\dot{m}_{hb}T_h - \dot{m}_{eb}T_{eb}) \tag{3.47}$$

Defining the work differential in the compression and expansion spaces as equations 3.48 and 3.49.

$$dW_c = PdV_c \tag{3.48}$$

$$dW_e = PdV_e \tag{3.49}$$

Summing equations 3.49 and 3.50, yields the total work differential.

$$dW = PdV_c + PdV_e \tag{3.50}$$

Integrating this equation over a cycle, we obtain equation 3.51.

$$\oint dW = \oint (dW_c + dW_e)$$

$$W = W_c + W_e \tag{3.51}$$

Equation 3.52 is the cycle efficiency which is calculated at the end of a cycle.

$$\eta = \frac{W_{net}}{Q_{h,net}} \tag{3.52}$$

3.3.8 Method of Solution

There is no analytical solution to the differential equations for the Stirling cycle second order ideal adiabatic model. This lack of solution is due to the adiabatic working space assumption, and it is therefore required that iterative methods be used to solve the system of equations.

To solve the system of equations the 4th order Runge-Kutta method is used to solve for the first four angular steps and to follow this the 4th order Adams-Bashforth method is used. The reason for this is that the Adams-Bashforth method is a linear multi-step method and utilises previously computed derivatives rather than using derivatives computed at intermediate steps, thus allowing for a more computationally efficient iterative method [84]. The computational scheme is terminated once convergence is reached, the criteria for convergence is when the initial and final temperatures in the compression and expansion spaces are equal. The equations that are used in these two iterative schemes can be seen under the two headings that follow. The Adam's-Bashforth method is a linear multi-step method which is not L-stable like the Runge-Kutta method, which because of this property is good for integrating stiff equations. However, in the case of the ideal adiabatic model a sufficiently small step size is chosen to increase the accuracy of the mass flow rate calculations, this means that the linear multi-step method is a suitable method and significantly speeds up the iterative scheme.

4th Order Runge Kutta Method

The 4th order Runge-Kutta method is made up of equations 3.53, 3.54, 3.55, 3.56 & 3.57.

$$\bar{k}_1 = \bar{h} f(t_i, y_i) \tag{3.53}$$

$$\bar{k}_2 = \bar{h} f(t_i + \frac{1}{2}\bar{h}, y_i + \frac{1}{2}\bar{k}_1) \tag{3.54}$$

$$\bar{k}_3 = \bar{h} f(t_i + \frac{1}{2}\bar{h}, y_i + \frac{1}{2}\bar{k}_2) \tag{3.55}$$

$$\bar{k}_4 = \bar{h} f(t_i + \bar{h}, y_i + \mathbf{k}_3) \tag{3.56}$$

The next y value is computed using equation 3.57 which requires the $\bar{k}$ values computed in equations 3.53, 3.54, 3.55 and 3.56.

$$y_{i+1} = y_i + \frac{1}{6}\Big(\bar{k}_1 + 2\bar{k}_2 + 2\bar{k}_3 + \bar{k}_4\Big) \tag{3.57}$$

4th Order Adams-Bashforth Method

The 4th order Adams-Bashforth iterative method can be seen as equation 3.58.

$$y_{i+1} = y_i + \frac{\bar{h}}{24}\Big(55f(t_i, y_i) - 59f(t_{i-1}, y_{i-1}) + 37f(t_{i-2}, y_{i-2}) - 9f(t_{i-3}, y_{i-3})\Big) \tag{3.58}$$

3.4 Model Description

The Stirling engine model consists of five working spaces which are serially connected along with source and sink streams which interface with the heater and cooler. A diagram of the Stirling engine model showing these serially connected components, and the source and sink streams can be seen in figure 3.7.

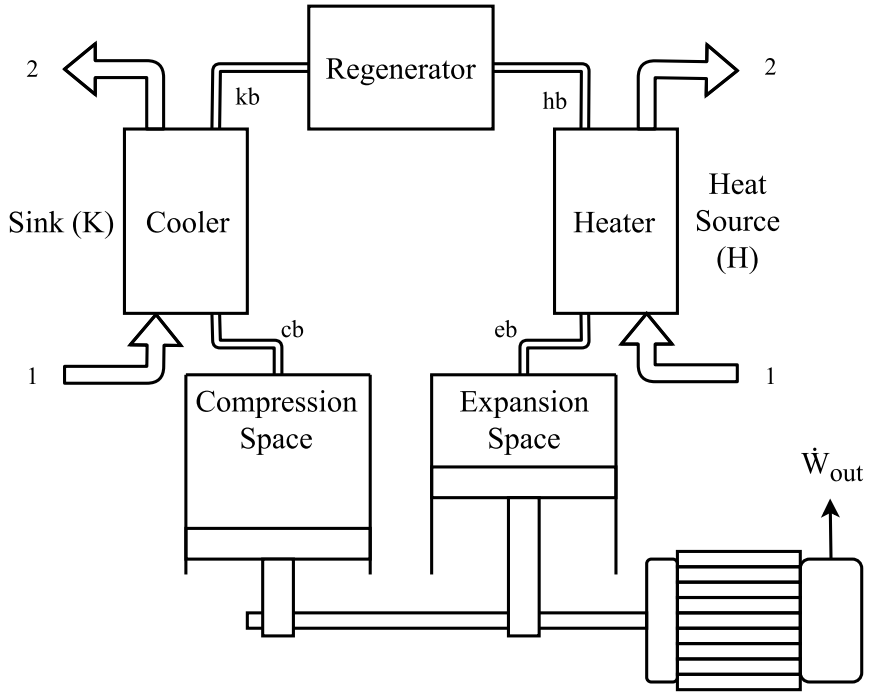

Figure 3.7: Diagram of Stirling engine configuration

In the analysis there will be two different models used, the first model assumes constant heat exchanger wall temperature and the second assumes finite heat capacity rates. These two different approaches as to the treatment of the heater and cooler have been chosen because in the literature both have been used in the analysis of Stirling engines.

3.4.1 Constant Wall Temperature

The constant wall temperature assumption has been used to analyse Stirling engines in many studies. This assumption maintains that the heat exchanger wall temperature in the cooler and the heater is constant. The compartment temperature diagram for the constant wall temperature case is shown in figure 3.8.

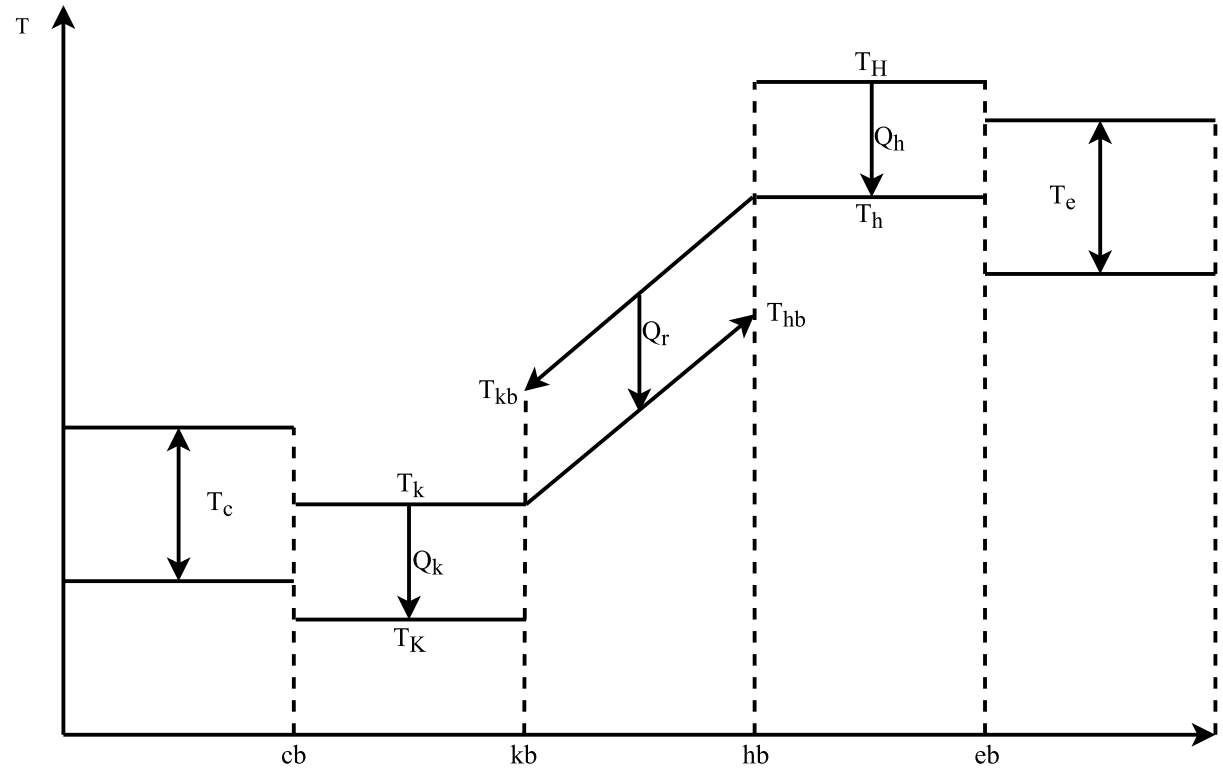

Figure 3.8: Compartment temperature diagram for constant heat exchanger wall temperature

This approach has been used in chapter 6 in the validation of the model and GPU-3 analysis. The reason for this is that the models of the GPU-3 engine seen in literature also make the constant wall temperature assumption. This study allows for the easy comparison of the new results to the existing results for the analysis of the GPU-3 engine, seen in chapter 6.

3.4.2 Finite Heat Capacity Rate

The finite heat capacity rate assumption maintains that the heat capacity rate of the external heat transfer fluid in the cooler and the heater is finite. The compartment temperature diagram for the finite heat capacity rate case is shown in figure 3.9.

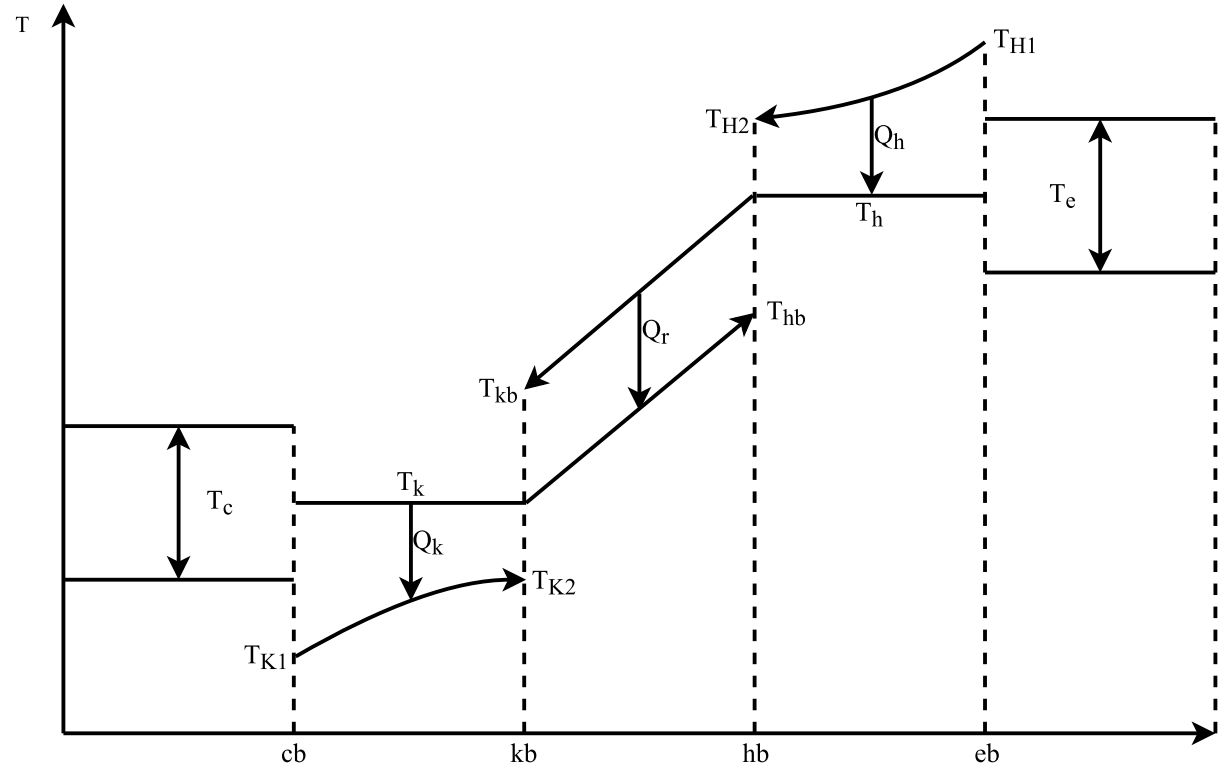

Figure 3.9: Compartment temperature diagram for heat source and sink of finite heat capacity rate

The finite heat capacity rate case has been used in some Stirling cycle analyses as it is a more realistic representation of the heat transfer in the heater and cooler. This approach has been used in chapter 7 in the optimisation of the geometry of the Stirling engine with finite heat capacity rates in the heater and cooler.

3.5 Heat Transfer and Flow Friction Relations

To calculate the heat transfer and pressure drop in the heat exchangers, empirical relations are required. These relations couple the geometric features and the thermodynamics of the system, allowing for the application of the second law so that the irreversibility rate can be determined. In the case of the Stirling engine, the flow is extremely complicated as it is unsteady and reverses direction during each cycle of the engine. This flow characteristic means that the working fluid flow rate through the different heat exchangers dramatically varies in magnitude and changes direction during each rotation of the crank. However, the empirical relations rely on the Reynolds number which requires the average flow velocity and fluid properties. It has also been found that the pressure drop is lower in oscillating flow cases than in unidirectional flow cases [64]. The quasi-steady flow assumption is made so that the empirical relations can be used. This assumption means that the average friction factor and heat transfer properties are calculated. The $NTU - \eta$ method is used to compute the effectiveness of the heat exchangers.

Sutherland's formula is used to calculate the viscosity of the working fluid in the different engine compartments [103]. This is seen as equation 3.59.

$$\mu = \mu_{reference} \left(\frac{T_{reference} + \bar{S}}{T + \bar{S}} \right) \left(\frac{T}{T_{reference}} \right)^{3/2} \tag{3.59}$$

As air and helium are the two different working fluids used in chapters 6 and 7, the inputs required for equation 3.52 differ. The reference values for these two different cases can be seen in table 3.1.

Table 3.1: Table of air and helium reference values for the Sutherland formula

Symbol	Description	Air	Helium
S	Sutherland temperature (K)	112	80
$\mu_{reference}$	Reference viscosity $(kg.m^{-1}.s^{-1})$	1.708×10^{-5}	1.885×10^{-5}
$T_{reference}$	Reference temperature (K)	273	273

The two relations required to calculate the heat transfer and flow losses are the Nusselt number (Nu) and the Darcy friction factor (f_D). The flow is reversing, so we introduce the Reynolds friction factor which is the Darcy friction factor multiplied by the Reynolds number. The Reynolds number changes sign with changing flow direction, so using this method allows for the computation of the pressures at either end of the heat exchanger in

question through vector addition. Only the core frictional pressure drop is accounted for, the entrance, exit and momentum effects are ignored as the core frictional pressure drop typically account for 90% or more of the pressure drop in compact gas heat exchangers [95].

Equation 3.60 is the Reynolds friction factor and equation 3.61 is the pressure drop. These two equations are used to calculate the flow losses in each of the heat exchangers.

$$f_r = f_D Re \tag{3.60}$$

Where f_D is the Darcy friction factor, which should not be confused with the Fanning friction factor (f_F).

$$\Delta P = -\frac{2 f_r \mu v V}{A_{flow} d_{hyd}^2} \tag{3.61}$$

The pressure in the compression space is used as a reference pressure to which the pressure drops are added. Figure 3.10 is a diagram which shows the pressures in each compartment along the lengths of the particular heat exchanger for a given flow direction.

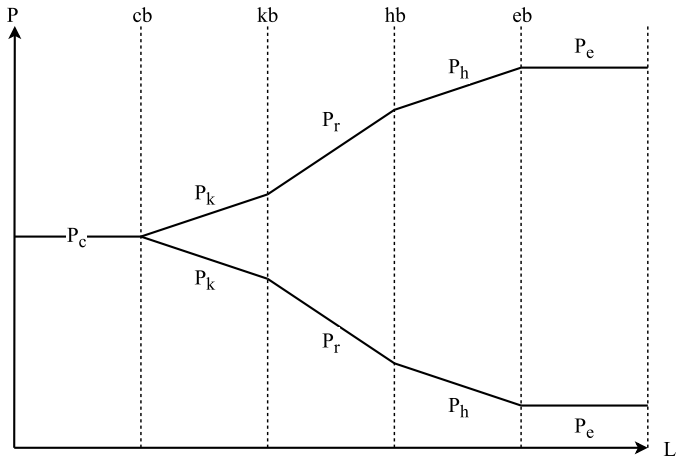

Figure 3.10: Compartment instantaneous pressure diagram

Equation 3.55 is used to calculate the heat transfer coefficient from the Nusselt number and equation 3.56 is used to calculate the number of transfer units, which in turn is used to calculate the heat exchanger effectiveness.

$$Nu = \frac{h D_{hyd}}{k} \tag{3.62}$$

$$NTU = \frac{U A_{surf}}{C_{min}} \tag{3.63}$$

The following two sections present the heat transfer and flow friction relations for the regenerator, and the heater and cooler.

3.5.1 Regenerator

Many relations have been proposed to calculate the friction factor and Nusselt number in the regenerator. The type and arrangement of regenerator material changes these relations.

Table 3.2 is a table of properties for different packs of wire mesh that are typically used in Stirling engine regenerators and were used by [104], in their experiments to determine regenerator relations. These mesh types have been used in chapter 7, as the relations have been shown experimentally to be suitable for calculating the Nusselt number and flow friction relations without significant error.

Table 3.2: Table of wire netting dimensions [104]

Symbol	Diameter (d_{mesh}) (mm)	Porosity (ϕ) (-)	Shape factor (ϵ) (-)
WN50	0.23	0.645	4.0
WN100	0.1	0.711	4.0
WN150	0.06	0.754	4.0
WN200	0.05	0.729	4.0

Equations 3.64 is the equation for the Darcy friction factor which is calculated using the maximum Reynolds number [104]. Equation 3.65 is the equation for Nusselt number and is calculated using the average Reynolds number [104]. Using the Nusselt number, the number of transfer units can be calculated and once this is known the effectiveness of the regenerator can be calculated. Equation 3.66 is used to calculate the effectiveness of the regenerator [104].

$$f_D = \frac{175}{Re_{max}} + 1.60 \tag{3.64}$$

$$Nu_{mean} = 0.33 Re_{mean}^{0.67} \tag{3.65}$$

$$\varepsilon_r = \frac{NTU}{NTU + 2} \tag{3.66}$$

3.5.2 Heater and Cooler

In Stirling engines, the heater and cooler are usually compact tube heat exchangers. These types of heat exchangers are suitable for the high pressure and temperature of the working fluid and thus have seen extensive usage. The experimental correlations for unidirectional flow are used to calculate the Darcy friction factor and the Nusselt number on the inside of the tubes. The heat loads in the heater and the cooler are defined in terms of the heat loads in the different heat exchangers and the regenerator effectiveness, seen as equations 3.67 and 3.68.

$$Q_{in} = Q_h + (1 - \varepsilon_r)Q_r \tag{3.67}$$

$$Q_{out} = Q_k + (1 - \varepsilon_r)Q_r \tag{3.68}$$

Recently improved relations for the friction factors inside smooth tubes were published in [50]. These relations can be seen as equations 3.69 and 3.70, each representing a different range of Reynolds numbers in the turbulent regime. The reason for this is that the flow in the heater and cooler is always assumed to be turbulent, which is due to the oscillating nature of the flow.

$$f_D = 0.351Re^{-0.255} \quad 3050 < Re < 240000 \tag{3.69}$$

$$f_D = 0.118Re^{-0.165} \quad 240000 < Re < \infty \tag{3.70}$$

To calculate the Nusselt number on the inside of the tubes it is suggested that the Gnielinski relation [42, 19] be used, seen as equation 3.71.

$$Nu = \frac{(f_D/8)(Re - 1000)Pr}{1 + 12.7(f_D/8)^{1/2}(Pr^{2/3} - 1)} \quad 3000 < Re < 5 \times 10^6 \tag{3.71}$$

Constant Wall Temperature

The constant wall temperature case calculates the rate of heat transfer based on the temperature difference between the heat exchanger wall and working fluid. Equation 3.72 is the rate of heat transfer in the heater.

$$\dot{Q}_{in} = h_h A_h (T_H - T_h) \tag{3.72}$$

Equation 3.73 is the rate of heat transfer in the cooler.

$$\dot{Q}_{out} = h_k A_k (T_K - T_k) \tag{3.73}$$

Equations 3.72 and 3.73 are used to calculate the required temperature difference between the heat exchanger wall and working fluid for the necessary rate of heat transfer. These equations are incorporated into the numerical scheme to solve for the heater and cooler gas temperatures using an iterative scheme.

Finite Heat Capacity Rate

In the finite heat capacity rate case, the external heat transfer fluid is assumed to have a finite heat capacity. In calculating the effectiveness of the heat exchanger, the overall heat transfer coefficient is required. It is assumed that the heat exchanger tubes are of a negligible thickness and the heat transfer coefficient on the inside of the tubes is the limiting factor. Therefore, the overall heat transfer coefficient is defined as equation 3.74, and assumed to be the same as the internal heat transfer coefficient.

$$U \approx h_{internal} \tag{3.74}$$

With the overall heat transfer coefficient, the number of transfer units can be calculated and with this the effectiveness of the respective heat exchangers. It has been suggested by [1], that the effectiveness of the heat exchangers be computed using equations 3.75 and 3.76 for the heater and cooler respectively.

$$\varepsilon_h = 1 - e^{-NTU_h} \tag{3.75}$$

$$\varepsilon_k = 1 - e^{-NTU_k} \tag{3.76}$$

These equations are for the case where the heat capacity of one of the fluids is infinite which is a result of the isothermal heater and cooler assumption. They are traditionally used in the case of latent heating or cooling.

Equation 3.77 is the rate of heat transfer in the heater

$$\dot{Q}_{in} = \varepsilon_h C_H (T_{H1} - T_h) = C_H (T_{H1} - T_{H2}) \tag{3.77}$$

Equation 3.78 is the rate of heat transfer in the cooler.

$$\dot{Q}_{out} = \varepsilon_k C_K (T_{K1} - T_k) = C_K (T_{K1} - T_{K2}) \tag{3.78}$$

Equations 3.77 and 3.78 are incorporated into the numerical scheme to solve for the heater and cooler gas temperature using an iterative approach.

3.5.3 Conductive Thermal Bridging Loss

The conductive thermal bridging loss is included in the analysis as heat is conducted between the hot and cold parts of the engine through the regenerator. The rate of conduction is assumed to be proportional to the regenerator material cross-sectional area and the temperature difference between the hot and cold parts of the engine, and inversely proportional to the length of the regenerator. Equation 3.79 is the rate of heat conduction between the heater and cooler.

$$\dot{Q}_{cond} = \frac{k_{cond} A_{cond}}{L_r}(T_h - T_k) \tag{3.79}$$

3.6 Entropy Generation Equations

The following section outlines the formulation of the rate of entropy generation equations for each Stirling engine heat exchanger. The heater and cooler rate of entropy generation equations are each formulated twice. The one formulation is for the constant wall temperature case and the other for the finite heat capacity rate case.

The formulation of the objective functions begins with the second law of thermodynamics. The mathematical formulation of the second law of thermodynamics, can be seen as equation 3.80.

$$\frac{dS}{dt} = \sum_i \frac{\dot{Q}_i}{T_i} + \sum_{in} \dot{m}s - \sum_{out} \dot{m}s + \dot{S}_{gen} \tag{3.80}$$

In the case of a heat exchanger with two streams, the rate of entropy generation can be defined as equation 3.81. This equation is used to calculate the degree of thermodynamic imperfection in the component under steady flow conditions [76].

$$\dot{S}_{gen} = \dot{m}_1(s_{1,in} - s_{1,out}) + \dot{m}_2(s_{2,in} - s_{2,out}) \tag{3.81}$$

Therefore, expressing the equation in terms of the inlet and outlet pressures and temperatures, equation 3.82 is obtained.

$$\dot{S}_{gen,total} = (\dot{m}C_p)_1 \ln\left(\frac{T_{1,out}}{T_{1,in}}\right) - (\dot{m}R)_1 \ln\left(\frac{P_{1,out}}{P_{1,in}}\right) + (\dot{m}C_p)_2 \ln\left(\frac{T_{2,out}}{T_{2,in}}\right) - (\dot{m}R)_2 \ln\left(\frac{P_{2,out}}{P_{2,in}}\right) \quad (3.82)$$

In the Stirling cycle, the derivation of the rate of entropy generation equation is not straightforward, as the steady flow assumption cannot be made. The constant temperature assumption in the heater and cooler makes the rate of entropy generation due to temperature effects in these components zero ($\dot{S}_{gen,\Delta T} = 0$), this is the same as the endo-reversible assumption which has been made in a number of the Stirling cycle irreversibility analyses seen in the literature. However, the entropy generation due to the pressure drop is accounted for ($\dot{S}_{gen,\Delta P} \neq 0$), which makes this analysis the first of its kind. In the regenerator the rates of entropy generation due to pressure drop and heat transfer are both accounted for ($\dot{S}_{gen,\Delta P}, \dot{S}_{gen,\Delta T} \neq 0$). To see a full derivation of the equations for the rate of entropy generation in the heater, cooler and regenerator, see Appendix B.

3.6.1 Heater

The rate of entropy generation in the heater is formulated for the constant wall temperature and the finite heat capacity rate cases.

Constant Wall Temperature

Equation 3.83 is the rate of entropy generation in the heater, for the constant wall temperature case.

$$\dot{S}_{gen,h} = \frac{R}{2\pi} \int_0^{2\pi} |\dot{m}_h(\theta)| \left| \ln\left(\frac{P_{eb}(\theta)}{P_{hb}(\theta)}\right) \right| d\theta - \frac{\dot{Q}_{in}}{T_H} \quad (3.83)$$

Finite Heat Capacity Rate

Equation 3.84 is the rate of entropy generation in the heater, for the finite heat capacity rate case.

$$\dot{S}_{gen,h} = C_h \ln\left(\frac{T_{H1} - \varepsilon_h(T_{H1} - T_h)}{T_{H1}}\right) + \frac{R}{2\pi} \int_0^{2\pi} |\dot{m}_h(\theta)| \left| \ln\left(\frac{P_{eb}(\theta)}{P_{hb}(\theta)}\right) \right| d\theta \quad (3.84)$$

3.6.2 Regenerator

In analysing the regenerator the rate of entropy generation due to heat transfer and pressure drop is calculated. Equation 3.85 is the definition of heat exchanger effectiveness for the regenerator [68].

$$\varepsilon_r = \frac{\dot{Q}}{\dot{Q}_{max}} = \frac{T_{hb} - T_k}{T_h - T_k} = \frac{T_{kb} - T_h}{T_k - T_h} \tag{3.85}$$

The quasi-steady flow approach is used to calculate the heat transfer characteristics in the regenerator. Using a similar method as presented in [68], the rate of entropy generation due to heat transfer using the temperatures T_{hb} and T_{kb} is calculated, seen as the first term in equation 3.86. Using these temperatures and the pressure drop the rate of entropy generation can be calculated as equation 3.86.

$$\dot{S}_{gen,r} = \frac{C_p}{4\pi} ln\left(\frac{T_{hb}T_{kb}}{T_k T_h}\right) \int_0^{2\pi} |\dot{m}_r(\theta)| d\theta + \frac{R}{2\pi} \int_0^{2\pi} |\dot{m}_r(\theta)| \left| \ln\left(\frac{P_{hb}(\theta)}{P_{kb}(\theta)}\right)\right) \Bigg| d\theta \tag{3.86}$$

3.6.3 Cooler

In the same way, as for the heater, the rate of entropy generation in the cooler is also formulated for the constant wall temperature and finite heat capacity rate cases.

Constant Wall Temperature

Equation 3.87 is the rate of entropy generation in the cooler, for the constant wall temperature case.

$$\dot{S}_{gen,k} = \frac{R}{2\pi} \int_0^{2\pi} |\dot{m}_k(\theta)| \left| \ln\left(\frac{P_{kb}(\theta)}{P_{cb}(\theta)}\right)\right| d\theta + \frac{\dot{Q}_{out}}{T_K} \tag{3.87}$$

Finite Heat Capacity Rate

Equation 3.88 is the rate of entropy generation in the cooler, for the finite heat capacity rate case.

$$\dot{S}_{gen,k} = C_k \ln\left(\frac{T_{K1} + \varepsilon_k(T_k - T_{K1})}{T_{K1}}\right) + \frac{R}{2\pi} \int_0^{2\pi} |\dot{m}_k(\theta)| \left| \ln\left(\frac{P_{kb}(\theta)}{P_{cb}(\theta)}\right)\right| d\theta \tag{3.88}$$

3.6.4 Total Entropy Generation

To calculate the total rate of entropy generation, the rate of entropy generation in each component is summed. Summing the entropy generation rate in the cooler, heater and regenerator, equation 3.89 is obtained.

$$\dot{S}_{gen,total} = \dot{S}_{gen,h} + \dot{S}_{gen,r} + \dot{S}_{gen,k} \tag{3.89}$$

Equation 3.89 does not include the rate of entropy generation in the expansion space and compression space. The reason for this is that the rate of entropy generation in the compression and expansion spaces is assumed to be negligible ($\dot{S}_{gen,e} = \dot{S}_{gen,c} = 0$). Therefore, writing the equations for total rate of entropy generation including all terms yields equations 3.90 and 3.91.

Constant Wall Temperature

The total rate of entropy generation for the case of constant wall temperature in the heater and cooler, can be seen as equation 3.90.

$$\begin{aligned}\dot{S}_{gen,total} = {} & \frac{R}{2\pi}\int_0^{2\pi} |\dot{m}_h(\theta)| \left| \ln\left(\frac{P_{eb}(\theta)}{P_{hb}(\theta)}\right)\right| d\theta - \frac{\dot{Q}_{in}}{T_H} \\ & + \frac{C_p}{4\pi} ln\left(\frac{T_{hb}T_{kb}}{T_k T_h}\right)\int_0^{2\pi} |\dot{m}_r(\theta)| d\theta + \frac{R}{2\pi}\int_0^{2\pi} |\dot{m}_r(\theta)| \left| \ln\left(\frac{P_{hb}(\theta)}{P_{kb}(\theta)}\right)\right)\right| d\theta \\ & + \frac{R}{2\pi}\int_0^{2\pi} |\dot{m}_k(\theta)| \left| \ln\left(\frac{P_{kb}(\theta)}{P_{cb}(\theta)}\right)\right| d\theta + \frac{\dot{Q}_{out}}{T_K}\end{aligned} \tag{3.90}$$

Finite Heat Capacity Rate

The total rate of entropy generation for the case of finite heat capacity rate in the heater and cooler, can be seen as equation 3.91.

$$\begin{aligned}\dot{S}_{gen,total} = {} & C_h \ln\left(\frac{T_{H1} - \varepsilon_h(T_{H1} - T_h)}{T_{H1}}\right) + \frac{R}{2\pi}\int_0^{2\pi} |\dot{m}_h(\theta)| \left| \ln\left(\frac{P_{eb}(\theta)}{P_{hb}(\theta)}\right)\right| d\theta \\ & + \frac{C_p}{4\pi} ln\left(\frac{T_{hb}T_{kb}}{T_k T_h}\right)\int_0^{2\pi} |\dot{m}_r(\theta)| d\theta + \frac{R}{2\pi}\int_0^{2\pi} |\dot{m}_r(\theta)| \left| \ln\left(\frac{P_{hb}(\theta)}{P_{kb}(\theta)}\right)\right)\right| d\theta \\ & + C_k \ln\left(\frac{T_{K1} + \varepsilon_k(T_k - T_{K1})}{T_{K1}}\right) + \frac{R}{2\pi}\int_0^{2\pi} |\dot{m}_k(\theta)| \left| \ln\left(\frac{P_{kb}(\theta)}{P_{cb}(\theta)}\right)\right| d\theta\end{aligned} \tag{3.91}$$

3.7 Exergy Analysis

This section presents the exergy analysis, which leads to the formulation of the objective functions. The objective function is thus the work potential, availability or maximum amount of thermodynamic work that can be delivered by the engine [11]. The exergy analysis begins with the exergy balance for a control volume, seen as equation 3.92.

$$\dot{X}_{in} - \dot{X}_{out} - \dot{I} - \dot{W}_{net} = 0 \tag{3.92}$$

Rearranging equation 3.92 to explicitly give the maximum available rate of thermodynamic work yields equation 3.93.

$$\dot{W}_{net} = \dot{X}_{in} - \dot{X}_{out} - T_0 \dot{S}_{gen,total} \tag{3.93}$$

The exergy analysis equations that are described are used in the analysis to define the maximum power that the engine can produce. The exergy equation for the constant wall temperature case is used in chapter 6 in the study of the GPU-3 Stirling engine and the finite heat capacity rate exergy equation is used in chapter 7 in the optimisation of the Stirling engine example presented.

3.7.1 Exergy Equations

The two objective functions for the constant wall temperature and the finite heat capacity rate cases are seen below:

Constant Wall Temperature

Substituting equation 3.90 into equation 3.93 yields the equation for the maximum power that the engine can produce, for the constant wall temperature case, yielding equation 3.94.

$$\begin{aligned}\dot{W}_{net} = \dot{Q}_{in}\left(1-\frac{T_0}{T_H}\right) - \dot{Q}_{out}\left(1-\frac{T_0}{T_K}\right) \\ - T_0\left[\frac{R}{2\pi}\int_0^{2\pi}|\dot{m}_h(\theta)|\left|\ln\left(\frac{P_{eb}(\theta)}{P_{hb}(\theta)}\right)\right|d\theta - \frac{\dot{Q}_{in}}{T_H}\right]_{heater} \\ - T_0\left[\frac{C_p}{4\pi}ln\left(\frac{T_{hb}T_{kb}}{T_kT_h}\right)\int_0^{2\pi}|\dot{m}_r(\theta)|d\theta + \frac{R}{2\pi}\int_0^{2\pi}|\dot{m}_r(\theta)|\left|\ln\left(\frac{P_{hb}(\theta)}{P_{kb}(\theta)}\right)\right)\right|d\theta\right]_{regenerator} \\ - T_0\left[\frac{R}{2\pi}\int_0^{2\pi}|\dot{m}_k(\theta)|\left|\ln\left(\frac{P_{kb}(\theta)}{P_{cb}(\theta)}\right)\right|d\theta + \frac{\dot{Q}_{out}}{T_K}\right]_{cooler}\end{aligned} \tag{3.94}$$

Finite Heat Capacity Rate

Substituting equation 3.91 into equation 3.93 yields the equation for the maximum power that the engine can produce, for the finite heat capacity rate case, yielding equation 3.95.

$$\begin{aligned}\dot{W}_{net} = C_h\varepsilon_h(T_{H1}-T_h) - T_0C_hln\left(\frac{T_{H1}}{T_{H1}-\varepsilon_h(T_{H1}-T_h)}\right) \\ - C_k\varepsilon_k(T_k-T_{K1}) - T_0C_k\ln\left(\frac{T_{K1}}{T_{K1}+\varepsilon_k(T_k-T_{K1})}\right) \\ - T_0\left[C_h\ln\left(\frac{T_{H1}-\varepsilon_h(T_{H1}-T_h)}{T_{H1}}\right) + \frac{R}{2\pi}\int_0^{2\pi}|\dot{m}_h(\theta)|\left|\ln\left(\frac{P_{eb}(\theta)}{P_{hb}(\theta)}\right)\right|d\theta\right]_{heater} \\ - T_0\left[\frac{C_p}{4\pi}ln\left(\frac{T_{hb}T_{kb}}{T_kT_h}\right)\int_0^{2\pi}|\dot{m}_r(\theta)|d\theta + \frac{R}{2\pi}\int_0^{2\pi}|\dot{m}_r(\theta)|\left|\ln\left(\frac{P_{hb}(\theta)}{P_{kb}(\theta)}\right)\right)\right|d\theta\right]_{regenerator} \\ - T_0\left[C_k\ln\left(\frac{T_{K1}+\varepsilon_k(T_k-T_{K1})}{T_{K1}}\right) + \frac{R}{2\pi}\int_0^{2\pi}|\dot{m}_k(\theta)|\left|\ln\left(\frac{P_{kb}(\theta)}{P_{cb}(\theta)}\right)\right|d\theta\right]_{cooler}\end{aligned} \tag{3.95}$$

3.8 Conclusion

In this chapter the functions that describe the exergy equation of the Stirling cycle, based on the constant wall temperature and finite heat capacity rate assumptions are presented. The total rate of entropy generation is calculated by summing the rates of entropy generation in each component. This expression is then substituted into the exergy equation to formulate the objective function. The heat transfer and flow friction relations used in the Stirling engine model to calculate the irreversibility rate are presented along with the equations that describe the volume variations and the equations that link the engine geometry to the thermodynamic equations.

The ideal adiabatic model presented in the first part of the chapter is used in chapter 5, which is the dead-volume analysis. The constant wall temperature exergy equation, seen as equation 3.94 is used in chapter 6 to analyse and optimise the GPU-3 Stirling engine prototype. The exergy equation for the finite heat capacity rate case is seen as equation 3.95 is used in chapter 7 to optimise the 1000 cm^3 alpha and beta type Stirling engines, for maximum power output.

Chapter 4

Optimisation Procedure

The following chapter presents the optimisation procedure that is used to optimise the Stirling engine geometry for maximum work output as seen in chapter 7. The concept of optimisation is first introduced along with the different types of optimisation algorithms, the optimisation problem and algorithm choice are then explained. Two books by C.T. Kelley were used a great deal in the writing of this chapter [53, 54]. The titles of these two books are: "Iterative Methods for Optimization" and "Implicit Filtering."

4.1 Introduction

The standard form of a constrained minimisation problem can be seen as equation 4.1.

$$\min_{x \in \Omega} f(x) \tag{4.1}$$

Where Ω is a hyper-rectangle in $\mathbb{R}^N$ and L_i and U_i are the lower and upper bounds on the i-th component of the vector x, shown as equation 4.2.

$$\Omega\{x \in \mathbb{R}^N | L_i \leq (x)_i \leq U_i|\} \tag{4.2}$$

There have been many different optimisation algorithms that have been developed for a wide variety of optimisation problems. These algorithms can be loosely defined under two different categories, namely local optimisation algorithms and global optimisation algorithms [118]. Typically local optimisation algorithms are gradient-based, whereas global optimisation algorithms are not. In the following three subsections these two categories are explained. Function properties and how they affect the choice of optimisation algorithm is also discussed.

4.1.1 Local Optimisation Algorithms

Most local optimisation algorithms are gradient-based. These techniques can solve a wide variety of optimisation problems. They do however have some drawbacks, which make them unsuitable for use in many cases. They are susceptible to noise, discontinuities, and are often complicated and inefficient to implement. These methods typically use a two-step iterative process, step one is the computing of the search direction and step two is using a line search method to calculate the distance in that search direction to progress [98].

The most well known local optimisation algorithm is Newton's method, which requires the gradient vector and the Hessian of the function that is being optimised. However, this is not always available or easy to compute. Therefore, a whole class of different methods known as quasi-Newton methods have been developed which use many different approaches to approximate the Hessian [53]. These types of algorithms are well suited to problems where there are a large number of variables, the analysis is computationally expensive, and gradients are easily computed [118].

4.1.2 Global Optimisation Algorithms

Global optimisation algorithms seek to find a global optimum, and many different techniques can be used to do this. All of the local optimisation algorithms mentioned previously can be implemented in a manner that is aimed at finding the global optimum. The way this is achieved is by using a multi-start approach. In this method multiple starting points are used to detect multiple local minima, these minima are then compared to find the global minimum. Evolutionary/Genetic algorithms have also been used extensively for global optimisation problems. These algorithms do not require gradient information but rather generate sets of solutions and use a heuristic process, typically inspired by nature. These heuristics seek to 'evolve' these solutions towards the optimal through many different steps [61]. These algorithms are often very computationally expensive and do not guarantee convergence to a global or even local minimum. However, they are robust algorithms that are well suited to discontinuous solution spaces. These algorithms are better suited to problems with few variables, where noise is a problem, it is difficult or impossible to compute the gradient, and a global optimum is required [54].

There are also some direct search/sampling methods that have been designed for finding global minimums, the most famous being the Nelder-Mead or downhill simplex algorithm

developed by John Nelder and Roger Mead [74]. Another direct optimisation method is the pattern search method, with the earliest variant of this technique dating back to the Manhattan Project work at the Los Alamos National Laboratory [31].

4.1.3 Function Properties and Optimisation

As stated in [118], " no single optimisation technique is suitable for all optimisation problems." The reason that so many different optimisation algorithms have been developed is precisely for this reason, as it has been found that many of the algorithms developed are unsuitable for a whole variety of real-world optimisation problems [98]. The properties of functions that cause many optimisation methods to fail are listed below:

1. The function is discontinuous.
2. The function is non-smooth.
3. There is a degree of numerical noise.
4. There is little information about the solution space.
5. Each function evaluation is computationally expensive.
6. The function is stochastic.

The mathematical model and objective function developed in the previous chapter exhibits properties 1 to 5. Therefore, a specialised optimisation procedure is required that can handle these properties, which would cause conventional optimisation algorithms to fail.

4.2 Stirling Engine Optimisation

The Stirling engine model with finite heat capacity rates at the source and sink presented in the previous chapter is optimised for maximum work output in chapter 7. This model exhibits many characteristics that make it unsuitable for classic gradient-based optimisation techniques. The function is a 'black box' function, and therefore numerical methods are required to compute the gradient vector and the Hessian.

Equation 4.3 is the gradient vector.

$$\nabla f(x) = g(x) = \begin{bmatrix} \dfrac{\partial f}{\partial x_1}(x) \\ \dfrac{\partial f}{\partial x_2}(x) \\ \vdots \\ \dfrac{\partial f}{\partial x_n}(x) \end{bmatrix} \tag{4.3}$$

Equation 4.4 is the Hessian matrix.

$$\nabla^2 f(x) = H(x) = \begin{bmatrix} \dfrac{\partial^2 f}{\partial x_1^2}(x) & \dfrac{\partial^2 f}{\partial x_1 \partial x_2}(x) & \cdots & \dfrac{\partial^2 f}{\partial x_1 \partial x_n}(x) \\ \dfrac{\partial^2 f}{\partial x_2 \partial x_1}(x) & \dfrac{\partial^2 f}{\partial x_2^2}(x) & \cdots & \dfrac{\partial^2 f}{\partial x_2 \partial x_n}(x) \\ \vdots & \vdots & \ddots & \vdots \\ \dfrac{\partial^2 f}{\partial x_n \partial x_1}(x) & \dfrac{\partial^2 f}{\partial x_n \partial x_2}(x) & \cdots & \dfrac{\partial^2 f}{\partial x_n^2}(x) \end{bmatrix} \tag{4.4}$$

The optimal value in the case of the objective function is maximum positive work so to optimise the function it has to be written as a negative ($f(x) = -f(x)$). This is done as the implicit filtering algorithm seeks to minimise a function of several variables.

The function is also discontinuous, non-smooth, noisy, computationally expensive to evaluate and very little is known about the solution space, specifically in what region extrema are located. All of these properties mean that a specialised optimisation procedure that can effectively deal with these function properties is required. Therefore, the implicit filtering algorithm will be used to try and overcome these problems, and find the optimum design point within the constraints. The variables that are input into the function have been defined as ratios. This technique has been used as it reduces the number of variables to be optimised, thus increasing the speed of the optimisation. Other variables have been assumed based on results from other studies, which further reduces the complexity.

4.3 Implicit Filtering

The following section describes the implicit filtering algorithm as developed by C.T. Kelley and his students at North Carolina State University [53, 54].

The implicit filtering algorithm is a deterministic sampling method for bound constraint optimisation. The algorithm has been developed to minimise noisy functions which are non-smooth, discontinuous and are not defined at all points in the solution space. The algorithm solves bound optimisation problems and seeks to exploit the advantages of both pure sampling methods and gradient-based methods. The power of pure sampling methods is their ability not to get stuck at non-stationary points, and the strength of gradient-based methods is fast convergence to a local minimum. In its most basic form, the implicit filtering algorithm is a quasi-Newton method that uses finite difference gradients, where the difference increment varies as the scheme progresses [54].

As explained in [54], the implicit filtering algorithm consists of two iterations, these are the outer and inner iterations, and each serves a different purpose. The outer iteration stores information about the scale of the coordinate search and the budget. The inner iteration evaluates the stencil to check for stencil failure and computes the stencil gradient. This gradient is used to apply the quasi-Newton method until stencil failure is detected, at this point the scale is reduced, and the stencil is re-evaluated. The implicit filtering algorithm extends a classic coordinate search by computing the gradient of the stencil and using it to try and do better than the stencil in finding a better point. This additional operation is done without much added computational expense as the function has already been evaluated in the coordinate search.

The following two subsections describe the coordinate search method that is used to evaluate the stencil and the gradient-based quasi-Newton method.

4.3.1 Coordinate Search

The coordinate search method is a sampling method used to evaluate the stencil. Two iterations of the coordinate search can be seen in figure 4.1

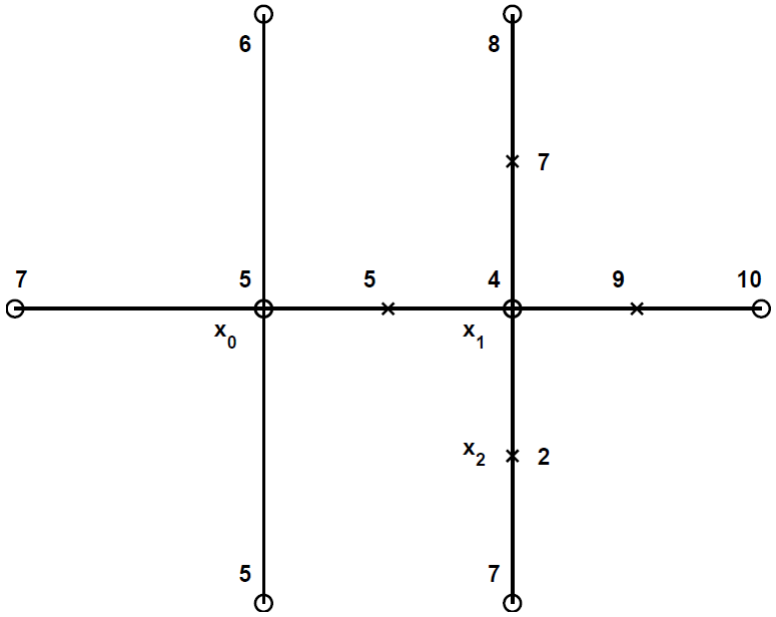

Figure 4.1: Two iterations of the coordinate search [54]

Initially the algorithm scales the variables in terms of the upper (U) and lower (L) bounds, as seen in equation 4.5. This normalises the variables such that the bounds are 0 and 1.

$$0 \leq (z)_i = \frac{(x)_i - L_i}{U_i - L_i} \leq 1 \tag{4.5}$$

The algorithm then evaluates f at $2N$ points on the stencil, around the starting point x.

$$S(x, h) = \{z | z = x \pm he_i\} \tag{4.6}$$

The entire stencil is then sampled and x is replaced with x_{min}.

$$f(x_{min}) = \min_{z \in S(x,h)} f(z) \tag{4.7}$$

If no other x returns a function value lower than the starting x function value ($f(x_{min}) \geq f(x)$), the stencil is deemed to have failed. If this is the case, the stencil is shrunk by a factor of 2. If stencil failure is not detected, the stencil gradient is computed using forward

differencing. This gradient is then used to compute the path of steepest descent, used in the quasi-Newton method.

4.3.2 Quasi-Newton Method (BFGS Update)

The quasi-Newton method is an iterative method that seeks to find the best value of x to minimise f. The method requires both the gradient vector and the Hessian matrix, however in many real-world applications, the exact first and second derivatives of a function are unknown. Therefore, the gradient vector and Hessian matrix have to be approximated, and following this a line search method is used to compute the next value in the optimisation.

Figure 4.2 is a few iterations of the line search method that is explained in this section, where U is the vector in the direction of Steepest decent.

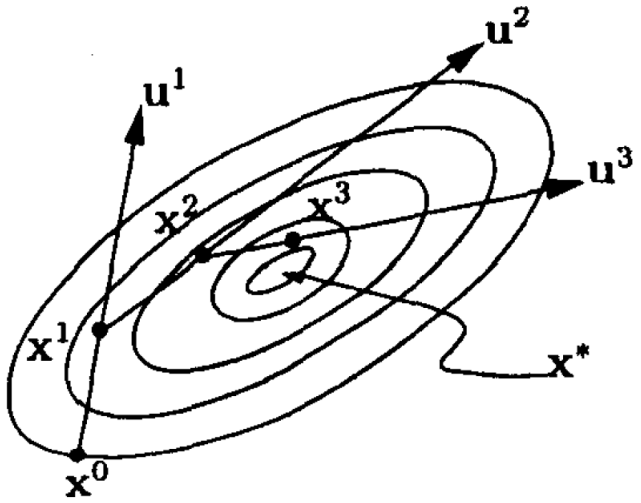

Figure 4.2: A few iterations of the line search method [98]

Quasi-Newton methods are named as such because they update an approximation of the Hessian, whereas Newton's method requires the actual Hessian. The theory behind this technique is to find a sequence of Hessians that perform well when the iteration is far from a local minimiser and rapidly converges when near a point that satisfies the second order sufficiency conditions, seen as equations 4.8 and 4.9.

$$\nabla f(x^*) = 0 \tag{4.8}$$

$$\nabla^2 f(x^*) > 0 \quad (Positive\ \ Definite) \tag{4.9}$$

The gradient vector is required and is approximated using finite forward differences, seen as equation 4.10. In this scheme, attention needs to be paid in choosing the finite difference step size. If the selected step size is too small, the error will be differentiated and not the slope of the function. This error differentiation will give an incorrect gradient and send the optimisation algorithm in the wrong direction.

$$\frac{\partial f(x)}{\partial x_i} \approx \frac{\Delta f(x)}{\delta_i} = \frac{f(x+\delta_i) - f(x)}{\delta_i} \tag{4.10}$$

The Hessian is approximated using the BFGS (Broyden, Fletcher, Goldfarb, Shanno) method. This method is defined as a secant method, as it satisfies equation 4.11.

$$H_+ S = y \tag{4.11}$$

This method updates an approximation of the Hessian (H_+), using the current approximation of the Hessian (H_c), current point (x_c) and future point (x_+). Each iteration is completed in the following four steps, seen below:

1. First the search direction is computed.

$$d = -H_c^{-1} \nabla f(x_c) \tag{4.12}$$

2. Then the Armijo rule [6], which is a line search technique is used to calculate the step size.

$$f(x_c + \lambda d) - f(x_c) < \alpha \lambda \nabla f(x_c)^T d \tag{4.13}$$

3. Using the step size λ, the next x value is computed.

$$x_+ = x_c + \lambda d \tag{4.14}$$

4. Using the values for x_c, x_+ and H_c, H_c is updated using the BFGS method to obtain H_+

$$H_+ = H_c + \frac{yy^T}{y^T S} - \frac{(H_c S)(H_c S)^T}{S^T H_c S} \tag{4.15}$$

These four steps are then repeated for each iteration and are used to move iteratively towards the minimum/optimal value.

4.4 Start point

The implicit filtering algorithm is exceptionally effective at finding the local minimum when the solution space does not oscillate quickly. In the case where the solution space does oscillate quickly, the problem is better tackled with an unstructured algorithm [54]. In the case of the Stirling engine model presented in chapter 3 very little is known about the solution space or where the optimal design points may lie, but the constraints are known. Therefore, consideration needs to be given as to the selection of the starting point. The approach used in the case of this Stirling engine model is to use a multi-start method for the first iteration at the first source temperature. Once this optimal point is found, it is used as the start point for the next source temperature. The reason for this is that the temperature change is relatively small, therefore, the optimal design points are relatively close to one another.

4.5 Conclusion

This chapter describes the optimisation algorithm that will be used to find the optimal geometry of a Stirling engine with finite heat capacity rates at the source and the sink, as presented in chapter 7. The implicit filtering algorithm is explained and discussed along with the implementation of the algorithm. The algorithm uses a combined coordinate search and gradient-based optimisation algorithm to find an optimal solution. This method coupled with an appropriate start point will be used to find the optimal geometry for maximum work output of 1000 cm^3 alpha and beta type Stirling engines with finite heat capacity rates at the source and the sink.

Chapter 5

Dead-Volume Analysis

5.1 Introduction

This chapter analyses the effects that dead-volume ratio and allocation of volume have on the performance of Stirling engines. The analysis uses the ideal adiabatic model which is presented in the first part of chapter 3 and the ideal isothermal model which is presented in Appendix C. These models are both used to analyse the effects of dead-volume ratio on performance, given the assumptions made in the respective models. The results of the analysis are used in the subsequent chapters to help explain some of the phenomena observed when analysing the effects that different parameters have on Stirling engine performance. This analysis is important, as the ideal adiabatic model is used in chapters 6 and 7, and the effects of dead-volume ratio need to be understood in their entirety so that the analysis can be properly understood. This chapter aims to give a thermal designer insight into the effect that dead-volume has on the Stirling engine, as well as to show that there is an optimal dead-volume ratio for LTD and MTD engines. The reason there is a whole chapter devoted to the seemingly simple concept of dead-volume and the analysis of the effects of dead-volume on engine performance is as follows: This is an area of Stirling engine analysis that is often overlooked when it could, in fact, have an integral effect on engine performance. Whether it positively or negatively affects performance is dependant on the temperature difference and the desired engine performance.

The analysis presented is for a Stirling engine which has a phase difference between the compression and expansion spaces of 90°. This model would, therefore, be best classified as an alpha type Stirling engine. The dead-volume is the unswept volume in a Stirling engine,

which is made up of the heat exchanger volumes and the cylinder clearance volumes. For a standard Stirling engine where the clearance volumes are included, this is seen as equation 5.1.

$$V_{dead} = V_{ccl} + V_k + V_r + V_h + V_{ecl} \tag{5.1}$$

In this analysis, the total volume is not the instantaneous maximum volume but rather the overall volume when both pistons are at bottom dead centre (BDC). In operation, this volume wouldn't ever be achieved. However, it is a design variable that is easily measured. Therefore, the total volume is seen as equation 5.2.

$$V_{total} = V_{c,swept} + V_{ccl} + V_k + V_r + V_h + V_{ecl} + V_{e,swept} \tag{5.2}$$

The dead-volume ratio, is the ratio of these two volumes defined as equations 5.1 and 5.2 and is seen as equation 5.3.

$$K = \frac{V_{dead}}{V_{total}} \tag{5.3}$$

In the subsequent analysis, the heater to cooler temperature ratio and the ratio of regenerator void volume to dead-volume are required. These two parameters are defined as follows, equation 5.4 is the heater to cooler temperature ratio and equation 5.5 is the regenerator void volume to dead-volume ratio.

$$X = \frac{T_h}{T_k} \tag{5.4}$$

$$\zeta = \frac{V_r}{V_{dead}} \tag{5.5}$$

Almost all dead-volume analysis in literature has been completed using an isothermal working space approach. However, in reality, it is known that the Stirling engine working spaces are not isothermal, as Stirling engine cylinder walls are usually not designed for heat transfer. It is, therefore, more appropriate to use an approach which assumes the working spaces are adiabatic [116, 115]. The general agreement in the literature is that any dead-volume reduces performance and therefore should be minimised as far as possible [57]. The impact of the dead-volume ratio is analysed using the ideal adiabatic model and the ideal isothermal model. The ideal isothermal model used is the same as the one used by Kongtragool and Wongwises in their dead-volume analysis [57]. The reason this model is used as a comparison is that the work by Kongtragool and Wongwises is the most cited dead-volume analysis in the open literature and is, therefore, a good basis for comparison and as a result, has been used extensively. The difference between the ideal adiabatic model and ideal isothermal models

are that the ideal isothermal model assumes that the processes occur sequentially and the ideal adiabatic model assumes they occur simultaneously. The derivation and validation of the ideal isothermal model can be seen in Appendix C.

The ideal adiabatic and ideal isothermal models require gas constants as inputs. To model the cycle, the working fluid is assumed to be air, and it is considered to be an ideal gas. Table 5.1 below is a table of the gas constants and phase angle used in the model.

Table 5.1: Table of constants

Symbol	Description	Value	Units
C_p	Constant pressure specific heat	1.005	$kJ.kg^{-1}.K^{-1}$
C_v	Constant volume specific heat	0.718	$kJ.kg^{-1}.K^{-1}$
γ	Ratio of specific heats	1.4	-
R	Ideal gas constant	0.287	$kJ.kg^{-1}.K^{-1}$
α	Phase angle	$\pi/2$	rad

The chapter begins by comparing the effect of dead-volume ratio on the two different models. The impact of the allocation of volume is then analysed, and this is followed by the optimisation of the LTD and MTD Stirling engines in terms of dead-volume ratio.

5.2 Model Comparison

The following section analyses the effects of dead-volume ratio on the ideal isothermal and the ideal adiabatic models. The effects of dead-volume ratio on specific input energy, specific work output and efficiency for the varying heater to cooler temperature ratios are analysed and discussed.

5.2.1 Input Energy

Figure 5.1 is a plot of specific input energy versus dead-volume ratio for the ideal isothermal and ideal adiabatic models at different temperature ratios.

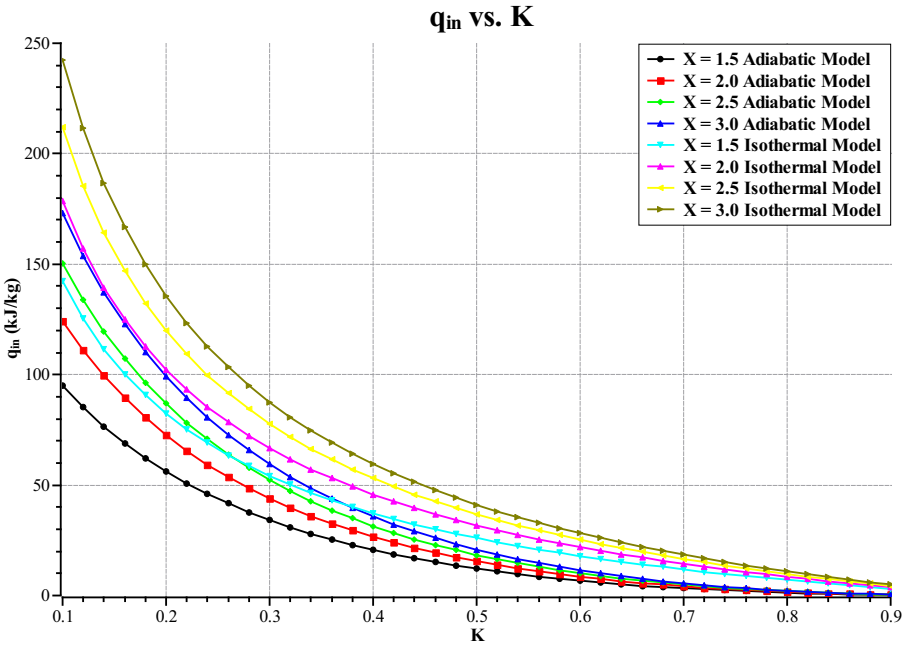

Figure 5.1: Specific input energy (q_{in}) versus dead-volume ratio (K), with varying temperature ratio (X) and model

From figure 5.1 it can be seen that the curves all have a similar trend in that the specific input energy decreases with increasing dead-volume ratio. Furthermore, the specific input energy requirement for the ideal adiabatic model is lower than for the ideal isothermal model.

5.2.2 Specific Work

Figure 5.2 is a graph of specific work output versus dead-volume ratio for the ideal isothermal and ideal adiabatic models at different temperature ratios.

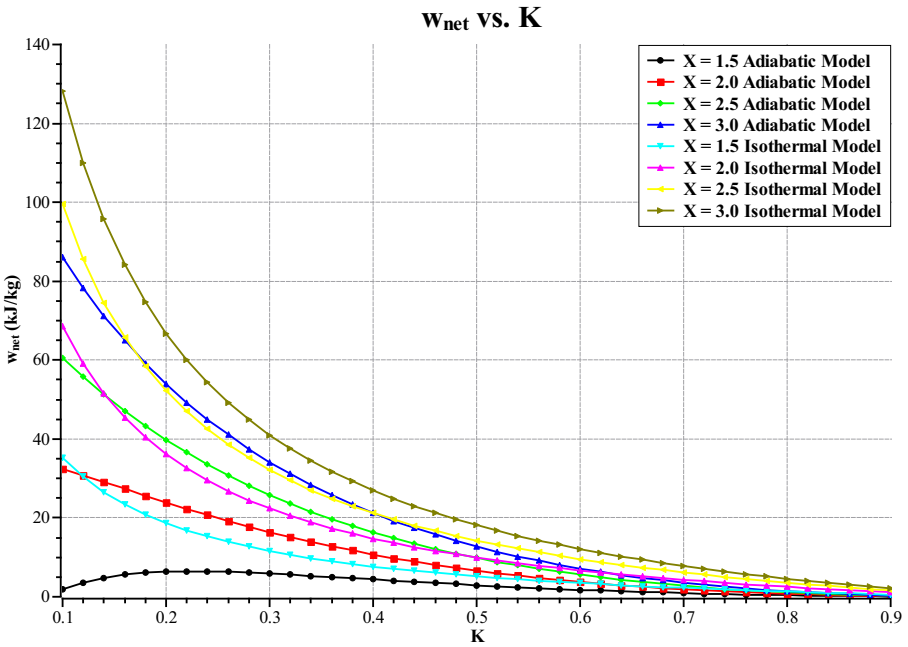

Figure 5.2: Specific work output (w_{net}) versus dead-volume ratio (K), with varying temperature ratio (X) and model

From figure 5.2 it can be seen that the effects of dead-volume ratio are comparable with one another in the case of the higher heater to cooler temperature ratios. However, for the ideal adiabatic model the curve representing the heater to cooler temperature ratio of 1.5 has a maximum value at a non-zero dead-volume ratio. Whereas, the ideal isothermal model does not.

To investigate this further, figure 5.3 has been plotted which is a graph of normalised specific work output versus dead-volume ratio for the ideal adiabatic model, looking at lower heater to cooler temperature ratios. These lower heater to cooler temperature ratios represent Stirling engines that would usually be classified as LTD or MTD engines. This is the case because the heater wall temperatures would be in the LTD or MTD range [61].

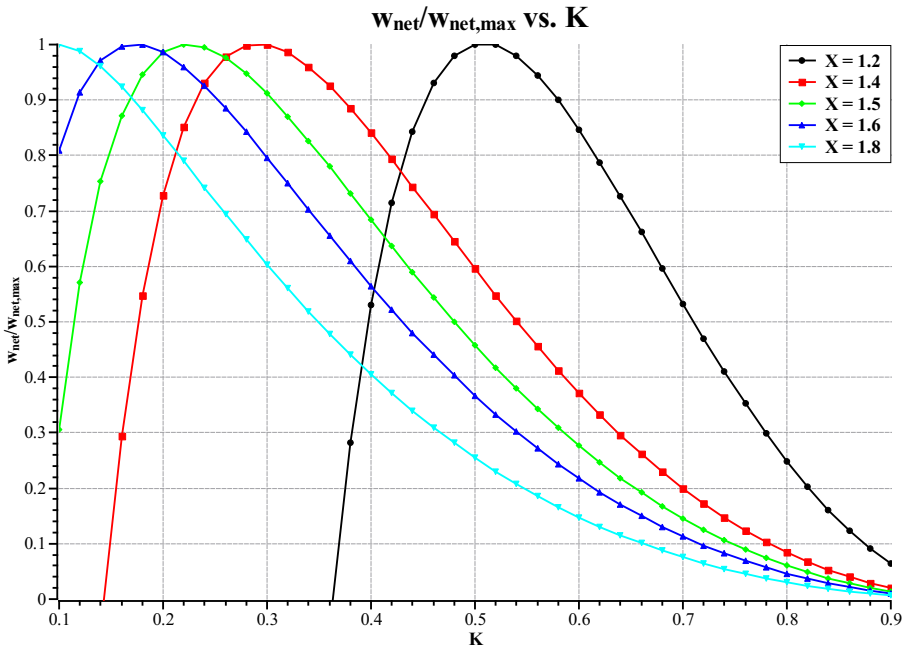

Figure 5.3: Normalised specific work output ($w_{net}/w_{net,max}$) versus dead-volume ratio (K) for the ideal adiabatic model at different LTD and MTD temperature ratios (X)

In figure 5.3 there is an optimal dead-volume ratio that gives maximised specific work output for the lower heater to cooler temperature ratios. The reason for this maximum specific work output at a particular dead-volume ratio is due in part to two different phenomena, listed below:

1. The decrease in specific work output after the maximum is because as the dead-volume ratio increases the swept volume decreases, resulting in there not being a large enough swept volume to give significant work output. In this case, while the specific work output decreases the thermal efficiency is seen to increase.

2. The decrease in specific work output before the maximum is due to the variation of temperature in the expansion and compression spaces. The compression and expansion space swept volumes increasing results in the temperature variation in these spaces increasing. This increase in working space temperature results in a decrease in specific work output as the compression work becomes greater relative to the expansion work.

5.2.3 Efficiency

Figures 5.4 and 5.5 are graphs of efficiency versus dead-volume ratio for the ideal isothermal model and ideal adiabatic model.

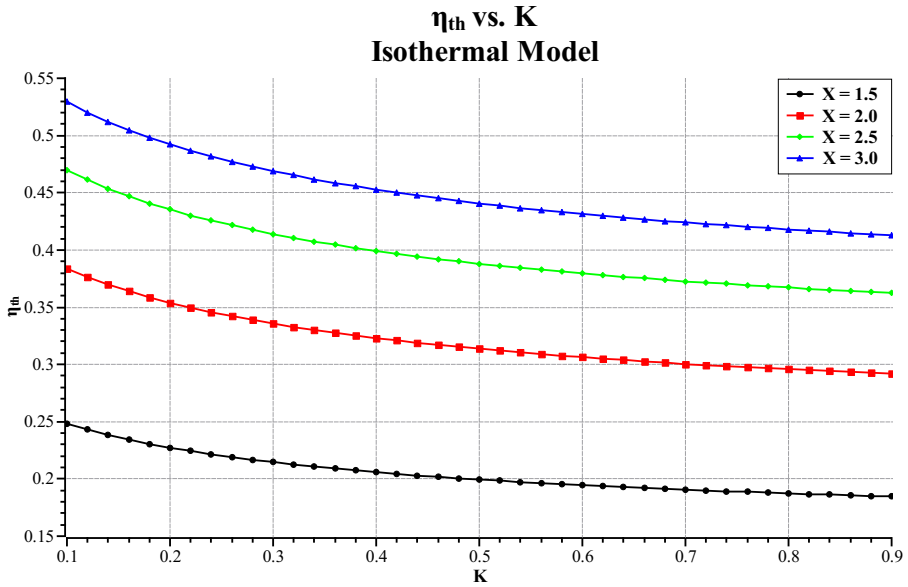

Figure 5.4: Efficiency (η_{th}) versus dead-volume ratio (K) for the ideal isothermal model at different temperature ratios (X)

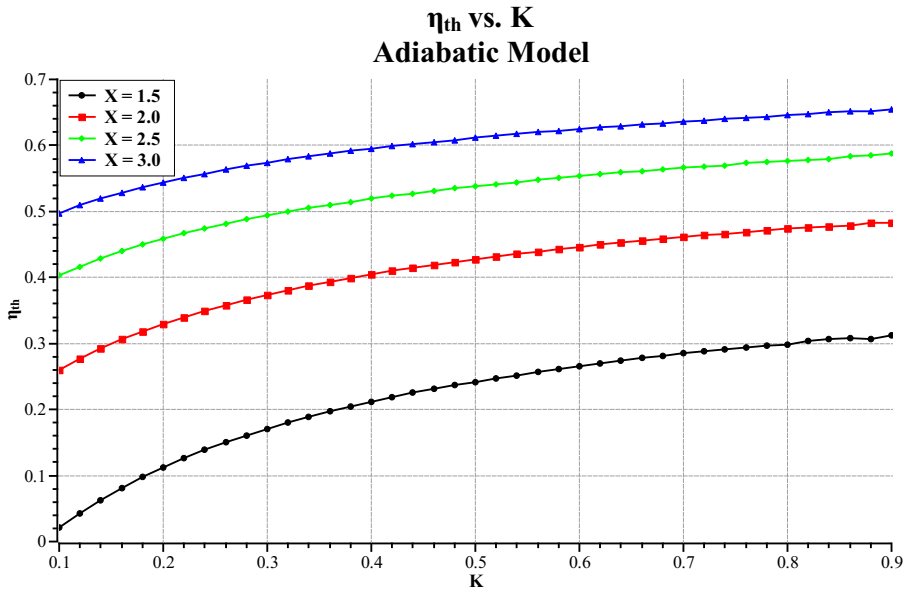

Figure 5.5: Efficiency (η_{th}) versus dead-volume ratio (K) for the ideal adiabatic model at different temperature ratios (X)

Figures 5.4 and 5.5 illustrate that the effect of dead-volume ratio on the efficiency is opposite to the effects on specific work output. The efficiency of the ideal isothermal model decreases with increasing dead-volume ratio, but in the case of the ideal adiabatic model, it increases. The reason the efficiency decreases in the case of the ideal isothermal model is that the increase in dead-volume ratio means there is more dead-volume that absorbs and rejects energy without contributing to the work output. In the case of the ideal adiabatic model, the increase in dead-volume ratio causes the mass flow through the heat exchangers to decrease, and the temperature variation in the expansion and compression spaces to decrease. This decrease in working space temperature variation results in less heat being absorbed in the heater and rejected in the cooler. Thus, as the dead-volume ratio tends towards 1, the thermal efficiency of the ideal adiabatic model asymptotically tends towards the Carnot efficiency. Whereas, the opposite is seen in the case of the ideal isothermal model.

Figure 5.6, illustrates that the efficiency of the ideal adiabatic model tends towards Carnot efficiency with increasing dead-volume ratio.

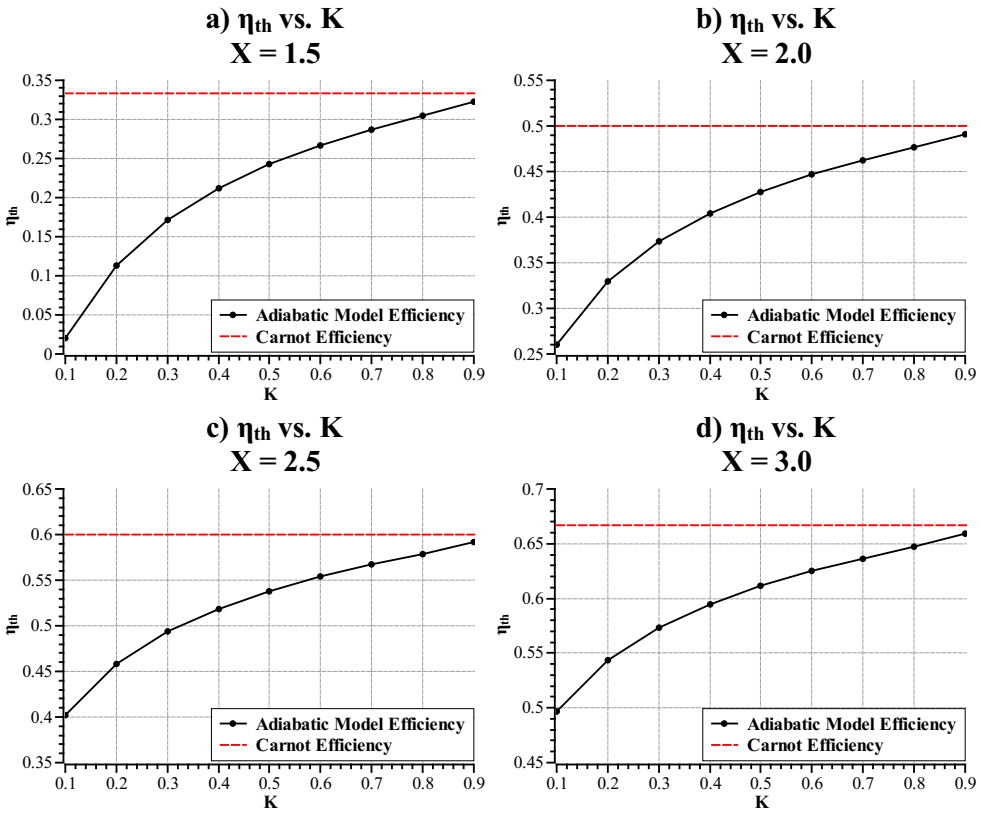

Figure 5.6: Efficiency (η_{th}) versus dead-volume ratio (K) for the ideal adiabatic model at different temperature ratios (X), showing Carnot efficiency

5.3 Optimal Allocation of Volume in LTD and MTD Engines

To better understand the effects of dead-volume ratio and the impact of volume allocation, a number of graphs have been plotted. The parameters analysed are namely the heater to cooler volume ratio (V_h/V_k), the swept volume ratio or compression space to expansion space volume ratio (V_c/V_e) and the regenerator to dead volume ratio (ζ). The effects of all these parameters are analysed at three different heater to cooler temperature ratios (X), namely: 1.25, 1.5 and 1.75.

5.3.1 Swept Volumes

The following section looks at the effect that swept volume ratio has on the engine specific work output and efficiency. Five different swept volume ratios are plotted on each graph, they are: 0.5, 0.6, 0.7, 0.8, 0.9 and 1.0.

Figures 5.7 and 5.8 are graphs of specific work output versus dead-volume ratio and efficiency versus dead-volume ratio. They show the effect of varying swept volume ratios at a heater to cooler temperature ratio of 1.25.

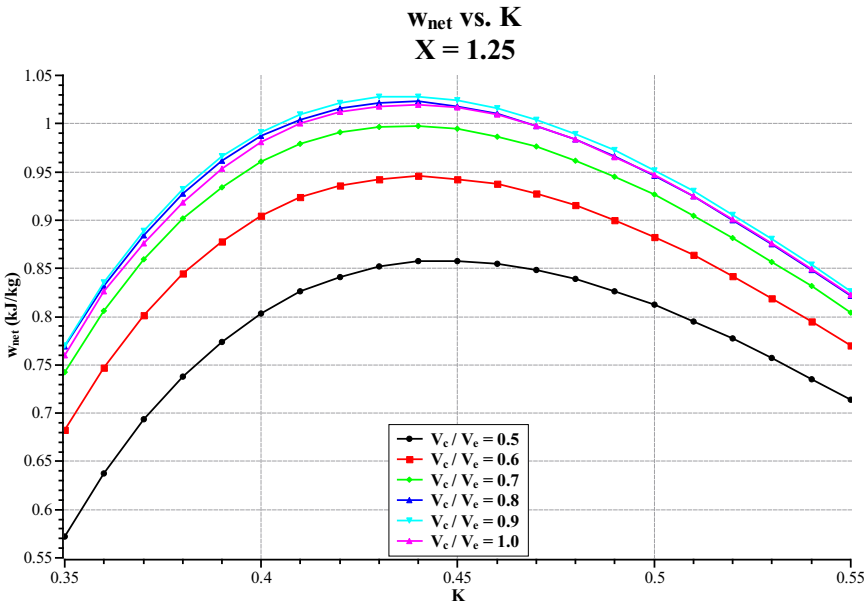

Figure 5.7: Specific work output (w_{net}) versus dead-volume ratio (K) for varying swept volume ratio (V_c/V_e) and $X = 1.25$

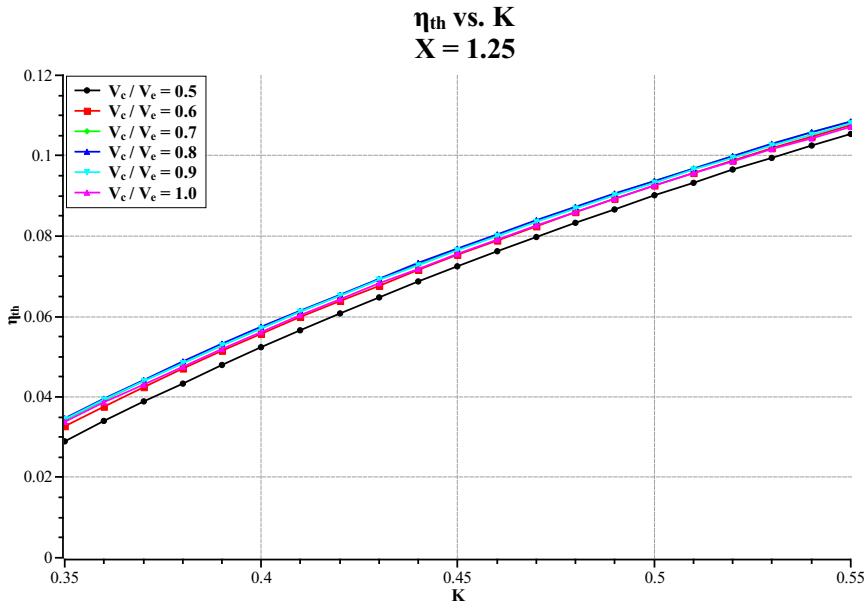

Figure 5.8: Efficiency (η_{th}) versus dead-volume ratio (K) for varying swept volume ratio (V_c/V_e) and $X = 1.25$

Figures 5.9 and 5.10 are graphs of specific work output versus dead-volume ratio and efficiency versus dead-volume ratio. They show the effect of varying swept volume ratios at a heater to cooler temperature ratio of 1.5.

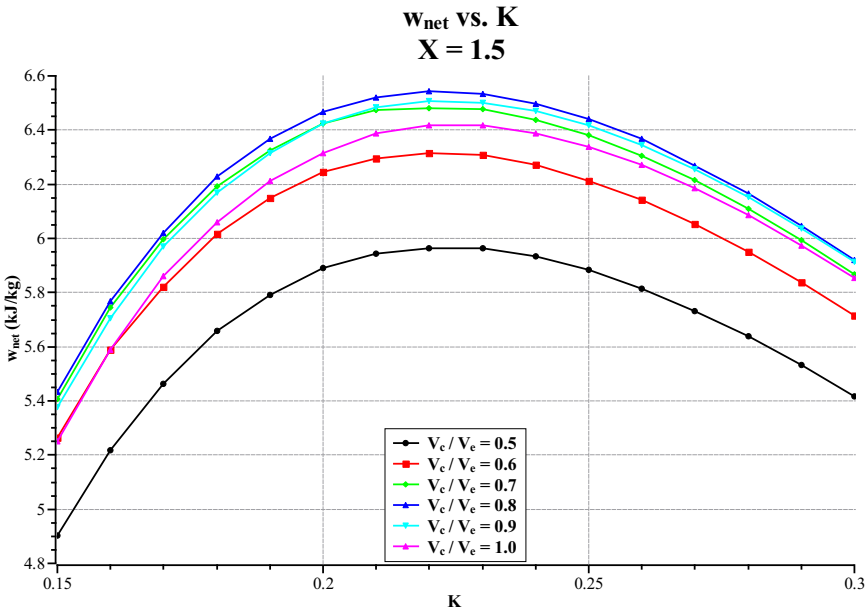

Figure 5.9: Specific work output (w_{net}) versus dead-volume ratio (K) for varying swept volume ratio (V_c/V_e) and $X = 1.5$

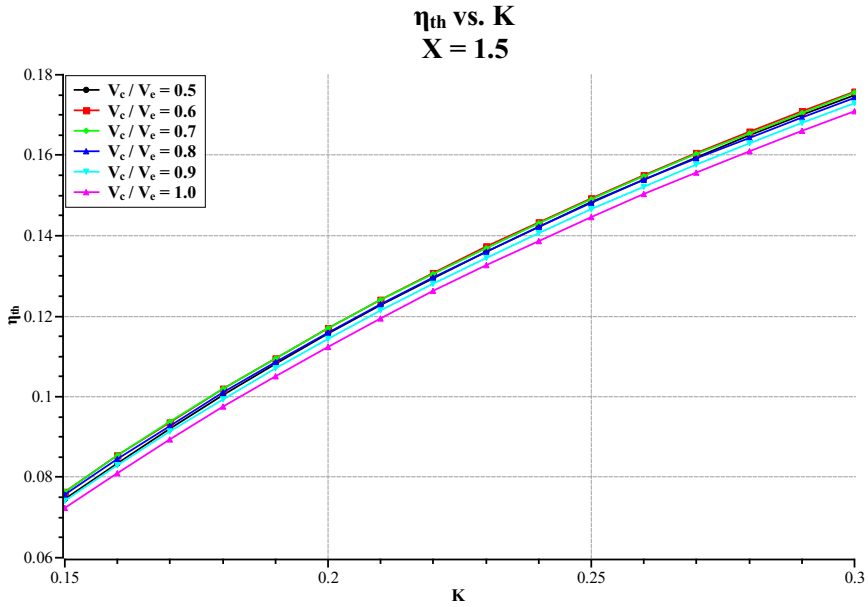

Figure 5.10: Efficiency (η_{th}) versus dead-volume ratio (K) for varying swept volume ratio (V_c/V_e) and $X = 1.5$

Figures 5.11 and 5.12 are graphs of specific work output versus dead-volume ratio and efficiency versus dead-volume ratio. They show the effect of varying swept volume ratios at a heater to cooler temperature ratio of 1.75.

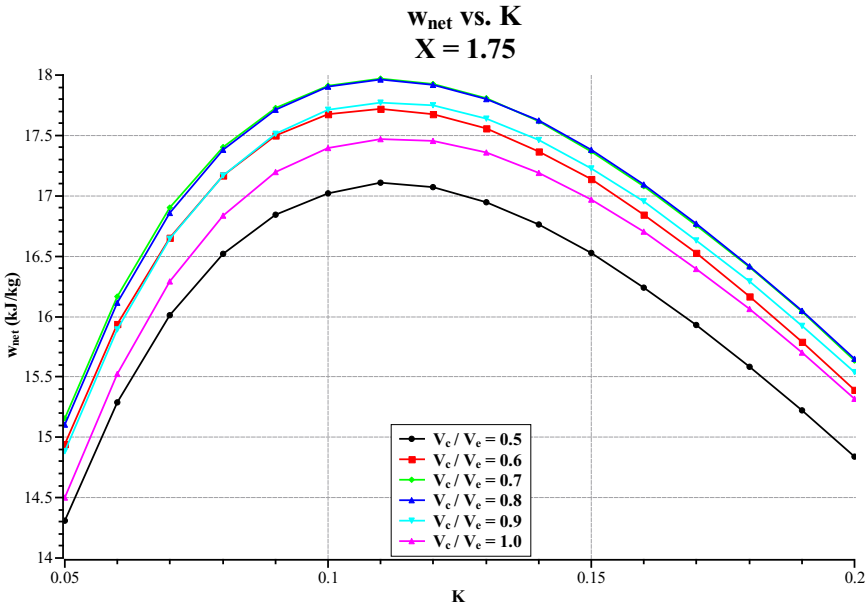

Figure 5.11: Specific work output (w_{net}) versus dead-volume ratio (K) for varying swept volume ratio (V_c/V_e) and $X = 1.75$

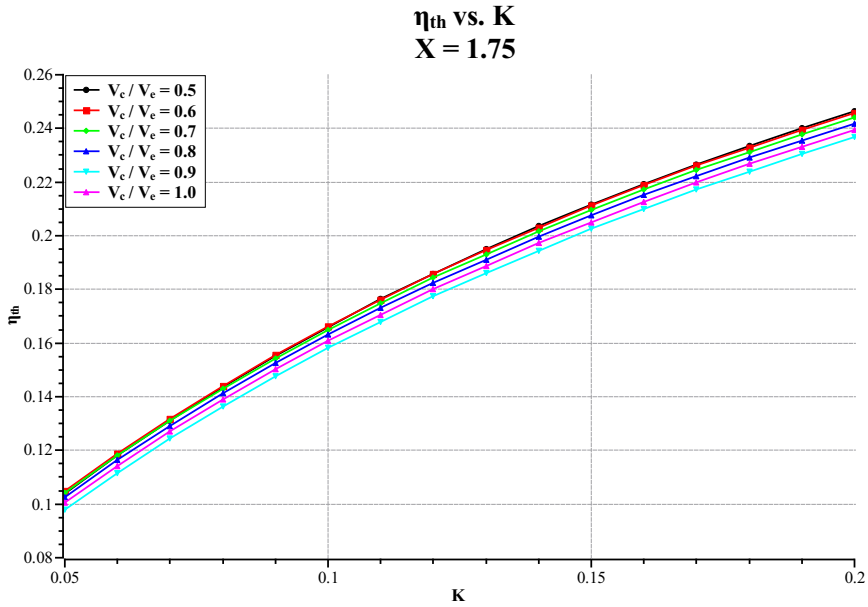

Figure 5.12: Efficiency (η_{th}) versus dead-volume ratio (K) for varying swept volume ratio (V_c/V_e) and $X = 1.75$

From figures 5.7 and 5.8 it can be seen that the optimal swept volume ratio for maximum specific work output is 0.9. Whereas, for maximum efficiency, the optimal swept volume ratio is 0.8.

From figures 5.9 and 5.10 it can be seen that the optimal swept volume ratio for maximum specific work output is 0.8. Whereas, for maximum efficiency, the optimal swept volume ratio is 0.6.

From figures 5.11 and 5.12 it can be seen that the optimal swept volume ratio for maximum specific work output is 0.7. Whereas, for maximum efficiency, the optimal swept volume ratio is 0.6.

5.3.2 Heat Exchanger Volumes

For each temperature ratio, the effects of the heater to cooler volume ratio and regenerator to dead-volume ratio are analysed. The heater to cooler volume ratios are: 0.25, 1.0 and 4.0 and the regenerator to dead-volume ratios are: 0.25, 0.5 and 0.75.

Figure 5.13 shows three specific work output versus dead-volume ratio plots for the case of a heater to cooler temperature ratio of 1.25. In the figure, each graph represents a different regenerator to dead-volume ratio, and each curve represents a different heater to cooler volume ratio.

Figure 5.14 shows three specific work output versus dead-volume ratio plots for the case of a heater to cooler temperature ratio of 1.5. In the figure, each graph represents a separate regenerator to dead-volume ratio, and each curve represents a different heater to cooler volume ratio.

Figure 5.15 shows three specific work output versus dead-volume ratio plots for the case of a heater to cooler temperature ratio of 1.75. In the figure, each graph represents a separate regenerator to dead-volume ratio, and each curve represents a different heater to cooler volume ratio.

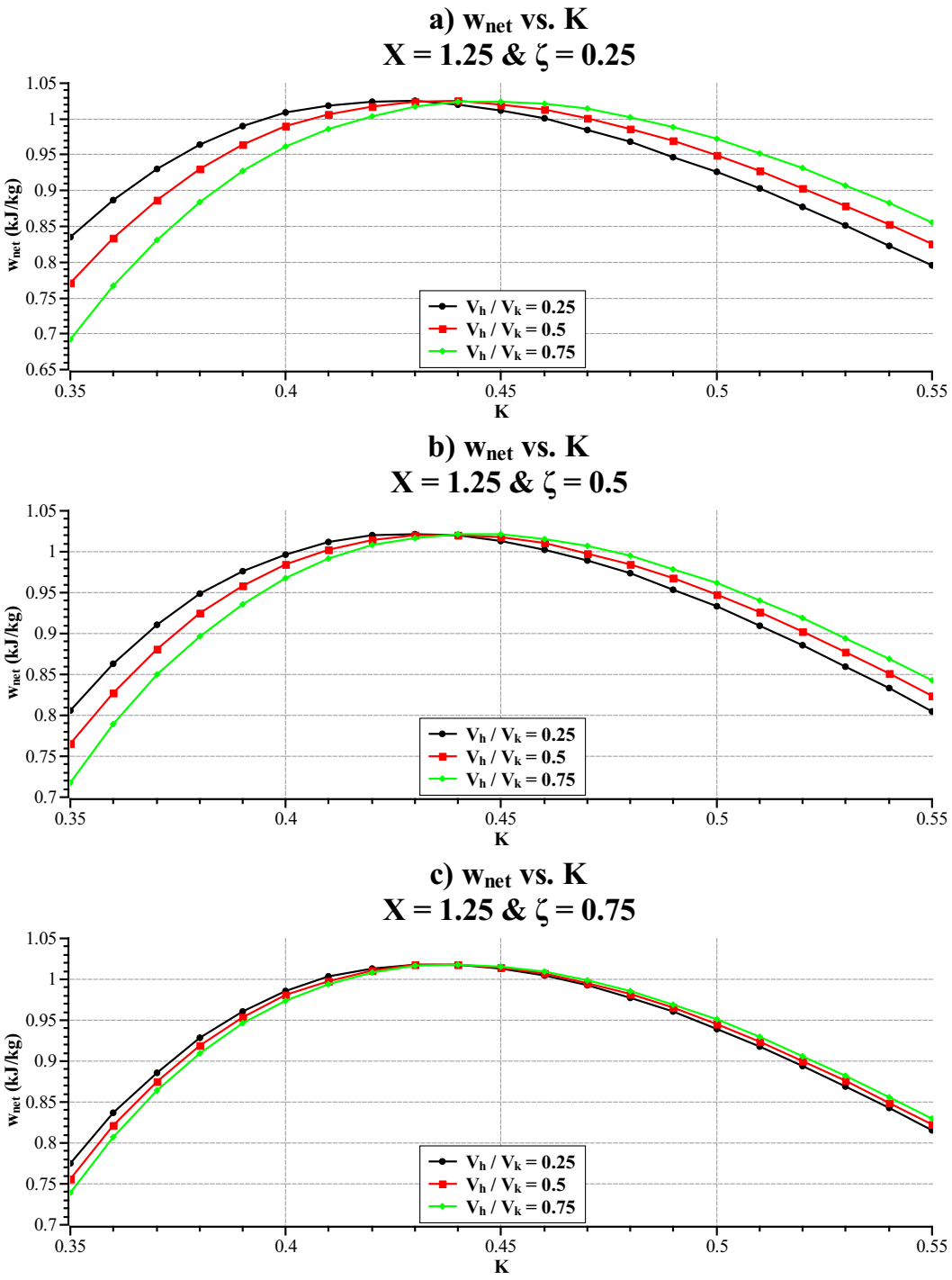

Figure 5.13: Specific work output (w_{net}) versus dead-volume ratio (K) for varying heater to cooler volume ratio (V_h/V_k), varying regenerator volume ratio (ζ) and $X = 1.25$

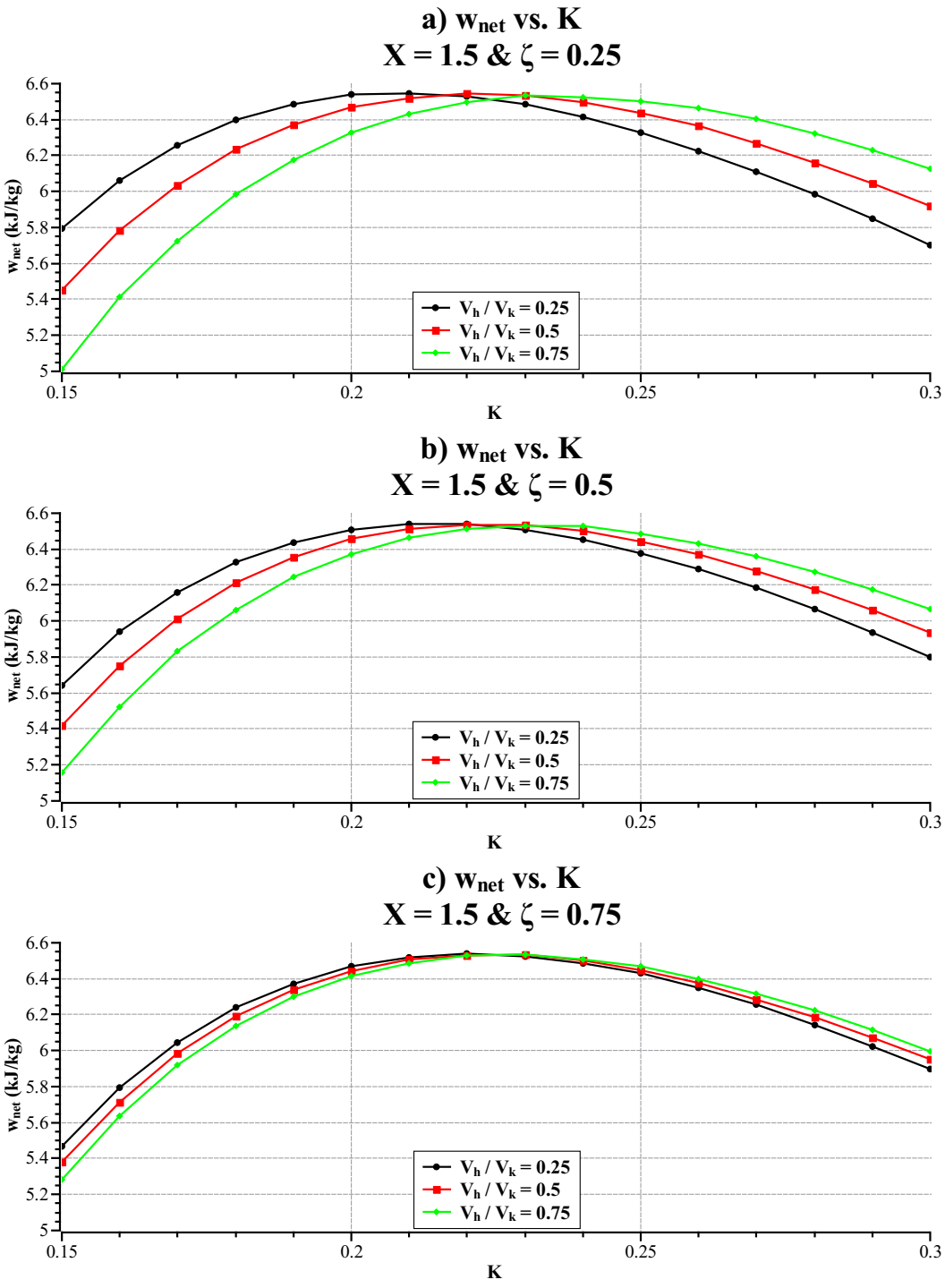

Figure 5.14: Specific work output (w_{net}) versus dead-volume ratio (K) for varying heater to cooler volume ratio (V_h/V_k), varying regenerator volume ratio (ζ) and $X = 1.5$

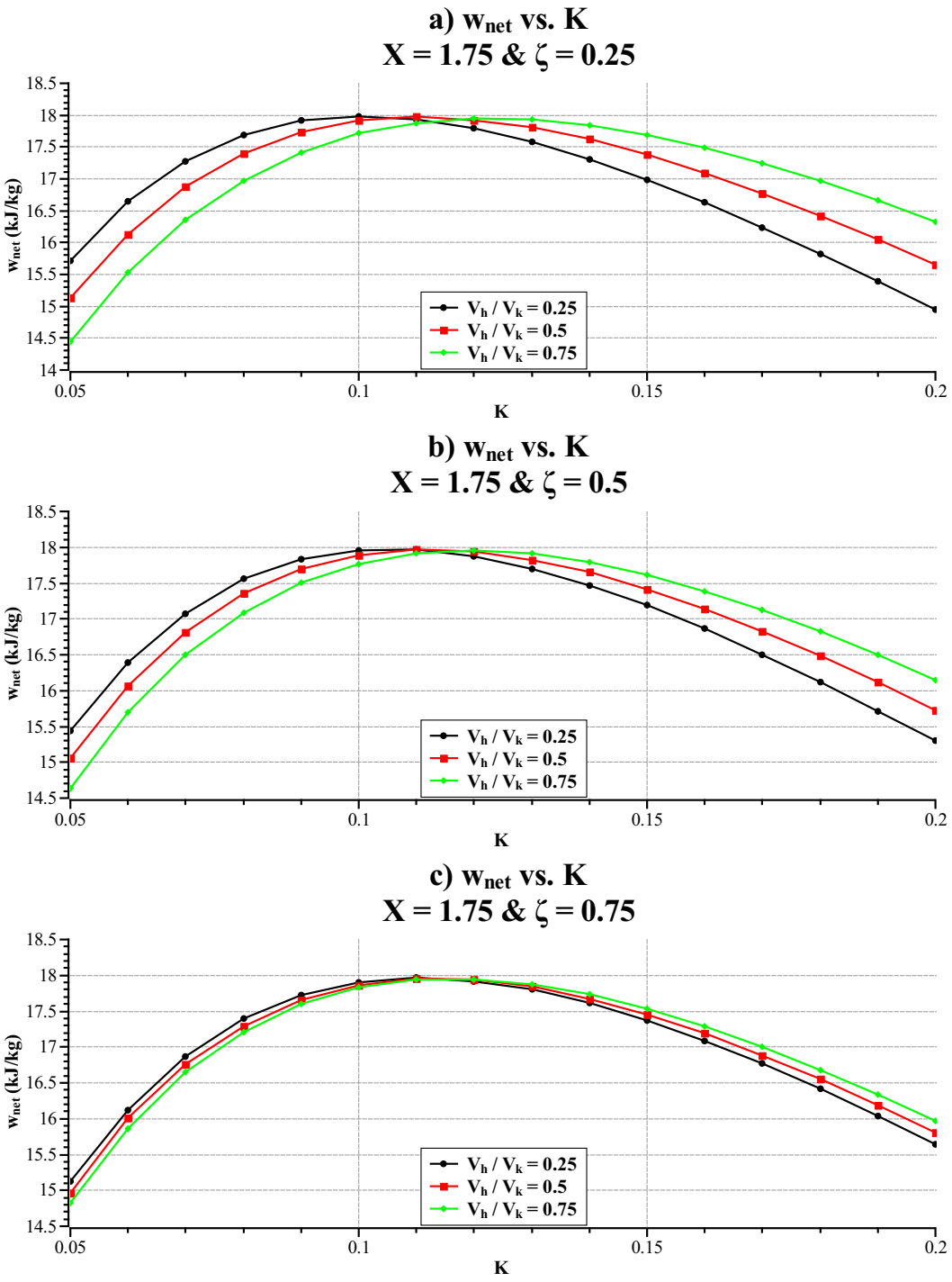

Figure 5.15: Specific work output (w_{net}) versus dead-volume ratio (K) for varying heater to cooler volume ratio (V_h/V_k), varying regenerator volume ratio (ζ) and $X = 1.75$

Figures 5.13, 5.14 and 5.15 illustrate the effect that the regenerator to dead-volume ratio and the heater to cooler volume ratio have on the optimal dead-volume ratio and the specific work output of the Stirling engine.

The regenerator to dead-volume ratio is seen to not affect the optimal dead-volume ratio for the case of a heater to cooler volume ratio of 1. It does, however, increase the effect of the heater to cooler volume ratio when it is not 1. There is an inverse relationship, the smaller the regenerator to dead-volume ratio the more significant the effect of the heater to cooler volume ratio and vice versa. The plots show that the heater to cooler volume ratio has a negligible impact on the maximum specific work output and only has a slight effect on the optimal dead-volume ratio. The influence that the heater to cooler volume ratio has becomes more pronounced at higher temperature ratios. Additionally, these results are seen to be largest when the dead-volume ratio moves away from optimal.

This is of significance for Stirling engine designers, as in practice the Stirling engine requires a high heat transfer rate in the cooler to keep the thermal efficiency high [109, 1]. It is shown in the graphs that the heater to cooler volume ratio can be chosen such that the cooler volume is far larger than the heater volume with negligible effect on the specific work output. This is only the case when the dead-volume ratio is at the optimal. Thus, higher surface area requirements in the cooler can be satisfied without introducing the substantial pressure drop associated with fine tube heat exchangers.

5.4 Optimal Dead-Volume Ratio for the LTD and MTD Cases

The following section looks at the optimisation of the Stirling cycle in terms of dead-volume ratio. As the ideal adiabatic model is considered a more accurate model of the real Stirling engine [116, 115], it is of importance to use this model when designing LTD and MTD engines. Figure 5.16 is a plot that shows the specific work output versus dead-volume ratio curves for different LTD and MTD heater to cooler temperature ratios. Also, the curve of optimal specific work output versus dead-volume ratio is shown.

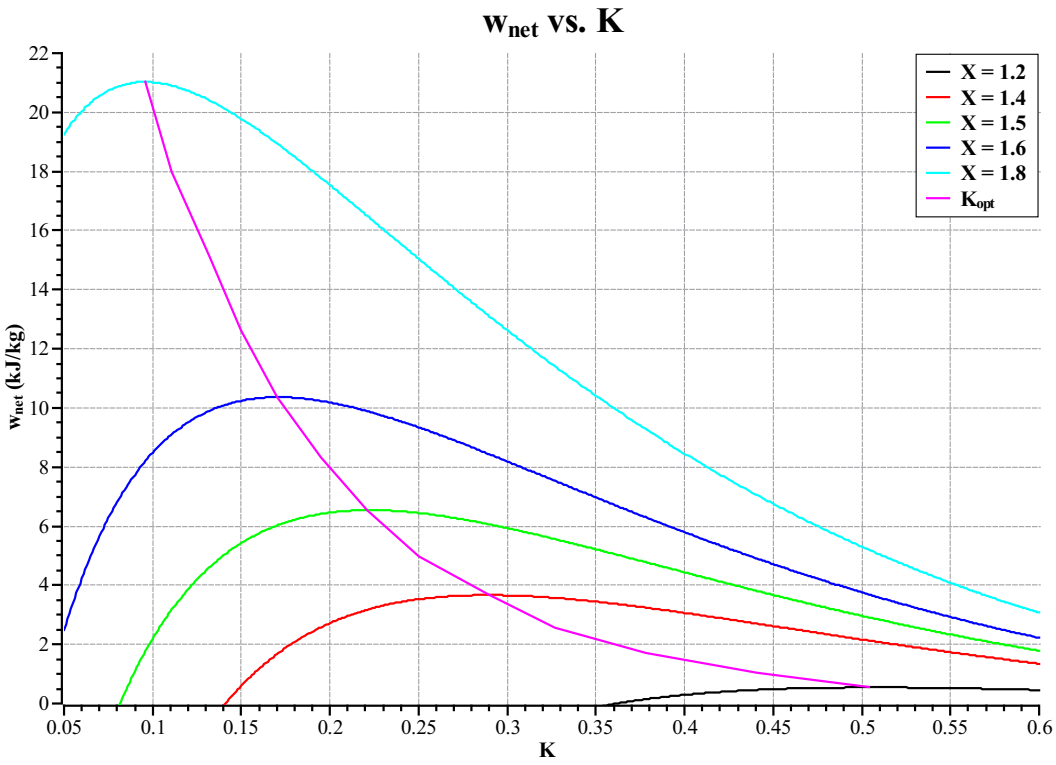

Figure 5.16: Specific work output (w_{net}) versus dead-volume ratio (K) for varying temperature ratio (X), showing the optimal specific work output curve

Figure 5.17 is a plot of optimal dead-volume ratio versus temperature ratio, using a logarithmic scale.

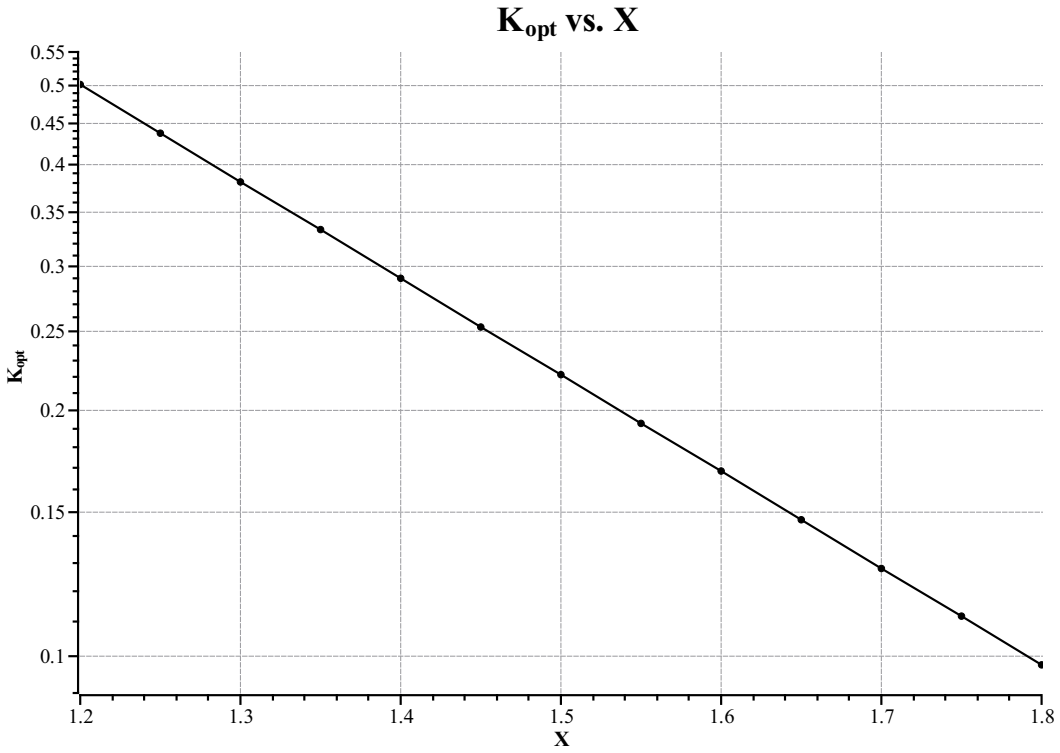

Figure 5.17: Optimal dead-volume ratio (K_{opt}) versus temperature ratio (X)

Figure 5.17 can be used by a thermal designer if he has a known heater to cooler working fluid temperature ratio. As is expected the plot shows that the optimal dead-volume ratio decreases with increasing heater to cooler temperature ratio.

5.5 Conclusion

The effects of dead-volume ratio on the performance of the ideal isothermal and ideal adiabatic models are presented and compared. The ideal adiabatic model which is considered a more accurate representation of real Stirling engines is then used to optimise the dead-volume ratio for maximum specific work output. Following this, the allocation of swept volume is optimised to maximise specific work output. Thus, insight into the effect that allocation of heat exchanger volume has on engine performance is gained.

The comparison of the results from the ideal isothermal and ideal adiabatic models has indicated that there is a difference in performance trends between the two models. The most notable differences being that the effect of dead-volume ratio on efficiency is seen to be the opposite. It is furthermore observed that at lower heater to cooler temperature ratios there exists an optimal dead-volume ratio that gives maximum specific work output. Whereas, for the ideal isothermal model there is not. From the investigation, it can be seen that the choice of the dead-volume ratio is an important decision for the Stirling engine designer, as it has a sizeable effect on engine performance. With LTD and MTD engines becoming of commercial interest it is imperative that these factors be taken into account as power density is an essential aspect of the design that needs to be considered. This is important to drive down cost and make these engines more economically competitive. Due to the low limiting efficiency of these engines, a big engine is required to produce significant power. Therefore, it is essential to optimise the engine for maximum power density because it represents a saving in cost and space. This chapter gives the reader valuable insight into the effect of the dead-volume ratio that is needed for the complete analysis and understanding of Stirling engines. In the coming chapters that look to analyse and optimise the Stirling engine, it is seen that changing design parameters can counter-intuitively impact the engine performance. This is usually due to the effects of dead-volume ratio, and these results are often overlooked.

Chapter 6

GPU-3 Stirling Engine Analysis

6.1 Introduction

The following chapter presents the analysis of the GPU-3 Stirling engine. This Stirling engine was developed in the 1960's and has been used extensively in Stirling engine analysis, as there is considerable experimental data that has been published.

This chapter aims to validate the model introduced in chapter 3 by comparing the results to the results from other numerical models and experimental efforts. The developed model is then used to analyse the sensitivity of GPU-3 engine performance to changing engine parameters.

6.2 The GPU-3 Stirling Engine Model

The GPU-3 Stirling engine (GPU - Ground Power Unit) is a Stirling engine generator that was developed by General Motors (GM) in 1965. The unit was developed for the United-States military and was designed to produce a maximum of 7.5 kW using hydrogen as the working fluid. The performance of the engine has been well documented in many technical reports produced by the NASA Lewis research centre [107, 105, 106]. These tests were conducted to map the engine performance under a wide variety of operating conditions using both hydrogen and helium as the working fluids. The test results used in the validation are those of the low baseline tests. The reason is that these are the results used in the models seen in the literature, which are compared to the model developed in this dissertation. The GPU-3 engine has been modelled in many studies [116, 110, 40, 115, 112, 113, 5]. Therefore,

the model presented in this dissertation can be validated by comparing the results to the results from these studies and experimental efforts. A diagram showing the GPU-3 Stirling engine and components can be seen as figure 6.1.

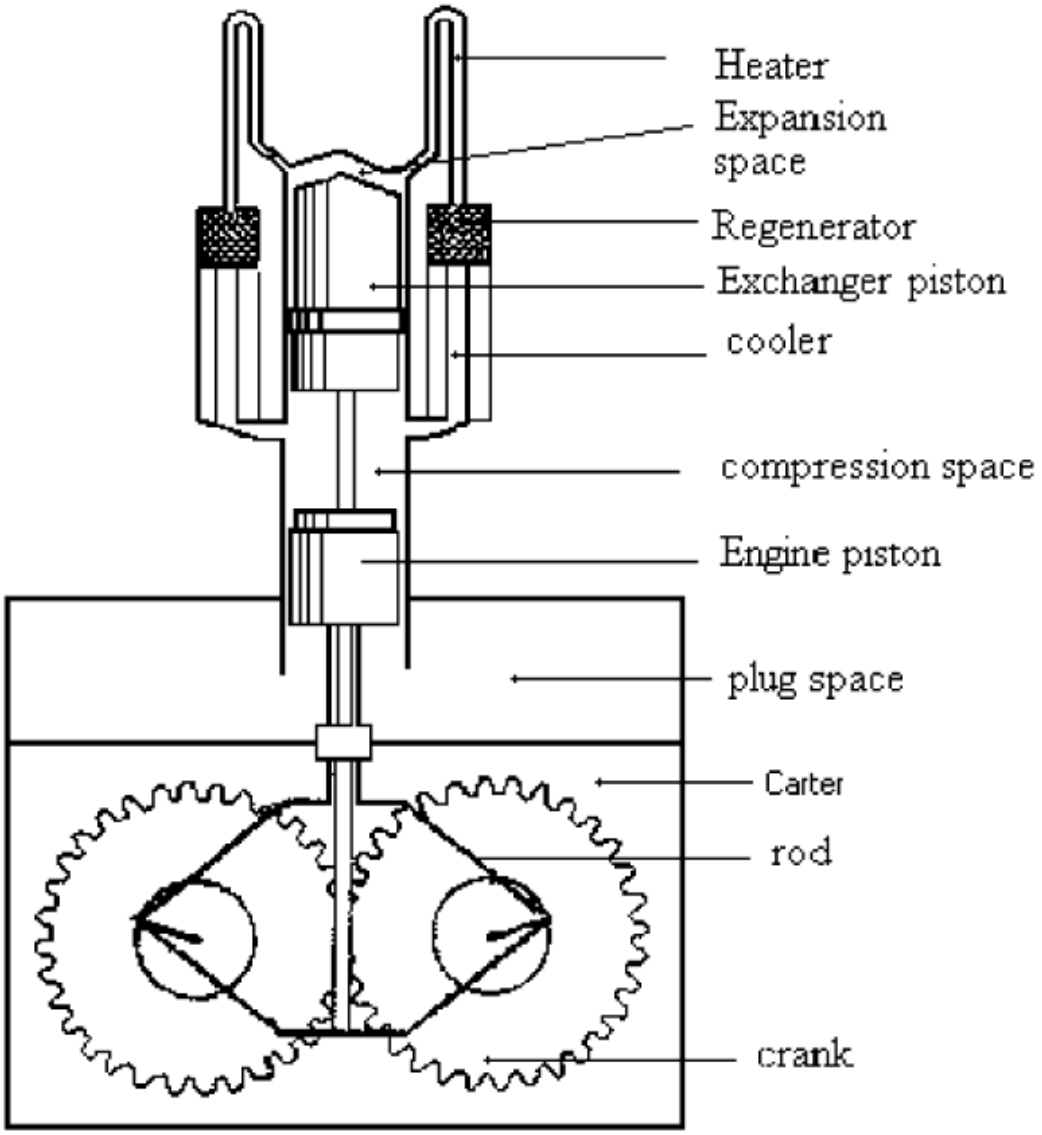

Figure 6.1: GPU-3 Stirling engine diagram showing labelled components [110]

Figure 6.1 shows that the GPU-3 Stirling engine utilises a unique drive mechanism, which is known as the Rhombic drive and was first developed in 1959 by Jan Meijer [71, 116]. At the time Meijer was working for Philips, a company conducting considerable research into Stirling engine design and optimisation. This drive mechanism was developed as a means of minimising gas leakage by reducing the force between the piston and cylinder walls.

Table 6.1 is a table of the operating conditions for the GPU-3 engine during the low power baseline tests.

Table 6.1: GPU-3 operating conditions [105]

Parameter	Symbol	Value	Units
Heater wall temperature	T_H	977	K
Cooler wall temperature	T_K	288	K
Operating frequency	f	41.72	Hz
Mean pressure	P_{mean}	4.13	MPa
Working fluid	-	Helium	-

To model the engine, the equations that describe the volume variation in the compression and expansion spaces need to be defined in terms of the engines geometric features. Figure 6.2 is a diagram showing the layout of the engine and the geometric features.

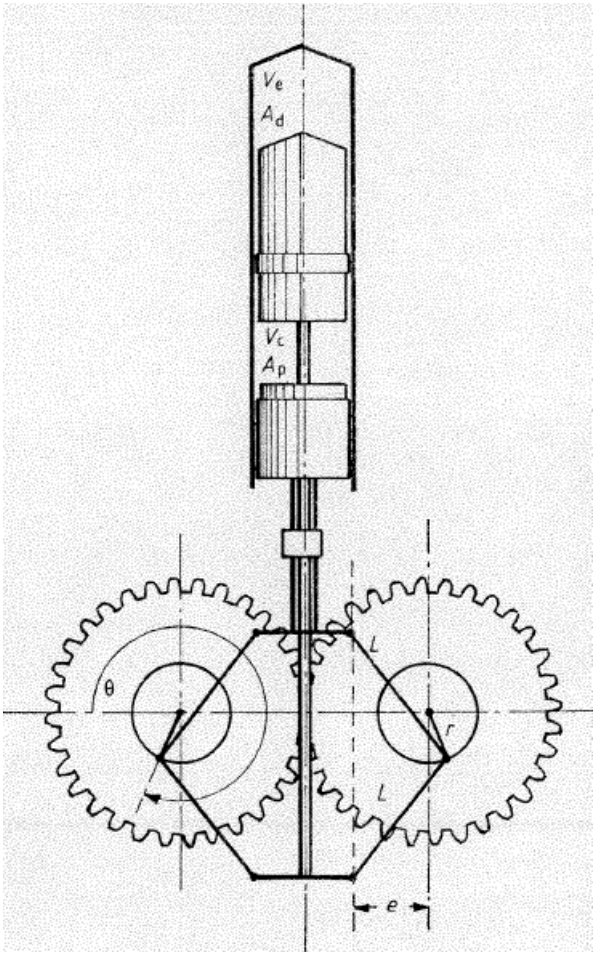

Figure 6.2: GPU-3 Stirling engine diagram showing dimensions [116]

The following three equations are used to simplify the expressions for expansion and compression space volume and volume differential, these expressions are for b_1, b_2 and b_θ seen below:

$$b_1 = \sqrt{L^2 - (e-r)^2} \quad ; \quad b_2 = \sqrt{(L-r)^2 - e^2} \quad ; \quad b_\theta = \sqrt{L^2 - (e + r\cos(\theta))^2}$$

Equations 6.1 and 6.2 are the equations which describe the volumes in the compression space and expansion space respectively.

$$V_c = V_{ccl} + 2A_p(b_1 - b_\theta) \tag{6.1}$$

$$V_e = V_{ecl} + A_d(b_\theta - b_2 - r\sin\theta) \tag{6.2}$$

Equations 6.3 and 6.4 are the equations which describe the volume differentials in the compression space and expansion space respectively.

$$\frac{dV_c}{d\theta} = -\frac{2A_p r\sin(\theta)(e + r\cos(\theta))}{b_\theta} \tag{6.3}$$

$$\frac{dV_e}{d\theta} = -\frac{dV_c}{d\theta}\frac{A_d}{2A_p} - A_d r\cos(\theta) \tag{6.4}$$

Table 6.2 is the table of the GPU-3 Stirling engine dimensions and component properties that are used in the numerical model.

Table 6.2: GPU-3 engine dimensions [116]

Parameter	Value	Units	Parameter	Value	Units
Clearance volumes			Cooler		
Compression space	28.68	cm^3	Number of tubes	312	-
Expansion space	30.52	cm^3	Tube diameter	1.08	mm
Swept Volumes			Tube length	46.1	mm
Compression space	114.13	cm^3	Heat transfer length	35.5	mm
Expansion space	120.82	cm^3	Void volume	13.18	cm^3
Heater			Regenerator		
Number of tubes	40	-	Number of units	8	-
Tube diameter	3.02	mm	Diameter	22.6	mm
Tube length	245.6	mm	Length	22.6	mm
Heat transfer length	155.4	mm	Porosity	0.697	-
Void volume	70.28	cm^3	Wire diameter	40	μm
			Thermal conductivity	15	$W.m^{-1}K^{-1}$
			Void volume	50.55	cm^3

Table 6.2 gives the dimensions of the GPU-3 Stirling engine. These dimensions are input into the model outlined in chapter 3, to calculate the performance of the engine. In the analysis, the constant wall temperature assumption is made and used to calculate the rate of entropy generation and the engine performance.

6.3 Model Results

The following section outlines the results of the GPU-3 Stirling engine simulation for the baseline test and compares the result to other numerical and experimental results.

Figure 6.3 is a plot of pressure versus volume for the compression and expansion spaces.

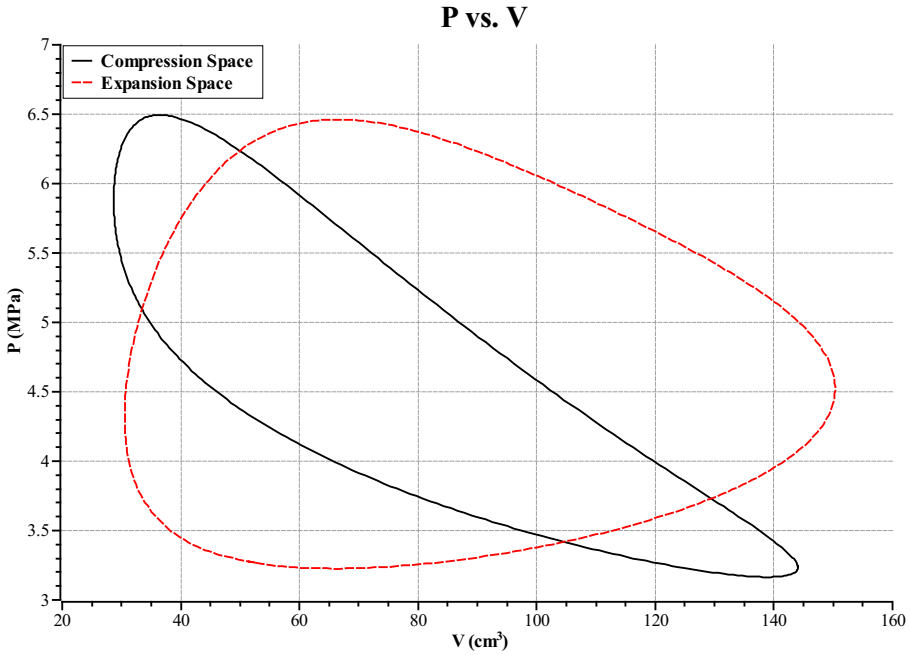

Figure 6.3: Pressure (P) versus volume (V) for the GPU-3 Stirling engine

Figure 6.3 shows the two pressure-volume curves, each one for a different compartment. It can be seen that the area encompassed by expansion space curve is larger than the compression space curve, thus indicating a positive work output per cycle.

Figure 6.4 is a plot of pressure versus crank angle for the compression and expansion spaces.

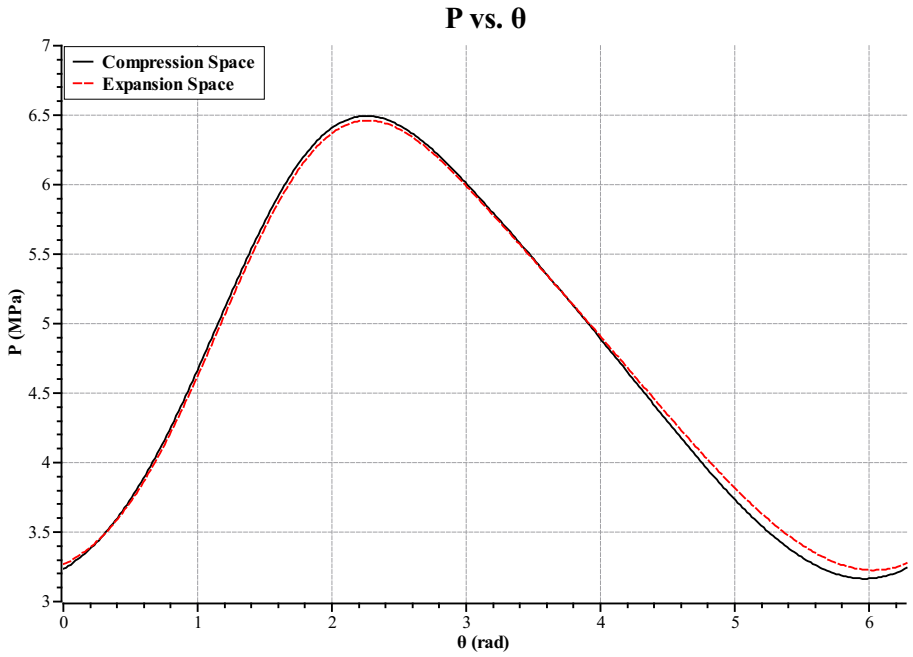

Figure 6.4: Pressure (P) versus crank angle (θ) for the GPU-3 Stirling engine

From figures 6.4 it can be seen that the pressure drop is low compared to the change in pressure with crank angle. It can also be seen that to allow for the flow of working fluid between the spaces at maximum engine pressure, the pressure in the compression space is higher than in the expansion space. When at the minimum pressure the pressure in the expansion space is higher than in the compression space, as this facilitates flow in the opposite direction.

These graphs are comparable with the figures for the actual GPU-3 Stirling engine. This result is expected, as the results are generated in the same way as in the quasi-steady flow approach [116, 115]. This model has been extensively experimentally validated and is one of the most cited Stirling engine analyses seen in the literature. The model also predicts the average heat exchanger gas temperatures, seen in table 6.3.

Table 6.3: Heat exchanger gas temperatures

Output	Value	Units
Heater gas temperature	887.86	K
Cooler gas temperature	341.09	K

To compare the results of the different approaches, the definition of work output using the method proposed by Urieli and Berchowitz needs to be defined [116, 115]. The description of work output is the work produced over a cycle, minus the pumping power consumed by the engine due to the pressure drop through the heat exchangers. This formulation of work output will be used to compare the results and validate the exergy analysis approach. The equation for cyclic work output as defined by Urieli and Berchowitz in their SIMPLE analysis can be seen as equation 6.5.

$$W = W_i - \Delta W = \oint P(dV_c + dV_e) - \oint \sum \Delta P dV_e \tag{6.5}$$

Table 6.4 shows the performance of the model in this study compared to other models in the literature.

Table 6.4: Model comparison

Description	Power (W)	Efficiency (%)
Adiabatic Model	8286.7	62.0
Urieli and Berchowitz	7400	53.1
Timoumi dynamic model	6372.4	53.3
Urieli and Berchowitz Quasi-Steady flow	6700	52.5
Timoumi Dynamic Best Model	4273	38.5
Experimental Results	3958	35.0
Current Model 2nd Law	**5736.4**	**43.0**
Current Model 1st Law (SIMPLE)	**5969.8**	**44.7**

Table 6.4 shows that the model used compares well with the models seen in the literature. When comparing the results to the experimental results, it can be seen that the first law approach (SIMPLE) predicts the power output within 50.8 % and the second law within 44.9 %. Concerning efficiency the first law (SIMPLE) approach predicts the efficiency within 27.7 % and the second law within 22.9 %. These discrepancies while significant are far better than the predictions of other Stirling engine models. There are many reasons for the difference between the model results and the experimental results, one of the most significant is that none of the models take into account the mechanical losses. The steady flow heat transfer relations are also seen to overestimate the heat transfer coefficients in the heater and the cooler. It is important to mention that the application of the exergy analysis approach to a Stirling engine numerical model is the first of its kind, and the results show that it performs better than many other approaches to Stirling engine modelling and compares well with the experimental results.

6.4 Performance Analysis

The following section presents the analysis and optimisation of the GPU-3 Stirling engine. The section looks at the impact that changes in working fluid mass, engine speed and regenerator dimensions have on the engine performance.

6.4.1 Mass of Working Fluid

Figure 6.5 is a plot of power output and efficiency versus the mass of working fluid.

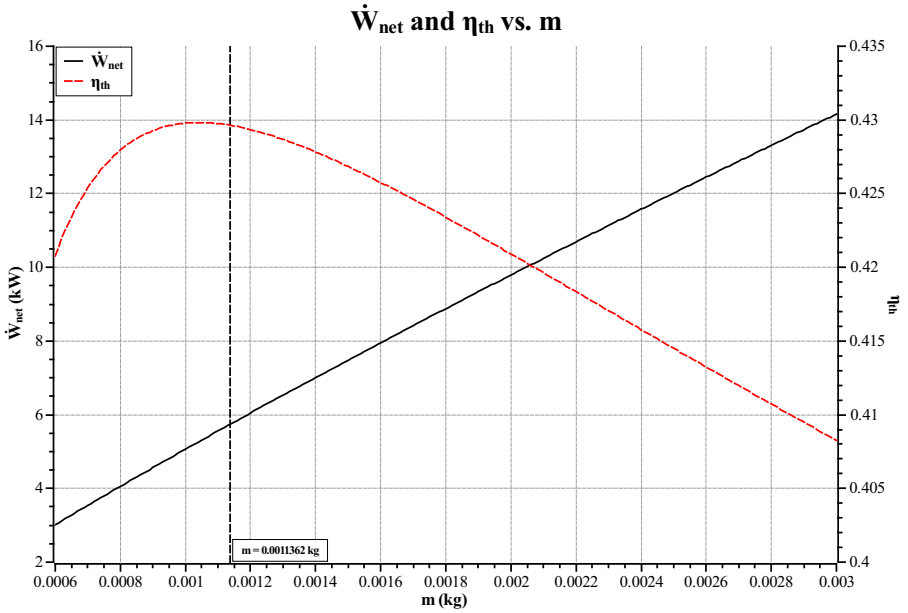

Figure 6.5: Power output ($\dot{W}_{net}$) and efficiency (η_{th}) versus the mass of working fluid (m) for the GPU-3 Stirling engine

From figure 6.5 it can be seen that the power output increases with increasing working fluid mass and that there is an optimal working fluid mass that gives maximum efficiency. The increase in power output due to the increase in mass of working fluid is caused by the increase in mass flow rate through the heat exchangers. This results in more energy being absorbed and rejected in the heater and cooler. However, there is a trade-off as the increased mass flow rate increases the irreversibility rate. The optimal efficiency occurs when the ratio of irreversibility rate to energy input is at a minimum, and this occurs when the irreversibility rates are balanced relative to the input energy. The portion of the curve before the optimal point is where the irreversibility rate is low in the regenerator and high in the heater and cooler. This is because the regenerator effectiveness is high and the pressure drop is low.

However, the mass flow rates in the heater and cooler are low, and the temperature difference between the working fluid and the heat exchanger walls is high. The portion of the curve after the optimal is where the irreversibility rates in the heater and cooler are low because the mass flow rates are high and the temperature difference between the working fluid and heat exchanger walls is decreased. However, the irreversibility rate in the regenerator is high due to the lower effectiveness and significant pressure drop. It is important to note that after the optimal efficiency point the irreversibility rates in the heater and cooler decrease up until a point, after which the rate of entropy generation becomes pressure drop dominant and the irreversibility rate increases.

Figure 6.6 is a plot of irreversibility to energy input ratio and energy rates versus the mass of working fluid.

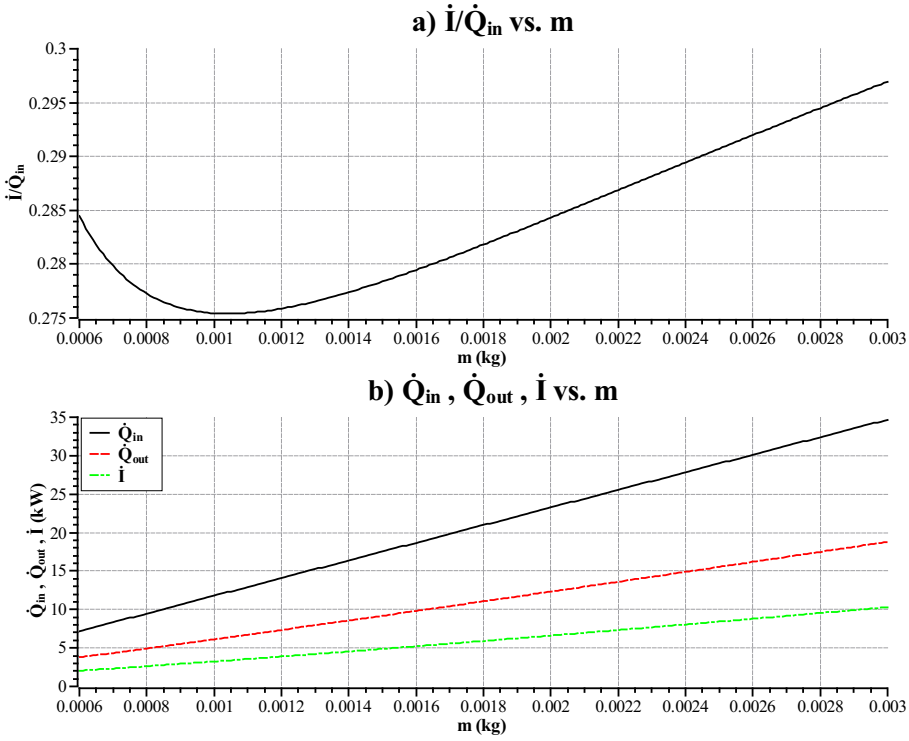

Figure 6.6: Ratio of irreversibility to input energy ($\dot{I}/\dot{Q}_{in}$) and energy rates ($\dot{Q}_{in}$,$\dot{Q}_{out}$,$\dot{I}$) versus the mass of working fluid (m) for the GPU-3 Stirling engine

From figure 6.6 the optimal ratio of irreversibility to input energy can be seen. This optimal corresponds to a working fluid mass of 0.0011 kg and can be seen to correspond to the maximum efficiency point.

6.4.2 Operating Frequency

Figure 6.7 is a plot of power output and efficiency versus operating frequency.

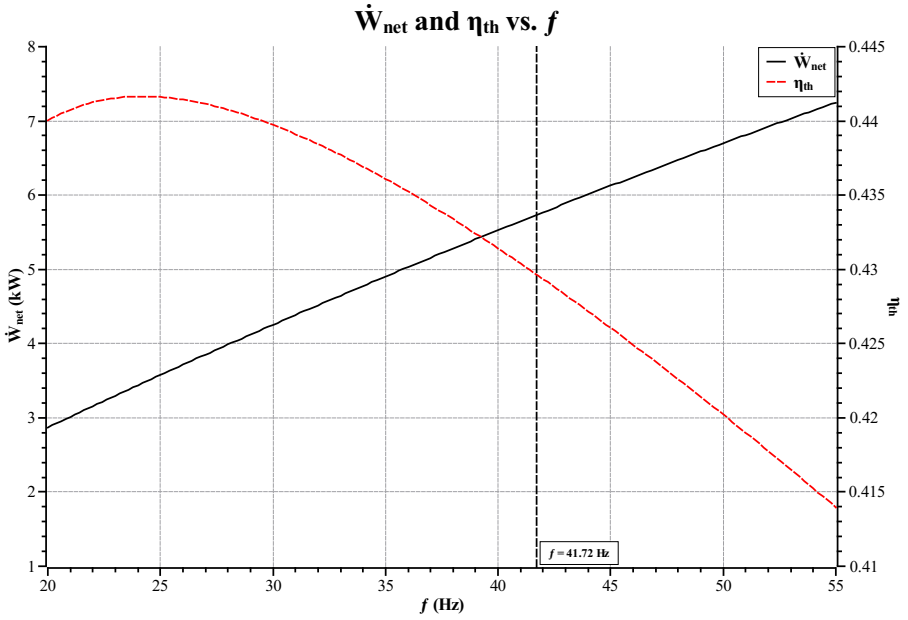

Figure 6.7: Power output ($\dot{W}_{net}$) and efficiency (η_{th}) versus operating frequency (f) for the GPU-3 Stirling engine

From figure 6.7 it can be seen that the power increases and the efficiency decreases with increasing operating frequency. It is also seen that there is an optimal operating frequency for maximum efficiency. This effect is due to the mass flow rates in the heat exchangers, which was mentioned in the previous subsection. At the optimal efficiency point, the irreversibility rates in all the Stirling engine components are balanced such that the ratio of irreversibility rate to energy input is a minimum. Before the optimal point, the irreversibility rate in the regenerator is low, but the irreversibility rates in the heater and cooler are high. Whereas, after the optimal point the irreversibility rate in the regenerator is high and the irreversibility rates in the heater and cooler are low. This occurs up until the point at which the entropy generation due to pressure drop becomes dominant.

This plot shows how the engine operating frequency can be changed during operation to change the performance characteristics of the engine. The device can be designed for high-efficiency steady state operation and then when there is a higher demand for power the engine speed can be increased to meet the demand. However, there will be a decrease in engine efficiency.

Figure 6.8 is a plot of irreversibility to energy input ratio and energy rates versus operating frequency.

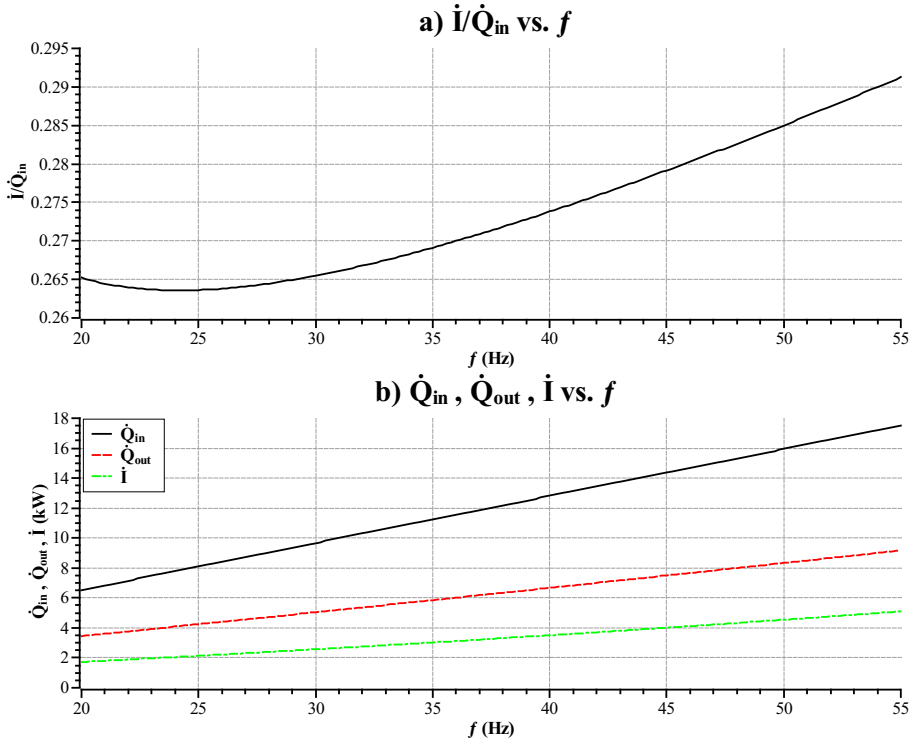

Figure 6.8: Ratio of irreversibility to input energy ($\dot{I}/\dot{Q}_{in}$) and energy rates ($\dot{Q}_{in}$,$\dot{Q}_{out}$,$\dot{I}$) versus operating frequency (f) for the GPU-3 Stirling engine

From figure 6.8 the optimal ratio of irreversibility to input energy can be seen. This optimal corresponds to an operating frequency of 24 Hz and can be seen to correspond to the maximum efficiency point. The analysis shows that the tests resulted in an operating frequency that was significantly higher than the maximum efficiency operating point. This would have been due to the alternator used, as the power produced by the engine and consumed by the alternator must be equal for there to be steady state operation. It is also important to mention that the mechanical losses due to friction are a function of engine speed and in this model mechanical losses have not been included. Therefore, the increase in operating frequency may not increase the power output by as much as is predicted.

6.4.3 Regenerator Dimensions

The regenerator has a significant impact on engine performance. Therefore the effect of these dimensions on engine performance has been analysed.

Figure 6.9 is a plot of power output and efficiency versus regenerator length.

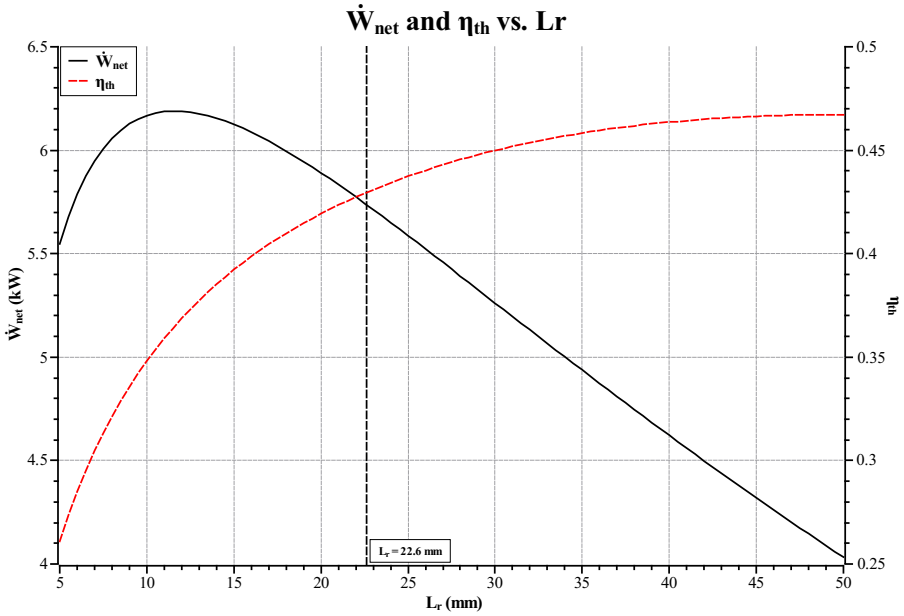

Figure 6.9: Power output ($\dot{W}_{net}$) and efficiency (η_{th}) versus regenerator length (L_r) for the GPU-3 Stirling engine

From figure 6.9 it can be seen that there is an optimal regenerator length for maximum power output. It is also seen that this doesn't correspond to the maximum for efficiency, as the efficiency is seen to increase with increasing regenerator length.

The reason for the optimal power output is that as the regenerator length increases the effectiveness of the regenerator increases, however the pressure drop through the regenerator also increases. The dead-volume ratio is also seen to increase with increasing regenerator length, which as shown in chapter 5 decreases the power output and increases the efficiency.

Concerning the power output before the optimal point, increasing the regenerator length results in an increase in power output as the increase in regenerator effectiveness decreases the loads in the heater and cooler. Increasing the regenerator length also increases the dead-volume ratio and pressure drop, which both reduce power output. However, the increased regenerator effectiveness has the more significant impact on performance. After the optimal

point, the power output decreases as the effects of the dead-volume and pressure drop become dominant over the effect of increased regenerator effectiveness, thus decreasing power output.

Concerning the efficiency, increasing the length of the regenerator increases the dead-volume ratio and the regenerator effectiveness, which both improve the efficiency. This is why there is a difference between the optimal power output and the optimal efficiency points. It is seen that the regenerator length chosen for the engine by the designers is a trade-off between the optimal power output point and optimal efficiency point.

Figure 6.10 is a plot of power output and efficiency versus regenerator diameter.

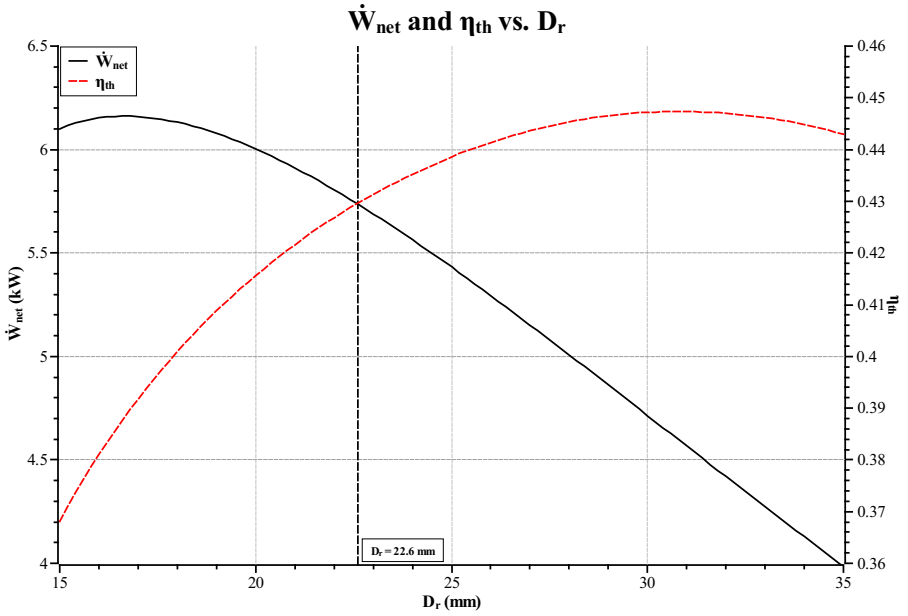

Figure 6.10: Power output ($\dot{W}_{net}$) and efficiency (η_{th}) versus regenerator diameter (D_r) for the GPU-3 Stirling engine

From figure 6.10 it can be seen that there is an optimal regenerator diameter that gives maximum power output.

As the regenerator diameter increases the dead-volume increases, however, the mass flow rate per unit area decreases resulting in a higher effectiveness and lower pressure drop. Before the optimal regenerator diameter that gives maximum power output, increasing the diameter increases the effectiveness and decreases pressure drop, such that the negative impact of dead-volume is outweighed. Whereas, after this point, the dead-volume effect dominates and the power output decreases. Concerning the efficiency, increasing the diameter increases

the effectiveness, decreases pressure drop and increases the dead-volume - improving engine efficiency. It is seen that the regenerator diameter chosen for the engine by the designers is a trade-off between the optimal power output point and optimal efficiency point.

Figure 6.11 is a plot of power output and efficiency versus regenerator mesh porosity.

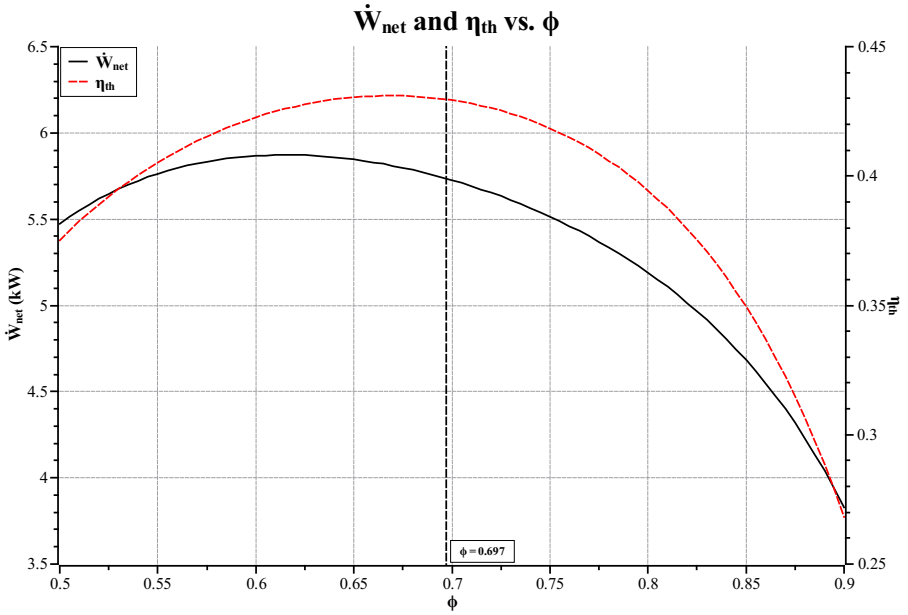

Figure 6.11: Power output ($\dot{W}_{net}$) and efficiency (η_{th}) versus regenerator mesh porosity (ϕ) for the GPU-3 Stirling engine

From figure 6.11 it can be seen that there is an optimal regenerator mesh porosity for maximum power output and for maximum efficiency. It can also be seen that these design points are close together.

The porosity of the regenerator mesh is seen to have a significant impact on engine performance. The porosity affects the hydraulic diameter of the mesh, the dead-volume, the gas velocity, heat transfer surface area, and effectiveness [110]. The power output and the efficiency decrease with increasing porosity as the effectiveness of the regenerator decreases. Therefore, it is better to have a regenerator of lower porosity, however, when the porosity gets too small the pressure drop increases, decreasing performance. Thus, an optimal regenerator porosity exists.

Figure 6.12 is a plot of power output and efficiency versus regenerator mesh wire diameter.

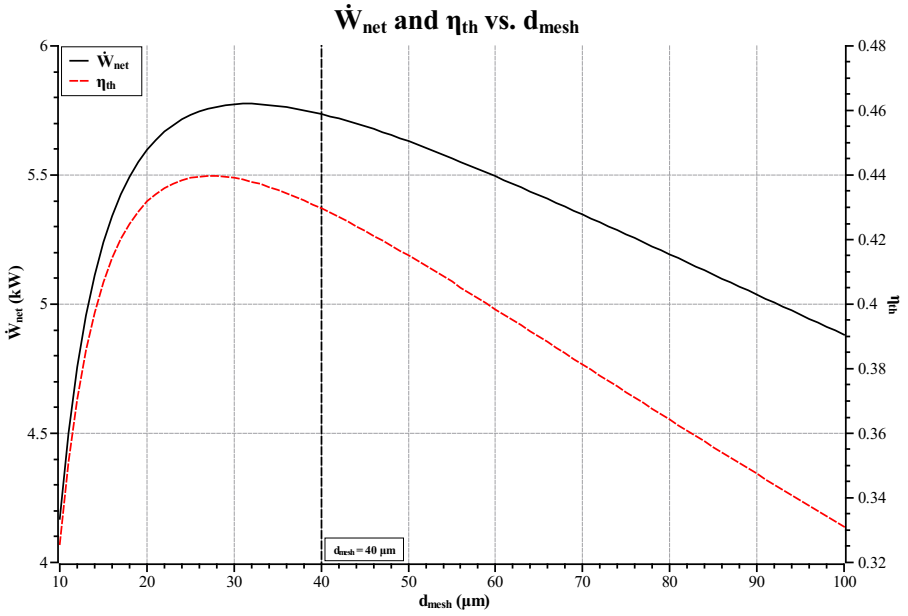

Figure 6.12: Power output ($\dot{W}_{net}$) and efficiency (η_{th}) versus regenerator mesh wire diameter (d_{mesh}) for the GPU-3 Stirling engine

From figure 6.12 it can be seen that there is an optimal regenerator mesh wire diameter for maximum power output and maximum efficiency.

The analysis shows that an optimal regenerator mesh wire diameter exists, as changing the regenerator mesh wire diameter changes the hydraulic diameter of the regenerator. Therefore, it directly influences the pressure drop and the heat transfer characteristics of the regenerator. The optimal values are seen to be sharp and very close together between 20 μm and 40 μm. The reason for this decrease in performance at the lower mesh wire diameters is due to the increased pressure drop associated with fine meshes. At the larger mesh wire diameters, the pressure drop is decreased which in turn increases performance. However, increasing the mesh wire diameter also decreases heat transfer rate, which increases irreversibility rate and causes an overall decrease in engine performance.

Wire mesh screens used in Stirling engines are usually manufactured at a fixed diameter and porosity. The significant impact of these parameters on performance should, therefore be considered in Stirling engine design so that the engine is optimised around these parameters. This approach is seen in chapter 7, where the regenerator mesh type is specified, and the rest of the engine geometry is optimised around this.

6.5 Conclusion

This chapter presented the analysis of the GPU-3 Stirling engine. The analysis showed the impact that different engine parameters have on performance and how changing the operating frequency or mass of working fluid can vary the performance characteristic depending on whether maximum efficiency or maximum power output is required. The analysis also shows where the engine design can be improved, as the engine has low power output when compared to internal combustion engines of a similar size.

From the model, it can be seen that the optimal operating point is different depending on whether the desired performance is for maximum power output or maximum efficiency. This result makes sense from a finite time and finite size engine standpoint, as in the literature it is acknowledged that the maximum power and maximum efficiency design points are very different [90]. In these cases, the literature suggests using the Ecological function as a basis for optimisation, as it is the tradeoff between maximum power output and maximum efficiency [23]. In the case of the GPU-3 Stirling engine, if maximum power output is required the best way to increase the performance is to increase the mass of working fluid in the engine as it will increase the power output. However, it will also decrease the efficiency. Another way to significantly alter the engine performance is to change the engine operating frequency. Increasing the operating frequency increases the power output of the engine and decreases the efficiency. Reducing the operating frequency, decreases the power output but increases efficiency. The geometry of the regenerator can also be changed to optimise performance. However, these parameters cannot be changed during operation like the mass of working fluid and operating frequency. The regenerator length and diameter are complex design parameters as they affect the efficiency and power output differently which makes optimising them difficult. Therefore, it is crucial to optimise these geometric features when desired efficiency and power output is known, or if the cost of the engine and cost of operation can be combined to calculate the levelised cost of electricity (LCOE), which can then be minimised.

In future, this approach can be used with more intricate loss mechanisms included to more accurately predict engine performance and refine the design parameters further. Due to the existence of the maximum efficiency and maximum power output points, it is quite straightforward to see that a Pareto optimal set exists from which an optimal solution can be selected.

Chapter 7

Exergy Analysis of the Stirling Cycle

7.1 Introduction

The following chapter introduces the exergy analysis of the alpha, and beta type Stirling engines. The chapter aims to apply the exergy analysis methodology to the numerical model of the Stirling engine and use this model to optimise the engine geometry for maximum power output using the implicit filtering algorithm. This approach has been applied to highly idealised Stirling engine mathematical models, however, these idealised models don't accurately predict the mass flow rates through the engine or the heat loads.

The chapter presents and explains the results of the optimisation of the 1000 cm^3 alpha and beta type Stirling engines. The results of the optimisation are presented as optimal values for several design parameters, at several source temperatures. The reason the engines are optimised for maximum power output is that Stirling engines have been cited as suffering from poor power density when compared to other power cycles. Therefore, optimising the engine for maximum power output is of economic interest. In the analysis only the alpha and beta type engines are analysed, the reason for this is that beta and gamma-type engines are very similar and it is assumed that the optimal design for the beta type engine holds for a gamma type engine of the same initial specifications.

In this optimisation, the size of the engine (total volume) is constrained, and the input energy is allowed to float. The reason for this is that if the engine size were allowed to float the engine would get exceptionally large, and operate at a very low operating frequency. This optimal solution to the design problem is not of interest as the engine would be economically uncompetitive. Therefore, the engine size is constrained, and it is optimised for maximum

power output. The numerical example shown is one that would be used in the initial Stirling engine design phase. This period in the design stage is when there is limited knowledge about the design of the engine, but the existence of optimal solutions can still be found to narrow down the design scope, and thus decrease the time and cost of testing and conducting a complex multi-dimensional analysis.

7.2 Numerical Example

The following example was chosen as a means of applying the exergy analysis methodology described in chapter 3 and to show the optimisation procedure described in chapter 4. The numerical example represents a case where the total volume of the Stirling engine is fixed, the working fluid is assumed to be air and to behave as an ideal gas, the regenerator thermal conductivity is known, and the heat capacity rates of the hot and cold streams are known. The numerical example chosen has the following parameters seen in table 7.1, these parameters were chosen based on the values for the GPU-3 Stirling engine [107, 105, 106].

Table 7.1: Table of parameters used in the numerical example

Symbol	Description	Value	Units
N_h	Number of heater tubes	100	-
N_k	Number of cooler tubes	300	-
P_{mean}	Mean engine pressure	5	MPa
A_r/A_c	Regenerator to heat exchanger flow area ratio	8	-
C_h	Source heat capacity rate	0.25	$kJ.K^{-1}$
C_k	Sink heat capacity rate	0.25	$kJ.K^{-1}$
C_p	Constant pressure specific heat	1.005	$kJ.kg^{-1}.K^{-1}$
C_v	Constant volume specific heat	0.718	$kJ.kg^{-1}.K^{-1}$
γ	Ratio of specific heats	1.4	-
T_{K1} & T_0	Sink temperature	298	K
R	Ideal gas constant	0.287	$kJ.kg^{-1}.K^{-1}$
Pr	Prandtl number	0.71	-
k	Regenerator thermal conductivity	0.05	$kJ.m^{-1}.K^{-1}$
L	Total heat exchanger length	300	mm
α	Phase angle	$\pi/2$	rad

The values seen in table 7.1 are fixed values that are assumed to be known before the optimisation of the engine. Using these values the other parameters are optimised to give maximum power output.

The values to be optimised are listed in table 7.2.

Table 7.2: Table of parameters to be optimised

Symbol	Description	Units
K	Dead-volume ratio	-
L_r	Regenerator length	mm
L_h	Heater tube length	mm
L_k	Cooler tube length	mm
V_c	Compression space volume	cm^3
V_e	Expansion space volume	cm^3
f	Operating frequency	Hz

These values are illustrated in the diagrams of the alpha and beta type engines, which are seen as figures 7.1 and 7.2 respectively.

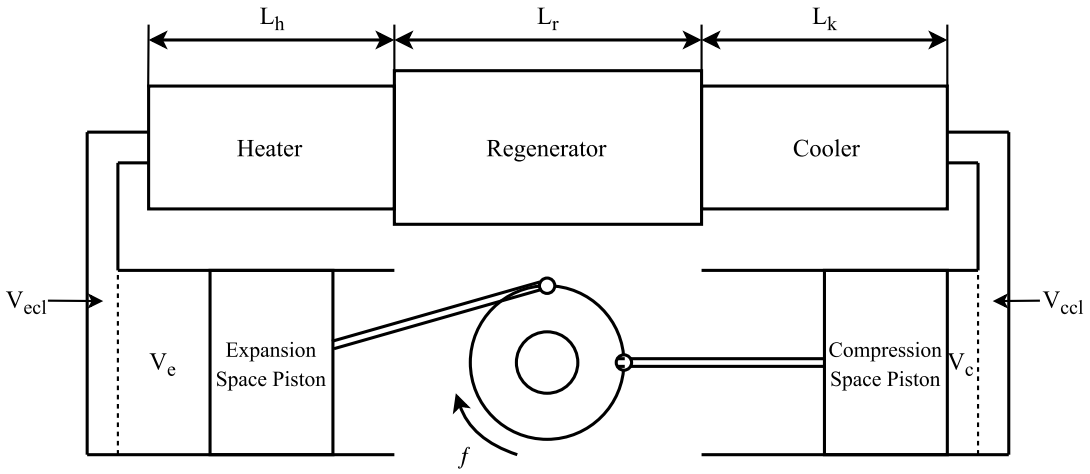

Figure 7.1: Schematic of the alpha type engine showing the variables to be optimised

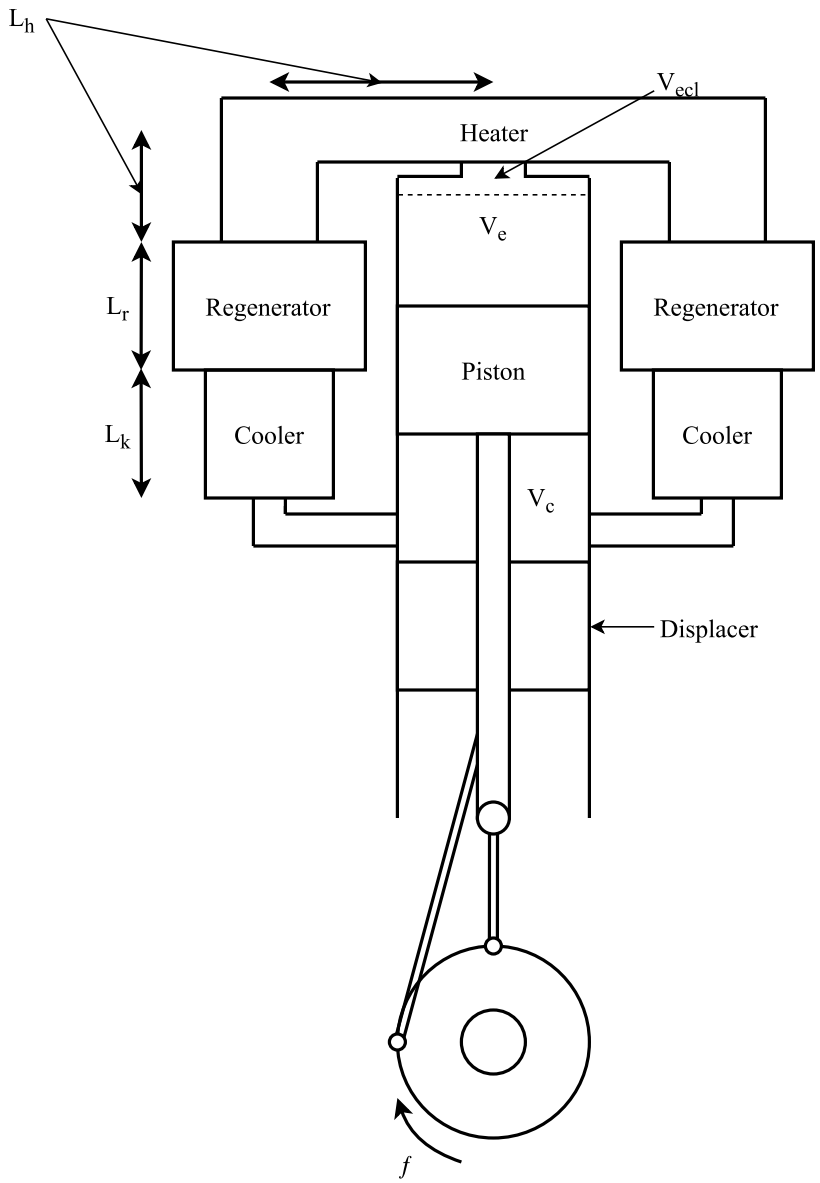

Figure 7.2: Schematic of the beta type engine showing the variables to be optimised

7.3 Optimisation

The following section presents the results of the exergy analysis and optimisation of the Stirling engine, for a range of source temperatures. Different optimal engine parameters are presented and discussed in each subsection. Each plot contains four curves, each representing a different regenerator mesh type. The regenerator mesh data was obtained from [104] and the empirical flow relations are known to hold for these mesh types.

7.3.1 Power Output

Figure 7.3 is a plot of power output versus source temperature for the alpha and beta type Stirling engines.

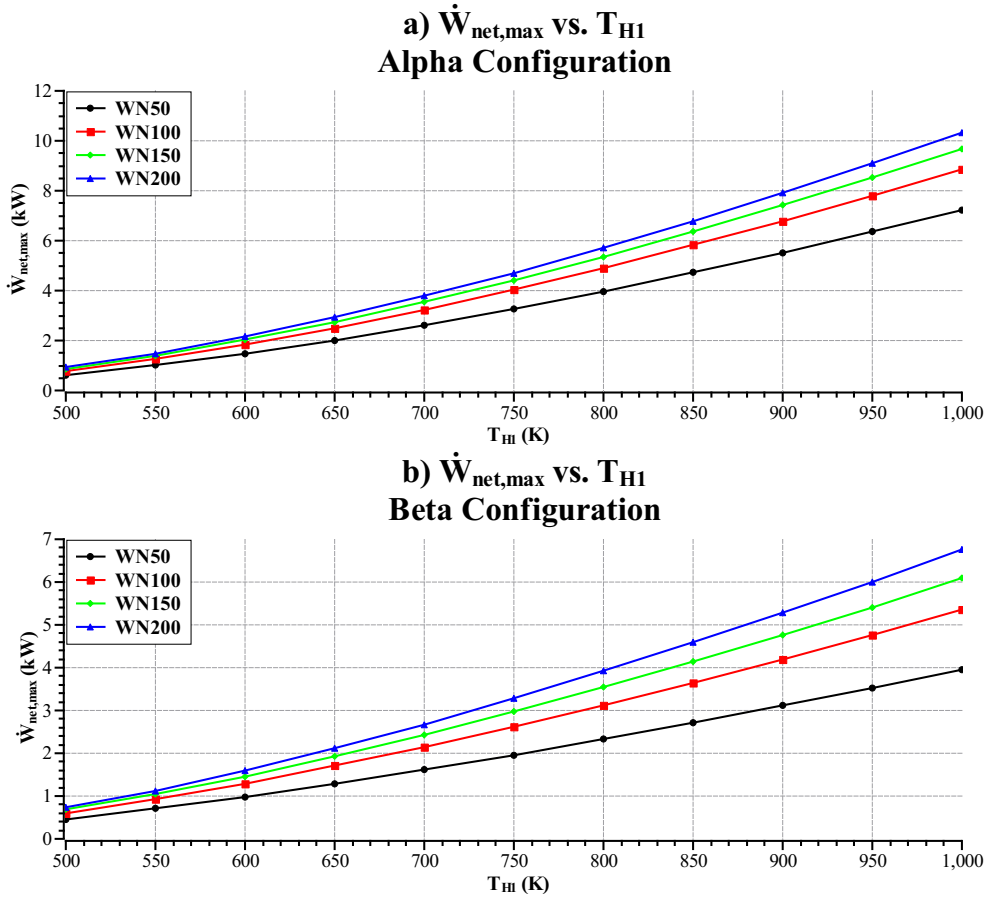

Figure 7.3: Maximum power output ($\dot{W}_{net,max}$) versus source temperature (T_{H1})

From figure 7.3 it is seen that the alpha type Stirling engine offers a higher power output than the beta type Stirling engine. The reason for this is that the alpha type Stirling engine configuration allows for an optimal swept volume ratio, greater heat exchanger volume and greater optimal operating frequency. The plot also shows that the WN200 mesh type offers the best performance from a maximum power output perspective. The reason for this is that the WN200 mesh is the finest mesh and therefore provides the highest heat transfer area per unit volume which gives a far shorter regenerator and thus a smaller pressure drop and greater regenerator effectiveness. The smaller regenerator also means that there is less void volume which means more of the available dead-volume can be allocated to the heater

and cooler, thus increasing the performance of these heat exchangers and increasing the performance of the engine as a whole.

7.3.2 Efficiency

Figure 7.4 is a plot of efficiency at maximum power output versus source temperature for the alpha and beta type Stirling engines.

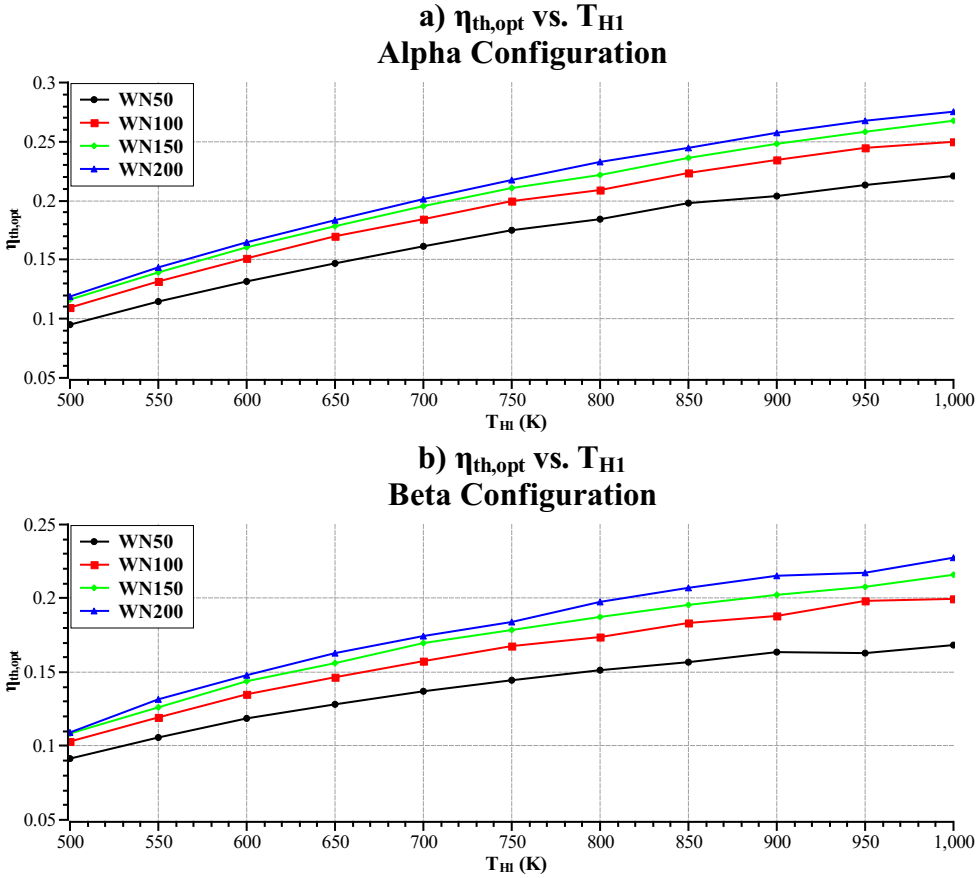

Figure 7.4: Efficiency at maximum power output ($\eta_{th,opt}$) versus source temperature (T_{H1})

From figure 7.4 it can be seen that the efficiency of Stirling engine is low considering the source temperature. The reason for this is that the engines are optimised for maximum power output which means these efficiencies represent the lowest efficiency design point in the Pareto optimal set of solutions. The alpha type Stirling engine yields a higher efficiency than the beta type Stirling engine. However, the difference in performance is not as pronounced as the difference seen in the case of power. Additionally, it can be seen that from an efficiency perspective the thermal bridging loss has an effect on the performance at lower

source temperatures. The reason for this is that the optimal cross-sectional area of the regenerator becomes larger increasing the thermal bridging loss between the hot and cold compartments which is due to there being more area for heat to conduct through. This loss is the reason the efficiency curves for the WN150 and WN200 mesh types appear to converge at the lower source temperatures.

7.3.3 Heat Exchanger Effectiveness

The following subsection presents the plots of optimal heat exchanger effectiveness versus source temperature for the four different mesh types. These effectivenesses are calculated using the flow relations seen in chapter 3.

Figure 7.5 is a plot of optimal regenerator effectiveness versus source temperature for the alpha and beta type Stirling engines.

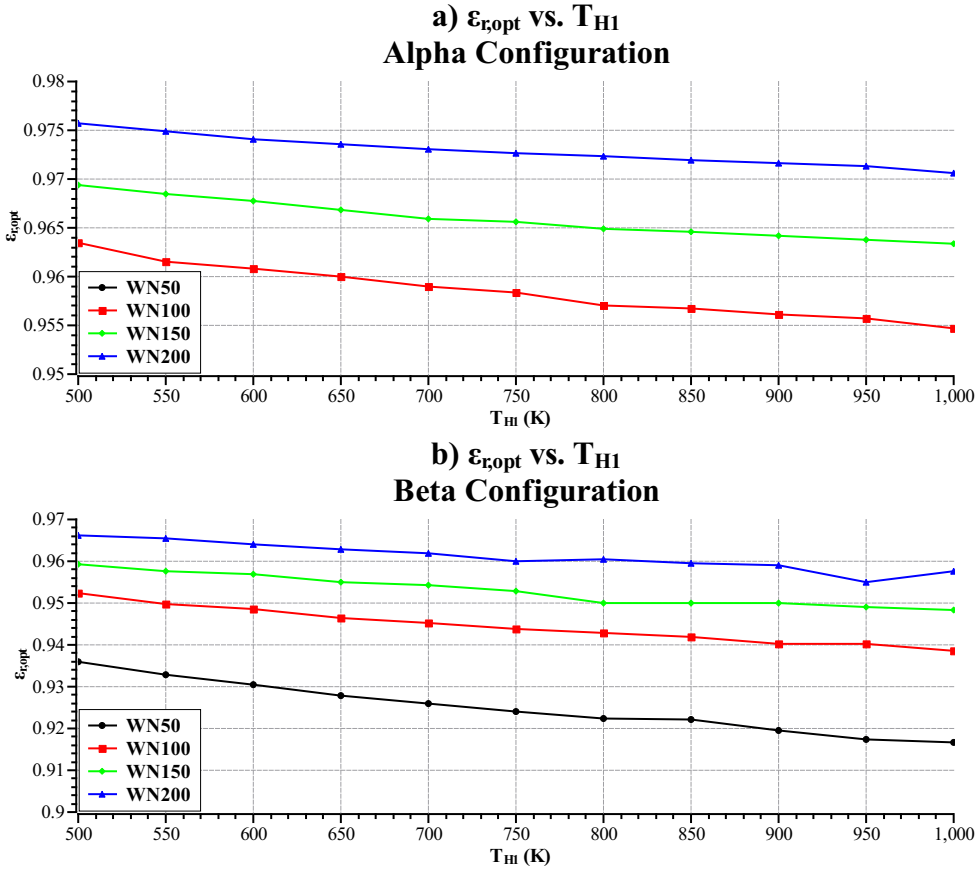

Figure 7.5: Optimal regenerator effectiveness ($\varepsilon_{r,opt}$) versus source temperature (T_{H1})

From figure 7.5 it can be seen that the effectiveness of the regenerator is very high in all cases and that at optimal Stirling engine operating conditions the regenerator effectiveness is the most influential parameter. When the configuration of the engine is allowed to float, the design will always 'morph' towards a design point with a high regenerator effectiveness. This result is evident when comparing the three plots, figures 7.5, 7.6 and 7.7 as it can be seen that in all cases the effectiveness of the regenerator is significantly higher than that of the cooler and heater.

Figure 7.6 is a plot of optimal cooler effectiveness versus source temperature for the alpha and beta type Stirling engines.

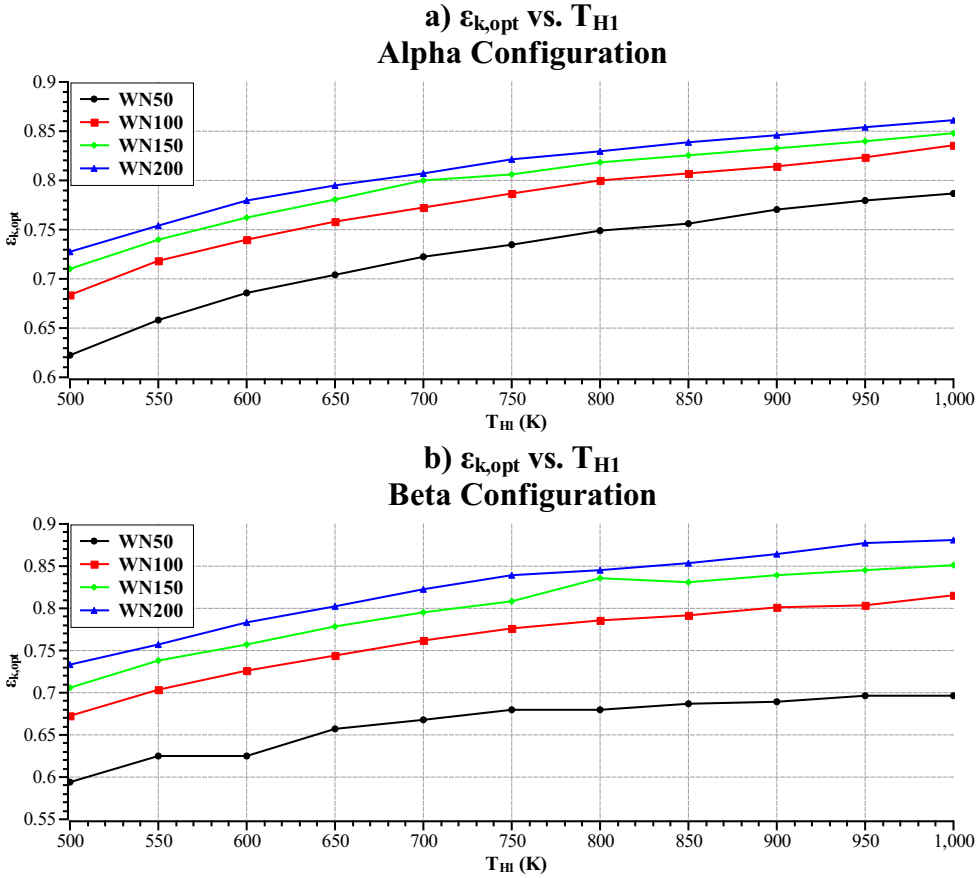

Figure 7.6: Optimal cooler effectiveness ($\varepsilon_{k,opt}$) versus source temperature (T_{H1})

Figure 7.7 is a plot of optimal heater effectiveness versus source temperature for the alpha and beta type Stirling engines.

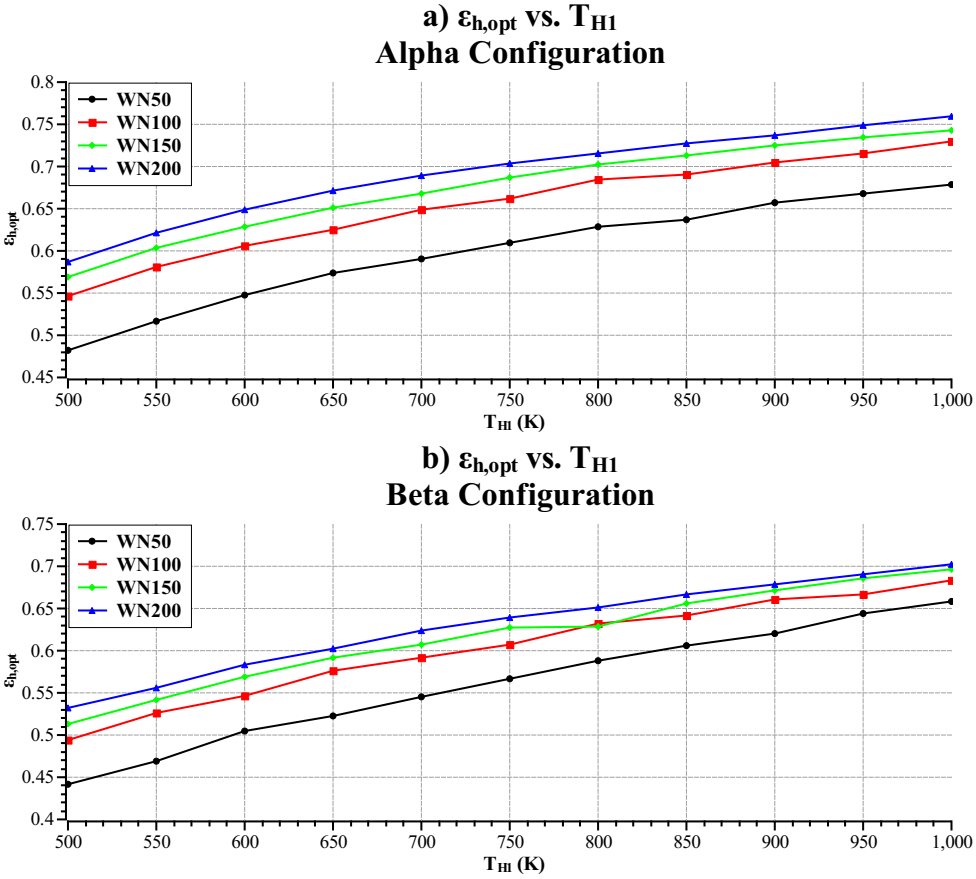

Figure 7.7: Optimal heater effectiveness ($\varepsilon_{h,opt}$) versus source temperature (T_{H1})

From figures 7.6 and 7.7 it can be seen that between configurations the alpha type engine has a higher heater and cooler effectivenesses than the beta type engine. There are two reasons for this. The first is the higher operating frequency at which the alpha type engine operates, as this directly affects the mass flow rates through the heat exchangers which increases the heat transfer coefficients. The second reason is the greater heat exchanger surface areas seen in the alpha type engine when compared to the beta type engine. This is due to the higher optimal dead-volume ratios seen in the alpha type engine when compared to the beta type engine. The effectivenesses are also seen to increase with increasing source temperature, and this is due to the increase in optimal operating frequency which increases the heat transfer coefficients.

Analysing figures 7.5, 7.6 and 7.7 together, allows for conclusions to be drawn about the nature of Stirling engine optimisation and how the configuration 'morphs' to give maximum power output. The analysis shows the importance of regenerator effectiveness on engine performance compared to the effectiveness of the heater and cooler. The reason for this is that the greater the effectiveness of the regenerator, the smaller the heat load in the heater and cooler. This increased load has a significant effect on performance especially at the lower temperature differences, as the temperature difference between the heater wall and the working fluid is proportional to the heat transfer load. This is why the regenerator effectiveness is seen to decrease slightly with increasing source temperature. The increase in heat transfer load is offset by the increase in engine power output, gained through the increase in engine operating frequency which decreases the effectiveness of the regenerator. This means more heat is transferred into the engine through the heater, and out of the engine through the cooler, resulting in a net gain in power output.

7.3.4 Rate of Entropy Generation

Figure 7.8 is a plot of optimal entropy generation rate versus source temperature for the alpha type Stirling engine.

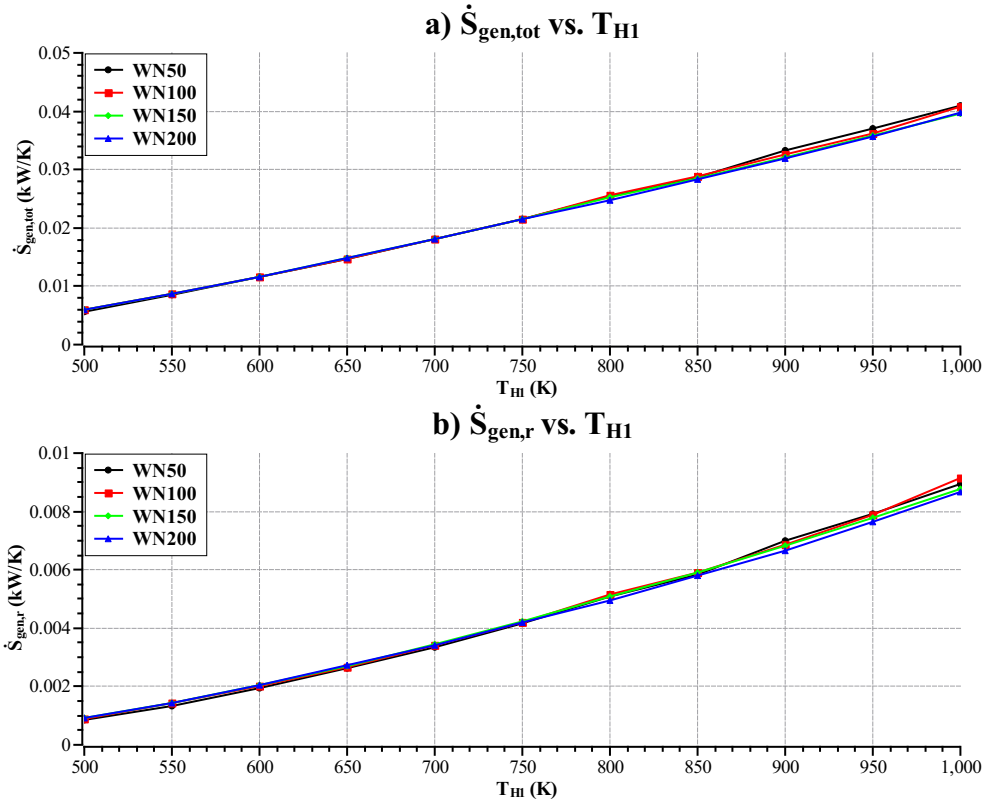

Figure 7.8: Rate of entropy generation ($\dot{S}_{gen,tot}$, $\dot{S}_{gen,r}$) versus source temperature (T_{H1}) for the alpha type Stirling engine

From figure 7.8 it can be seen that the rate of entropy generation increases with increasing source temperature. The reason for this, is that as the source temperature increases the mass flow rates and heat loads increase, thus increasing the rate of entropy generation. However, the engine performance still improves. The plot also shows the rate of entropy generation in the regenerator, which follows the same trend as the total rate of entropy generation.

Figure 7.9 is a plot of optimal entropy generation rate versus source temperature for the beta type Stirling engine

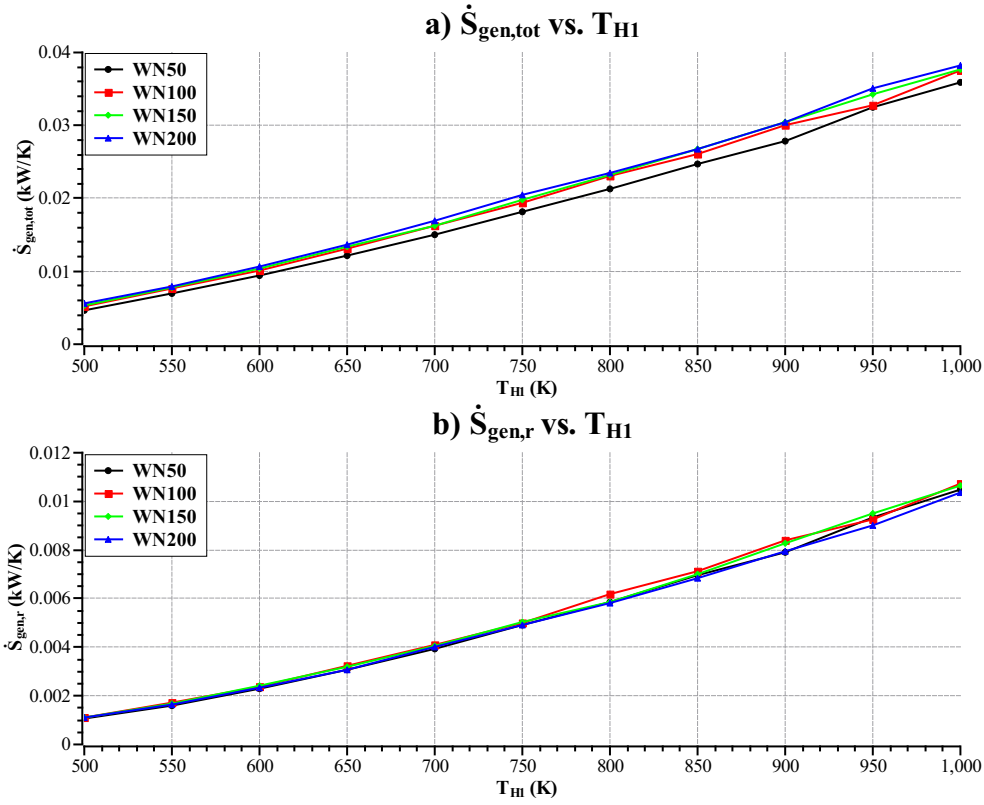

Figure 7.9: Rate of entropy generation ($\dot{S}_{gen,tot}$, $\dot{S}_{gen,r}$) versus source temperature (T_{H1}) for the beta type Stirling engine

Figure 7.9 shows the rate of entropy generation in the beta type Stirling engine. The beta type engine exhibits the same characteristics as the alpha type engine in that the rate of entropy generation increases with increasing source temperature. Comparing figures 7.8 and 7.9, it can be seen that the rates of entropy generation are higher in the alpha type engine than the beta type engine. This is because the alpha type engine has a higher optimal operating frequency which means the mass flow rates and heat exchanger loads are greater, resulting in a higher rate of entropy generation.

7.3.5 Optimal Engine Geometry

The following section presents the optimal heat exchanger geometry for the alpha and beta type Stirling engines at maximum power conditions.

Figure 7.10 is a plot of optimal dead-volume ratio versus source temperature for the alpha and beta type Stirling engines.

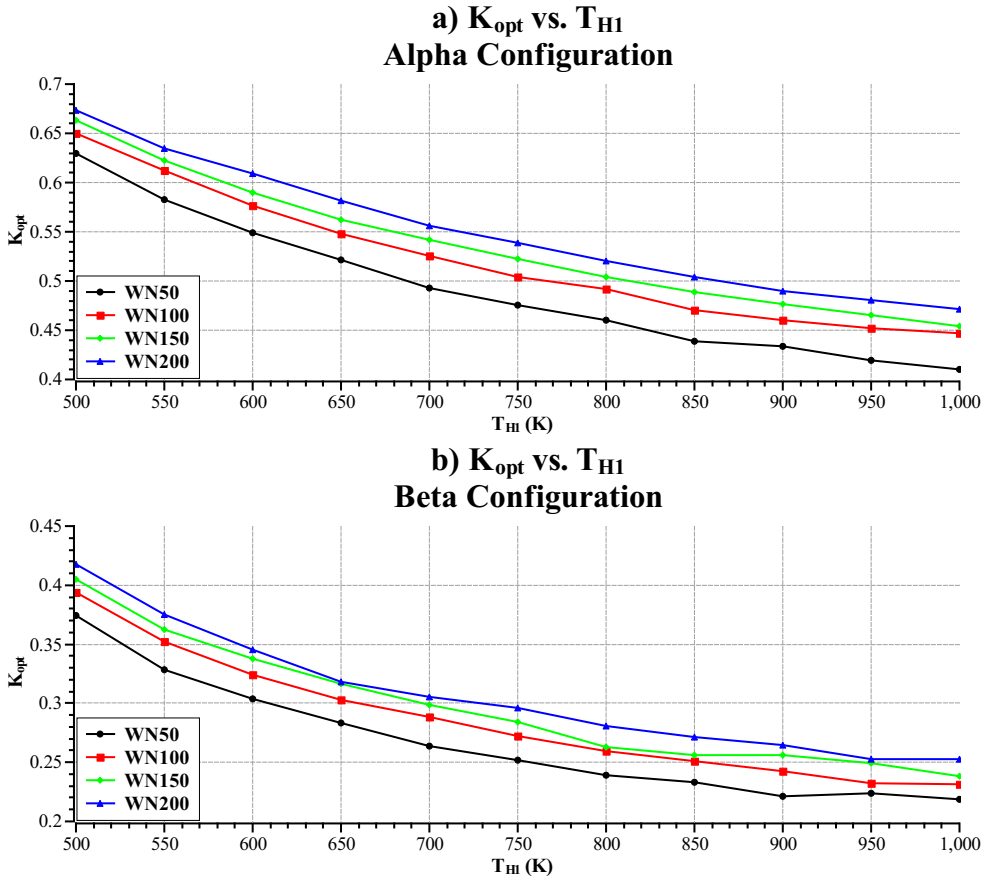

Figure 7.10: Optimal dead-volume ratio (K_{opt}) versus source temperature (T_{H1})

Figure 7.10 shows that the optimal dead-volume ratio differs substantially between the engine types and also varies with a change in regenerator mesh type. The beta type Stirling engine has a much lower optimal dead-volume ratio than the alpha type Stirling engine. The alpha type coupling means that the phase difference between the volumes is 90°, whereas for the beta type engine it is not. This means that the effective dead-volume in the compression space is much larger than the clearance volume, as the coupling doesn't allow the whole space to be swept by the piston and displacer such that the minimum volume is the clearance volume. This is why different crank mechanisms or piston displacer overlap is often employed in the beta type engine, as it reduces this effect and increases the power output of the engine. The optimal dead-volume ratios are also seen to decrease with increasing source temperature, the reasons for this are discussed in detail in chapter 5.

Figure 7.11 is a plot of optimal heater tube diameter versus source temperature for the alpha and beta type Stirling engines.

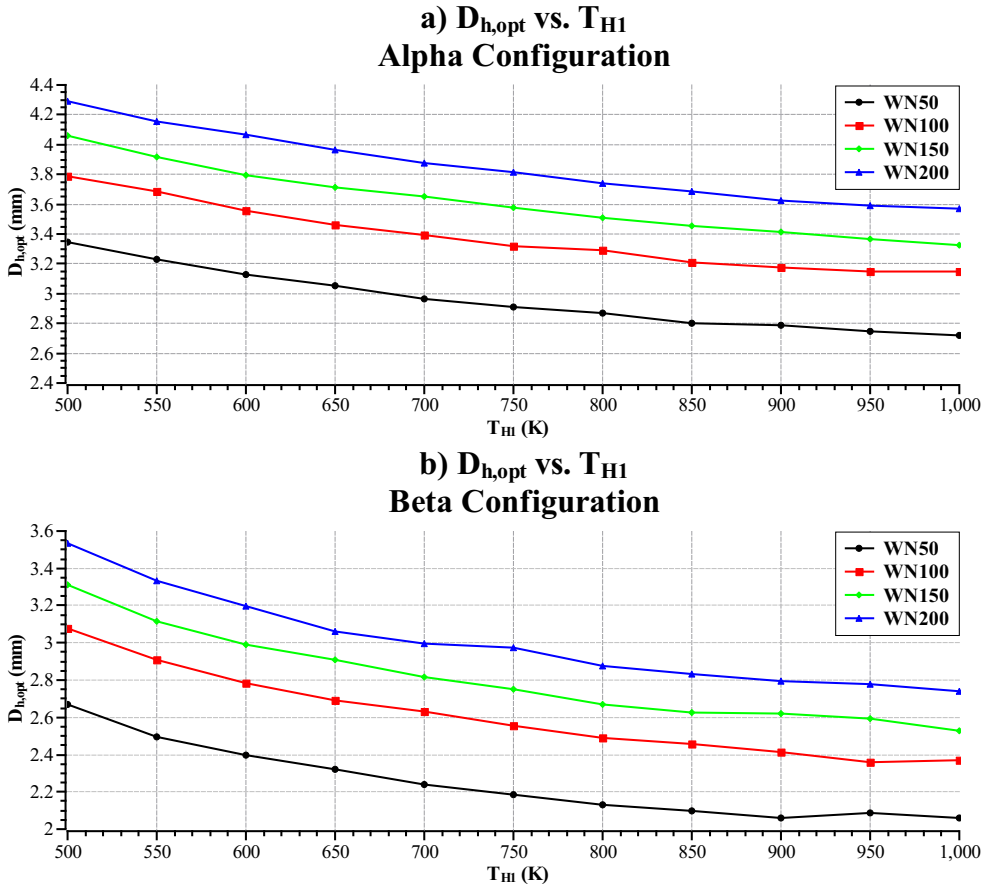

Figure 7.11: Optimal heater tube diameter ($D_{h,opt}$) versus source temperature (T_{H1})

Figure 7.11 is a plot that shows the optimal heater tube diameter versus source temperature. It shows that as the source temperature increases the optimal heater tube diameter decreases. This is due to many different factors. Firstly, as is discussed in chapter five the optimal dead-volume ratio should reduce with increasing source temperature, and therefore the tube diameter must decrease to accommodate this. This results in a decrease in surface area, however, this is offset by the increase in operating frequency which results in increased heat transfer coefficients in the heat exchangers, improving the heat exchanger performance. The WN200 mesh gives a larger diameter heater compared to the other mesh types, and the reason for this is that it yields a shorter and wider regenerator which allows more dead-volume to be allocated to the heater, thus giving a larger tube diameter that offers a larger surface area and better heat transfer performance.

Figure 7.12 is a plot of optimal cooler tube diameter versus source temperature for the alpha and beta type Stirling engines.

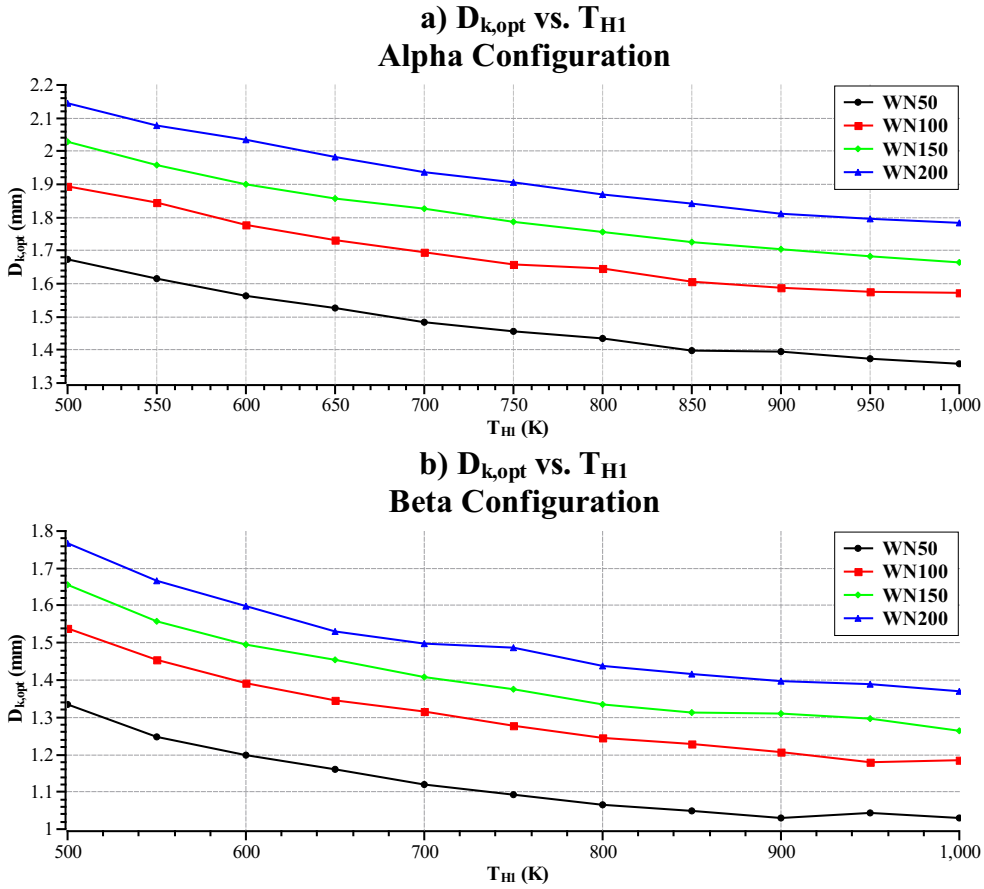

Figure 7.12: Optimal cooler tube diameter ($D_{k,opt}$) versus source temperature (T_{H1})

Figure 7.12 is a plot that shows the optimal cooler tube diameter versus source temperature. The plot shows that as the source temperature increases the optimal cooler tube diameter decreases. The reason for this is the same as for the heater tube diameter which was mentioned previously. The dead-volume effects and the heat exchanger requirements 'compete', as the heat exchanger load seeks to increase the heat exchanger volume to decrease the rate of entropy generation. Whereas, the dead-volume effects try to decrease the heat exchanger volume to increase the engine performance, as is discussed in detail in chapter 5.

Figure 7.13 is a plot of optimal regenerator length versus source temperature for the alpha and beta type Stirling engines.

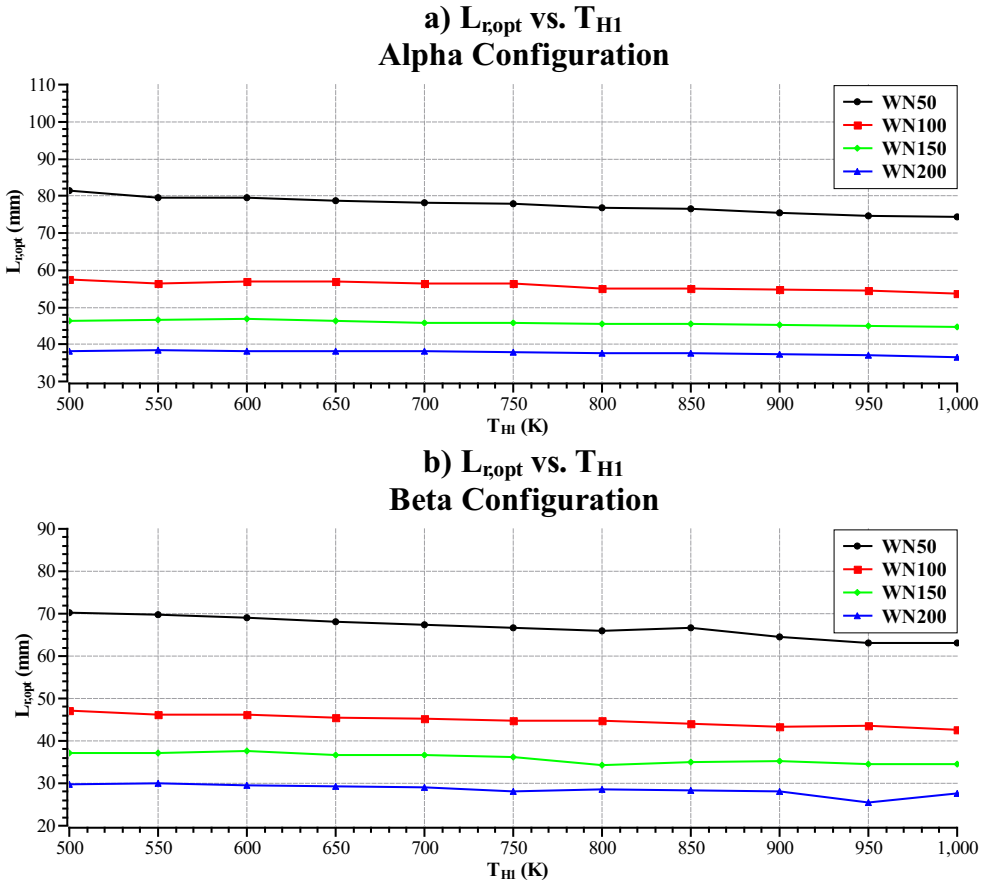

Figure 7.13: Optimal regenerator length ($L_{r,opt}$) versus source temperature (T_{H1})

From figure 7.13 it can be seen that the regenerator length remains approximately constant for all source temperatures and only the mesh type affects the regenerator length. The WN200 mesh which is the finest mesh is seen to give the shortest regenerator, whereas the WN50 mesh is seen to give the longest regenerator. The reason for this is that the heat transfer area increases as the mesh gets finer thus increasing the effectiveness per unit volume of the regenerator, resulting in a smaller regenerator. This is directly linked to the increased engine performance with finer meshes, as they give a smaller regenerator which means more of the available dead-volume can be allocated to the heat exchangers, increasing heater and cooler effectiveness. The shorter regenerator also has a far smaller pressure drop which means the engine can run at a far higher operating frequency, resulting in a larger power output.

Figure 7.14 is a plot of optimal heater tube length versus source temperature for the alpha and beta type Stirling engines.

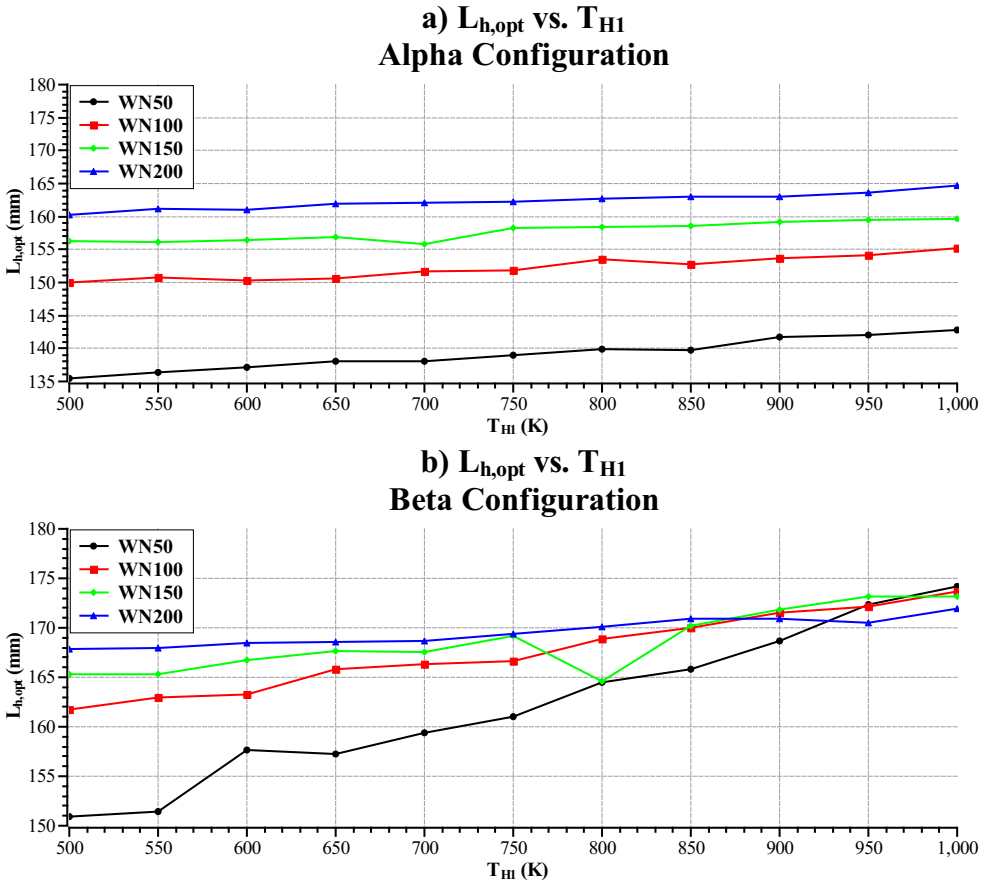

Figure 7.14: Optimal heater length ($L_{h,opt}$) versus source temperature (T_{H1})

From figure 7.14 it can be seen that the heater length remains approximately constant with changing source temperature, with only the mesh type affecting the optimal length. This result is expected as the total heat exchanger length is constrained. The WN200 mesh gives the longest heater tube, and the WN50 mesh gives the shortest heater tube. This directly affects the performance of the engine as the heat transfer area, and thus the effectiveness of the heater is impacted. The reason for this length difference is that the WN200 mesh type yields the shortest regenerator, which means more of the available heat exchanger length can be allocated to the heater.

Figure 7.15 is a plot of optimal cooler tube length versus source temperature.

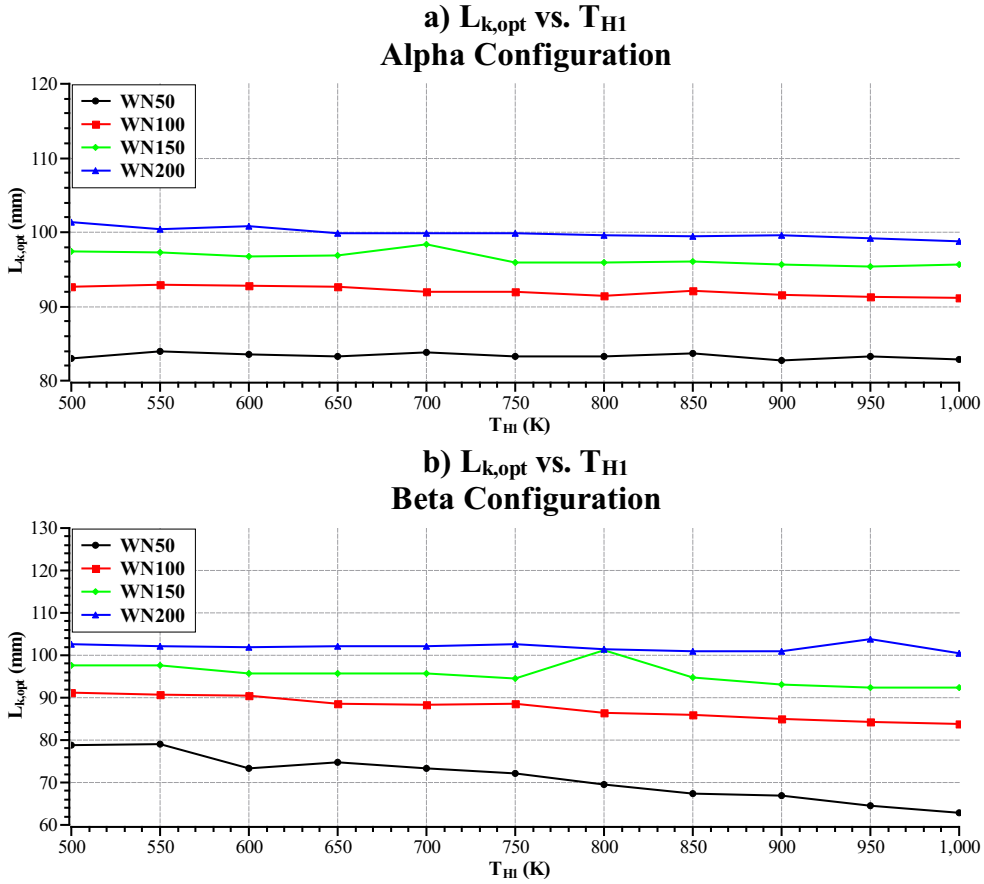

Figure 7.15: Optimal cooler Length ($L_{k,opt}$) versus source temperature (T_{H1})

From figure 7.15 it can be seen that the cooler length remains approximately constant with changing source temperature, with only the mesh type affecting the optimal length. This result is expected as the total heat exchanger length is constrained. The reasons for the mesh type difference are the same as for the heater tube length mentioned previously.

Figure 7.16 is a plot of optimal allocation of swept volume versus source temperature for the alpha type Stirling engine.

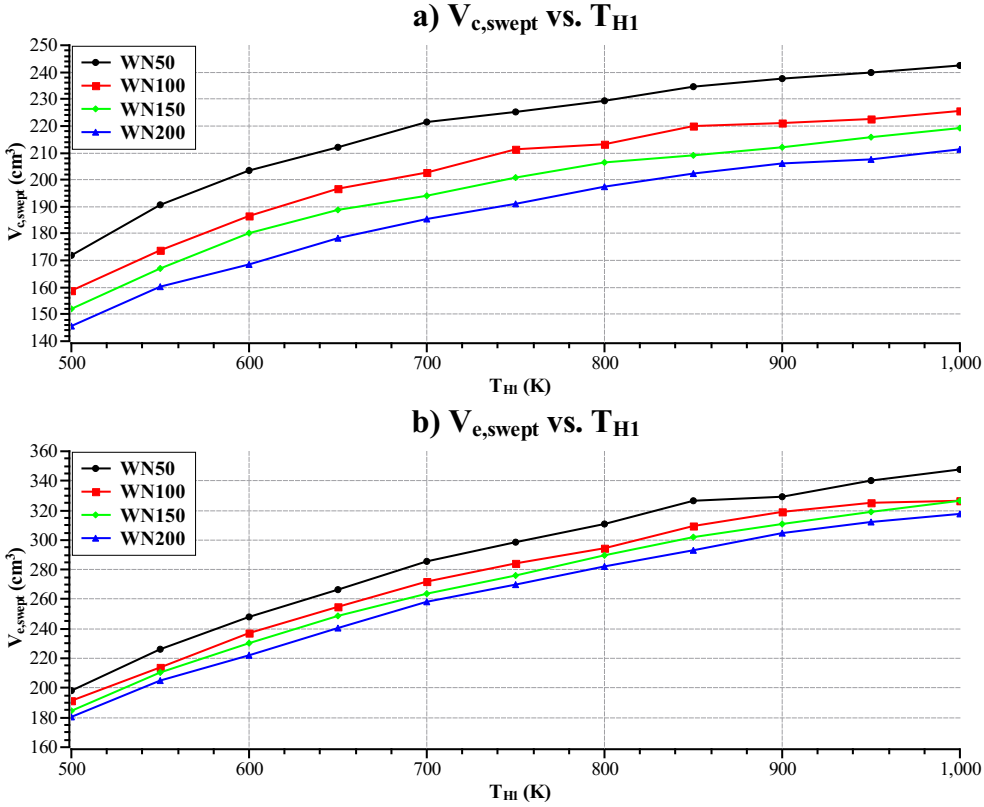

Figure 7.16: Optimal compression and expansion space swept volumes ($V_{c,swept}$,$V_{e,swept}$) versus source temperature (T_{H1}) for the alpha type Stirling engine

From figure 7.16 it can be seen that the optimal ratio of compression space to expansion space volume is less than one for the alpha type engine. It can also be seen that the optimal swept volumes increase with increasing source temperature. This result is expected and can be easily predicted from the analysis presented in chapter 5.

Figure 7.17 is a plot of optimal allocation of swept volume versus source temperature for the beta type Stirling engine.

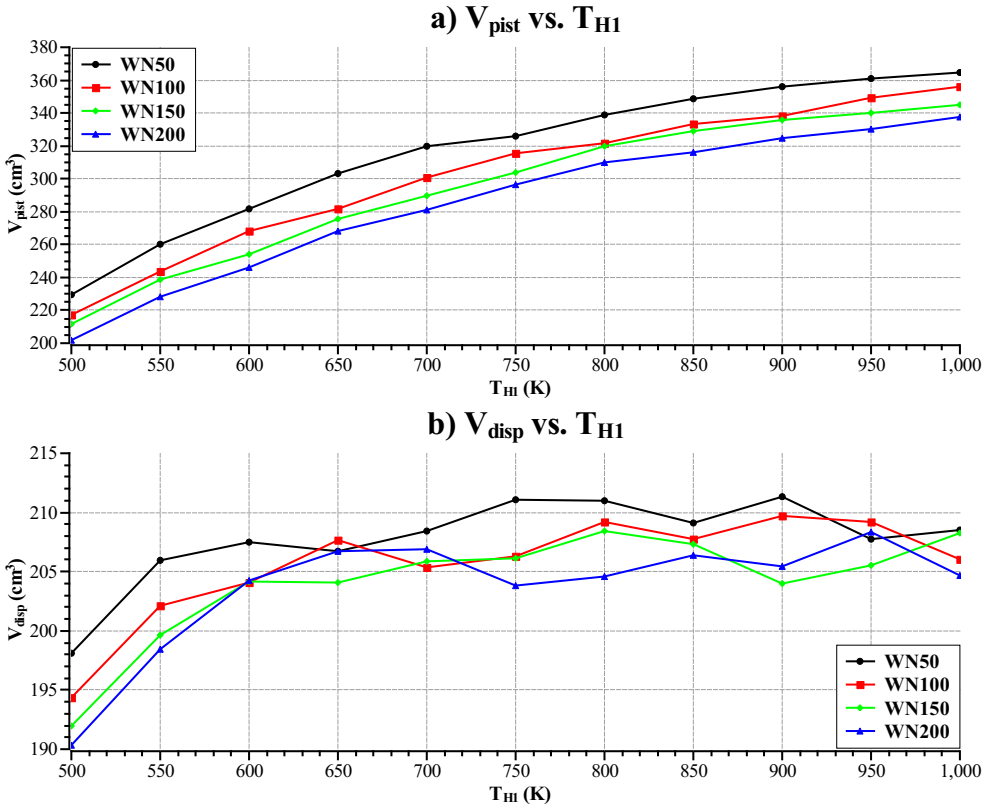

Figure 7.17: Optimal piston and displacer swept volumes (V_{pist},V_{disp}) versus source temperature (T_{H1}) for the beta type Stirling engine

From figure 7.17 it can be seen that the optimal ratio of displacer swept volume to piston volume is less than one for the beta type engine. It can also be seen that the optimal piston volume increases with increasing source temperature, whereas the displacer volume remains relatively unchanged.

7.3.6 Optimal Engine Speed

Figure 7.18 is a plot of optimal operating frequency versus source temperature for the alpha and beta type Stirling engines.

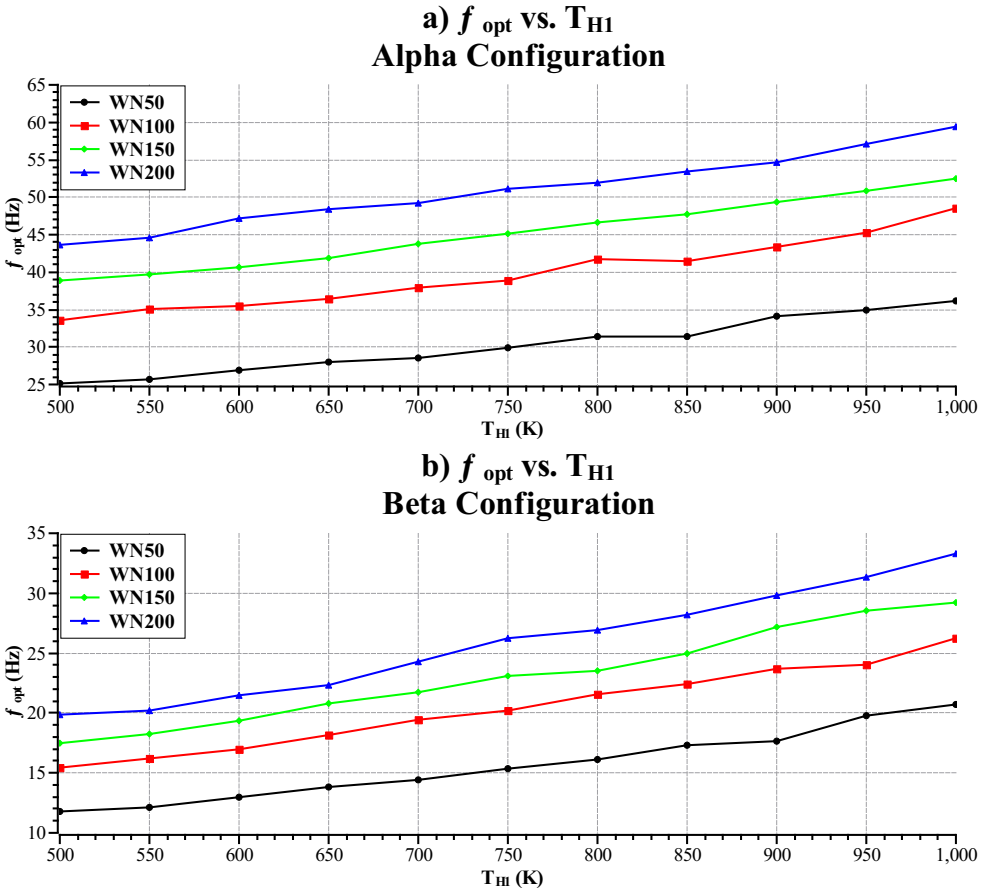

Figure 7.18: Optimal Operating frequency (f_{opt}) versus source temperature (T_{H1})

From figure 7.18 it can be seen that the optimal operating frequency of the engine increases with increasing source temperature for both the alpha and beta type engines. It can also be seen that the optimal operating frequencies are much higher for the alpha type engine when compared to the beta type engine. This is due to the greater heat exchanger volume in the alpha type engine compared to the beta type engine. This greater volume allows the optimal operating frequency to be greater because the heat exchanger flow and surface areas are greater, resulting in a smaller pressure drop through the heat exchanger at a fixed operating frequency. This also explains the superior heat transfer performance of the alpha type engine when compared to the beta type engine.

This optimisation of the operating frequency as a variable in the design is unique, as most Stirling engine studies specify the operating frequency and optimise the geometry around this specified operating frequency. Whereas, this study has allowed the frequency to vary with the geometry which results in a better solution than would otherwise be obtained.

7.4 Conclusion

The analysis presented gives clear insights into the effects that different engine parameters have on Stirling engine performance. The analysis shows how the exergy analysis methodology can be used with a second order numerical model to quickly and effectively optimise a Stirling engine with limited inputs. These results are significant as they show that this model can be used by a thermal designer to locate near optimal design points that will give an optimal engine subject to either maximum power output (shown in this chapter) or a different objective such as maximum efficiency, maximum ecological function, or minimum cost.

The results of the analysis show the importance of the regenerator in Stirling engine design and the significant effect that it has on engine performance. The optimal solution seems to always 'morph' towards maximising the regenerator effectiveness. This result was expected as the literature shows through many studies that the regenerator has the most significant effect on engine performance and its effectiveness should be maximised. The impact of the dead-volume ratio was also observed in the analysis, and the result is in agreement with the study presented in chapter 5. The optimal dead-volume ratio decreases with increasing source temperature as was expected because the ideal adiabatic has been used, this motivates the analysis that was presented in chapter 5.

It is clear that concerning maximum power output the alpha type Stirling engine performs better than the beta type engine. However, in reality, beta type engines are more practical as they are far cheaper engines to manufacture. The reason for this, is that the alpha type engine requires the sealing of two cylinders, whereas the beta type engine only involves the sealing of a single cylinder. In the case of the alpha type engine, this is problematic as sealing the hot expansion space cylinder is difficult because the piston and cylinder are subject to significant thermal expansion. This characteristic drives up the cost of these engines drastically making them economically uncompetitive. The beta configuration with a slider crank mechanism, on the other hand, doesn't require this sealing but it also doesn't

offer the same performance. This is why many different linkages have been invented over the course of Stirling engine development history. These different linkages have tried to allow for working space volume variation with a phase difference of 90 °, but with a beta or gamma coupling. Thus, not requiring expensive sealing.

Chapter 8

Conclusions

The outcomes of this dissertation are presented in chapters 5,6 and 7. Chapter 5 is the dead-volume analysis, chapter 6 is the analysis of the GPU-3 Stirling engine, and chapter 7 is the optimisation of a 1000 cm^3 engine with finite heat capacity rates at the source and the sink.

In my study, the effects of dead-volume on engine performance were thoroughly analysed, and the exergy analysis methodology was applied to the Stirling engine second order adiabatic model. This application of the exergy analysis methodology to a numerical model of the Stirling cycle is the first of its kind and has not been seen in the literature. The methodology has however been applied to Stirling engine mathematical models, and this work took those techniques and applied them to the ideal adiabatic numerical model. The conclusions of these analyses have been summarised in point form below:

Dead-volume analysis, seen in chapter 5.

- The results obtained in my study and the results presented in the literature differ significantly. The reason for this is that the studies performed in the literature use an ideal isothermal model, whereas this analysis uses the ideal adiabatic model.
- The dead-volume ratio is an important design parameter that dramatically affects the performance of the Stirling engine. Therefore, the dead-volume ratio needs to be carefully considered in the design of real Stirling engines.
- As the dead-volume ratio increases the efficiency of the engine increases. The reason for this is that the temperature change in the compression and expansion spaces is reduced and the working spaces tend towards being isothermal.

- In the case of low-temperature difference (LTD) and medium-temperature difference (MTD) engines there exists an optimal dead-volume ratio which gives maximum specific work output.
- The allocation of volume plays a significant role in performance, and there exists an optimal swept volume ratio for a given source and sink temperature ratio.
- The heat exchanger volume ratio has an insignificant effect on engine performance, so long as the dead-volume ratio is optimal.

The GPU-3 analysis, seen in chapter 6.

- The results obtained from the exergy analysis of the GPU-3 Stirling engine compare well with the experimental and numerical results seen in the literature.
- The model shows that the engine design can be improved by changing particular design parameters.
- Resizing the regenerator and using a finer regenerator mesh will increase the engine performance.
- Increasing the operating frequency of the engine will increase the power output, and there is an optimal operating frequency that gives maximum efficiency.
- Increasing the mass of working fluid in the engine will increase the power output, and there is an optimal mass of working fluid that gives maximum efficiency.

Exergy analysis of the alpha and beta type Stirling engines with finite heat capacity rates at the source and sink, seen in chapter 7.

- The exergy analysis of the alpha and beta type Stirling engines shows that optimal design parameters for the 1000 cm^3 numerical example exist.
- The optimal dead-volume ratio is seen to decrease with increasing source temperature. This shows the effect that dead-volume ratio has on engine performance, motivating the work presented in chapter 5.
- The optimal regenerator length is seen to be robust and not change with changing temperature ratio. However, it does change with choice of mesh type.

- The regenerator effectiveness is the most critical parameter that affects the engine performance, and the design will always 'morph' towards maximising the regenerator effectiveness.
- The alpha type engine outperforms the beta type engine regarding maximum power output for a sinusoidal volume variation with a crank difference of 90 °.
- The WN200 mesh gives the best engine performance regarding power output and efficiency and results in the smallest regenerator.
- There exists an optimal engine operating frequency for each engine configuration, mesh type and source temperature that gives maximum power output. It is important to mention that this may differ from experimentally derived optimal operating frequency as the model developed in this dissertation did not take into account mechanical friction losses.

One of the conclusions drawn from this study is the importance of dead-volume ratio and heat exchanger volume in the analysis and performance optimisation of Stirling engines. My research shows that dead-volume ratio is a critical parameter that needs to be seriously considered in Stirling engine design. My study also indicates that there exist optimal geometries for the Stirling engine that give maximum power output, along with the usefulness of the implicit filtering algorithm for Stirling engine optimisation. The effect of regenerator mesh type is analysed using four different standard regenerator mesh types, and it is shown that finer meshes outperform coarser meshes. This is because the thinner wire mesh provides greater heat transfer area per unit volume, which gives a smaller optimal regenerator resulting in lower dissipative losses and a higher effectiveness. However, this can negatively affect the thermal efficiency of the device as the thermal bridging loss is proportional to the length of the regenerator and the analysis shows that care needs to be taken to properly insulate the regenerator, as this loss mechanism can severely reduce efficiency.

The analysis shows that the alpha configuration gives better power output than the beta/gamma configuration. However, as is discussed, the beta/gamma type engine is easier and cheaper to manufacture than the alpha type engine and it, therefore, sees more widespread use.

Chapter 9

Recommendations

This dissertation presented a study that analysed the effects of dead-volume ratio and developed a model that has taken the first steps in the exergy analysis of the Stirling cycle numerical model. The methodology presented can be used in the initial phases of Stirling engine design and in predicting the existence of near-optimal engine geometries. These optimal geometries can be used to narrow down the search for optimal operating conditions when more complex models are employed or prototypes developed.

To better understand the effects that the different parameters have on engine performance, more complex models need to be developed and used in numerical experiments. The model presented in this dissertation should be updated as the literature is updated, and coupled to entire energy systems to optimise the system as a whole using the exergy analysis approach.

The following recommendations have been made for future Stirling engine research:

- Analyse the effects of dead-volume ratio using more complex multidimensional models to establish the actual impact of dead-volume ratio on engine performance.
- Once relations become available for oscillating flow in the heater and cooler update the model with these relations and analyse the effects on performance. In the literature, oscillating flow relations were only found for the regenerator, and steady flow equations for the heat transfer coefficient and friction factor were used in the heater and cooler.
- Use multi-objective optimisation criteria to find the optimal engine geometry for optimal power output and efficiency or to develop the Pareto set of optimal solutions. Another approach would be to include a levelised cost of electricity (LCOE) function,

which can be minimised to find the optimal operating conditions from an economic standpoint.

- The development of a more accurate Stirling cycle numerical model that does not assume the heater and cooler to be isothermal. This increase in accuracy could be achieved by breaking the heater and cooler up into multiple control volumes which are all assumed to vary in temperature. These temperature differences could then be used to compute the rate of entropy generation due to temperature effects in the heater and cooler, thus increasing the accuracy of the exergy equation.

- Inclusion of the conduction and external heat transfer coefficient to more accurately model the performance of the heater and cooler.

- Include external loss mechanisms into the model to increase accuracy.

- Coupling of the model to a parabolic dish or another system that supplies heat to model an entire system and optimise the geometry and characteristics of the whole system using an exergy analysis approach.

- A wider variety of regenerator materials and configurations, should be tested and modelled so that the optimal regenerator material and geometry can be selected to give optimal engine performance. It is recommended that a Constructal law methodology (where the regenerator configuration is allowed to fit the body of the flow) be utilised to reduce the temperature oscillation in the entrance lengths, as this effect has been found to reduce engine performance significantly.

- Use the exergy analysis methodology in the analysis of Stirling refrigerators and cryocoolers. Stirling refrigerators and cryocoolers have been used extensively, and the exergy analysis methodology could be used to analyse and find optimal design points for these engines.

Bibliography

[1] Mohammad Hossein Ahmadi, Mohammad Ali Ahmadi, and Mehdi Mehrpooya. Investigation of the effect of design parameters on power output and thermal efficiency of a stirling engine by thermodynamic analysis. *Int. J. Low-Carbon Tech.*, 11(2):141–156, oct 2014.

[2] Mohammad Hossein Ahmadi, Hoseyn Sayyaadi, Saeed Dehghani, and Hadi Hosseinzade. Designing a solar powered stirling heat engine based on multiple criteria: Maximized thermal efficiency and power. *Energy Conversion and Management*, 75:282–291, nov 2013.

[3] Stig Kildegård Andersen, Henrik Carlsen, and Per Grove Thomsen. Numerical study on optimal stirling engine regenerator matrix designs taking into account the effects of matrix temperature oscillations. *Energy Conversion and Management*, 47(7-8):894–908, may 2006.

[4] Joseph A. Araoz, Evelyn Cardozo, Marianne Salomon, Lucio Alejo, and Torsten H. Fransson. Development and validation of a thermodynamic model for the performance analysis of a gamma stirling engine prototype. *Applied Thermal Engineering*, 83:16–30, 2015.

[5] Joseph A. Araoz, Marianne Salomon, Lucio Alejo, and Torsten H. Fransson. Non-ideal stirling engine thermodynamic model suitable for the integration into overall energy systems. *Applied Thermal Engineering*, 73(1):205–221, dec 2014.

[6] Larry Armijo. Minimization of functions having lipschitz continuous first partial derivatives. *Pacific Journal of mathematics*, 16(1):1–3, 1966.

[7] Mojtaba Babaelahi and Hoseyn Sayyaadi. A new thermal model based on polytropic numerical simulation of stirling engines. *Applied Energy*, 141:143–159, 2015.

[8] Enrico Barbier. Geothermal energy technology and current status: an overview. *Renewable and Sustainable Energy Reviews*, 6(1):3–65, 2002.

[9] İhsan Batmaz and Sleyman stn. Design and manufacturing of a v-type stirling engine with double heaters. *Applied Energy*, 85(11):1041–1049, nov 2008.

[10] Adrian Bejan. Entropy generation minimization: The new thermodynamics of finite-size devices and finite-time processes. *J. Appl. Phys.*, 79(3):1191, 1996.

[11] Adrian Bejan. *Advanced engineering thermodynamics*. John Wiley & Sons, Inc, 2006.

[12] Adrian Bejan, Sylvie Lorente, and Deok-Hong Kang. Constructal design of regenerators. *International Journal of Energy Research*, 37(12):1509–1518, oct 2012.

[13] T. Bello-Ochende, J.P. Meyer, and A. Bejan. Constructal ducts with wrinkled entrances. *International Journal of Heat and Mass Transfer*, 52(15-16):3628–3633, jul 2009.

[14] Tunde Bello-Ochende and Adrian Bejan. Fitting the duct to the body of the convective flow. *International journal of heat and mass transfer*, 46(10):1693–1701, 2003.

[15] David Berchowitz. A computer and experimental simulation of stirling cycle machines. Master's thesis, University of the Witwatersrand, 1978.

[16] David Berchowitz. *Stirling cycle engine design and optimisation*. PhD thesis, University of the Witwatersrand, 1986.

[17] I. M. Bugaje. Renewable energy for sustainable development in africa: a review. *Renewable and Sustainable Energy Reviews*, 10(6):603–612, 2006.

[18] M.C. Campos, J.V.C. Vargas, and J.C. Ordonez. Thermodynamic optimization of a stirling engine. *Energy*, 44(1):902–910, aug 2012.

[19] Y Cengel and A Ghajar. *Heat and mass transfer: fundamentals and applications*. McGraw-Hill, 4 edition, 2011.

[20] Paul Chambadal. *Les centrales nuclaires*, volume 321. Colin, 1957.

[21] Jincan Chen, Zijun Yan, Lixuan Chen, Bjarne Andresen, et al. Efficiency bound of a solar-driven stirling heat engine system. *International journal of energy research*, 22(9):805–812, 1998.

[22] Lingen Chen, Chih Wu, and Fengrui Sun. Finite time thermodynamic optimization or entropy generation minimization of energy systems. *Journal of Non-Equilibrium Thermodynamics*, 24(4):327–359, 2005.

[23] Lingen Chen, Wanli Zhang, and Fengrui Sun. Power, efficiency, entropy-generation rate and ecological optimization for a class of generalized irreversible universal heat-engine cycles. *Applied Energy*, 84(5):512–525, 2007.

[24] NCJ Chen and FP Griffin. Review of stirling-engine mathematical models. Technical report, Oak Ridge National Lab., TN (USA), 1983.

[25] Chin-Hsiang Cheng and Hang-Suin Yang. Theoretical model for predicting thermodynamic behavior of thermal-lag stirling engine. *Energy*, 49:218–228, 2013.

[26] Can Cinar and Halit Karabulut. Manufacturing and testing of a gamma type stirling engine. *Renewable Energy*, 30(1):57–66, jan 2005.

[27] Can Cinar, Serdar Yucesu, Tolga Topgul, and Melih Okur. Beta-type stirling engine operating at atmospheric pressure. *Applied Energy*, 81(4):351–357, aug 2005.

[28] M. Costea and M. Feidt. The effect of the overall heat transfer coefficient variation on the optimal distribution of the heat transfer surface conductance or area in a stirling engine. *Energy Conversion and Management*, 39(16-18):1753–1761, nov 1998.

[29] M. Costea, S. Petrescu, and C. Harman. The effect of irreversibilities on solar stirling engine cycle performance. *Energy Conversion and Management*, 40(15-16):1723–1731, oct 1999.

[30] F. L. Curzon. Efficiency of a carnot engine at maximum power output. *American Journal of Physics*, 43(1):22, 1975.

[31] William C Davidon. Variable metric method for minimization. *SIAM Journal on Optimization*, 1(1):1–17, 1991.

[32] P. C. T. de Boer. Maximum attainable performance of stirling engines and refrigerators. *Journal of Heat Transfer*, 125(5):911, 2003.

[33] P. C. T. de Boer. Optimal regenerator performance in stirling engines. *International Journal of Energy Research*, 33(9):813–832, jul 2009.

[34] Rodger W Dyson, Scott D Wilson, and Roy C Tew. Review of computational stirling analysis methods. In *Collect. Tech. Pap. Int. Energy Convers. Eng. Conf*, volume 1, pages 511–531, 2004.

[35] Omar Ellabban, Haitham Abu-Rub, and Frede Blaabjerg. Renewable energy resources: Current status, future prospects and their enabling technology. *Renewable and Sustainable Energy Reviews*, 39:748–764, 2014.

[36] L. Berrin Erbay and Hasbi Yavuz. Optimization of the irreversible stirling heat engine. *International Journal of Energy Research*, 23(10):863–873, aug 1999.

[37] L.Berrin Erbay and Hasbi Yavuz. Analysis of the stirling heat engine at maximum power conditions. *Energy*, 22(7):645–650, jul 1997.

[38] Ted Finkelstein. Generalized thermodynamic analysis of stirling engines. Technical report, SAE Technical Paper, 1960.

[39] Thomas P. Fluri. The potential of concentrating solar power in South Africa. *Energy Policy*, 37(12):5075–5080, dec 2009.

[40] Fabien Formosa and Ghislain Despesse. Analytical model for stirling cycle machine design. *Energy Conversion and Management*, 51(10):1855–1863, 2010.

[41] David Gedeon. Sage - object-oriented software for stirling machine design. In *Intersociety Energy Conversion Engineering Conference*. American Institute of Aeronautics and Astronautics (AIAA), aug 1994.

[42] Volker Gnielinski. New equations for heat and mass transfer in the turbulent flow in pipes and channels. *NASA STI/recon technical report A*, 75:8–16, 1975.

[43] Lavinia Grosu, Pierre Rochelle, and Nadia Martaj. An engineer-oriented optimisation of stirling engine cycle with finite-size finite-speed of revolution thermodynamics. *International Journal of Exergy*, 11(2):191, 2012.

[44] Hind El Hassani, N. Boutammachte, and M. Hannaoui. Study of some power influencing parameters of a solar low temperature stirling engine. *European Journal of Sustainable Development*, 3(2):109–118, jun 2014.

[45] Arif Hepbasli. A key review on exergetic analysis and assessment of renewable energy resources for a sustainable future. *Renewable and Sustainable Energy Reviews*, 12(3):593–661, 2008.

[46] Mounir Ibrahim, Roy C Tew, and James E Dudenhoefer. Two-dimensional numerical simulation of a stirling engine heat exchanger. In *Energy Conversion Engineering Conference, 1989. IECEC-89., Proceedings of the 24th Intersociety*, pages 2795–2802. IEEE, 1989.

[47] Seita ISSHIKI, Hidekazu SATO, Shoji KONNO, Hiroaki SHIRAISHI, Naotsugu ISSHIKI, Iwane FUJII, and Hiroyuki MIZUI. The experimental study of atmospheric stirling engines using pin-fin arrays' heat exchangers. *Journal of Power and Energy Systems*, 2(5):1198–1208, 2008.

[48] S Iwamoto, F Toda, K Hirata, M Takeuchi, and T Yamamoto. Comparison of low-and high-temperature differential stirling engines. In *Proceedings of the 8th international Stirling engine conference*, pages 29–38, 1997.

[49] Shoichi IWAMOTO, Koichi HIRATA, and Fujio TODA. Performance of stirling engines. arranging method of experimental results and performance prediction. *JSME International Journal Series B*, 44(1):140–147, 2001.

[50] Daniel D. Joseph and Bobby H. Yang. Friction factor correlations for laminar, transition and turbulent flow in smooth pipes. *Physica D: Nonlinear Phenomena*, 239(14):1318–1328, jul 2010.

[51] Soteris A. Kalogirou. Solar thermal collectors and applications. *Progress in Energy and Combustion Science*, 30(3):231–295, jan 2004.

[52] Mitsuo Kanzaka and Makio Iwabuchi. Study on heat transfer of heat exchangers in the stirling engine: heat transfer in a heated tube under the periodically reversing flow condition. *JSME international journal. Ser. 2, Fluids engineering, heat transfer, power, combustion, thermophysical properties*, 35(4):641–646, 1992.

[53] Carl T Kelley. *Iterative methods for optimization*. SIAM, 1999.

[54] Carl T Kelley. *Implicit filtering*. SIAM, 2011.

[55] Ivo Kolin, Sonja Koscak-Kolin, and Miroslav Golub. Geothermal electricity production by means of the low temperature difference stirling engine. In *Proceedings World Geothermal Congress*, volume 2000, pages 3199–203, 2000.

[56] Bancha Kongtragool and Somchai Wongwises. A review of solar-powered stirling engines and low temperature differential stirling engines. *Renewable and Sustainable Energy Reviews*, 7(2):131–154, 2003.

[57] Bancha Kongtragool and Somchai Wongwises. Thermodynamic analysis of a stirling engine including dead volumes of hot space, cold space and regenerator. *Renewable Energy*, 31(3):345–359, mar 2006.

[58] Bancha Kongtragool and Somchai Wongwises. Performance of a twin power piston low temperature differential stirling engine powered by a solar simulator. *Solar Energy*, 81(7):884–895, 2007.

[59] Bancha Kongtragool and Somchai Wongwises. Performance of low-temperature differential stirling engines. *Renewable Energy*, 32(4):547–566, 2007.

[60] Bancha Kongtragool and Somchai Wongwises. A four power-piston low-temperature differential stirling engine using simulated solar energy as a heat source. *Solar Energy*, 82(6):493–500, 2008.

[61] Kwanchai Kraitong. *Numerical modelling and design optimisation of stirling engines for power production.* PhD thesis, Northumbria University, 2012.

[62] Kwanchai Kraitong and K Mahkamov. Optimisation of low temperature difference solar stirling engines using genetic algorithm. In *Proceedings of the World Renewable Energy Congress – Sweden, 8–13 May, 2011, Linkoping, Sweden.* Linkoping University Electronic Press, 2011.

[63] M. Kuosa, J. Kaikko, and L. Koskelainen. The impact of heat exchanger fouling on the optimum operation and maintenance of the stirling engine. *Applied Thermal Engineering*, 27(10):1671–1676, jul 2007.

[64] M. Kuosa, K. Saari, A. Kankkunen, and T.-M. Tveit. Oscillating flow in a stirling engine heat exchanger. *Applied Thermal Engineering*, 45-46:15–23, dec 2012.

[65] Martin LaMonica. NRG energy deploying dean kamens solar-smart in-home generator.

[66] W. G. le Roux, T. Bello-Ochende, and J. P. Meyer. Thermodynamic optimisation of the integrated design of a small-scale solar thermal brayton cycle. *International Journal of Energy Research*, 36(11):1088–1104, may 2011.

[67] Willem Gabriel le Roux. Maximum net power output from an integrated design of a small scale open and direct solar thermal brayton cycle. Master's thesis, University of Pretoria, 2011.

[68] N. Martaj, L. Grosu, and P. Rochelle. Exergetical analysis and design optimisation of the stirling engine. *International Journal of Exergy*, 3(1):45, 2006.

[69] Nadia Martaj, Lavinia Grosu, and Pierre Rochelle. Thermodynamic study of a low temperature difference stirling engine at steady state operation. *International Journal of Thermodynamics*, 10(4):165–176, 2007.

[70] William R Martini. *Stirling engine design manual*. US Department of Energy, Office of Conservation and Solar Applications, Division of Transportation Energy Conservation, 1978.

[71] Roelf Jan Meijer. *The Philips Stirling thermal engine: analysis of the rhombic drive mechanism and efficiency measurements*. PhD thesis, TU Delft, Delft University of Technology, 1960.

[72] D. Mills. Advances in solar thermal electricity technology. *Solar Energy*, 76(1-3):19–31, jan 2004.

[73] Manish Mishra, P.K. Das, and Sunil Sarangi. Second law based optimisation of cross-flow plate-fin heat exchanger design using genetic algorithm. *Applied Thermal Engineering*, 29(14-15):2983–2989, oct 2009.

[74] John A Nelder and Roger Mead. A simplex method for function minimization. *The computer journal*, 7(4):308–313, 1965.

[75] I. I. Novikov. Efficiency of an atomic power generating installation. *The Soviet Journal of Atomic Energy*, 3(11):1269–1272, nov 1957.

[76] Juan Carlos Ordonez and Adrian Bejan. Entropy generation minimization in parallel-plates counterflow heat exchangers. *International Journal of Energy Research*, 24(10):843–864, 2000.

[77] N. L. Panwar, S. C. Kaushik, and Surendra Kothari. Role of renewable energy sources in environmental protection: A review. *Renewable and Sustainable Energy Reviews*, 15(3):1513–1524, 2011.

[78] Nezaket Parlak, Andreas Wagner, Michael Elsner, and Hakan S. Soyhan. Thermodynamic analysis of a gamma type stirling engine in non-ideal adiabatic conditions. *Renewable Energy*, 34(1):266–273, jan 2009.

[79] S. Petrescu, M. Costea, C. Harman, and T. Florea. Application of the direct method to irreversible stirling cycles with finite speed. *International Journal of Energy Research*, 26(7):589–609, 2002.

[80] Alfred Brian Pippard. *Elements of classical thermodynamics: for advanced students of physics*. Cambridge University Press, 1964.

[81] Pascal Puech and Victoria Tishkova. Thermodynamic analysis of a stirling engine including regenerator dead volume. *Renewable Energy*, 36(2):872–878, feb 2011.

[82] R.V. Rao and V.K. Patel. Thermodynamic optimization of cross flow plate-fin heat exchanger using a particle swarm optimization algorithm. *International Journal of Thermal Sciences*, 49(9):1712–1721, sep 2010.

[83] P. S. Ren. Renewables 2015 global status report. *Ren*, 2015.

[84] J. Douglas Faires Richard L. Burden. *Numerical Analysis*. BROOKS COLE PUB CO, 2010.

[85] W. G. Le Roux, T. Bello-Ochende, and J. P. Meyer. Optimum small-scale open and direct solar thermal brayton cycle for pretoria, south africa. In *ASME 2012 6th International Conference on Energy Sustainability, Parts A and B*. ASME International, jul 2012.

[86] W.G. Le Roux, T. Bello-Ochende, and J.P. Meyer. Operating conditions of an open and direct solar thermal brayton cycle with optimised cavity receiver and recuperator. *Energy*, 36(10):6027–6036, oct 2011.

[87] W.G. Le Roux, T. Bello-Ochende, and J.P. Meyer. Optimum performance of the small-scale open and direct solar thermal brayton cycle at various environmental conditions and constraints. *Energy*, 46(1):42–50, oct 2012.

[88] W.G. Le Roux, T. Bello-Ochende, and J.P. Meyer. A review on the thermodynamic optimisation and modelling of the solar thermal brayton cycle. *Renewable and Sustainable Energy Reviews*, 28:677–690, dec 2013.

[89] W.G. Le Roux, T. Bello-Ochende, and J.P. Meyer. The efficiency of an open-cavity tubular solar receiver for a small-scale solar thermal brayton cycle. *Energy Conversion and Management*, 84:457–470, aug 2014.

[90] Peter Salamon, Karl Heinz Hoffmann, Sven Schubert, R. Stephen Berry, and Bjarne Andresen. What conditions make minimum entropy production equivalent to maximum power production? *Journal of Non-Equilibrium Thermodynamics*, 26(1), jan 2001.

[91] Gustav Schmidt. Classical analysis of operation of stirling engine. *A report published in German engineering union (Original German)*, 15:1–12, 1871.

[92] James R Senft. *Ringbom stirling engines*. Oxford University Press, USA, 1993.

[93] James R. Senft. Theoretical limits on the performance of stirling engines. *International Journal of Energy Research*, 22(11):991–1000, sep 1998.

[94] James R. Senft. Optimum stirling engine geometry. *International Journal of Energy Research*, 26(12):1087–1101, 2002.

[95] Shah. *Fundamentals of Heat Exchanger Design*. WILEY ACADEMIC, 2003.

[96] Terrence W Simon and Jorge R Seume. A survey of oscillating flow in stirling engine heat exchangers. *NASA*, 1988.

[97] Jiri Skorpik. Stirlinguv motor-english version. *Transformacni technologie*, 2009.

[98] Jan Snyman. *Practical mathematical optimization: an introduction to basic optimization theory and classical and new gradient-based algorithms*, volume 97. Springer Science & Business Media, 2005.

[99] Angkee Sripakagorn and Chana Srikam. Design and performance of a moderate temperature difference stirling engine. *Renewable Energy*, 36(6):1728–1733, jun 2011.

[100] William B Stine and Richard B Diver. A compendium of solar dish/stirling technology. Technical report, DTIC Document, 1994.

[101] William B Stine and Michael Geyer. *Power from the Sun*. Power from the sun. net, 2001.

[102] Robert Stirling. Patent no. 4081. *Stirling air engine and the heat regenerator*, 1816.

[103] William Sutherland. Lii. the viscosity of gases and molecular force. *The London, Edinburgh, and Dublin Philosophical Magazine and Journal of Science*, 36(223):507–531, 1893.

[104] Makoto Tanaka, Iwao Yamashita, and Fumitake Chisaka. Flow and heat transfer characteristics of the stirling engine regenerator in an oscillating flow. *JSME international journal. Ser. 2, Fluids engineering, heat transfer, power, combustion, thermophysical properties*, 33(2):283–289, 1990.

[105] Lanny G Thieme. Low-power baseline test results for the gpu 3 stirling engine. *NASA*, 1979.

[106] Lanny G Thieme. High-power baseline and motoring test results for the gpu-3 stirling engine. *NASA*, 1981.

[107] Lanny G Thieme and Roy C Tew Jr. Baseline performance of the gpu 3 stirling engine. *NASA*, 1978.

[108] Mirunalini Thirugnanasambandam, S. Iniyan, and Ranko Goic. A review of solar thermal technologies. *Renewable and Sustainable Energy Reviews*, 14(1):312–322, jan 2010.

[109] D. G. Thombare and S. K. Verma. Technological development in the stirling cycle engines. *Renewable and Sustainable Energy Reviews*, 12(1):1–38, 2008.

[110] Youssef Timoumi, Iskander Tlili, and Sassi Ben Nasrallah. Performance optimization of stirling engines. *Renewable Energy*, 33(9):2134–2144, sep 2008.

[111] Iskander Tlili, Youssef Timoumi, and Sassi Ben Nasrallah. Analysis and design consideration of mean temperature differential stirling engine for solar application. *Renewable Energy*, 33(8):1911–1921, aug 2008.

[112] Somayeh Toghyani, Alibakhsh Kasaeian, and Mohammad H. Ahmadi. Multi-objective optimization of stirling engine using non-ideal adiabatic method. *Energy Conversion and Management*, 80:54–62, apr 2014.

[113] Somayeh Toghyani, Alibakhsh Kasaeian, Seyyed Hasan Hashemabadi, and Morteza Salimi. Multi-objective optimization of GPU3 stirling engine using third order analysis. *Energy Conversion and Management*, 87:521–529, nov 2014.

[114] S K Tyagi, S C Kaushik, and R Salhotra. Ecological optimization and performance study of irreversible stirling and ericsson heat engines. *Journal of Physics D: Applied Physics*, 35(20):2668–2675, oct 2002.

[115] Israel Urieli. Stirling cycle machine analysis, 2016.

[116] Israel Urieli and David M. Berchowitz. *Stirling cycle engine analysis*. Taylor & Francis, 1984.

[117] Jose V.C. Vargas and Adrian Bejan. Thermodynamic optimization of finned crossflow heat exchangers for aircraft environmental control systems. *International Journal of Heat and Fluid Flow*, 22(6):657–665, dec 2001.

[118] Gerhard Venter. Review of optimization techniques. *Encyclopedia of aerospace engineering*, 2010.

[119] Graham Walker. *Stirling Engines*. Oxford University Press, 1980.

[120] Scott Wilson, Rodger Dyson, Roy Tew, and Mounir Ibrahim. Multi-d cfd modeling of free-piston stirling convertor at nasa grc. In *2nd International Energy Conversion Engineering Conference*, page 5673, 2004.

[121] Feng Wu, Lingen Chen, Chih Wu, and Fengrui Sun. Optimum performance of irreversible stirling engine with imperfect regeneration. *Energy Conversion and Management*, 39(8):727–732, jun 1998.

[122] Gang Xiao, Conghui Chen, Bingwei Shi, Kefa Cen, and Mingjiang Ni. Experimental study on heat transfer of oscillating flow of a tubular stirling engine heater. *International Journal of Heat and Mass Transfer*, 71:1–7, apr 2014.

[123] Li Yaqi, He Yaling, and Wang Weiwei. Optimization of solar-powered stirling heat engine with finite-time thermodynamics. *Renewable Energy*, 36(1):421–427, jan 2011.

Appendix A

Isothermal Schmidt Analysis Equation Derivations

The following two sections (derivations) are for calculating the mass of working fluid from a specified mean pressure. The equations derived are used in the ideal adiabatic model as a means of quickly calculating the mass of working fluid that results in a specified mean engine pressure for the specific engine configuration. The following derivations assume that the pistons are connected by a slider crank mechanism and that the resultant piston motion is sinusoidal.

A.1 Alpha Type Fluid Mass

Defining the volumes in the compression and expansion spaces in terms of crank angle, yields equations A.1 and A.2.

$$V_c = V_{ccl} + \frac{V_{c,swept}}{2}(1 + \cos(\theta)) \tag{A.1}$$

$$V_e = V_{ecl} + \frac{V_{e,swept}}{2}(1 + \cos(\theta + \alpha)) \tag{A.2}$$

Defining the derivatives with respect to crank angle of equations A.1 and A.2, yields equations A.3 and A.4.

$$dV_c/d\theta = -\frac{V_{c,swept}}{2}\sin(\theta) \tag{A.3}$$

$$dV_e/d\theta = -\frac{V_{e,swept}}{2}\sin(\theta + \alpha) \tag{A.4}$$

Calculating the pressure throughout the engine yields equation A.5.

$$P = mR/\Big(\frac{V_c}{T_k} + \frac{V_k}{T_k} + \frac{V_r}{T_r} + \frac{V_h}{T_h} + \frac{V_e}{T_h}\Big) \tag{A.5}$$

Defining the constants in equation A.5 as s, yields equation A.6.

$$s = \frac{V_{ccl}}{T_k} + \frac{V_{c,swept}}{2T_k} + \frac{V_k}{T_k} + \frac{V_r}{T_r} + \frac{V_h}{T_h} + \frac{V_{ecl}}{T_h} + \frac{V_{e,swept}}{2T_h} \tag{A.6}$$

Therefore, equation A.5 can be written as equation A.7.

$$P = mR/\Big(s + \frac{V_{c,swept}}{2T_k}\cos(\theta) + \frac{V_{e,swept}}{2T_h}\cos(\theta+\alpha)\Big) \tag{A.7}$$

Expanding the trigonometric functions, yields equation A.8.

$$P = mR/\Big(s + \Big(\frac{V_{c,swept}}{2T_k} + \frac{V_{e,swept}}{2T_h}\cos(\alpha)\Big)\cos(\theta) - \Big(\frac{V_{e,swept}}{2T_h}\sin(\alpha)\Big)\sin(\theta)\Big) \tag{A.8}$$

To simplify equation A.8, constants A and β can be defined. These can be seen as equations A.9 and A.10.

$$A\sin(\beta) = \frac{V_{e,swept}}{2T_h}\sin(\alpha) \tag{A.9}$$

$$A\cos(\beta) = \frac{V_{c,swept}}{2T_k} + \frac{V_{e,swept}}{2T_h}\cos(\alpha) \tag{A.10}$$

Defining the constants A and β explicitly yields equations A.11 and A.12.

$$A = \frac{1}{2}\sqrt{\Big(\frac{V_{e,swept}}{T_h}\Big)^2 + 2\frac{V_{e,swept}V_{c,swept}}{T_hT_k}\cos(\alpha) + \Big(\frac{V_{c,swept}}{T_k}\Big)^2} \tag{A.11}$$

$$\beta = \tan^{-1}\Big(\frac{V_{e,swept}\sin(\alpha)/T_h}{V_{c,swept}/T_k + V_{e,swept}\cos(\alpha)/T_h}\Big) \tag{A.12}$$

Therefore the expression for pressure can be written as equation A.13.

$$P = \frac{mR}{s(1 + B\cos(\phi))} \tag{A.13}$$

Where

$$B = A/s$$

and

$$\phi = \theta + \beta$$

Evaluating A.13, it can be seen that the maximum and minimum pressures can be expressed as equations A.14 and A.15 respectively.

$$P_{max} = \frac{mR}{s(1-B)} \tag{A.14}$$

$$P_{min} = \frac{mR}{s(1+B)} \tag{A.15}$$

In order to calculate the mean pressure, equation A.13 is integrated over a cycle, yielding equation A.16.

$$P_{mean} = \frac{mR}{s}\int_0^{2\pi} \frac{1}{1+B\cos(\phi)}d\phi = \frac{mR}{s\sqrt{1-B^2}} \tag{A.16}$$

Rearranging equation A.16 to explicitly give the mass of working fluid, yields equation A.17.

$$m = \frac{P_{mean}s\sqrt{1-B^2}}{R} \tag{A.17}$$

A.2 Beta and Gamma Type Fluid Mass

Defining the volumes in the compression and expansion spaces in terms of crank angle, yields equations A.18 and A.19.

$$V_c = V_{ccl} + \frac{V_{c,disp}}{2}(1-\cos(\theta+\alpha)) + \frac{V_{c,pist}}{2}(1+\cos(\theta)) \tag{A.18}$$

$$V_e = V_{ecl} + \frac{V_{e,swept}}{2}(1+\cos(\theta+\alpha)) \tag{A.19}$$

Defining the derivatives with respect to crank angle of equations A.18 and A.19, yields equations A.20 and A.21.

$$dV_c/d\theta = \frac{V_{c,disp}}{2}\sin(\theta+\alpha) - \frac{V_{c,pist}}{2}\sin(\theta) \tag{A.20}$$

$$dV_e/d\theta = -\frac{V_{e,swept}}{2}\sin(\theta+\alpha) \tag{A.21}$$

Calculating the pressure throughout the engine yields equation A.22.

$$P = mR/\Big(\frac{V_c}{T_k} + \frac{V_k}{T_k} + \frac{V_r}{T_r} + \frac{V_h}{T_h} + \frac{V_e}{T_h}\Big) \tag{A.22}$$

Defining the constant values in equation A.22 as s, yields equation A.23.

$$s = \frac{V_{ccl}}{T_k} + \frac{V_{c,pist}}{2T_k} + \frac{V_{c,disp}}{2T_k} + \frac{V_k}{T_k} + \frac{V_r}{T_r} + \frac{V_h}{T_h} + \frac{V_{ecl}}{T_h} + \frac{V_{e,swept}}{2T_h} \tag{A.23}$$

Therefore, equation A.23 can be written as equation A.24.

$$P = mR/\Big(s + \frac{V_{c,pist}}{2T_k}\cos(\theta) - \frac{V_{c,disp}}{2T_k}\cos(\theta+\alpha) + \frac{V_{e,swept}}{2T_h}\cos(\theta+\alpha)\Big) \tag{A.24}$$

Expanding the trigonometric functions, yields equation A.25.

$$\begin{aligned} P = mR/\Big(s + \Big(\frac{V_{c,pist}}{2T_k} - \frac{V_{c,disp}}{2T_k}\cos(\alpha) + \frac{V_{e,swept}}{2T_h}\cos(\alpha)\Big)\cos(\theta) \\ + \Big(\frac{V_{c,disp}}{2T_k}\sin(\alpha) - \frac{V_{e,swept}}{2T_h}\sin(\alpha)\Big)\sin(\theta)\Big) \end{aligned} \tag{A.25}$$

To simplify equation A.25, constants A and β can be defined. These can be seen as equations A.26 and A.27.

$$A\sin(\beta) = \frac{V_{c,disp}}{2T_k}\sin(\alpha) - \frac{V_{e,swept}}{2T_h}\sin(\alpha) \tag{A.26}$$

$$A\cos(\beta) = \frac{V_{c,pist}}{2T_k} - \frac{V_{c,disp}}{2T_k}\cos(\alpha) + \frac{V_{e,swept}}{2T_h}\cos(\alpha) \tag{A.27}$$

Defining the constants A and β explicitly yields equations A.28 and A.29.

$$\begin{aligned} A = \\ \frac{1}{2}\sqrt{\Big(\frac{V_{c,pist}}{2T_k} - \frac{V_{c,disp}}{2T_k}\cos(\alpha) + \frac{V_{e,swept}}{2T_h}\cos(\alpha)\Big)^2 + \Big(\frac{V_{c,disp}}{2T_k}\sin(\alpha) - \frac{V_{e,swept}}{2T_h}\sin(\alpha)\Big)^2} \end{aligned} \tag{A.28}$$

$$\beta = \tan^{-1}\Big(\frac{V_{c,disp}\sin(\alpha)/T_k - V_{e,swept}\sin(\alpha)/T_h}{V_{c,pist}/T_k - V_{c,disp}\cos(\alpha)/T_k + V_{e,swept}\cos(\alpha)/T_h}\Big) \tag{A.29}$$

Therefore the expression for pressure can be written as equation A.30.

$$P = \frac{mR}{s(1 + B\cos(\phi))} \tag{A.30}$$

Where

$$B = A/s$$

and

$$\phi = \theta - \beta$$

Evaluating A.30, it can be seen that the maximum and minimum pressures can be expressed as equations A.31 and A.32 respectively.

$$P_{max} = \frac{mR}{s(1-B)} \tag{A.31}$$

$$P_{min} = \frac{mR}{s(1+B)} \tag{A.32}$$

In order to calculate the mean pressure, equation A.30 is integrated over a cycle, yielding equation A.33.

$$P_{mean} = \frac{mR}{s}\int_0^{2\pi} \frac{1}{1+B\cos(\phi)}d\phi = \frac{mR}{s\sqrt{1-B^2}} \tag{A.33}$$

Rearranging equation A.33 to explicitly give the mass of working fluid, yields equation A.34.

$$m = \frac{P_{mean}s\sqrt{1-B^2}}{R} \tag{A.34}$$

Appendix B

Entropy Equation Derivation

B.1 Entropy Generation Equation Derivation

Defining the change in entropy with respect to change in crank angle in a compartment in the Stirling engine as equation B.1.

$$\frac{dS}{d\theta} = \sum_i \frac{1}{T_i}\frac{dQ}{d\theta}\Big|_i + \sum_{in} \frac{dm}{d\theta}s - \sum_{out} \frac{dm}{d\theta}s + \frac{dS_{gen}}{d\theta} \tag{B.1}$$

In order to calculate the amount of entropy generated per cycle, the function is integrated between the initial and final states. This yields equation B.2.

$$\int_0^{2\pi} \frac{dS}{d\theta}d\theta = \int_0^{2\pi} \frac{1}{T}\frac{dQ}{d\theta}d\theta + \int_0^{2\pi} \frac{dm_{in}}{d\theta}(\theta)s_{in}(\theta)d\theta - \int_0^{2\pi} \frac{dm_{out}}{d\theta}(\theta)s_{out}(\theta)d\theta + \int_0^{2\pi} \frac{dS_{gen}}{d\theta}d\theta \tag{B.2}$$

Assuming that the integral of entropy change with angle is zero because the initial and final states are the same.

$$\int_0^{2\pi} dS = S(2\pi) - S(0) = 0 \tag{B.3}$$

Therefore, the entropy produced per cycle is equation B.4

$$S_{gen} = \int_0^{2\pi} \frac{dm_{out}}{d\theta}(\theta)s_{out}(\theta) - \frac{dm_{in}}{d\theta}(\theta)s_{in}(\theta)d\theta - \frac{Q}{T} \tag{B.4}$$

Assuming that the mass flow in equals the mass flow out, and that it is the average of the two mass flows.

$$\frac{dm}{d\theta} = \frac{1}{2}\Big(\frac{dm_{in}}{d\theta} + \frac{dm_{out}}{d\theta}\Big)$$

Therefore, the expression for entropy generation per cycle simplifies to equation B.5

$$S_{gen,net} = \int_0^{2\pi} \frac{dm}{d\theta}(\theta)\big(s_{out}(\theta) - s_{in}(\theta)\big)d\theta - \frac{Q}{T} \tag{B.5}$$

Looking at the Tds relation seen as equation B.6.

$$Tds = dh - VdP \tag{B.6}$$

Assuming that $dh = C_p(T)dT$ and $V/T = R/P$, equation B.7 is obtained.

$$ds = C_p(T)\frac{dT}{T} - R\frac{dP}{P} \tag{B.7}$$

Assuming constant specific heats and integrating between points 1 and 2, yields equation B.8

$$\int_1^2 ds = C_p \int_1^2 \frac{dT}{T} - R\int_1^2 \frac{dP}{P} \tag{B.8}$$

Therefore, evaluating the integral yields equation B.9.

$$s_2 - s_1 = C_p \ln\left(\frac{T_2}{T_1}\right) - R\ln\left(\frac{P_2}{P_1}\right) \tag{B.9}$$

Therefore, the equation B.10 describes the change in entropy.

$$s_{out} - s_{in} = C_p \ln\left(\frac{T_{out}}{T_{in}}\right) - R\ln\left(\frac{P_{out}}{P_{in}}\right) \tag{B.10}$$

Substituting equation B.10 into equation B.5, yields equation B.11

$$S_{gen} = \int_0^{2\pi} \frac{dm}{d\theta}(\theta)\left(C_p \ln\left(\frac{T_{out}(\theta)}{T_{in}(\theta)}\right) - R\ln\left(\frac{P_{out}(\theta)}{P_{in}(\theta)}\right)\right)d\theta - \frac{Q}{T} \tag{B.11}$$

Defining the angular velocity of the engine and the time per cycle, the rate of entropy generation can be defined as equation B.12.

$$\omega = \frac{d\theta}{dt} = 2\pi f$$

$$\Delta t = \frac{1}{f}$$

$$\dot{S}_{gen} = \frac{dS_{gen}}{dt} = \frac{\Delta S_{gen}}{\Delta t} = f S_{gen} \tag{B.12}$$

$$\dot{m} = \frac{dm}{dt} = \frac{dm}{d\theta}\frac{d\theta}{dt} = \omega \frac{dm}{d\theta} \tag{B.13}$$

$$\dot{Q} = \frac{dQ}{dt} = fQ \tag{B.14}$$

Therefore.

$$\dot{S}_{gen} = \frac{1}{2\pi}\int_0^{2\pi} \dot{m}(\theta)\left(C_p \ln\left(\frac{T_{out}(\theta)}{T_{in}(\theta)}\right) - R\ln\left(\frac{P_{out}(\theta)}{P_{in}(\theta)}\right)\right)d\theta - \frac{\dot{Q}}{T} \tag{B.15}$$

B.2 Heater and Cooler

The heater is assumed to be isothermal, therefore:

$$\ln\left(\frac{T_{out}}{T_{in}}\right) = 0$$

As the expressions are numerically integrated, the absolute values of each term are taken to aid in applying the numerical integration scheme.

$$\dot{S}_{gen,h} = \frac{R}{2\pi}\int_0^{2\pi} |\dot{m}_h(\theta)|\left|\ln\left(\frac{P_{eb}(\theta)}{P_{hb}(\theta)}\right)\right|d\theta - \frac{\dot{Q}_h}{T_{source}} \tag{B.16}$$

$$\dot{S}_{gen,k} = \frac{R}{2\pi}\int_0^{2\pi} |\dot{m}_k(\theta)|\left|\ln\left(\frac{P_{kb}(\theta)}{P_{cb}(\theta)}\right)\right|d\theta + \frac{\dot{Q}_k}{T_{sink}} \tag{B.17}$$

In the case of the finite capacity rate assumption the $\frac{\dot{Q}}{T}$ term is replaced by the equation which describes the entropy change of the external fluid.

B.3 Regenerator

Defining the rate of entropy generation in the regenerator as equation B.18.

$$\dot{S}_{gen,r} = \frac{1}{2\pi}\int_0^{2\pi} \dot{m}_r(\theta)\left(C_p \ln\left(\frac{T_{out}(\theta)}{T_{in}(\theta)}\right) - R\ln\left(\frac{P_{out}(\theta)}{P_{in}(\theta)}\right)\right)d\theta \tag{B.18}$$

therefore.

$$\dot{S}_{gen,r} = \frac{C_p}{2\pi}\int_0^{\pi} \dot{m}_r(\theta)\ln\left(\frac{T_{hb}}{T_k}\right)d\theta + \frac{C_p}{2\pi}\int_{\pi}^{2\pi} \dot{m}_r(\theta)\ln\left(\frac{T_{kb}}{T_h}\right)d\theta - \frac{R}{2\pi}\int_0^{2\pi} \dot{m}_r(\theta)\ln\left(\frac{P_{out}(\theta)}{P_{in}(\theta)}\right)d\theta \tag{B.19}$$

$$\dot{S}_{gen,r} = \frac{C_p}{2\pi}\ln\left(\frac{T_{hb}}{T_k}\right)\int_0^{\pi} \dot{m}_r(\theta)d\theta + \frac{C_p}{2\pi}\ln\left(\frac{T_{kb}}{T_h}\right)\int_{\pi}^{2\pi} \dot{m}_r(\theta)d\theta - \frac{R}{2\pi}\int_0^{2\pi} \dot{m}_r(\theta)\ln\left(\frac{P_{out}(\theta)}{P_{in}(\theta)}\right)d\theta \tag{B.20}$$

Assuming the average mass flow for each direction is equal and opposite in direction.

$$\int_0^{\pi} |\dot{m}_r(\theta)|d\theta = \int_{\pi}^{2\pi} |\dot{m}_r(\theta)|d\theta = \frac{1}{2}\int_{\pi}^{2\pi} |\dot{m}_r(\theta)|d\theta$$

As the expressions are numerically integrated, the absolute values of each term are taken to aid in applying the numerical integration scheme. This yields equation B.21 which is used to calculate the rate of entropy generation in the regenerator.

$$\dot{S}_{gen,r} = \frac{C_p}{4\pi} ln\left(\frac{T_{hb}T_{kb}}{T_k T_h}\right)\int_0^{2\pi} |\dot{m}_r(\theta)|d\theta + \frac{R}{2\pi}\int_0^{2\pi} |\dot{m}_r(\theta)|\left|\ln\left(\frac{P_{out}(\theta)}{P_{in}(\theta)}\right)\right|d\theta \tag{B.21}$$

Appendix C

Ideal Isothermal Model (Kongtragool and Wongwises)

C.1 Mathematical Derivation

Defining the pressure in the device as equation C.1.

$$P = mR/(\frac{V_c}{T_k} + \frac{V_k}{T_k} + \frac{V_r}{T_r} + \frac{V_h}{T_h} + \frac{V_e}{T_e}) \tag{C.1}$$

Defining the regenerator temperature as the arithmetic mean of the hot and cold space temperatures, seen as equation C.2.

$$T_r = \frac{T_h + T_k}{2} \tag{C.2}$$

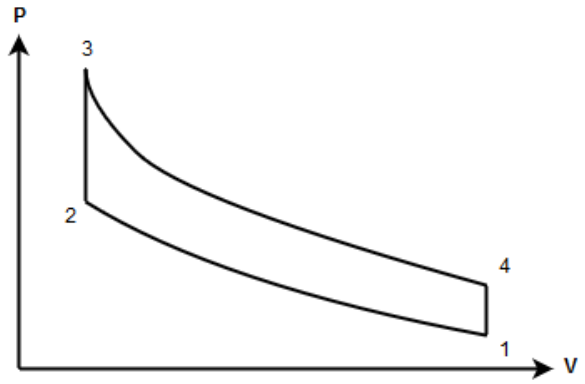

Figure C.1: Ideal pressure-volume diagram

Looking at the pressure-volume diagram and defining the engine volumes we obtain:

$$V_1 = V_c + V_{dead}$$

$$V_2 = V_3 = V_{dead}$$

$$V_4 = V_e + V_{dead}$$

Defining the work and the energy equations for the isothermal compression process, yields equation C.3.

$$Q_{1-2} = W_{1-2} = \int_{V_1}^{V_2} P dV_c \tag{C.3}$$

Defining the work and the energy equations for the isothermal expansion process, yields equation C.4.

$$Q_{3-4} = W_{3-4} = \int_{V_3}^{V_4} P dV_e \tag{C.4}$$

Therefore, evaluating the integral for the compression process, yields equation C.5

$$Q_{1\to2} = W_{1\to2} = mRT_k ln\left(\frac{V_{dead} + V_{ccl} + T_k(V_{ecl}/T_h + Y)}{V_c + V_{dead} + V_{ccl} + T_k(V_{ecl}/T_h + Y)}\right) \tag{C.5}$$

Therefore, evaluating the integral for the expansion process, yields equation C.6

$$Q_{3\to4} = W_{3\to4} = mRT_h ln\left(\frac{V_e + V_{dead} + V_{ecl} + T_h(V_{ccl}/T_k + Y)}{V_{dead} + V_{ecl} + T_h(V_{ccl}/T_k + Y)}\right) \tag{C.6}$$

Since energy is absorbed during the expansion process, we can define equation C.7 as the energy absorbed per cycle.

$$Q_{in} = mRT_k ln\left(\frac{V_{dead} + V_{ccl} + T_k(V_{ecl}/T_h + Y)}{V_c + V_{dead} + V_{ccl} + T_k(V_{ecl}/T_h + Y)}\right) \tag{C.7}$$

Since energy is rejected during the compression process, we can define equation C.8 as the energy rejected per cycle.

$$Q_{out} = mRT_h ln\left(\frac{V_e + V_{dead} + V_{ecl} + T_h(V_{ccl}/T_k + Y)}{V_{dead} + V_{ecl} + T_h(V_{ccl}/T_k + Y)}\right) \tag{C.8}$$

Therefore defining the work as the difference between the energy absorbed and rejected, yields equation C.9.

$$W = mRT_k ln\left(\frac{V_{dead} + V_{ccl} + T_k(V_{ecl}/T_h + Y)}{V_c + V_{dead} + V_{ccl} + T_k(V_{ecl}/T_h + Y)}\right) - mRT_h ln\left(\frac{V_e + V_{dead} + V_{ecl} + T_h(V_{ccl}/T_k + Y)}{V_{dead} + V_{ecl} + T_h(V_{ccl}/T_k + Y)}\right) \quad \text{(C.9)}$$

Defining the efficiency, yields equation C.10.

$$\eta = \left(T_h ln\left(\frac{V_e + V_{dead} + V_{ecl} + T_h(V_{ccl}/T_k + Y)}{V_{dead} + V_{ecl} + T_h(V_{ccl}/T_k + Y)}\right) - T_k ln\left(\frac{V_{dead} + V_{ccl} + T_k(V_{ecl}/T_h + Y)}{V_c + V_{dead} + V_{ccl} + T_k(V_{ecl}/T_h + Y)}\right)\right) / T_h ln\left(\frac{V_e + V_{dead} + V_{ecl} + T_h(V_{ccl}/T_k + Y)}{V_{dead} + V_{ecl} + T_h(V_{ccl}/T_k + Y)}\right) \quad \text{(C.10)}$$

C.2 Validation Matlab Code

```
%DEAD-VOLUME ANALYSIS VALIDATION CODE-----------------------------------------
%JAMES WILLS 2016-------------------------------------------------------------
%-----------------------------------------------------------------------------
%DEFINING CONSTANTS-----------------------------------------------------------
TH = 923;
TK = 338;
VP = 50000;
VD = 75000;
Ksh = 0.2;
Ksr = 0.6;
Ksc = 0.2;
p = 101300;
R = 287;
Cv = 718;
Cp = 1005;
%-----------------------------------------------------------------------------
%CALCULATING THE REGENERATOR TEMPERATURE--------------------------------------
TR = (TH + TK)/2;
%-----------------------------------------------------------------------------
%CALCULATING THE CYLINDER VOLUMES---------------------------------------------
VC1 = VD + VP;
VC2 = VD;
%-----------------------------------------------------------------------------
%DEFINING THE VECTORS---------------------------------------------------------
Kst = [0  0.2  0.3333  0.5  0.6  0.66667];
%-----------------------------------------------------------------------------
%PREALLOCATION----------------------------------------------------------------
W12 = zeros(1,numel(Kst));
W34 = zeros(1,numel(Kst));
Wnet = zeros(1,numel(Kst));
m = zeros(1,numel(Kst));
Vs = zeros(1,numel(Kst));
K = zeros(1,numel(Kst));
Ksdp = zeros(1,numel(Kst));
%-----------------------------------------------------------------------------
for i = 1:numel(Kst)
    Ksdp(i) = Kst(i)/(1 - Kst(i));
    Vs(i) = Ksdp(i)*(VD + VP);
    Vdead = (Ksh + Ksr + Ksc)*Vs(i);
    K(i) = (Ksh/TH + Ksr/TR + Ksc/TK)*Vs(i);
    m(i) = (p/R)*(K(i) + VC1/TK);
    W12(i) = m(i)*R*TK*log((VD + K(i)*TK)/(VD + VP + K(i)*TK));
    W34(i) = m(i)*R*TH*log((VD + VP + K(i)*TH)/(VD  + K(i)*TH));
    Wnet(i) = W12(i) + W34(i);
end
Wnet1 = Wnet/max(Wnet);
W121 = W12/min(W12);
W341 = W34/max(W34);
m1 = m/min(m);
%-----------------------------------------------------------------------------
```

```
TR = (TH - TK)/log(TH/TK);
for i = 1:numel(Kst)
    Ksdp(i) = Kst(i)/(1 - Kst(i));
    Vs(i) = Ksdp(i)*(VD + VP);
    Vdead = (Ksh + Ksr + Ksc)*Vs(i);
    K(i) = (Ksh/TH + Ksr/TR + Ksc/TK)*Vs(i);
    m(i) = (p/R)*(K(i) + VC1/TK);
    W12(i) = m(i)*R*TK*log((VD + K(i)*TK)/(VD + VP + K(i)*TK));
    W34(i) = m(i)*R*TH*log((VD + VP + K(i)*TH)/(VD  + K(i)*TH));
    Wnet(i) = W12(i) + W34(i);
end
Wnet2 = Wnet/max(Wnet);
W1212 = W12/min(W12);
W3412 = W34/max(W34);
m2 = m/min(m);
%-------------------------------------------------------------------------------
```

C.3 Validation Results

Figure C.2 is a plot of normalised mass versus dead-volume ratio.

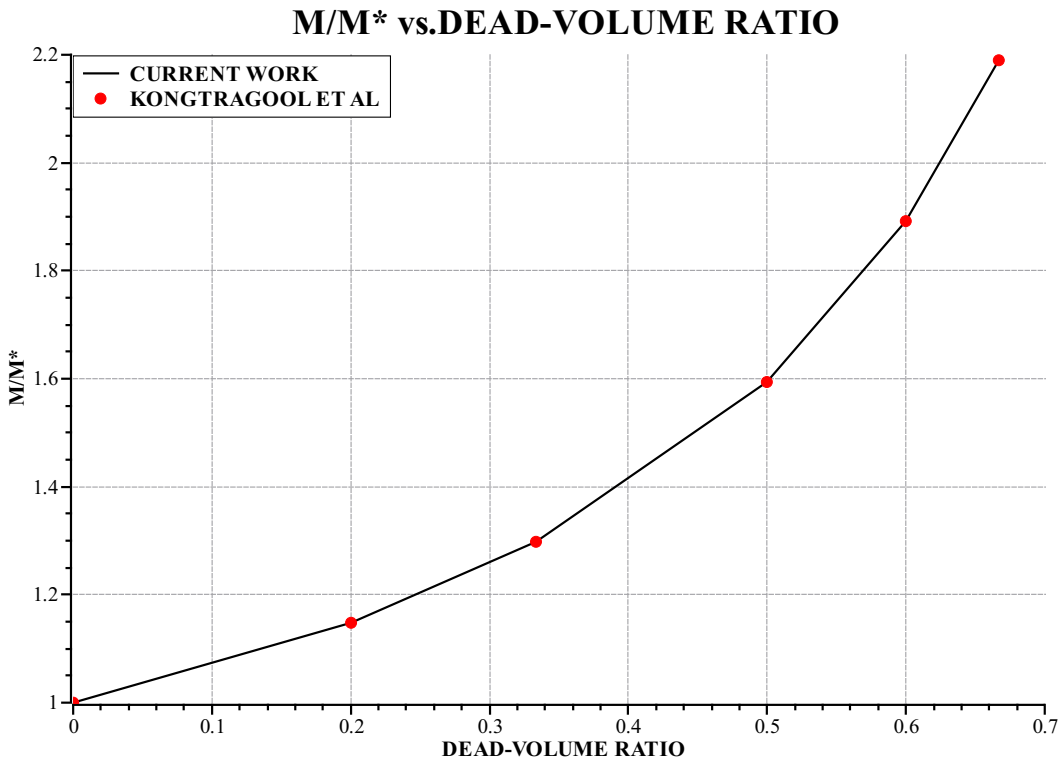

Figure C.2: Normalised mass versus dead-volume ratio

Figure C.3 is a plot of normalised work versus dead-volume ratio.

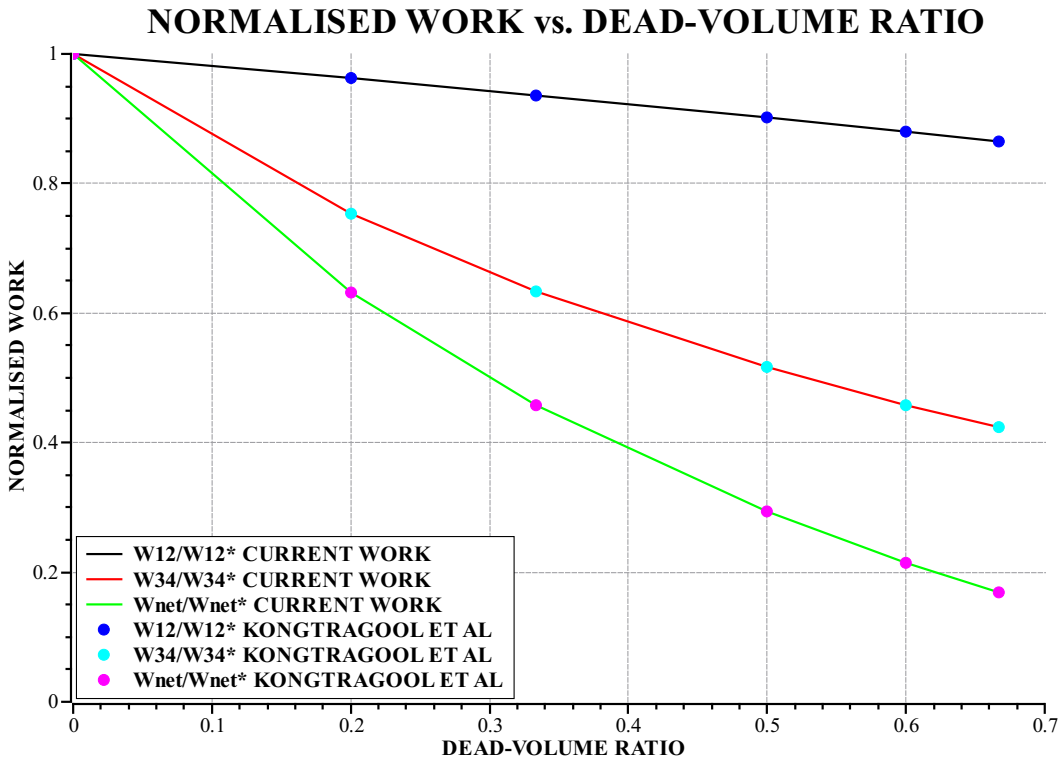

Figure C.3: Normalised work versus dead-volume ratio

It can be seen in both of the plots that the results are identical. This code is the same as the code used in chapter 5, the only difference being that in the chapter 5 analysis logarithmic regenerator temperature is used rather that arithmetic mean temperature.

Appendix D

Matlab Code

D.1 Adiabatic Model

D.1.1 Numerical Scheme for Adiabatic Model

```
%INITIALISING AND RUNNING THE NUMERICAL SCHEMES-----------------------------
%James Wills 2016/17--------------------------------------------------------
%---------------------------------------------------------------------------
function [Variables,dVariables] = NUMERICAL(Variables,dVariables,M,Th,Tk,Vh,Vr,Vk,Vccl,
    Vcswept,Vecl,Veswept)
%Note: Change function call if configuration changes
%INITIALISING VALUES--------------------------------------------------------
Variables(17,1) = Tk;
Variables(18,1) = Th;
Variables(2,360) = Th;
Variables(1,360) = Tk;
h = 2*pi/359;
n = 0;
while (abs(Variables(1,1)-Variables(1,360)) + abs(Variables(2,1)-Variables(2,360))) > 0.05
    n = n+1;
    Theta = 0;
    Variables(3,1) = 0;
    Variables(4,1) = 0;
    Variables(5,1) = 0;
    Variables(6,1) = 0;
    Variables(7,1) = 0;
    Variables(10,1) = 0;
    Variables(1,1) = Variables(1,360);
    Variables(2,1) = Variables(2,360);
    [Variables(:,1),dVariables(:,1)] = feval('ADIABEQUATIONS',0,Variables(:,1),M,Th,Tk,Vh,Vr
        ,Vk,Vccl,Vcswept,Vecl,Veswept);
    for i = 1:5;
        [Theta, Variables(:,i+1),dVariables(:,i+1)] = RUNGEKUTTA4('ADIABEQUATIONS',7,Theta,
            Variables(:,i),M,Th,Tk,Vh,Vr,Vk,Vccl,Vcswept,Vecl,Veswept,h);
```

```
27      end
28      for i = 5:359
29          [Theta, Variables(:,i+1),dVariables(:,i+1)] = AB4('ADIABEQUATIONS',7,Variables(:,i),
                dVariables(:,i),dVariables(:,i-1),dVariables(:,i-2),dVariables(:,i-3),Theta,M,Th
                ,Tk,Vh,Vr,Vk,Vccl,Vcswept,Vecl,Veswept,h);
30      end
31      if n>30
32          break
33      end
34  end
35  %-------------------------------------------------------------------------
```

D.1.2 Adiabatic Equations

```
1   %ADIABATIC EQUATIONS---------------------------------------------------------
2   %James Wills 2016/17---------------------------------------------------------
3   %-----------------------------------------------------------------------------
4   function [f,df] = ADIABEQUATIONS(theta,f,M,Th,Tk,Vh,Vr,Vk,Vccl,Vcswept,Vecl,Veswept)
5   %Note: Change function call if configuration changes
6   global Ri
7   global Cpi
8   global Cvi
9   global ki
10  %DEFINING THE INDICES--------------------------------------------------------
11  Tc = 1;
12  Te = 2;
13  Qk = 3;
14  Qr = 4;
15  Qh = 5;
16  Wc = 6;
17  We = 7;
18  Vc = 8;
19  Ve = 9;
20  W = 10;
21  P = 11;
22  mc = 12;
23  mk = 13;
24  mr = 14;
25  mh = 15;
26  me = 16;
27  Tcb = 17;
28  Teb = 18;
29  mcb = 19;
30  mkb = 20;
31  mhb = 21;
32  meb = 22;
33  %REGENERATOR TEMPERATURE-----------------------------------------------------
34  Tr = (Th-Tk)/log(Th/Tk);                                                %K
35  %VOLUME AND VOLUME DERIVATIVES-----------------------------------------------
36  %ALPHA TYPE------------------------------------------------------------------
37  f(Vc) = Vccl + (Vcswept/2)*(1 + cos(theta));                            %m^3
38  f(Ve) = Vecl + (Veswept/2)*(1 + cos(theta + pi/2));                     %m^3
```

```
39 df(Vc) = -(Vcswept/2)*sin(theta);                                    %m^3/
       theta
40 df(Ve) = -(Veswept/2)*sin(theta + pi/2);                             %m^3/
       theta
41 %BETA TYPE-----------------------------------------------------------------
42 %f(Vc) = Vccl + (Vcdisp/2)*(1 - cos(theta + pi/2)) + (Vcpist/2)*(1 + cos(theta));  %m^3
43 %f(Ve) = Vecl + (Veswept/2)*(1 + cos(theta + pi/2));                   %m^3
44 %df(Vc) = (Vcdisp/2)*sin(theta + pi/2) - (Vcpist/2)*sin(theta);       %m^3/
       theta
45 %df(Ve) = -(Veswept/2)*sin(theta + pi/2);                             %m^3/
       theta
46 %PRESSURE and PRESSURE DERIVATIVE-------------------------------------------
47 f(P) = M*Ri/(f(Vc)/f(Tc) + Vk/Tk + Vr/Tr + Vh/Th + f(Ve)/f(Te));      %kPa
48 df(P) = -ki*f(P)*(df(Vc)/f(Tcb) + df(Ve)/f(Teb))/(f(Vc)/f(Tcb) + ki*(Vk/Tk + Vr/Tr + Vh/Th)
       + f(Ve)/f(Teb)); %kPa/theta
49 %MASS and MASS DERIVATIVES---------------------------------------------------
50 f(mc) = f(P)*f(Vc)/(Ri*f(Tc));                                        %kg
51 f(mk) = f(P)*Vk/(Ri*Tk);                                              %kg
52 f(mr) = f(P)*Vr/(Ri*Tr);                                              %kg
53 f(mh) = f(P)*Vh/(Ri*Th);                                              %kg
54 f(me) = f(P)*f(Ve)/(Ri*f(Te));                                        %kg
55 df(mc) = (f(P)*df(Vc) + (f(Vc)*df(P)/ki))/(Ri*f(Tcb));               %kg/theta
56 df(mk) = f(mk)*df(P)/f(P);                                           %kg/theta
57 df(mr) = f(mr)*df(P)/f(P);                                           %kg/theta
58 df(mh) = f(mh)*df(P)/f(P);                                           %kg/theta
59 df(me) = (f(P)*df(Ve) + (f(Ve)*df(P)/ki))/(Ri*f(Teb));               %kg/theta
60 %MASS FLOWS-----------------------------------------------------------------
61 f(mcb) = -df(mc);                                                    %kg/theta
62 f(mkb) = f(mcb) - df(mk);                                            %kg/theta
63 f(meb) = df(me);                                                     %kg/theta
64 f(mhb) = f(meb) + df(mh);                                            %kg/theta
65 %CONDITIONAL TEMPERATURES----------------------------------------------------
66 if f(mcb) > 0
67     f(Tcb) = f(Tc);                                                  %K
68 else f(Tcb) = Tk;                                                    %K
69 end
70 if f(meb) > 0
71     f(Teb) = Th;                                                     %K
72 else f(Teb) = f(Te);                                                 %K
73 end
74 %TEMPERATURE DERIVATIVES-----------------------------------------------------
75 df(Tc) = f(Tc)*(df(P)/f(P) + df(Vc)/f(Vc) - df(mc)/f(mc));           %K/theta
76 df(Te) = f(Te)*(df(P)/f(P) + df(Ve)/f(Ve) - df(me)/f(me));           %K/theta
77 %ENERGY EQUATIONS------------------------------------------------------------
78 df(Qk) = Vk*df(P)*Cvi/Ri - Cpi*(f(Tcb)*f(mcb) - Tk*f(mkb));          %kJ/theta
79 df(Qr) = Vr*df(P)*Cvi/Ri - Cpi*(Tk*f(mkb) - Th*f(mhb));              %kJ/theta
80 df(Qh) = Vh*df(P)*Cvi/Ri - Cpi*(Th*f(mhb) - f(Teb)*f(meb));         %kJ/theta
81 df(Wc) = f(P)*df(Vc);                                               %kW/theta
82 df(We) = f(P)*df(Ve);                                               %kW/theta
83 df(W) = df(Wc) + df(We);                                            %kW/theta
84 f(W) = f(Wc) + f(We);                                               %kW
85 %---------------------------------------------------------------------------
```

D.1.3 Runge-Kutta Numerical Method

```
%RUNGE-KUTTA OF ORDER 4----------------------------------------------------------------------
%James Wills 2016/17-------------------------------------------------------------------------
%--------------------------------------------------------------------------------------------
function [x,f,df] = RUNGEKUTTA4(Equations,num,x0,f0,M,Th,Tk,Vh,Vr,Vk,Vccl,Vcswept,Vecl,
    Veswept,h)
[f,k1] = feval(Equations,x0,f0,M,Th,Tk,Vh,Vr,Vk,Vccl,Vcswept,Vecl,Veswept);
W2 = f;
W3 = f;
W4 = f;
for i = 1:num
    W2(i) = f(i) + 0.5*h*k1(i);
end
xmid = x0 + 0.5*h;
[~,k2] = feval(Equations,xmid,W2,M,Th,Tk,Vh,Vr,Vk,Vccl,Vcswept,Vecl,Veswept);
for i = 1:num
    W3(i) = f(i) + 0.5*h*k2(i);
end
[~,k3] = feval(Equations,xmid,W3,M,Th,Tk,Vh,Vr,Vk,Vccl,Vcswept,Vecl,Veswept);
for i = 1:num
    W4(i) = f(i) + h*k3(i);
end
x = x0 + h;
[~,k4] = feval(Equations,x,W4,M,Th,Tk,Vh,Vr,Vk,Vccl,Vcswept,Vecl,Veswept);
for i = 1:num
    f(i) = f(i) + (h/6)*(k1(i) + 2*k2(i) + 2*k3(i) + k4(i));
end
[f,df] = feval(Equations,x,f,M,Th,Tk,Vh,Vr,Vk,Vccl,Vcswept,Vecl,Veswept);
%--------------------------------------------------------------------------------------------
```

D.1.4 Adam's-Bashforth Numerical Method

```
%ADAMS BASHFORTH ORDER 4 ---------------------------------------------------------------------
%James Wills 2016/17-------------------------------------------------------------------------
%--------------------------------------------------------------------------------------------
%df1 = derivative at i
%df2 = derivative at i-1
%df3 = derivative at i-2
%df4 = derivative at i-3
function [Theta,f,df] = AB4(Equations,num,f0,df1,df2,df3,df4,Theta,M,Th,Tk,Vh,Vr,Vk,Vccl,
    Vcswept,Vecl,Veswept,h)
f = f0;
for i = 1:num
    f(i) = f0(i) + (h/24)*(55*df1(i) - 59*df2(i) + 37*df3(i) - 9*df4(i));
end
Theta = Theta + h;
[f,df] = feval(Equations,Theta,f,M,Th,Tk,Vh,Vr,Vk,Vccl,Vcswept,Vecl,Veswept);
%--------------------------------------------------------------------------------------------
```

D.2 Dead-Volume Scripts

D.2.1 Adiabatic Dead-Volume Analysis

```
%STIRLING ENGINE ADIABATIC MODEL DEAD VOLUME ANALYSIS
%James Wills 2016
%
%DEFINING GLOBAL VARIABLES
global R
global Cp
global Cv
global k
global Th
global Tr
global Tk
global M
global Vr
global Vh
global Vk
global Vemax
global Vcmax
global Vccl
global Vecl
%GAS CONSTANTS
R = 0.2870;
Cp = 1.005;
Cv = 0.718;
k = 1.4;
%ENGINE VOLUMES AND MASS
Vtot = 1;
DVR = 0.1:0.02:0.9;
V = 1;
M = 1;
x = [1.5 2.0 2.5 3.0];
%DEFINING TEMPERATURES
Tk = 300;
Efficiency = zeros(numel(x),numel(DVR));
HEATER = zeros(numel(x),numel(DVR));
WORK = zeros(numel(x),numel(DVR));
%FOR LOOP
for n = 1:numel(x)
    Th = x(n)*Tk;
    Tr = (Th - Tk)/log(Th/Tk);
for j = 1:numel(DVR)
    Vdead = V*DVR(j);
    Vemax = 0.5*(V - Vdead);
    Vcmax = 0.5*(V - Vdead);
    Vccl = (5/100)*Vdead;
    Vk = ((30/100)*Vdead);
    Vr = (30/100)*Vdead;
    Vh = (30/100)*Vdead;
    Vecl = (5/100)*Vdead;
```

```
49      %PREALLOCATION OF MATRICES AND ANGLE VECTOR----------------------------------
50      Variables = zeros(25,360);    %Setting up variables matrix-----------------
51      dVariables = zeros(16,360);   %Setting up derivatives matrix---------------
52      Theta1 = linspace(0,2*pi,360);
53      h = Theta1(2) - Theta1(1);
54      %INITIAL VALUES--------------------------------------------------------------
55      Variables(17,1) = Tk;
56      Variables(18,1) = Th;
57      Variables(2,360) = Th;
58      Variables(1,360) = Tk;
59      while (abs(Variables(1,1) - Variables(1,360)) + abs(Variables(2,1) - Variables(2,360)))
            > 0.1
60          Theta = 0;
61          Variables(3,1) = 0;
62          Variables(4,1) = 0;
63          Variables(5,1) = 0;
64          Variables(6,1) = 0;
65          Variables(7,1) = 0;
66          Variables(10,1) = 0;
67          Variables(1,1) = Variables(1,360);
68          Variables(2,1) = Variables(2,360);
69          Variables(8,1) = Variables(8,360);
70          Variables(9,1) = Variables(9,360);
71          Variables(11,1) = Variables(11,360);
72          for i = 1:5;
73              [Theta, Variables(:,i+1),dVariables(:,i+1)] = RUNGEKUTTA('DVEQUATIONS',7,Theta,h
                    ,Variables(:,i));
74          end
75          for i = 5:359
76              [Theta, Variables(:,i+1),dVariables(:,i+1)] = AB4('DVEQUATIONS',7,Variables(:,i)
                    ,dVariables(:,i),dVariables(:,i-1),dVariables(:,i-2),dVariables(:,i-3),Theta
                    ,h);
77          end
78      end
79      Efficiency(n,j) = (Variables(5,360)+Variables(3,360))/Variables(5,360);
80      HEATER(n,j) = Variables(5,360);
81      WORK(n,j) = Variables(5,360)+Variables(3,360);
82  end
83  end
84  %----------------------------------------------------------------------------
```

D.2.2 LTD and MTD Dead-Volume Analysis

```
1   %STIRLING ENGINE LTD ANALYSIS-----------------------------------------------
2   %James Wills 2016-----------------------------------------------------------
3   %---------------------------------------------------------------------------
4   %DEFINING GLOBAL VARIABLES--------------------------------------------------
5   global R
6   global Cp
7   global Cv
8   global k
9   global Th
```

```
10 global Tr
11 global Tk
12 global M
13 global Vr
14 global Vh
15 global Vk
16 global Vemax
17 global Vcmax
18 global Vccl
19 global Vecl
20 %GAS CONSTANTS----------------------------------------------------------------
21 R = 0.2870;
22 Cp = 1.005;
23 Cv = 0.718;
24 k = 1.4;
25 %ENGINE VOLUMES AND MASS--------------------------------------------------------
26 Vtot = 1;
27 DVR = 0.1:0.02:0.9;
28 V = 1;
29 M = 1;
30 x = [1.2 1.4 1.5 1.6 1.8];
31 %DEFINING TEMPERATURES----------------------------------------------------------
32 Tk = 300;
33 Efficiency = zeros(numel(x),numel(DVR));
34 HEATER = zeros(numel(x),numel(DVR));
35 WORK = zeros(numel(x),numel(DVR));
36 %FOR LOOP------------------------------------------------------------------------
37 for n = 1:numel(x)
38     Th = x(n)*Tk;
39     Tr = (Th - Tk)/log(Th/Tk);
40 for j = 1:numel(DVR)
41     Vdead = V*DVR(j);
42     Vemax = 0.5*(V - Vdead);
43     Vcmax = 0.5*(V - Vdead);
44     Vccl = (5/100)*Vdead;
45     Vk = ((30/100)*Vdead);
46     Vr = (30/100)*Vdead;
47     Vh = (30/100)*Vdead;
48     Vecl = (5/100)*Vdead;
49     %PREALLOCATION OF MATRICES AND ANGLE VECTOR-------------------------------
50     Variables = zeros(25,360);    %Setting up variables matrix----------
51     dVariables = zeros(16,360);   %Setting up derivatives matrix---------
52     Theta1 = linspace(0,2*pi,360);
53     h = Theta1(2) - Theta1(1);
54     %INITIAL VALUES-----------------------------------------------------------
55     Variables(17,1) = Tk;
56     Variables(18,1) = Th;
57     Variables(2,360) = Th;
58     Variables(1,360) = Tk;
59     while (abs(Variables(1,1) - Variables(1,360)) + abs(Variables(2,1) - Variables(2,360)))
           > 0.001
60         Theta = 0;
```

```
61            Variables(3,1) = 0;
62            Variables(4,1) = 0;
63            Variables(5,1) = 0;
64            Variables(6,1) = 0;
65            Variables(7,1) = 0;
66            Variables(10,1) = 0;
67            Variables(1,1) = Variables(1,360);
68            Variables(2,1) = Variables(2,360);
69            Variables(8,1) = Variables(8,360);
70            Variables(9,1) = Variables(9,360);
71            Variables(11,1) = Variables(11,360);
72            for i = 1:5;
73                [Theta, Variables(:,i+1),dVariables(:,i+1)] = RUNGEKUTTA('DVEQUATIONS',7,Theta,h
                      ,Variables(:,i));
74            end
75            for i = 5:359
76                [Theta, Variables(:,i+1),dVariables(:,i+1)] = AB4('DVEQUATIONS',7,Variables(:,i)
                      ,dVariables(:,i),dVariables(:,i-1),dVariables(:,i-2),dVariables(:,i-3),Theta
                      ,h);
77            end
78        end
79        Efficiency(n,j) = (Variables(5,360)+Variables(3,360))/Variables(5,360);
80        HEATER(n,j) = Variables(5,360);
81        WORK(n,j) = Variables(5,360)+Variables(3,360);
82    end
83    end
84    %POINTS ------------------------------------------------------------------------
85    DVRP = 0.1:0.1:0.9;
86    WORKP = [WORK(:,1),WORK(:,11),WORK(:,21),WORK(:,31),WORK(:,41),WORK(:,51),WORK(:,61),WORK
          (:,71),WORK(:,81)];
87    %MAXIMUM WORK------------------------------------------------------------------------
88    MW1 = max(WORK(1,:));
89    MW2 = max(WORK(2,:));
90    MW3 = max(WORK(3,:));
91    MW4 = max(WORK(4,:));
92    MW5 = max(WORK(5,:));
93    %------------------------------------------------------------------------
```

D.2.3 Heat Exchanger Volume Analysis

```
1   %STIRLING ENGINE ADIABATIC MODEL HEAT EXCHANGER VOLUME ANALYSIS----------
2   %James Wills 2016------------------------------------------------------------
3   %----------------------------------------------------------------------------
4   %DEFINING GLOBAL VARIABLES----------------------------------------------------
5   global R
6   global Cp
7   global Cv
8   global k
9   global Th
10  global Tr
11  global Tk
12  global M
```

```
13 global Vr
14 global Vh
15 global Vk
16 global Vemax
17 global Vcmax
18 global Vccl
19 global Vecl
20 %GAS CONSTANTS-------------------------------------------------------------------
21 R = 0.2870;
22 Cp = 1.005;
23 Cv = 0.718;
24 k = 1.4;
25 %ENGINE VOLUMES AND MASS-----------------------------------------------------------
26 Vtot = 1;
27 DVR = 0.05:0.01:0.2;
28 V = 1;
29 M = 1;
30 REG = [0.25 0.5 0.75];
31 HEAT = [0.25 1.0 4.0];
32 r = 0.8;
33 X = 1.75;
34 %DEFINING TEMPERATURES-------------------------------------------------------------
35 Tk = 300;
36 %----------------------------------------------------------------------------------
37 Efficiency = zeros(numel(r)*numel(X),numel(DVR));
38 HEATER = zeros(numel(r)*numel(X),numel(DVR));
39 WORK = zeros(numel(r)*numel(X),numel(DVR));
40 %FOR LOOP---------------------------------------------------------------------------
41 for n = 1:numel(REG)
42     Th = X*Tk;
43     Tr = (Th - Tk)/log(Th/Tk);
44     for l = 1:numel(HEAT)
45         for j = 1:numel(DVR)
46             Vdead = V*DVR(j);
47             Vemax = (V - Vdead)/(1 + r);
48             Vcmax = (V - Vdead) - Vemax;
49             Vccl = (5/100)*Vdead;
50             Vk = ((0.9 - REG(n))*Vdead)/(1 + HEAT(l));
51             Vr = REG(n)*Vdead;
52             Vh = (0.9 - REG(n))*Vdead - Vk;
53             Vecl = (5/100)*Vdead;
54             %PREALLOCATION OF MATRICES AND ANGLE VECTOR-----------------------------
55             Variables = zeros(25,360);    %Setting up variables matrix-------------
56             dVariables = zeros(16,360);   %Setting up derivatives matrix-----------
57             Theta1 = linspace(0,2*pi,360);
58             h = Theta1(2) - Theta1(1);
59             %INITIAL VALUES---------------------------------------------------------
60             Variables(17,1) = Tk;
61             Variables(18,1) = Th;
62             Variables(2,360) = Th;
63             Variables(1,360) = Tk;
64             while (abs(Variables(1,1) - Variables(1,360)) + abs(Variables(2,1) - Variables
```

```
                    (2,360))) > 0.01
65                  Theta = 0;
66                  Variables(3,1) = 0;
67                  Variables(4,1) = 0;
68                  Variables(5,1) = 0;
69                  Variables(6,1) = 0;
70                  Variables(7,1) = 0;
71                  Variables(10,1) = 0;
72                  Variables(1,1) = Variables(1,360);
73                  Variables(2,1) = Variables(2,360);
74                  Variables(8,1) = Variables(8,360);
75                  Variables(9,1) = Variables(9,360);
76                  Variables(11,1) = Variables(11,360);
77                  for i = 1:5;
78                      [Theta, Variables(:,i+1),dVariables(:,i+1)] = RUNGEKUTTA('DVEQUATIONS'
                            ,7,Theta,h,Variables(:,i));
79                  end
80                  for i = 5:359
81                      [Theta, Variables(:,i+1),dVariables(:,i+1)] = AB4('DVEQUATIONS',7,
                            Variables(:,i),dVariables(:,i),dVariables(:,i-1),dVariables(:,i-2),
                            dVariables(:,i-3),Theta,h);
82                  end
83              end
84              Efficiency(l + (n-1)*numel(REG),j) = (Variables(5,360)+Variables(3,360))/
                    Variables(5,360);
85              HEATER(l + (n-1)*numel(REG),j) = Variables(5,360);
86              WORK(l + (n-1)*numel(REG),j) = Variables(5,360) + Variables(3,360);
87          end
88      end
89  end
90  %-------------------------------------------------------------------------------
```

D.2.4 Swept Volume Analysis

```
1   %STIRLING ENGINE ADIABATIC MODEL SWEPT VOLUME ANALYSIS-----------------------
2   %James Wills 2016-------------------------------------------------------------
3   %-----------------------------------------------------------------------------
4   %DEFINING GLOBAL VARIABLES----------------------------------------------------
5   global R
6   global Cp
7   global Cv
8   global k
9   global Th
10  global Tr
11  global Tk
12  global M
13  global Vr
14  global Vh
15  global Vk
16  global Vemax
17  global Vcmax
18  global Vccl
```

```
19  global Vecl
20  %GAS CONSTANTS----------------------------------------------------------------------
21  R = 0.2870;
22  Cp = 1.005;
23  Cv = 0.718;
24  k = 1.4;
25  %ENGINE VOLUMES AND MASS------------------------------------------------------------
26  Vtot = 1;
27  DVR = 0.05:0.01:0.6;
28  V = 1;
29  M = 1;
30  X = [1.25 1.5 1.75];
31  r = [0.5 0.6 0.7 0.8 0.9 1.0];
32  %DEFINING TEMPERATURES--------------------------------------------------------------
33  Tk = 300;
34  %----------------------------------------------------------------------------------
35  Efficiency = zeros(numel(r)*numel(X),numel(DVR));
36  HEATER = zeros(numel(r)*numel(X),numel(DVR));
37  WORK = zeros(numel(r)*numel(X),numel(DVR));
38  %FOR LOOP---------------------------------------------------------------------------
39  for n = 1:numel(X)
40      Th = X(n)*Tk;
41      Tr = (Th - Tk)/log(Th/Tk);
42      for l = 1:numel(r)
43          for j = 1:numel(DVR)
44              Vdead = V*DVR(j);
45              Vemax = (V - Vdead)/(1 + r(l));
46              Vcmax = (V - Vdead) - Vemax;
47              Vccl = (5/100)*Vdead;
48              Vk = ((30/100)*Vdead);
49              Vr = (30/100)*Vdead;
50              Vh = (30/100)*Vdead;
51              Vecl = (5/100)*Vdead;
52              %PREALLOCATION OF MATRICES AND ANGLE VECTOR-----------------------------
53              Variables = zeros(25,360);    %Setting up variables matrix-------------
54              dVariables = zeros(16,360);   %Setting up derivatives matrix-----------
55              Theta1 = linspace(0,2*pi,360);
56              h = Theta1(2) - Theta1(1);
57              %INITIAL VALUES---------------------------------------------------------
58              Variables(17,1) = Tk;
59              Variables(18,1) = Th;
60              Variables(2,360) = Th;
61              Variables(1,360) = Tk;
62              while (abs(Variables(1,1) - Variables(1,360)) + abs(Variables(2,1) - Variables
                    (2,360))) > 0.1
63                  Theta = 0;
64                  Variables(3,1) = 0;
65                  Variables(4,1) = 0;
66                  Variables(5,1) = 0;
67                  Variables(6,1) = 0;
68                  Variables(7,1) = 0;
69                  Variables(10,1) = 0;
```

```
                    Variables(1,1) = Variables(1,360);
                    Variables(2,1) = Variables(2,360);
                    Variables(8,1) = Variables(8,360);
                    Variables(9,1) = Variables(9,360);
                    Variables(11,1) = Variables(11,360);
                    for i = 1:5;
                        [Theta, Variables(:,i+1),dVariables(:,i+1)] = RUNGEKUTTA('DVEQUATIONS'
                            ,7,Theta,h,Variables(:,i));
                    end
                    for i = 5:359
                        [Theta, Variables(:,i+1),dVariables(:,i+1)] = AB4('DVEQUATIONS',7,
                            Variables(:,i),dVariables(:,i),dVariables(:,i-1),dVariables(:,i-2),
                            dVariables(:,i-3),Theta,h);
                    end
                end
                Efficiency(l + (n-1)*numel(r),j) = (Variables(5,360)+Variables(3,360))/Variables
                    (5,360);
                HEATER(l + (n-1)*numel(r),j) = Variables(5,360);
                WORK(l + (n-1)*numel(r),j) = Variables(5,360) + Variables(3,360);
            end
        end
    end
%-------------------------------------------------------------------------------
```

D.2.5 Dead-Volume Ratio Optimisation

```
%STIRLING ENGINE ADIABATIC MODEL OPTIMUM DEAD VOLUME FUNCTION-----------------
%James Wills 2016-------------------------------------------------------------
%-----------------------------------------------------------------------------
%DEFINING GLOBAL VARIABLES----------------------------------------------------
global R
global Cp
global Cv
global k
global Th
global Tr
global Tk
global M
global Vr
global Vh
global Vk
global Vemax
global Vcmax
global Vccl
global Vecl
%GAS CONSTANTS---------------------------------------------------------------
R = 0.2870;
Cp = 1.005;
Cv = 0.718;
k = 1.4;
%ENGINE VOLUMES AND MASS-----------------------------------------------------
Vtot = 1;
```

```
27 DVR = 0.05:0.001:0.6;
28 V = 1;
29 M = 1;
30 X = 1.2:0.05:1.8;
31 r = 0.8;
32 %DEFINING TEMPERATURES----------------------------------------------------------------
33 Tk = 300;
34 %---------------------------------------------------------------------------------------
35 count = 0;
36 Efficiency = zeros(numel(r)*numel(X),numel(DVR));
37 HEATER = zeros(numel(r)*numel(X),numel(DVR));
38 WORK = zeros(numel(r)*numel(X),numel(DVR));
39 MAXWORK = zeros(1,numel(X));
40 OPTIDVR = zeros(1,numel(X));
41 %FOR LOOP-------------------------------------------------------------------------------
42 for n = 1:numel(X)
43     count = count + 1;
44     for j = 1:numel(DVR)
45         Th = X(n)*Tk;
46         Tr = (Th + Tk)/2;
47         Vdead = V*DVR(j);
48         Vemax = (V - Vdead)/(1 + r);
49         Vcmax = (V - Vdead) - Vemax;
50         Vccl = (5/100)*Vdead;
51         Vk = ((30/100)*Vdead);
52         Vr = (30/100)*Vdead;
53         Vh = (30/100)*Vdead;
54         Vecl = (5/100)*Vdead;
55         %PREALLOCATION OF MATRICES AND ANGLE VECTOR-----------------------------
56         Variables = zeros(25,360);    %Setting up variables matrix-----------
57         dVariables = zeros(16,360);   %Setting up derivatives matrix---------
58         Theta1 = linspace(0,2*pi,360);
59         h = Theta1(2) - Theta1(1);
60         %INITIAL VALUES---------------------------------------------------------
61         Variables(17,1) = Tk;
62         Variables(18,1) = Th;
63         Variables(2,360) = Th;
64         Variables(1,360) = Tk;
65         while (abs(Variables(1,1) - Variables(1,360)) + abs(Variables(2,1) - Variables
               (2,360))) > 0.001
66             Theta = 0;
67             Variables(3,1) = 0;
68             Variables(4,1) = 0;
69             Variables(5,1) = 0;
70             Variables(6,1) = 0;
71             Variables(7,1) = 0;
72             Variables(10,1) = 0;
73             Variables(1,1) = Variables(1,360);
74             Variables(2,1) = Variables(2,360);
75             Variables(8,1) = Variables(8,360);
76             Variables(9,1) = Variables(9,360);
77             Variables(11,1) = Variables(11,360);
```

```
78                for i = 1:5;
79                    [Theta, Variables(:,i+1),dVariables(:,i+1)] = RUNGEKUTTA('DVEQUATIONS',7,
                          Theta,h,Variables(:,i));
80                end
81                for i = 5:359
82                    [Theta, Variables(:,i+1),dVariables(:,i+1)] = AB4('DVEQUATIONS',7,Variables
                          (:,i),dVariables(:,i),dVariables(:,i-1),dVariables(:,i-2),dVariables(:,i
                          -3),Theta,h);
83                end
84            end
85            Efficiency(n,j) = (Variables(5,360)+Variables(3,360))/Variables(5,360);
86            HEATER(n,j) = Variables(5,360);
87            WORK(n,j) = Variables(5,360) + Variables(3,360);
88        end
89        ind = find(WORK(n,:) == max(WORK(n,:)));
90        OPTIDVR(n) = DVR(ind);
91        MAXWORK(n) = WORK(n,ind);
92    end
93    %-------------------------------------------------------------------------------
```

D.3 Heat Exchangers

D.3.1 Regenerator Properties

```
%FUNCTION THAT CALCULATES THE REGENERATOR PROPERTIES AND DIMENSIONS
%James Wills 2016/17
%
function [Dh,Vr,Armat,Arsurf] = REGENERATORPROPERTIES(type,L,Aflow)
if strcmp(type,'WN50') == 1
    Diam = 0.23e-3;                                          %m
    Poros = 0.645;
elseif strcmp(type,'WN100') == 1
    Diam = 0.1e-3;                                           %m
    Poros = 0.711;
elseif strcmp(type,'WN150') == 1
    Diam = 0.06e-3;                                          %m
    Poros = 0.754;
elseif strcmp(type,'WN200') == 1
    Diam = 0.05e-3;                                          %m
    Poros = 0.729;
end
ShapeFactor = 4.0;
%CALCULATING THE HYDRAULIC DIAMETER
Dh = 4*Poros*Diam/(ShapeFactor*(1-Poros));                   %m
%CALCULATING THE FLOW AREA
Across = Aflow/Poros;                                        %m^2
%CALCULATING THE REGENERATOR GAS VOLUME
Vr = Poros*Across*L;                                         %m^3
%CALCULATING THE REGENERATOR MATERIAL AREA
Armat = Across - Aflow;                                      %m^2
%CALCULATING THE REGENERATOR HEAT TRANSFER SURFACE AREA
Arsurf = (4*Poros/Dh)*Vr;                                    %m^2
%
```

D.3.2 Regenerator Flow

```
%REGENERATOR FUNCTION CALCULATES FLOW LOSSES AND HEAT TRANSFER
%James Wills 2016/17
%
function [Eff,delP] = REGENERATOR(T,Mave,Mass,Aflow,D,L,Vr)
global Pri
%CALCULATING THE VISCOSITY
Visc = (1.458e-6)*(T^1.5)/(T + 110.4);                       %kg/m.s
%CALCULATING THE REYNOLDS NUMBER
Re = Mave*D/(Visc*Aflow);
Reave = mean(abs(Re));
Remax = max(abs(Re));
%PRESSURE DROP CALCULATIONS
f = (175/Remax) + 1.6;
Cre = f*Reave;
delP = -(Cre.*Mave*Visc*L*Vr)./(2000*Mass*Aflow*(D^2));      %kPa
%HEAT TRANSFER CALCULATIONS
```

```
Nu = 0.33*(Reave^0.67);
NTU = 4*Nu*L/(Pri*Reave*D);
Eff = NTU/(NTU+2);
%-------------------------------------------------------------------------
```

D.3.3 Cooler and Heater Flow

```
%HEAT EXCHANGER FUNCTION CALCULATES FLOW LOSSES AND HEAT TRANSFER--------
%James Wills 2016/17----------------------------------------------------
%-----------------------------------------------------------------------
function [Eff,delP,Reave] = HEATEXCHANGER(T,Mave,Mass,C,N,D,L)
%Eff and h, interchangeable depending on wall assumption----------------
global Pri
global Cpi
%CALCULATING THE VISCOSITY OF THE WORKING FLUID-------------------------
Visc = (1.458e-6)*(T^1.5)/(T + 110.4);                          %kg/m.s
%FLOW AREA, SURFACE AREA AND VOLUME-------------------------------------
Aflow = 0.25*N*pi*(D^2);                                        %m^2
Vol = Aflow*L;                                                  %m^3
Asurf = N*pi*D*L;                                               %m^2
%CALCULATING THE REYNOLDS NUMBERS, AVERAGE AND MAXIMUM------------------
Re = ((Mave/Aflow)*D)/Visc;
Reave = mean(abs(Re));
%PRESSURe DROP THROUGH THE HEAT EXCHANGER-------------------------------
if Reave <= 240000
    f = 0.351*Reave^-0.255;
else
    f = 0.118*Reave^-0.165;
end
Cre = f*Reave;
delP = -(Cre.*Mave*Visc*L*Vol)./(2000*Mass*Aflow*(D^2));         %kPa
%INTERNAL HEAT TRANSFER-------------------------------------------------
NUi = (f/8)*(Reave-1000)*Pri/(1 + 12.7*((f/8)^0.5)*(Pri^(2/3)-1));
ki = Visc*Cpi/Pri;                                              %kW/mK
hi = ki*NUi/D;                                                  %kW/m^2.K

%This section is only required for finite capactance rate assumption----
%NTU--------------------------------------------------------------------
NTU = hi*Asurf/C;
%EFFECTIVENESS----------------------------------------------------------
Eff = 1 - exp(-NTU);
%-----------------------------------------------------------------------
```

D.4 Mass and Mass Flows

D.4.1 Alpha Type Mass

```
%MASS OF WORKING FLUID IN THE ENGINE-----------------------------------------------
%James Wills 2016/17---------------------------------------------------------------
%----------------------------------------------------------------------------------
function M = ENGMASS(Pmean,Vcswept,Vccl,Veswept,Vecl,Vk,Vr,Vh,Th,Tk)
global Ri
%----------------------------------------------------------------------------------
s = Vcswept/(2*Tk) + Vccl/Tk + Vk/Tk + Vr*log(Th/Tk)/(Th-Tk) + Vh/Th + Veswept/(2*Th) + Vecl
    /Th;
c =0.5*sqrt((Veswept/Th)^2 + 2*(Veswept/Th)*(Vcswept/Tk)*cos(pi/2) + (Vcswept/Tk)^2);
b = c/s;
%MASS OF WOKING FLUID--------------------------------------------------------------
M = Pmean*s*sqrt(1-b^2)/Ri;
%----------------------------------------------------------------------------------
```

D.4.2 Beta Type Mass

```
%MASS OF WORKING FLUID IN THE ENGINE-----------------------------------------------
%James Wills 2016/17---------------------------------------------------------------
%----------------------------------------------------------------------------------
function M = ENGMASS(Pmean,Vcdisp,Vcpist,Vccl,Vedisp,Vecl,Vk,Vr,Vh,Th,Tk)
global Ri
%----------------------------------------------------------------------------------
s = (Vcdisp + Vcpist)/(2*Tk) + Vccl/Tk + Vk/Tk + Vr*log(Th/Tk)/(Th-Tk) + Vh/Th + Vedisp/(2*
    Th) + Vecl/Th;
c =0.5*sqrt((Vcpist/(2*Tk) - (Vcdisp/(2*Tk))*cos(pi/2) + (Vedisp/(2*Th))*cos(pi/2))^2 + ((
    Vcdisp/(2*Tk))*sin(pi/2) + (Vedisp/(2*Th))*sin(pi/2))^2);
b = c/s;
%MASS OF WOKING FLUID--------------------------------------------------------------
M = Pmean*s*sqrt(1-b^2)/Ri;
%----------------------------------------------------------------------------------
```

D.4.3 Mass Flow Rates

```
%COMPONENT MASSFLOWS---------------------------------------------------------------
%James Wills 2016/17---------------------------------------------------------------
%----------------------------------------------------------------------------------
function Massflow = MASSFLOWS(Massflow,Mcb,Mkb,Mhb,Meb,thetadot)
%FLOW THROUGH THE COOLER-----------------------------------------------------------
Massflow(1,:) = 0.5*(Mcb + Mkb)*thetadot;                                    %kg/s
%FLOW THROUGH THE REGENERATOR-----------------------------------------------------
Massflow(2,:) = 0.5*(Mkb + Mhb)*thetadot;                                    %kg/s
%FLOW THROUGH THE HEATER----------------------------------------------------------
Massflow(3,:) = 0.5*(Mhb + Meb)*thetadot;                                    %kg/s
%----------------------------------------------------------------------------------
```

D.5 Entropy Generation

D.5.1 Constant Wall Temperature

```
%FUNCTION FOR CALCULATING AVERAGE RATE OF ENTROPY GENERATION
%James Wills 2016/17
%
function [Sgenr,Sgenk,Sgenh] = ENTROPYGEN(Mr,Mk,Mh,Tk,Th,T0,Tsource,Pcb,Pkb,Phb,Peb,Effr,Qk,
    Qh)
%Global Variables
global Cpi
global Ri
%Mass flow averages and angles
Mrave = mean(abs(Mr));
Theta = linspace(0,2*pi,numel(Mr));
%Entropy generation in the regenerator
Thb = Tk + Effr*(Th-Tk);
Tkb = Th - Effr*(Th-Tk);
Sgenr = Mrave*(Cpi/2)*log((Thb*Tkb)/(Tk*Th)) + (Ri/(2*pi))*trapz(Theta,abs(Mr).*abs(log(Phb
    ./Pkb)));
%Entropy generation in the cooler
Sgenk = (Ri/(2*pi))*trapz(Theta,abs(Mk).*abs(log(Pkb./Pcb))) + abs(Qk)/T0;
%Entropy generation in the heater
Sgenh = (Ri/(2*pi))*trapz(Theta,abs(Mh).*abs(log(Peb./Phb))) - abs(Qh)/Tsource;
```

D.5.2 Finite Capacity Rate

```
%FUNCTION FOR CALCULATING AVERAGE RATE OF ENTROPY GENERATION
%James Wills 2016/17
%
function [Sgenr,Sgenk,Sgenh] = ENTROPYGEN(Mr,Mk,Mh,CH,CK,Tk,Th,T0,Tsource,Pcb,Pkb,Phb,Peb,
    Effr,Effh,Effk)
%Global Variables
global Cpi
global Ri
%Mass flow averages and angles
Mrave = mean(abs(Mr));
Theta = linspace(0,2*pi,numel(Mr));
%Entropy generation in the regenerator
Thb = Tk + Effr*(Th-Tk);
Tkb = Th - Effr*(Th-Tk);
Sgenr =  Mrave*(Cpi/2)*log((Thb*Tkb)/(Tk*Th)) + (Ri/(2*pi))*trapz(Theta,abs(Mr).*abs(log(Phb
    ./Pkb)));
%Entropy generation in the cooler
TCL2 = T0 + Effk*(Tk-T0);
Sgenk = (Ri/(2*pi))*trapz(Theta,abs(Mk).*abs(log(Pkb./Pcb))) + CK*log(TCL2/T0);
%Entropy generation in the heater
THL2 = Tsource - Effh*(Tsource-Th);
Sgenh = (Ri/(2*pi))*trapz(Theta,abs(Mh).*abs(log(Peb./Phb))) + CH*log(THL2/Tsource);
```

D.6 GPU-3 Analysis

D.6.1 Analysis Script

```
%ANALYSIS FUNCTION
%James Wills 2016/17
%
%
%GAS CONSTANTS
global Ri
global Cpi
global Cvi
global ki
global Pri
Ri = 2.08;
Cpi = 5.19;
Cvi = 3.12;
ki = 1.667;
Pri = 0.72;
kreg = 0.015;
%
%TEMPERATURES
Tsource = 977;
T0 = 288;
%
%GEOMETRY
Vccl = 2.868e-5;
Vcswept = 0.00011413;
Vecl = 3.052e-5;
Veswept = 0.00012082;
%
Nh = 40;
Dh = 3.02e-3;
Lh = 0.2456;
LhHT = 0.1554;
Vh = 7.028e-5;
%
Nk = 312;
Dk = 1.08e-3;
Lk = 0.0461;
LkHT = 0.0355;
Vk = 1.318e-5;
%
Porosr = 0.697;
DiameterMesh = 4e-5;
Diamr = 0.0226;
Lr = 0.0226;
%Speed Calculations
freq = 41.72;
MASS = 0.0006:0.00005:0.003;
SECONDP = zeros(1,numel(MASS));
SECONDE = zeros(1,numel(MASS));
```

```
FIRSTP = zeros(1,numel(MASS));
FIRSTE = zeros(1,numel(MASS));
Effr = zeros(1,numel(MASS));
Qin = zeros(1,numel(MASS));
Qout = zeros(1,numel(MASS));
Sgen = zeros(1,numel(MASS));
%Calculating Geometry-------------------------------------------------------------
for i = 1:numel(MASS)
    freq = MASS(i);
    thetadot = freq*2*pi;
    %--------------------------------------------------------------------------
    Ahflow = Nh*(pi/4)*Dh^2;
    Akflow = Nk*(pi/4)*Dk^2;
    %--------------------------------------------------------------------------
    Aksurf = Nk*LkHT*pi*Dk;
    Ahsurf = Nh*LhHT*pi*Dh;
    %--------------------------------------------------------------------------
    Vk = Akflow*Lk;
    Armat = 8*(pi/4)*(Diamr^2)*(1-Porosr);
    Arflow = 8*(pi/4)*(Diamr^2)*Porosr;
    Dr = 4*Porosr*DiameterMesh/(4*(1-Porosr));
    Vr = Arflow*Lr;
    %PREALLOCATION------------------------------------------------------------
    Variables = zeros(22,361);
    dVariables = zeros(16,361);
    Massflows = zeros(3,361);
    Pressure = zeros(4,361);
    %INITIAL VALUES-----------------------------------------------------------
    Th = 0;
    Tk = 0;
    THEATER = Tsource;
    TCOOLER = T0;
    n = 0;
    while abs(TCOOLER - Tk) + abs(THEATER - Th) >= 0.0001
        Th = THEATER;
        Tk = TCOOLER;
        %M = 0.0011362;
        %REGENERATOR TEMPERATURE TO CALCULATE GAS PROPERTIES----------------
        Trmean  = (Th + Tk)/2;
        [Variables,dVariables] = NUMERICAL(Variables,dVariables,M,Th,Tk,Vh,Vr,Vk,Vccl,
            Vcswept,Vecl,Veswept);
        Massflows = MASSFLOWS(Massflows,Variables(19,:),Variables(20,:),Variables(21,:),
            Variables(22,:),thetadot);
        %REGENERATOR--------------------------------------------------------
        [Effr(i),delPr,NTUr,Nur,Reaver] = REGENERATOR(Trmean,Massflows(2,:),Variables(14,:),
            Arflow,Dr,Lr,Vr);
        %HEATER AND COOLER--------------------------------------------------
        [hh,delPh,Reh] = HEATEXCHANGER(Th,Massflows(3,:),Variables(15,:),Nh,Dh,Lh);
        [hk,delPk,Rek] = HEATEXCHANGER(Tk,Massflows(1,:),Variables(13,:),Nk,Dk,Lk);
        Qr = abs(max(Variables(4,:)) - min(Variables(4,:)));
        Qcond = (kreg*Armat/Lr)*(Th-Tk);
        Qin(i) = (Variables(5,360) + (1 - Effr(i))*Qr)*freq + Qcond;
```

```
98          Qout(i) = (abs(Variables(3,360)) + (1 - Effr(i))*Qr)*freq + Qcond;
99          THEATER = Tsource - Qin(i)/(Ahsurf*hh);
100         TCOOLER = T0 + Qout(i)/(Aksurf*hk);
101         %INFINITE LOOP BREAKER----------------------------------------------
102         n = n + 1;
103         %NON-CONVERGENCE----------------------------------------------------
104         if n > 300
105             break
106         else
107         end
108     end
109     %PRESSURE MATRIX----------------------------------------------------------
110     Pressure(1,:) = Variables(11,:);
111     Pressure(2,:) = Pressure(1,:) + delPk;
112     Pressure(3,:) = Pressure(2,:) + delPr;
113     Pressure(4,:) = Pressure(3,:) + delPh;
114     %PRESSUREDROP-------------------------------------------------------------
115     PumpLoss = 0;
116     dtheta = 2*pi/360;
117     for j = 1:numel(delPr)
118         PumpLoss = PumpLoss + (delPk(j) + delPr(j) + delPh(j))*dtheta*dVariables(9,j);
119     end
120     %ENTROPY GENERATION EQUATIONS---------------------------------------------
121     [Sgenr,Sgenk,Sgenh] = ENTROPYGEN(Massflows(2,:),Massflows(1,:),Massflows(3,:),Tk,Th,T0,
            Tsource,Pressure(1,:),Pressure(2,:),Pressure(3,:),Pressure(4,:),Effr(i),Qout(i),Qin(
            i));
122     Sgen(i) = Sgenr + Sgenh + Sgenk;
123     %WORK---------------------------------------------------------------------
124     Power = Qin(i)*(1-(T0/Tsource)) - Qout(i)*(1-(T0/T0)) - T0*Sgen(i);
125     %Constraining the reynolds number in heater and cooler--------------------
126     if Reh < 3050
127         Power = 0;
128     elseif Rek <3050
129         Power = 0;
130     else
131     end
132     if n > 300
133         Power = 0;
134     else
135     end
136     Eff = Power/Qin(i);
137     %VECTORS OF OUTPUTS-------------------------------------------------------
138     SECONDP(i) = Power;
139     SECONDE(i) = Eff;
140     FIRSTP(i) = Qin(i) - Qout(i) + PumpLoss*freq;
141     FIRSTE(i) = FIRSTP(i)/Qin(i);
142
143 end
```

D.7 Optimisation Functions

D.7.1 Maximum Power Function

```
%MAXIMUM POWER FUNCTION-------------------------------------------------------------------
%James Wills 2016/17----------------------------------------------------------------------
%-----------------------------------------------------------------------------------------
function [W, ifail, icount] = MAXPOWER(X0)
[WORK,~,~,~,~,~,~,~,~,~,~,~,~,~,~,~,~,~,~,~,~] = ANALYSIS(X0);
%EVALUATING THE POWER OUTPUT---------------------------------------------------------------
W = -WORK;
if isnan(WORK)
    ifail = 1;
    icount = 0;
else
    ifail = 0;
    icount = 1;
end
%-----------------------------------------------------------------------------------------
```

D.7.2 Power and Efficiency Function

```
%ANALYSIS FUNCTION------------------------------------------------------------------------
%James Wills 2016/17----------------------------------------------------------------------
%-----------------------------------------------------------------------------------------
function [Power, Eff, Effr, Effh, Effk, Sgen, Sgenr, Sgenh, Sgenk, Dh, Dk, Lr, Lh, Lk, Arsurf, Ahsurf,
    Aksurf, Vcswept, Veswept] = ANALYSIS(X)
%Note 1: The following function is for the Alpha type engine change way
%volumes are calculated for Beta type.
%Note 2: Finite capacity rates are assumed in order to change edit heat
%exchanger and entropy generation functions and the way the heater and
%cooler temperature is updated.
global Tsource
global T0
global RegenType
global CH
global CK
global Vtot
global N
global TubeRatio
global AreaRatio
global L
%-----------------------------------------------------------------------------------------
DVR = abs(X(1));
Regratio = abs(X(2));
LengthRatio = abs(X(3));
Vratio = abs(X(4));
Speed = abs(X(5));
%GAS CONSTANTS-----------------------------------------------------------------------------
global Ri
global Cpi
global Cvi
```

```
30  global ki
31  global Pri
32  Ri = 0.2870;
33  Cpi = 1.005;
34  Cvi = 0.718;
35  ki = 1.4;
36  Pri = 0.72;
37  kreg = 0.05;
38  %SPEED CALCULATIONS-------------------------------------------------------------------
39  freq = Speed/60;
40  thetadot = freq*2*pi;
41  %GEOMETRY CALCULATIONS----------------------------------------------------------------
42  Nk = round(N/(1 + TubeRatio));
43  Nh = N - Nk;
44  Vdead = DVR*Vtot;
45  Vswept = Vtot - Vdead;
46  Veswept = Vswept/(1+Vratio);
47  Vcswept = Vswept - Veswept;
48  Vccl = 0.05*Vcswept;
49  Vecl = 0.05*Veswept;
50  VHX = Vdead - Vccl - Vecl;
51  Lr = L*Regratio;
52  Ahflow = VHX/(Lr*(AreaRatio-1)+L);
53  Akflow = Ahflow;
54  Arflow = AreaRatio*Akflow;
55  Dh = sqrt(Ahflow/(Nh*(pi/4)));
56  Dk = sqrt(Ahflow/(Nk*(pi/4)));
57  Lk = (L-Lr)/(1+LengthRatio);
58  Lh = (L - Lr - Lk);
59  Vh = Nh*(pi/4)*(Dh^2)*Lh;
60  Vk = Nk*(pi/4)*(Dk^2)*Lk;
61  [Dr,Vr,Armat,Arsurf] = REGENERATORPROPERTIES(RegenType,Lr,Arflow);
62  Aksurf = Nk*Lk*pi*Dk;
63  Ahsurf = Nh*Lh*pi*Dh;
64  %PREALLOCATION------------------------------------------------------------------------
65  Variables = zeros(22,360);
66  dVariables = zeros(16,360);
67  Massflows = zeros(3,360);
68  Pressure = zeros(4,360);
69  %INITIAL VALUES-----------------------------------------------------------------------
70  Th = 0;
71  Tk = 0;
72  THEATER = Tsource;
73  TCOOLER = T0;
74  n = 0;
75  while abs(TCOOLER - Tk) + abs(THEATER - Th) >= 0.0005
76    Th = THEATER;
77    Tk = TCOOLER;
78    M = ENGMASS(5000,Vcswept,Vccl,Veswept,Vecl,Vk,Vr,Vh,Th,Tk);
79    %REGENERATOR TEMPERATURE TO CALCULATE GAS PROPERTIES----------------------------
80    Trmean  = (Th + Tk)/2;
81    [Variables,dVariables] = NUMERICAL(Variables,dVariables,M,Th,Tk,Vh,Vr,Vk,Vccl,Vcswept,Vecl
```

```
        ,Veswept);
82    Massflows = MASSFLOWS(Massflows,Variables(19,:),Variables(20,:),Variables(21,:),Variables
        (22,:),thetadot);
83    %REGENERATOR-----------------------------------------------------------------
84    [Effr,delPr] = REGENERATOR(Trmean,Massflows(2,:),Variables(14,:),Arflow,Dr,Lr,Vr) ;
85    %HEATER AND COOLER-----------------------------------------------------------
86    [Effh,delPh,Reh] = HEATEXCHANGER(Th,Massflows(3,:),Variables(15,:),CH,Nh,Dh,Lh);
87    [Effk,delPk,Rek] = HEATEXCHANGER(Tk,Massflows(1,:),Variables(13,:),CK,Nk,Dk,Lk);
88    Qr = abs(max(Variables(4,:)) - min(Variables(4,:)));
89    Qcond = (kreg/Lr)*Armat*(Th - Tk);
90    Qin = (Variables(5,360) + (1 - Effr)*Qr)*freq + Qcond;
91    Qout = (abs(Variables(3,360)) + (1 - Effr)*Qr)*freq + Qcond;
92    %Make change here depending on whether the asumption is finite capacity
93    %rate or constant wall temperature.
94    THEATER = Tsource - Qin/(Effh*CH);
95    TCOOLER = T0 + Qout/(Effk*CK);
96    %INFINITE LOOP BREAKER-------------------------------------------------------
97    n = n + 1;
98    %NON CONVERGENCE-------------------------------------------------------------
99  if n > 300
100     break
101 else
102 end
103 end
104 %PRESSURE MATRIX-------------------------------------------------------------
105 Pressure(1,:) = Variables(11,:);
106 Pressure(2,:) = Pressure(1,:) + delPk;
107 Pressure(3,:) = Pressure(2,:) + delPr;
108 Pressure(4,:) = Pressure(3,:) + delPh;
109 %ENTROPY GENERATION CALCULATION----------------------------------------------
110 [Sgenr,Sgenk,Sgenh] = ENTROPYGEN(Massflows(2,:),Massflows(1,:),Massflows(3,:),CH,CK,Tk,Th,T0
      ,Tsource,Pressure(1,:),Pressure(2,:),Pressure(3,:),Pressure(4,:),Effr,Effh,Effk);
111 Sgen = Sgenr + Sgenh + Sgenk;
112 %Work------------------------------------------------------------------------
113 Power = Qin - T0*CH*log(Tsource/(Tsource - Effh*(Tsource-Th))) - Qout - T0*CK*log(T0/(T0 +
      Effk*(Tk-T0))) - T0*Sgen;
114 %Constraining the reynolds number in heater and cooler----------------------
115 %REYNOLDS NUMBER CONSTRAINT--------------------------------------------------
116 if Reh < 3050
117     Power = 0;
118 elseif Rek <3050
119     Power = 0;
120 else
121 end
122 if n > 300
123    Power = 0;
124 else
125 end
126 %EFFICIENCY------------------------------------------------------------------
127 Eff = Power/Qin;
128 %----------------------------------------------------------------------------
```

D.7.3 Optimisation Script

```
%OPTIMIZATION PROGRAM-------------------------------------------------------------------
%James Wills 2016-----------------------------------------------------------------------
%---------------------------------------------------------------------------------------
global Tsource
global T0
global RegenType
global CH
global CK
global Vtot
global N
global TubeRatio
global AreaRatio
global L
%TEMPERATURES---------------------------------------------------------------------------
T0 = 298;
%REGENERATOR TYPE-----------------------------------------------------------------------
%Note 1: Manually define the regnerator type here.
RegenType = 'WN200';
%SINK AND SOURCE CAPACITY RATES---------------------------------------------------------
%Note 2: Not required if constant wall temperature
CH = 0.25;
CK = 0.25;
%ENGINE FEATURES------------------------------------------------------------------------
Vtot = 0.001;
TubeRatio = 0.25;
AreaRatio = 8;
N = 400;
L = 0.3;
THOTSIDE = 500:50:1000;
%PREALLOCATION--------------------------------------------------------------------------
n = 0;
OUTPUT = zeros(numel(THOTSIDE),19);
PROPS = zeros(numel(THOTSIDE),5);
lb = [0.1  0.05  0.5  0.5  150];
ub = [0.8  0.6  2  2  3000];
bounds = [lb' ub'];
%Note 3: define starting vector or matrix here
INITIAL = [.];
for i = 1:numel(THOTSIDE)
    n = n+1
    Tsource = THOTSIDE(i);
    [PROPS(i,:)] = imfil(INITIAL',@MAXPOWER,200,bounds);
    [OUTPUT(i,1),OUTPUT(i,2),OUTPUT(i,3),OUTPUT(i,4),OUTPUT(i,5),...
        OUTPUT(i,6),OUTPUT(i,7),OUTPUT(i,8),OUTPUT(i,9),OUTPUT(i,10),...
        OUTPUT(i,11),OUTPUT(i,12),OUTPUT(i,13),OUTPUT(i,14),...
        OUTPUT(i,15),OUTPUT(i,16),OUTPUT(i,17),OUTPUT(i,18),...
        OUTPUT(i,19)] = ANALYSIS(PROPS(i,:));
end
%---------------------------------------------------------------------------------------
```